ISSN: 0019-4824

The Indian Geographical Journal

Volume 98 2023 No.1 & 2

The Indian Geographical Society
Department of Geography
University of Madras
Guindy Campus
Chennai-600 025,India

Editor: K.Kumaraswamy
Assistant Editor: K.Balasubramani

Governing Council of The Indian Geographical Society

President:	Prof. N. Sivagnanam
Vice Presidents:	Prof. B. Hema Malini Prof. Sulochana Shekhar Prof. Smita Bhutani Prof. Subhash Anand Prof. Aravind Mulimanian
General Secretary:	Dr. R. Jaganathan
Joint Secretaries:	Prof. R. Jegankumar Dr. S. Sanjeevi Prasad Dr. G. Geetha
Treasurer:	Prof. M. Sakthivel
Council Members:	Prof. P.S. Tiwari Prof. V. Emayavaramban Prof. B. Srinagesh Prof. Dhanaraj Gownamani Dr. B. Mahalingam Dr. S. Eswari
Member Nominated to the EC:	Prof. P.S. Tiwari
Editor:	Prof. K. Kumaraswamy
Assistant Editor:	Dr. K. Balasubramani

For details about the IGS, visit: www.igschennai.org

Information to Authors

The Indian Geographical Journal is published half-yearly in June and December by The Indian Geographical Society, Chennai. The UGC-Care listed / peer-reviewed journal invites manuscripts of original research on any geographical field, providing information of importance to geography and related disciplines with an analytical approach. The manuscript should be submitted only through the **online submission form https://forms.gle/SLfL1wodtvLEVPcV8**

The manuscript should be uploaded in Microsoft Word Document (.doc, .docx) as follows: 1) **Title Page**: Title of the Manuscript, Author Name and Address (complete postal address with contact details including phone and email ID) and acknowledgements (if any). 2) **Full-Length Manuscript**: The main text part should not contain the author(s) name or identities. The main text can be divided into the sections viz. Title, Abstract, Keywords, Introduction (Background/Literature review), Study area, Methodology, Results, Discussion, Conclusion and References. 3) **Tables**: All tables should be consolidated in a single MS Word document with proper captions and footnotes (if applicable). 4) **Figures**: All figures/graphs/charts/maps should be submitted in JPEG/PNG format within a single MS Word document. Each figure should have a concise caption describing accurately what the figure depicts. The tables and figures should be numbered in a sequence (Table 1, Table 2 etc. and Figure 1, Figure 2 etc.) and cited in the manuscript at appropriate places.

The title should be brief, specific and amenable to indexing. No more than five keywords should be indicated separately; these should be chosen carefully and not phrases of several words. The abstract should be limited to 100-250 words and convey the main points of the study, outline the methods and results and explain the significance of the results. Acknowledgements of people, grants, funds, etc., should be placed in a separate section in the title page. The names of funding organisations should be written in full. The title page should also be accompanied by a letter stating that it has not been published or sent to any other journal and will not be submitted elsewhere for publication.

Maps and charts should be submitted in the final or near-final form. The authors should, however, agree to revise the maps and charts for reproduction after the article is accepted for publication. If you include figures that have already been published elsewhere, you must obtain permission from the copyright owner(s) for both the print and online format. Please be aware that some publishers do not grant electronic rights for free, and it is informed that IGS will not be able to refund any costs that may have occurred to receive these permissions.

References should be listed in alphabetical order as per MLA format. The list of references (limited to 20-25) should include only the published works or sites that are cited in the main text. You may refer to the IGS website (http://igschennai.org/IGJ.php) for detailed guidelines.

Corresponding Email: editorigs1926@gmail.com

The Indian Geographical Journal

Contents

The Indian Geographical Journal
Volume 98 (1) June - 2023, pp 01-16
ISSN 0019-4824

SPATIO–TEMPORAL ANALYSIS OF SPECTRAL INDICES AND IN-SITU EDAPHIC SALINITY ESTIMATION IN THE DELTAIC ECOSYSTEM OF INDIAN SUNDARBANS

Priyanka Das[1], Aditi Sarkar[2], Pabitra Banik[3]*, Michael A. Powell[4], and Krishna Chandra Rath[5]

[1] Agricultural and Ecological Research Unit, Indian Statistical Institute, Kolkata, India.

[2] Department of Mining Engineering, IIEST, Kolkata, India.

[3]* Agricultural and Ecological Research Unit, Indian Statistical Institute, Kolkata, India.

[4] Dept of Renewable Resources, University of Alberta, Alberta, Canada.

[5] Department of Geography, Utkal University, Bhubaneshwar, Odisha, India.

*Corresponding author. E-mail address: banikpabitra@gmail.com

ABSTRACT

The Sundarbans area represents the world's most extensive mangrove forests, formed by the confluence of the Ganga-Brahmaputra Rivers delta spread across 10000 km^2. The significance of the area was recognised by the United Nations Educational, Scientific and Cultural Organization (UNESCO) in 1987 when it was named a World Heritage Site. Past research has demonstrated that mangrove ecosystems are highly susceptible to climate change. The current study explores the relationship between different spectral indices derived from remote sensing using Landsat satellite's Multispectral Scanner (MSS), Thematic Mapper (TM), and Operational Land Imager (OLI) images as indicators of mangrove conditions. Specifically, this study analyses changes in the Normalized Difference Salinity Index (NDSI), the Normalized Difference Vegetation Index (NDVI), and the Land Surface Temperature (LST) index across the Sundarbans from 1972 to 2022. The index values for NDSI positively correlate with measured soil electrical conductivity (EC). The results show that NDVI declined while NDSI and LST increased during the study period. Over the last 50 years (1972-2022), the maximum NDVI values have decreased by 0.54, while the maximum NDSI has increased by 0.7. LST rose by about 0.9 ^{0}C between 1995 and 2022. The changes in these indices help identify potential safeguard measures to protect the fragile ecosystem, which help policies related to sustainable mangrove management in the Sundarbans.

Keywords: Land Surface Temperature, Mangrove, NDVI, NDSI, Sundarbans

1. INTRODUCTION

The Sundarbans is the world's largest coastal deltaic mangrove ecosystem and represents a susceptible area in terms of vulnerability to climatic change due to the intricate blend of estuarine and coastal environments (International Union for Conservation of Nature, 2010; Sievers et al., 2020). Moreover, the dynamic relationships between terrestrial and meteorological systems make them highly vulnerable to the effects of climate change. Plenty of previous research works have documented significant destruction of mangroves. Mitra et al. (2009) observed that the intensity of climate change's impact on the Sundarbans' mangrove forests exceeds the global average, i.e., 0.5 °C increase in surface temperature per decade. According to the U.N.'s Intergovernmental Panel on Climate Change (IPCC, 2013), the average global temperature is predicted to increase by up to 4.8° C by 2081–2100 relative to the 1986–2005 average. Over the past 30 years (1978-2008), the atmospheric temperature is estimated to have risen by 6.14 percent and 6.12 percent in the western and eastern sides of the Sundarbans, respectively. Both sides constitute an average annual increase of approximately 0.05°C yearly (Mitra et al., 2009). Increasing temperatures globally can result in a rise in sea levels (Thomas et al., 2014). A recent study estimates that the current rate of mangrove destruction globally is about 1-2% per year, especially due to rising sea levels (Alongi, 2015). The changing climate will likely generate more harsh effects, such as increased intensity and frequency of extreme floods, storm surges, and cyclones.

There are studies that have emphasised the ecological conditions of the Sundarbans using remote sensing and field data. Remote Sensing (RS) techniques have enhanced the capacity of researchers to provide a complete picture of inaccessible regions of the mangrove ecosystem. However, it is necessary to compare the satellite-derived spectral indices with the field measurements to accurately quantify and assess their ability to monitor and map the variables. In 2018, Deng et al. (2018) studied remote sensing combined with regression to analyse the impact of land-use change on Land Surface Temperature (LST) and Normalized Difference Vegetation Index (NDVI). Thakur et al. (2020) studied the impact of changing land use patterns on the LST and NDVI from 2000 to 2017 and found that the LST is an essential function of LULC. LST has been used mainly to show changes in temperature in urban areas. However, the LST application has recently broadened to include other areas, such as climate change on inland water bodies, crop management, water management, fire monitoring, and geological processes.

Several studies have examined the anthropogenic changes that are influencing different aspects of the Sundarbans' ecology, morphology, land use pattern (Ganguly et al., 2006; Hajra et al., 2017), mangrove loss (Mondal et al., 2018), and tidal channels (Ghosh et al., 2018) over the period. Soil salinity plays a vital role in defining the distribution of mangrove species in the Sundarbans. Soil salinization is also a root cause of soil degradation. The comprehensive literature review indicates limited studies evaluating salinity variation and its linkage with other image-based indicators in the Sundarban

regions. Analyzing the Normalized Difference Salinity Index (NDSI) with the soil electrical conductivity (EC) can provide a more substantial basis for updating the variations in salinity across inaccessible areas of the Sundarbans over time.

Improved documentation of ongoing changes in inhabited regions of the Sundarbans and a better understanding of the relationship between changes in soil salinity, soil electro-conductivity, land surface temperature vegetation, and similar environmental indicators will provide insights helpful in identifying ways to reduce future changes and improve the resilience of the Sundarbans' mangroves. The present research is intended to meet the primary objectives of 1) evaluating the broader ecosystem health in the Sundarbans through the spectral-based environmental indicators of mangroves, 2) enhancing the understanding of the spatial and temporal variations of spectral-based environmental indicators (i.e., NDVI, NDSI, and LST), and 3) examining the relationships between indicators (LST, NDSI, NDVI, soil EC) in Sundarbans mangroves.

2. STUDY AREA

Approximately 60% of the Sundarbans lie in Bangladesh, and the balance lies in India (Kundu et al., 2020) (Figure 1). The Sundarbans Biosphere Reserve (SBR) is segmented into a transition zone, a buffer zone, and a core zone. The Sundarbans landscape can be categorized by the different land features, i.e., sandy beaches, mud flats, coastal dunes, estuaries, creeks, inlets, and mangrove swamps. There are roughly 100 low-lying islands in the Indian part of the Sundarbans (the exact number varies over time due to the formation and inundation of smaller islands due to tidal flows and cyclones), and 50% are inhabited. These islands lie on marshy alluvial plains that undergo constant transformation due to siltation, flooding, cyclones, and tidal currents.

The Sundarbans experience a monsoon/rainy season with moderate temperatures throughout the year due to their proximity to the Bay of Bengal and the Indian Ocean. The Sundarbans suffer from frequent storms (cyclones or tropical depressions) between mid-March and November; major cyclones have caused extensive damage to the area (Kar et al., 2015).

Agriculture and fishing are principal sources of livelihood for households in this low-lying region. The mangrove forests of the Sundarbans also play an essential role in the livelihoods of households, such as fishing, logging, and gathering other resources for sale (e.g., honey and beeswax, Keora fruits, medicinal plants). In recent years, tourism has grown in the Sundarbans, providing residents with new opportunities to improve their livelihoods and raise their economic status. These activities, as well as the construction of water management infrastructure in the upstream regions, have profoundly affected water flow and the health of the mangroves in the Sundarbans, especially in the western area of the Indian Sundarbans (Rahman et al., 2011).

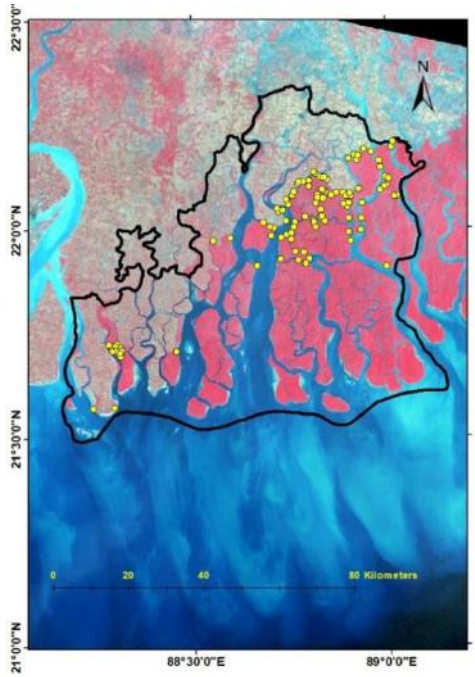

Figure 1. Delineation of the study area (Indian Sundarbans) and distribution of soil sampling sites

3. DATA AND METHODOLOGY

The primary data sources were optical satellite images from Landsat MSS, TM, and OLI sensors. Images were used to define and characterize mangrove areas and to record environmental indicators and their change in the Sundarbans. The spectral indices such as NDVI, NDSI, and LST were estimated for 1972, 1995, 2019, and 2022. In addition, soil samples were collected, and the EC of the soils was analysed. Garmin GPS, with an accuracy of ±5 meters, was used to geo-locate places where soil samples were collected. Subsequently, the statistical interpretation based on the Coefficient of Determination was calculated among the spectral indices and EC variables. Besides that, spatial and temporal variations in the spectral indices were also analysed simultaneously. A brief methodological flowchart is provided in Figure 2. Detailed methodology is discussed in the following sub-sections.

3.1 Satellite Data and Spectral Indicators

The Landsat series images such as MSS, TM, and OLI were obtained (tiff format) from the United States Geological Survey (USGS) Global Visualization Viewer (GLOVIS) website (Table 1). Erdas Imagine (version 9) and ArcMap (version 10) were used for image processing, spatial database creation, and data analyses. Images covered by water were excluded from the analysis. Spectral radiance values were used to retrieve land surface temperatures from Landsat TM 5, OLI 8, and OLI 9. The LST was extracted from the thermal band using band 6 of Landsat TM and bands 10 and 11 of Landsat 8 and 9.

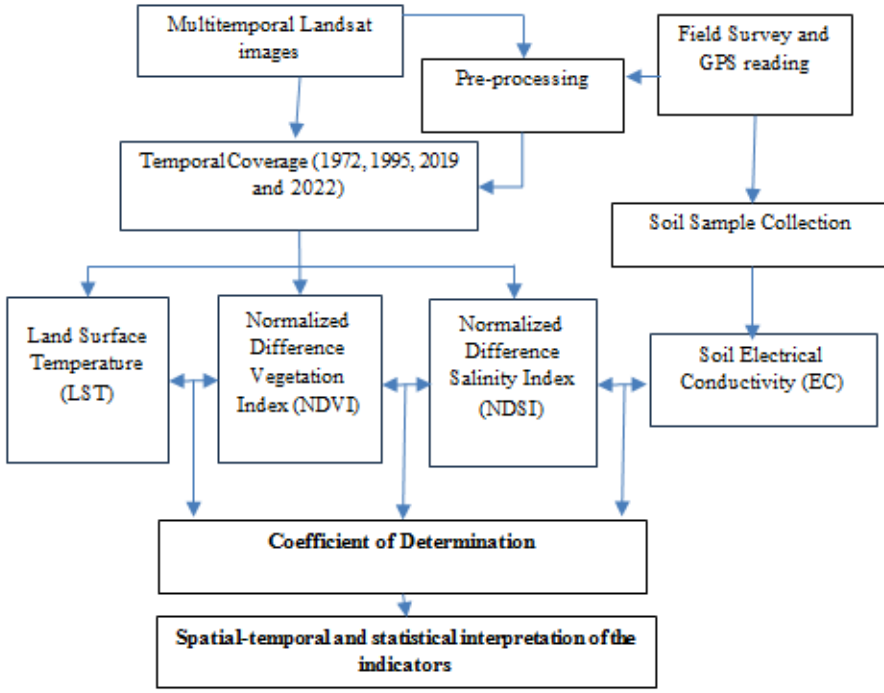

Figure 2. Methodological Flowchart

Table 1. Details of optical satellite images used in this study

DATA	BANDS	SENSOR (LANDSAT)	DATA FORMAT	ACQUISITION DATE	PATH ROW	SPATIAL RESOLUTION
Landsat 1	4	MSS	GEOTIFF	1972-11-05	P148/r45	60 m
Landsat 5	7	TM	GEOTIFF	1995-01-28	P138/r45	30 m
Landsat 8	11	OLI	GEOTIFF	2019-01-30	P138/r45	30 m
Landsat 9	11	OLI	GEOTIFF	2022-12-16	P138/r45	30 m

3.1.1 Generating Spectral Indicators: NDVI, NDSI, and LST

The Normalized Difference Vegetation Index was calculated using data from the Landsat Series according to Equation 1. The NDVI index is based on remotely sensed differences between vegetation's reflectance and absorption bands. High positive NDVI values (near +1) indicate healthy vegetation, while the lowest values (near zero) indicate a lack of vegetation. The steps mentioned in Jeevalaxhmi (2017) were followed to extract NDVI from the satellite images.

$$\boldsymbol{NDVI} = (\boldsymbol{NIR} - \boldsymbol{R})/(\boldsymbol{NIR} + \boldsymbol{R}) \quad (1)$$

Where NIR = Near Infrared band, R = Red band.

The spectral soil reflectance is influenced by the physical and chemical properties of the soil (e.g., types of salt found in the soil as well as levels of soil moisture, colour, and surface texture) and is well captured by the NIR region of the electromagnetic spectrum. The Normalized Difference Salinity Index (NDSI) is commonly used to record soil salinity fluctuations spatially and temporally; Landsat images (1972, 1995, 2019, and 2022) were used to derive the spectral-based salinity index based on Equation 2. NDSI values range between -1 to +1, where higher values indicate higher salinity.

$$\boldsymbol{NDSI} = (\boldsymbol{R} - \boldsymbol{NIR})/(\boldsymbol{R} + \boldsymbol{NIR}) \quad (2)$$

Where NIR = Near Infrared band, R = Red band.

Estimates of land surface temperatures were derived from geometrically corrected Landsat TM and OLI images. The split window method and the spectral radiance model were used to retrieve surface temperature using the thermal bands of Landsat images. The estimation of land surface emissivity (LSE) is also required to estimate LST since LSE is a proportionality factor that scales the black body radiance (Plank's law) to measure emitted radiance. Therefore, the NDVI threshold method was used to estimate the emissivity of different land covers, as suggested by Jeevalaxhmi (2017). Finally, LST was retrieved using Equation 3.

$$\boldsymbol{LST=[BT/(1+(\lambda*BT/\rho))*ln(\varepsilon)]} \quad (3)$$

where LST is in Celsius (C), *BT* is at-sensor brightness temperature (in C), λ is the average wavelength of thermal bands, ρ is ($h*(c/\sigma)$, which is equal to 1.438 x 10^{-2} meter Kelvin, σ is the Boltzmann constant (1.38 x 10^{-23} Joule per Kelvin), h is Plank's constant (6.626 x 10^{-34}), c is the velocity of light (3 x 10^{8} meters/second) and $\boldsymbol{\varepsilon}$ is the spectral surface emissivity (Jeevalaxhmi, 2017).

3.2 Ground-based Soil Salinity Measurements

One hundred soil samples were collected from different sites in the Sundarbans to validate the accuracy of NDSI estimates (Figure 1). A stratified random sampling technique was used to gather at least one soil sample from each accessible island in the broader Sundarbans area. Due to a legal prohibition on visitor access, soil samples could not be collected from the core area of the Sundarbans Biosphere Reserve. The soil samples were collected intermittently from December 2018 to March 2020. Soil samples were dried, crushed, and sieved through a 2 mm sieve. The electrical conductivity of each piece was measured using an auto-digital conductivity meter.

3.3 Statistical Metrics and Model Validation

The pixel level NDSI-2019 values were compared with soil EC measurements. In the present study, the validation was carried out with the EC values obtained from the

available soil sample locations. This cross-validation provides greater confidence in using remotely sensed-based NDSI to understand salinity in the Sundarbans. The relationships between pairs of environmental indicators were plotted in scatter diagrams and characterized based on linear regression estimates. The coefficient of determination (R^2) for these estimates were also calculated with P values at < 0.05 to test the statistical significance of the variables.

4. RESULTS AND DISCUSSION

The various estimated remote sensing-based environmental indicators provide different perspectives for understanding the past and current states of mangrove forests in the Sundarbans. The indices extracted from the study play an essential role in exhibiting the fluctuations of the Sundarbans in response to anthropogenic and environmental changes. Field observations in the intertidal zone of the Sundarbans are often difficult due to frequent inundations. Thus, the study used a satellite imaged-based spectral approach for a better interpretation of the dynamics in the Sundarbans.

4.1 Spatio-temporal Trends in NDVI and LST Estimates

NDVI is one of the most widely used indicators for differentiating vegetative cover from other land surfaces. Estimates of NDVI generated in this study (Figure 3) indicate that there is a decrease in vegetative cover between 1972 and 2022. The war that led to Bangladesh's independence from Pakistan in 1971 significantly increased the number of inhabitants in the Indian portion of the Sundarbans due to the influx of refugees from former East Bengal. According to the Census of India 2011, the population in the broader Sundarbans area increased from roughly 2 million in 1971 to 4.4 million in 2011. The rising population was associated with an increase in the Sundarbans' deforestation rate. During the 1980s, the Government of India enacted laws to protect the forests and restrict human activity in the core and buffer zones of the Sundarbans Biosphere Reserve (Ghosh et al., 2015). Government intervention has imposed limited human activity in the Sundarbans' core and buffer zones. However, despite increased population density since 1971, the extent of SBR has remained more stable.

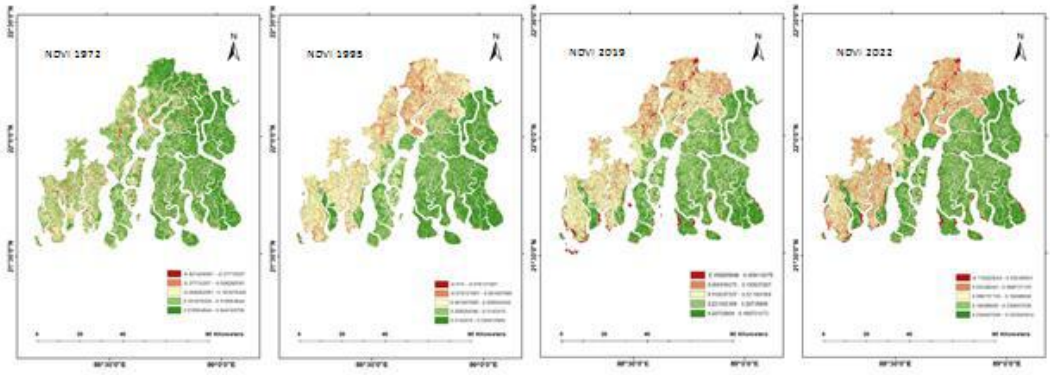

Figure 3. NDVI of 1972, 1995, 2019, and 2022 in the Indian Sundarbans

The deterioration of the vegetation health is often associated with frequent and prolonged saline water inundation. The maximum value recorded for the NDVI (0.84) was observed in 1972 and declined to 0.56 in 1995, 0.48 in 2019, and 0.35 in 2022. The decline suggests the loss of dense and healthy mangrove forests. The mean NDVI decreased from 0.23 to 0.14 during this same period.

The relationship between LST and NDVI suggests that declines in surface vegetation cover have been associated with rises in land surface temperature. Areas covered by mangroves showed considerably lower radiant temperatures than non-mangrove areas in 1995 and 2022 (Figure 4). Deforestation driven by increases in population and subsequent economic activity appears to have intensified recent temperature rises. According to the estimates, the maximum LST in the Sundarbans increased by 0.98 °C between 1995 and 2022. The average yearly increase in the maximum temperature observed from 1995-2022 is approximately 0.04° C.

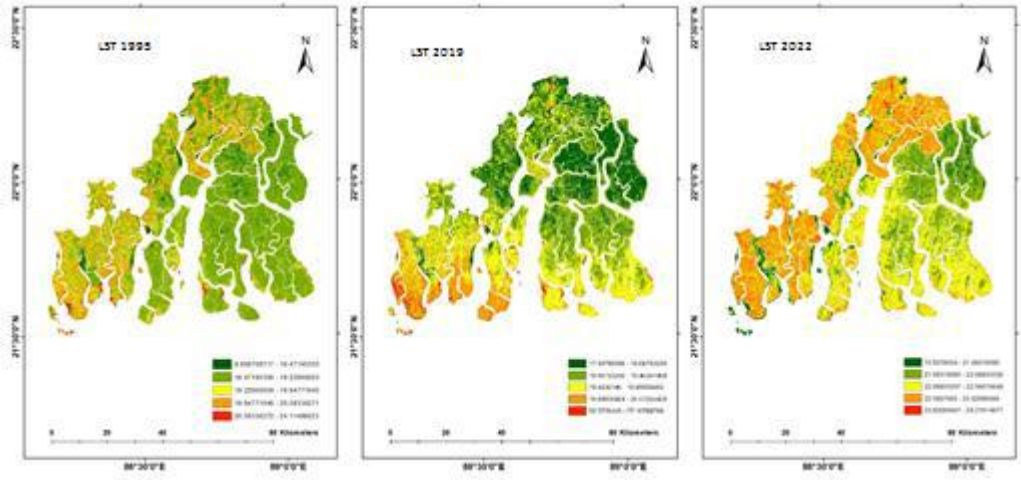

Figure 4. Land Surface Temperature in the Indian Sundarbans during 1995, 2019, and 2022

To understand variations in the increases in LST across the Sundarbans, we compared the differences between estimates made for Henry Island (located on the Southwest edge of the Sundarbans) and the *Burirdabri* area (in the Northeast portion, near the Bangladesh border) of the Indian Sundarbans. The estimated maximum LST in both *Henry Island* and *Burirdabri* show increasing trends, while NDVI estimates show a decreasing trend between 1995 and 2022. As shown in Figure 3, this is consistent with our finding that land without vegetation experienced more significant increases in surface temperatures, i.e., the eastern part of the Sundarbans is covered with relatively dense vegetation (mostly mangroves) compared with the western and southwestern parts.

Furthermore, Figure 5 exhibits that the two spots tracked in the southwestern islands of Sundarbans showed temperatures above 21°C in 1995. In 2019 and 2022, the south-central and northern parts of the island also exhibited a higher temperature (i.e., >21

°C). Hence, our study suggests that forest areas showed gradual and steadily increasing temperatures, suggesting that higher temperatures are not limited to human settlement areas. The reasons are the increased sea surface temperatures, the presence of sand/beach areas, and the degradation of healthy mangroves.

a) 1995

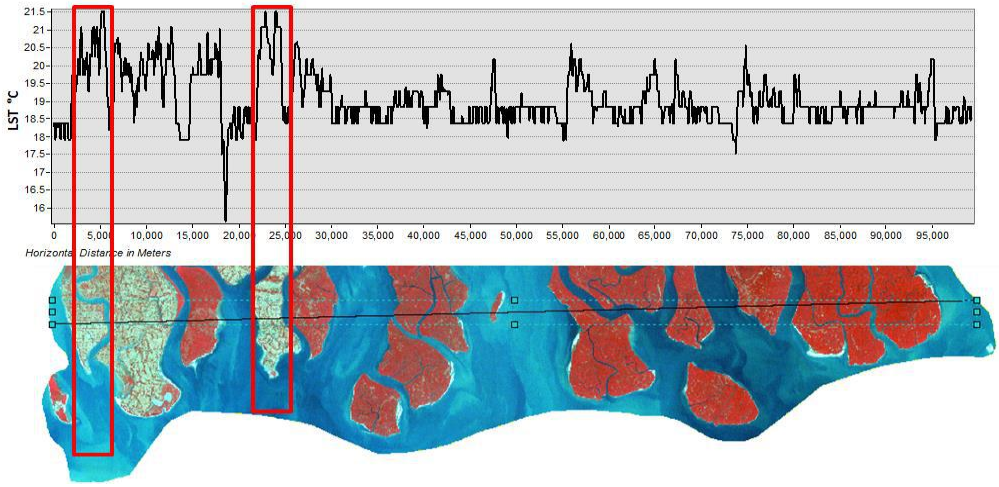

b) 2022

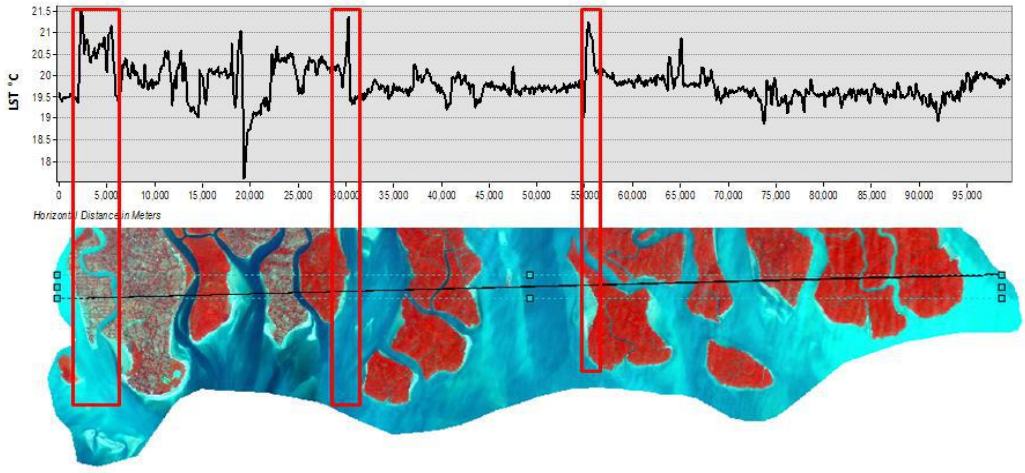

Figure 5. West–East Transect Profile of LST estimates a) 1995 and b) 2022 in the Sundarbans derived from Landsat Data

We generated scatterplots and calculated a regression estimate to examine the relationship between LST and NDVI. These also show that the two indicators are inversely related, both spatially and temporally. A single point change in NDVI is associated with a 3.48 °C decline in LST; the estimated R^2 was 0.267 (Figure 7).

Areas with vegetation frequently inundated by tidal flows display lower temperatures than areas with less vegetation. In comparison, upland areas lacking vegetation generally had higher temperatures. Forests adjacent to settlement zones showed higher temperature fluctuations compared to the interior, less populated parts of the Sundarbans. Estimates indicate that partially deforested islands, cultivated land, fallow lands, and human settlement areas tend to display more significant temperature fluctuations.

4.2 Relationship Between NDVI and NDSI

Salinity is essential in defining species' spatial distribution, assemblage, and density in deltaic mangrove forests. Most of the mangrove genera and families tend to be highly diversified. They have developed specific morphological, biological, physiological, and ecological characteristics that promote adaptability for thriving in the tidal environment (Giri et al., 2014). Soil salinity, present in excessive or insufficient quantities, is a limiting factor in determining the distribution and composition of mangrove species (Mitra et al., 2010). The NDSI is considered a good indicator for identifying salinity-stressed areas. However, relative to NDVI, NDSI is less widely used for mangrove studies. Since the highest salinity is reflected in water bodies, water bodies are removed from our estimates of NDSI. The findings are derived from the pixel values estimated from the islands' interior parts and lands affected by regular tidal flows.

Mangrove species that are highly tolerant of salinity are found in coastal tidal zones, while less tolerant species thrive in the interior parts of the islands. Less tidal water penetration and infrequent and less extreme seasonal inundation in the inland areas account for the lower soil salinity. High NDVI values (i.e., values near +1) indicate healthy vegetation, while NDSI (i.e., values near +1) indicate high salinity. NDSI reported in Figure 6 suggests that the various mangrove species regulate the salinity profile in densely forested areas. In contrast, the areas of greater human habitation display higher soil salinity levels, devastatingly affecting soil fertility and agricultural productivity. Orange- and red-tinted areas in Figure 6 indicate areas of high salinity corresponding to human settlement areas. These areas are concentrated in the northwest of the study area. Moreover, small pockets of highly saline soils are scattered across the Sundarbans and correspond to shallow, frequently inundated mangrove areas, where high evapotranspiration rates lead to high salinity.

Rising soil salinity will cause the agricultural areas to become unproductive, thus negatively affecting the economic conditions where most of the population depend on agriculture for their livelihoods. Moreover, blending sea water with the salty water found in mangrove swamps will have disastrous impacts on the health and biodiversity of the Sundarbans' mangroves. This study has found that the mean NDSI values increased from -0.24 in 1972, - 0.21 in 1995, to +0.17 in 2019, and + 0.19 in 2022 (Figure 6). Figure 7 suggests a moderate negative correlation between NDVI and NDSI values, suggesting that high salinity is inversely related to vegetation (with $R^2 = 0.533$ and p-value=0.43). Mangrove

species' spatial distribution and growth depend on the salinity profile at different topographical gradients. The relationship between estimated values of NDSI and NDVI varies spatially over the Sundarbans area (aside from the general relationship found in this study).

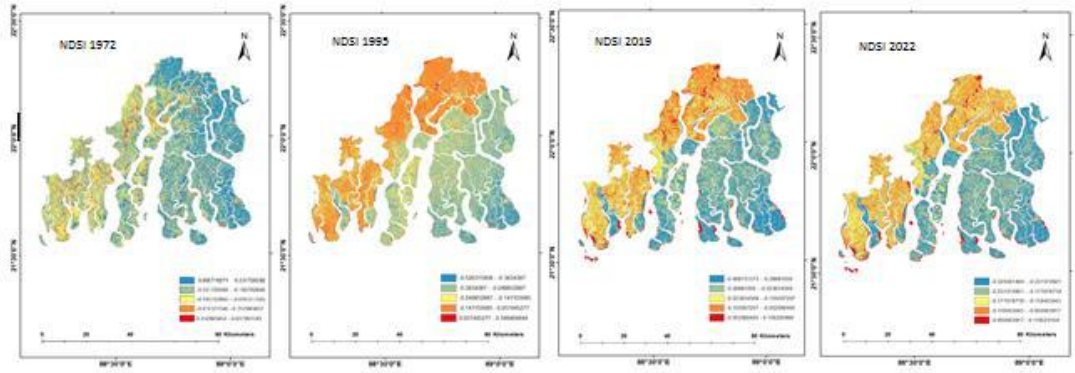

Figure 6. NDSI of 1972, 1995, 2019, and 2022 in the Sundarbans

4.3 Soil EC and NDSI Comparisons

In contrast to other tropical forests, where salt concentrations and variations are low, soil salinity in the deltaic zones fluctuates highly due to daily tidal activity and salt accumulation in the soil, producing a crucial salinity change that affects the spatial distribution of mangrove species. Joshi and Ghose (2003) showed that soil salinity tends to decrease from the tidal coast to the interior of the Lothian islands. The present study focuses on the analysis of soil salinity using both remote sensing techniques and conventionally measured soil EC.

EC offers a rapid, reliable, and easy measure of the number of dissolved ions (total dissolved species, TDS) in the soil solution (dS/m) and measures the ability of the water suspension to conduct electricity; higher salt concentrations to work more current (Corwin and Yemoto, 2017). EC and the total salt concentration of a soil solution are closely related by applying a simple conversion standard (depending on soil type). According to Sahana et al. (2020), the measured EC of the soil samples was highly correlated to the satellite-derived NDSI compared to other salinity indices. Abdul-Qadir et al. (2010) also found that the visible red band performs best among the Landsat bands for characterizing the pattern and features of soil salinity due to its high correlation with measured EC.

However, the accuracy of estimates declines when raster values are compared with corresponding ground location points where the topographical gradient varies significantly. It is likely because the exposed coastal areas subject to daily inundation of tidal flows are often misrepresented as water pixels in satellite imagery. This study overcame this challenge by comparing remote-sensed indicators to field data temporally and spatially. Field observations have potential uncertainties because sites that undergo daily inundation

are challenging to recognize in satellite imagery. In most cases, such areas appear as water pixels or bare mudflats with no vegetation.

The soil salinity was validated by comparing remote-sensed NDSI to measured soil EC. There is a high correlation between NDSI and measured EC of 0.601 (with p-value=0.00) (Figure 7). Our study's soil salinity measurements in coastal areas with daily inundated tidal flows found high soil salinity in remotely sensed data (NDSI). This was confirmed when compared to EC values from soil samples in the inhabited/accessible areas of the Sundarbans.

Based on the spatial location and distribution of EC points, corresponding values of NDSI (generated from Landsat 2019) were plotted on a scatter diagram (Figure 7). Regression of the NDSI and EC measures shows a moderately high positive trend (a one-point increase in NDSI is associated with a 20.7 MHOS/cm increase in EC) with an R^2 of 0.601 and p-value of 0.001. Two islands in the interior of the Sundarbans—*Panchmukhani* and *Khatuajuri,* showed higher values in measured EC (12.71, 13.91) and satellite-derived NDSI (0.38 and 0.30), respectively. The reason may be their interior location along tidal channels with minimum dilution with the freshwater from other creeks and channels.

4.4 Relationships Between Environmental Indicators

Our study found that there is a relationship between LST, NSDI and NDVI across the Sundarbans. In general, increasing soil salinity levels appear to directly alter the distribution and growth of mangrove species. Estimates of the statistical relationships between NDVI-NDSI, NDSI-EC and NDVI-LST explain such spatial variabilities of the mangrove ecosystem in the study area. Based on this study's estimated changes in vegetation, salinity, and temperature in recent decades, it is inferred that the mangrove forests in the Sundarbans are undergoing constant changes in terms of the composition of species due to rises in soil salinity and temperature, erratic rainfall, frequent flooding, and increasingly severe storms (Das et al., 2021). Overall, these changes are increasing the vulnerability of the Sundarbans. In the southwestern and northern portion of the study area, where human settlement is relatively dense, mangroves are relatively scarce, and vegetation is less dense. Proximity to human settlements and the degradation of mangrove forests due to anthropogenic activities likely contributed to the relatively high temperatures observed in these areas in 1995, 2019, and 2022. The discussions with the local respondents during the field visits confirmed that these locations were once densely forested and have now been converted to human settlements with intensive agricultural activity.

5. CONCLUSION

The remote sensing-based spectral analysis shows increased surface temperature and salinity over the period, while the vegetation cover decreased remarkably from 1972 to 1995. However, the net forested areas remained the same due to government policies, but the quality of the mangroves deteriorated over time. Overall, the spectral reflectance of

vegetation decreased by 6.19% from 1972-2022. The average surface temperature across the Sundarbans has increased by 14.9%, both in the human habitat and the mangrove zones. The salinity of the Sundarbans has also increased, and the abrupt increases in salinity have reduced the growth of less saline-resistant mangrove species, suggesting that salinity causes changes in species types and assemblage. The accelerating increase in salinity affects the spatial distribution of mangrove species along the topographical slope but not the density. The high salinity tolerant mangrove species tend to grow in the more frequently inundated newly formed islands spotted during our field survey. Moreover, the eustatic mean sea level and the frequency of storms and cyclones have increased the severity of saltwater intrusions in low-lying arable coastal parts of the Sundarbans. These factors will not only affect the distribution of mangrove species but also cause land degradation of low-lying inundation lands due to increased salinity, compromising agricultural productivity and the livelihoods of the local inhabitants.

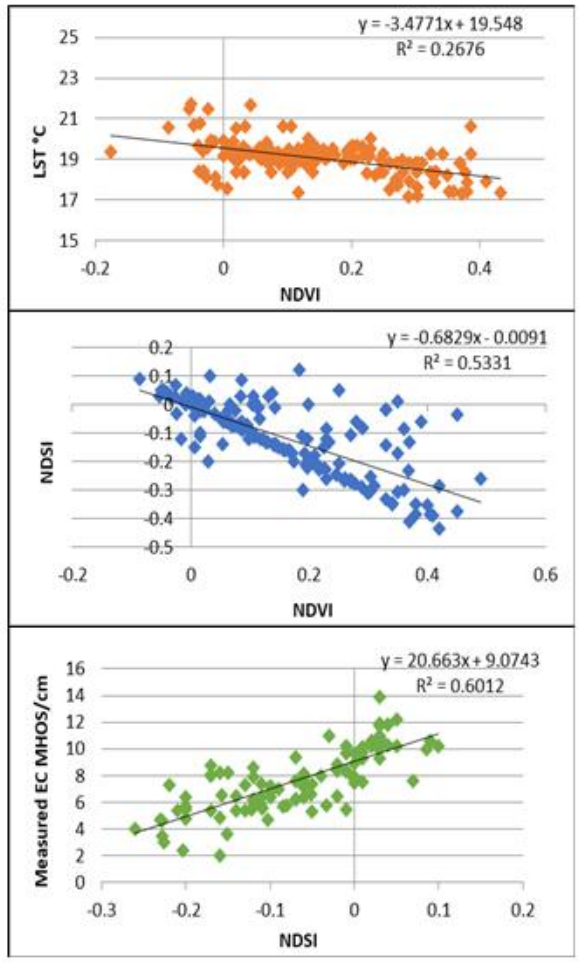

Figure 7. Scatter plots showing the relationship between spectral indices (i) NDVI-LST (ii) NDVI- NDSI (iii) NDSI-Measured EC

Our study found that the NDSI retrieved from Landsat was consistent with the EC values measured from the soil samples. Hence, NDSI can be used to replicate EC in other coastal areas where changes in salinity play an essential role in shaping local vegetation and its impact on livelihood. Given the importance of the Sundarbans mangrove ecosystem and the rising risks to mangrove survival and health, this study highlights the areas of rising temperatures (LST), increased salinity (NDSI), and decreased vegetative cover (NDVI) for implementing corrective measures to preserve and protect this important World Heritage site.

Acknowledgement

We are grateful to all the officials of the Sundarbans Biosphere Reserve for permitting us to collect the soil samples from Sajnekhali Wildlife Sanctuary and Buffer zone. We also wish to thank the Indian Statistical Institute for its constant encouragement and necessary support.

REFERENCES

1. Abdul-Qadir, A.M., Benni, T.J., (2010). Monitoring and evaluation of soil salinity in terms of spectral response using Landsat images and GIS in Mesopotamian plain Iraq. *Journal of Iraqi Desert Studies* 2, 19–32. ISSN: 1994-7801.
2. Alongi, D. M., (2015). The Impact of Climate Change on Mangrove Forests. *Current Climate Change Report*, 1 (30–39). DOI 10.1007/s40641-015-0002-x.
3. Corwin, D., Yemoto, K., (2017). Salinity: Electrical Conductivity and Total Dissolved Solids. *Methods of Soil Analysis* 2: 1-16. DOI: 10.2136/msa2015.0039.
4. Das, P., Banik, P. Rath, K.C. and Edmond, C., (2021). Precipitation extremes and anomalies of the Indian Sundarban 1984-2018. *MAUSAM*. 72, (847–858). DOI: https://doi.org/10.54302/mausam.v72i4.3552
5. Deng, Y., Wang, S., Bai, X., Tian, Y., Qian, Q., (2018). Relationship among land surface temperature and LUCC, NDVI in typical Karst area. *Scientific Reports* 8 1-12. DOI:10.1038/s41598-017-19088-x.
6. Ganguly, D., Mukhopadhyay, A., Pandey, R. K., and Mitra, D., (2006). Geomorphological study of Sundarban deltaic estuary. *Journal of the Indian Society of Remote Sensing*, 34(4), 431-435. https://doi.org/10.1007/BF02990928
7. Ghosh, M. K., Kumar, L., and Langat, P. K., (2018). Mapping tidal channel dynamics in the Sundarbans, Bangladesh, between 1974 and 2017, and implications for the sustainability of the Sundarbans mangrove forest. *Environmental Monitoring and Assessment*, 190(10), 582. DOI: 10.1007/s10661-018-6944-4
8. Ghosh, A., Schmidt, S., Fickert, T., and Nüsser, M., (2015). The Indian Sundarban mangrove forests: history, utilization, conservation strategies, and local perception. *Diversity*, 7(2), 149-169. doi:10.3390/d7020149.
9. Giri, S., Mukhopadhyay, A., Hazra, S., Mukherjee, S., Roy, D., Ghosh, S., and Mitra, D., (2014). A study on abundance and distribution of mangrove species in Indian Sundarban using remote sensing technique. *Journal of Coastal Conservation*, 18(4), 359-367. DOI 10.1007/s11852-014-0322-3.

10. Hajra, R., Ghosh, A., and Ghosh, T., (2017). Comparative assessment of morphological and land use/landcover change pattern of Sagar, Ghoramara, and Mousani island of Indian Sundarban delta through remote sensing. *Environment and Earth Observation* (pp. 153-172). Springer, Cham. DOI:10.1007/978-3-319-46010-9_11
11. Intergovernmental Panel on Climate Change (IPCC), (2013). Climate Change (2013): The Physical Science Basis. Contribution of Working Group I to the Fifth Assessment Report of the Intergovernmental Panel on Climate Change. Cambridge University Press, Cambridge, United Kingdom and New York, NY, USA, p.1535.
12. International Union for Conservation of Nature, (2010). Mangrove forests in worldwide decline, https://www.iucn.org/content/mangrove-forests-worldwide-decline (accessed DATE).
13. Jeevalaxhmi, D., Reddy, S.N., Manikiam, B., (2017). Land Surface Temperature Retrieval from LANDSAT data using Emissivity Estimation. *International Journal of Applied Engineering Research*, 12 (9679-9687).
14. Joshi, H., Ghose, M., (2003). Forest structure and species distribution along soil salinity and pH gradient in mangrove swamps of the Sundarbans. *Tropical Ecology* 44 (197-206).
15. Kar, N. S., and Bandyopadhyay, S., (2015). Tropical storm Aila in Gosaba block of Indian Sundarban: remote sensing-based assessment of impact and recovery. *Geography Review India*, 77(1), 40-54.
16. Kundu, K., Halder, P., and Mandal, J. K., (2020). Forest Cover Change Analysis in Sundarban Delta Using Remote Sensing Data and GIS. *In Intelligent Computing Paradigm: Recent Trends (pp. 85-101). Springer*, Singapore. https://doi.org/10.1007/978-981-13-7334-3_7.
17. Mallick, J., Kant, Y., Bharath, B.D., (2008). Estimation of Land Surface Temperature over Delhi Using Landsat-7 ETM+. *The Journal of Indian Geophysical Union*, 12 (131-140).
18. Mitra, A., Gangopadhyay, A., Dube, A., Schmidt, A., Banerjee, K., (2009). Observed changes in water mass properties in the Indian Sundarbans northwestern Bay of Bengal during 1980–2007. *Current Science* 971445–1452.
19. Mitra, D., and Karmaker, S. (2010). Mangrove Classification in Sundarban using High Resolution Multispectral Remote Sensing Data and GIS. *Asian Journal of Environment and Disaster Management*, 2(2). doi:10.3850/S179392402010000268.
20. Mondal, B., and Saha, A. K., (2018, June). Spatio-Temporal Analysis of Mangrove Loss in Vulnerable Islands of Sundarban World Heritage Site, India. In *The Annual International Conference on Geographic Information Science* (pp. 93-109). Springer, Cham.
21. Rahman, A. F., Dragoni, D., and El-Masri, B., (2011). Response of the Sundarbans coastline to sea level rise and decreased sediment flow: A remote sensing assessment. *Remote Sensing of Environment*, 115(12), 3121-3128. doi: 10.1016/j.rse.2011.06.019.
22. Sahana, M., Rehman, S., Patel, P. P., Dou, J., Hong, H., and Sajjad, H., (2020). Assessing the degree of soil salinity in the Indian Sundarban Biosphere Reserve using measured soil electrical conductivity and remote sensing data–derived salinity indices.

Arabian Journal of Geosciences, 13(24), 1-15. https://doi.org/10.1007/s12517-020-06310-w /.

23. Sievers, M., Chowdhury, M. R., Adame, M. F., Bhadury, P., Bhargava, R., Buelow, C., ... and Connolly, R. M., (2020). Indian Sundarbans mangrove forest considered endangered under Red List of Ecosystems, but there is cause for optimism. *Biological Conservation*, 251, 108751.
24. Thomas, J. V., Arunachalam, A., Jaiswal, R. K., Diwakar, P. G., and Kiran, B., (2014). Dynamic land use and coastline changes in active estuarine regions-a study of Sundarban delta. *The International Archives of Photogrammetry, Remote Sensing and Spatial Information Sciences*, 40(8), 133. doi:10.5194/isprsarchives-XL-8-133-2014.
25. Thakur, S., Maity, D., Mondal, I. *et al.* Assessment of changes in land use, land cover, and land surface temperature in the mangrove forest of Sundarbans, northeast coast of India. *Environ Dev Sustain* **23**, 1917–1943 (2021). https://doi.org/10.1007/s10668-020-00656-7

The Indian Geographical Journal
Volume 98 (1) June - 2023, pp 17-33
ISSN 0019-4824

CHANNEL MIGRATION AND INFLUENCING HYDROGEOMORPHIC ATTRIBUTES OF KULSI RIVER, NORTH EAST INDIA

G. Thakuriah[1] G. Sonowal[2]

[1] Department of Geography, Cotton University, Guwahati-781001
[2] Department of Geography, Darrang College, Tezpur, Assam

Corresponding Author: gulapsonowal15@gmail.com

Abstract

Morphological change over time in a river system is a natural process. The channel shifting mainly occurred due to weak geology, unusual stream discharge, intense meandering river bed, soil properties, land use, and involvement of human activities. The Kulsi River is a south-bank tributary of the Brahmaputra River. The river is well recognised for high discharge, sediment supply, and channel diversion. Therefore, the paper aims to study the channel migration pattern and its influencing attributes. Satellite images are used to identify the spatio-temporal changes in the course of the channel. The digitisation of the river channel is done in the GIS platform (ArcGIS 10.6), and the channel morphology of different periods is overlayed to find out the rate of magnitude and shifting of the river course from 1972 to 2018 at the five-year interval. The secondary data are collected from authentic governmental sources and publications for the preparation of base layers. The data on channel hydraulics are collected from the field surveys at eight channel shifting locations. The study noted that about 11 km away from the Ukiam, the river was suddenly shifted to the west in 1995 for about 1 km from its earlier path in the easterly direction. The longitudinal profile and sinuosity index show that the upper course of the catchment area is incised with more soil erosion and sediment supply to foothills near the Ukiam, where the river drifts to the west from the eastern direction in early 1990. The results help devise plans to mitigate flood hazards in the Kulsi River.

Keywords: Channel avulsion, Morphodynamics, Hydro-geomorphology, Remote sensing, GIS

1. INTRODUCTION

River morphology is unpredictable and dynamic in varying environmental landscapes over both spatio-temporal scales. An avulsion is a process by which flow is diverted from the parent channel into a new course in the floodplain (Sonowal et al., 2022). A local avulsion forms a new channel that joins its parent channel downstream (Heller and Paola, 1996). The channel hydro-geomorphic factors such as natural bank geometry (e.g. meander wavelength, meander length, the radius of curvature, amplitude, channel width arc

angle, and sinuosity), land use pattern, geologic structure, sedimentation, precipitation, bank erosion, discharges of various frequencies, vertical and horizontal heterogeneity of floodplain soils and distribution of riparian vegetation are some accountable factors for channel migration (Brice, 1982; Motta et al., 2012). Channel diversion mainly occurs within the floodplain region, and bank erosion is held because of lateral shifting of the course. Usually, it is a natural process, but with the age of time, it becomes semi-natural because of human intervention. Changing channel courses creates havoc on the physical and cultural landscapes. Sometimes, many people lose their household activities, agriculture fields, and substructures due to river migration and associated fluvial hazards. It is variable - some changes are gradual and unnoticeable, while others depend upon phenomena like extreme floods and droughts.

River abandonment to form a new channel at a lower elevation creates instability in the channel courses notably in the Mississippi in the United States (Fisk, 1947), the Kosi in India (Gole & Chitale, 1966), the Meander in Anatolia (Russell, 1954), the Saskatchewan in Canada (Smith & Perez-Arlucea, 1994), the Thomson in Australia (Brizga & Finlayson, 1990), and the Okavango in Africa (McCarthy at al., 1992). The experimental study of avulsion frequency and deposition rate (Bryant et al., 1995), along with the interpretation of geological records, shows that channel avulsion can result from high peak discharges, sediment accretion, tectonic upliftment, and channel jamming through the exogenous process (Jones & Schum, 1999). In India, the braided Koshi River stands out among the other rivers because of the high frequency of channel avulsion and other morphological changes, such as channel migration and channel width adjustment (Baniya et al., 2023). The Koshi River is one of the world's highest silt-yielding rivers, with an estimated annual sediment yield of 2.2 × 10 5 t/year (Baniya et al., 2023). Sinuous to meandering channel patterns are common in floodplains in the Koshi River course. A similar channel pattern is identified in the Kulsi River course because of the river's behaviour. The river experiences lateral shifting from the foothills of Meghalaya up to the floodplain region of the Brahmaputra. Every year, the Kulsi River causes a significant loss to the physical and cultural landscape near the bank of the river. Because of high discharge, the river raises its water level and submerges villages as well as hectares of productive land near the bank of the river annually. Besides, the region faces tremendous economic loss due to flood and lateral channel migrations. Another significant fluvial-geomorphic aspect of the Kulsi River is that it tends to form sand deposits due to high discharge. The river experienced a shifting at varied local scales after flowing into the foothills and the channels rejoining further downstream.

Geographical Information System (GIS) and multi-temporal satellite images are the most sophisticated tools to identify spatio-temporal river course changes (Hassan et al., 2017). The high-resolution images give accurate data for evaluating the trend of river shifting (Mohamad et al., 2018). This will be helpful for the assessment of the vulnerability of communities living on the floodplains. (Sonowal et al., 2022). The geospatial method has been applied in many world regimes and has proven effective in river course change

analysis (Petropoulos et al., 2015). Therefore, the paper uses remote sensing and GIS techniques to identify channel migration, its intensity, and the influence of hydro-geomorphic channel migration indicators in the Kulsi River.

2. STUDY AREA

The Kulsi River originates from the Meghalaya Plateau in Meghalaya, known as the Khri River, at an altitude of 1700 m above mean sea level. The tributaries like Um Krisinya, Um Siri, and Um Ngi confluence with the Khri River at Ukiam. After reaching the alluvial plain of Assam, it is known as Kulsi. Umkrisinya, Um Siri, and Um Ngi, Boko, Singra, Singua, Deosila are left bank tributary of Kulsi River. Batha and Umshru are the tributaries on the right bank (Thakuriah, 2023b). The Kulsi drains about 4,111.81 km^2 of geographical area on the southern bank of the Brahmaputra. Out of which about 1,956 km^2 area drains over Kamrup rural and Goalpara districts of Assam (India) within the geographical extension from 25˚31' 58.8" N to 26˚75' 3.33" N latitude and from 91˚E to 91˚48' 30" E longitude (Figure 1).

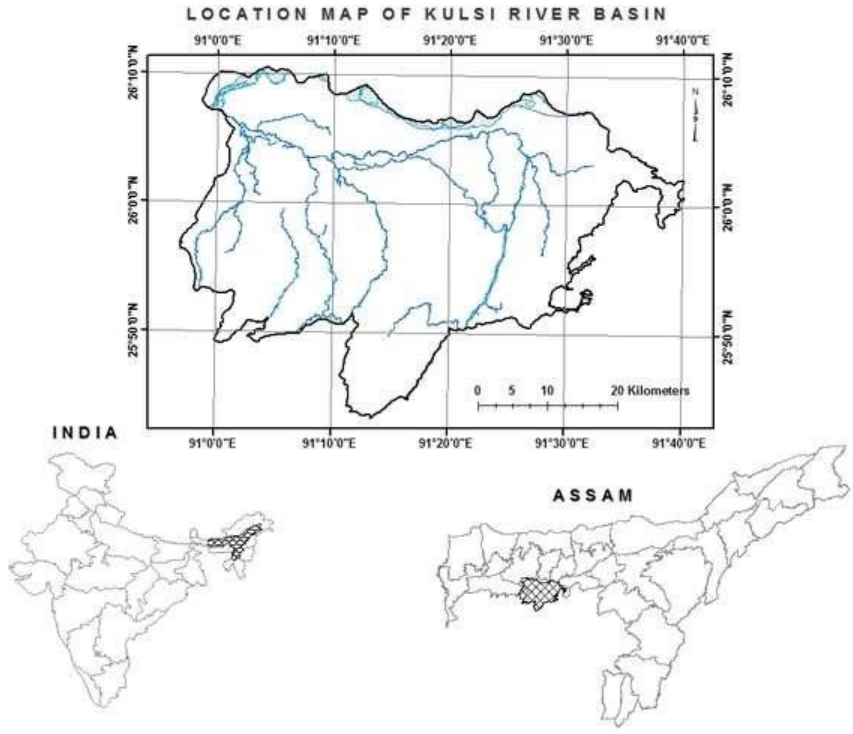

Figure 1: Location map of Kulsi River Basin

Structurally, the upper catchments area belongs to the age of Proterozoic with Assam-Meghalaya Gneissic complex with migmatite/banded Gneiss lithologic structure. The downstream belongs to the geological age of Meghalayan during the Barpeta-I

formation with white to greyish sand, silt, pebble, and clay lithologic structure (Thakuriah, 2023a). In upper reach, the Kulsi flow over four microtectonic fault lines. From the river source to the confluence to the Brahmaputra, the river has a more expansive valley due to bed sedimentation and frequent channel diversion due to flood discharges (Thakuriah, 2023c). The channel morphology includes level to nearly level sloping (0º-1º) in plain and steeps (15º-30º) in the upper catchment. The Kulsi River flows over fine to fine-loamy soil in the catchment and coarse-silty soil texture near the confluence. The section of the downstream is covered mainly by young alluvium. Soil gets easily erodible during the high discharge or heavy precipitation in the Kulsi river basin. At the same time, the soil characteristics of the upper reach from Ukium to Chandubi outlet covered a fine texture and steep morphology with moderately steep sloping (15o-30o), and thus, extreme soil drain conditions existed. From Chandubi Lake outlet to Kulsi bifurcated point, it covers fine-loamy soil texture and undulating morphology with a moderately sloping surface (8o-15o) and has well soil drainage (Thakuriah, 2023c). The Kulsi River basin is characterised by a southwest monsoon with maximum rainfall from May to September and minimum rainfall during the winter. The average annual rainfall of Boko station in the Kulsi river basin was 1,796 mm from 1993 to 2018. The average gauge discharge of the Kulsi River at Kukurmara station was recorded at 61.80 cumecs during 1991-2018. During this period, the highest average annual discharge was recorded at 99.78 cumecs in 2014 (Thakuriah, 2023b).

3. DATABASE AND METHODOLOGY

3.1 Database

The Kulsi River basin is delineated from the Survey of India topographical sheets No: 78 N/4, 78 N/8, 78 O/1, 78 O/2, 78 O/5, 78 O/6, 78 O/9, 78 O/10, and 78 O/14 at 1: 50,000 scale. Multi-temporal Landsat satellite data and IRS LISS IV data for the years 1972, 1977, 1988, 1995, 2001, 2006, 2011, and 2018 were used to understand the dynamic nature of the Kulsi River. The details of the satellite image are mentioned below in Table 1.

Table 1: Details of satellite images used in the study

Sensor	Date of acquisition	Bands used	Resolution
MSS	22 Nov 1972	MTL	60 m
MSS	24 Dec 1977	MTL	60 m
MSS	19 Feb 1988	4,3,2	60 m
MSS	26 Mar 1995	4,3,2	30 m
ETM+	15 Dec 2001	4,3,2	30 m
LISS IV	20 Mar2006	2,3,4	5 m
OLI and TIRS	06 Mar 2011	5,4,3	30 m
LISS IV	19 Feb 2018	2,3,4	5 m

To understand the flow characteristics of the river, the fluvial and geomorphic databases are collected from the field from the point of Ukium to Nagarbera, where it joins

the Brahmaputra River. We have also used secondary databases, especially the soil map, the geological map at the scale of 1:50,000 from the Geological Survey of India, rainfall data from the Indian Meteorological Department, Guwahati (Borjhor) and Regional Sericulture Research Station (RSRS), Boko, and discharge data from Central Water Commission, Shillong in order to know their role in lateral channel migration.

3.2 Channel Migration Assessment

To identify the spatio-temporal migration of the Kulsi River, the satellite images were projected with the coordinate system of WGS 1984 UTM Zone 46N. The dynamic nature of the Kulsi River courses over different years was digitised and analysed in ArcGIS 10.6 software. The morphometric parameters like longitudinal profile, sinuosity index, channel gradient and channel slopes are computed using the SOI toposheets at a scale of 1:50,000 and contour interval of 20 m.

Longitudinal Profile: The longitudinal profile is the natural law of the river and depends on the length and gradient of the channel from the source to the outlet point. The river carries the materials from the source and starts depositing the materials where the river finds the equilibrium point (Mackin, 1948). The longitudinal profile helps to identify the equilibrium state of the river. The profile waning takes place gradually depending on the nature of the topography, tectonic activity, geologic structure, sediment transport, flow resistance, discharge, depth and width. The longitudinal profile helps to measure channel slope, channel gradient, and stream length gradient index (SL). In this study, these parameters were calculated with the help of digitised contours from the SOI toposheets at 20 m contour intervals.

Channel gradient, $G = \frac{VD}{HD}$

Where, VD is the vertical drop of the slope and HD is the horizontal space of the slope.

Stream length gradient index, $SL = \Delta H \times \frac{L}{\Delta L}$

Where, ΔH is the change in elevation of the reach, L is the total stream length from the source to the reach of interest, ΔL is the length of the reach (Hack, 1973).

Sinuosity Index: The sinuosity index defines the channel pattern of a drainage basin. It is a major morphometric factor that affects the topography characteristics of the river course. According to Brice (1982), the sinuosity index is the ratio of the length of the channel to the length of the meander belt axis. The sinuosity pattern of the channel is analysed in the ArcGIS platform by applying the following formula Brice (1982).

S.I = $\frac{CL}{MB}$

Where, CL is the length of the channel and MB is the length of the meander belt axis

Hydraulic Attributes: Cross-sectional channel characteristics and flow characteristics of river channels were analysed through cross-sectional channel geometry, especially the channel width, depth, velocity, and discharge. From the point of Ukium to Nagarbera, eight cross-sectional hydraulic attributes were collected during the pre-monsoon season of 2019-2020 using wooden boats on the river course. The width, depth, and velocity are measured for each cross-section. A cup meter is used to measure the depth water velocity of each cross-section, and the surface velocity of water is read through the floating method. Spatial information of each cross-section, especially location and height, was collected from the field using handheld GPS. Figure 2 shows the location of the sample cross-sections at different channel diversion sites from the Ukium to Nagarbera.

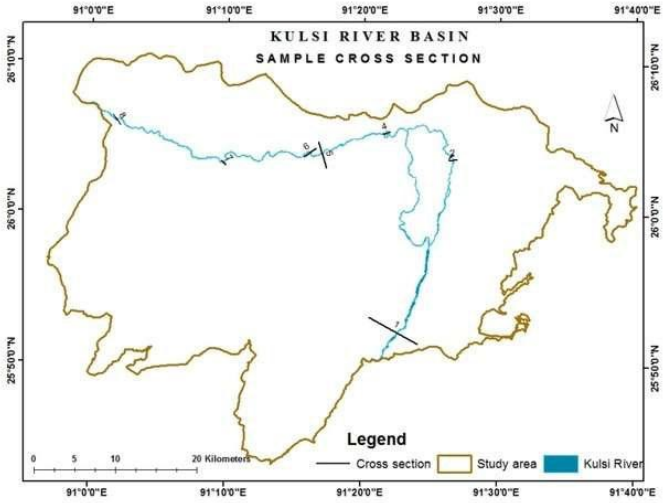

Figure 2: Location of the cross-sections at different channel migration sites from Ukium to Nagarbera

4 RESULTS

4.1 Morphological Changes in Kulsi River

To analyse the dynamic nature of the river, we have used the different years of a satellite image at the intervals of 5 years, i.e. 1972, 1977, 1988, 1995, 2001, 2006, 2011, and 2018. Kulsi River is more sinuous at the river's former course, creating channel bars. The multi-temporal satellite images show that the river's course underwent drastic changes after the 1990's. The 1972, 1977, and 1988 images show the river meandering through Langkher, Baregaon No.2, and Bherveri village. However, from 1990 to 1995, the river completely abandoned its old course and started flowing through the new course through the Pantan village. The detailed measurement of Lower Kulsi River channel diversion at some selected cross-sections is shown in Table 2. The year 1972 is taken as the base year, and at the interval of 5 years, the changes are shown up to 2018.

Table 2: Extent of cross-sectional channel changes at selected points across river Kulsi

Cross Section	1972-1977		1977-1988		1988-1995		1995-2001		2001-2006		2006-2011		2011-2018	
	R (Km)	L (Km)	R (Km)	L (Km)	R (Km)	L (Km)	R (Km)	L (Km)	R (Km)	L (Km)	R (Km)	L (Km)	R (Km)	L (Km)
A-A1				0.04w		**1.031w**		0.08w	0.018e	0.005w			0.011w	0.010w
B-B2			- 0.05w	-0.02e 0.79w	- 0.03w	-0.01e **0.792w**	0 0.03w	0		0.03w			- 0.008w	-0.008e
C-C3	0.09w	0.11w	0.26w	0.35w	02w	0.23w	0.28w	0.2w	0.01e	0.01e	0.03w	0.03w	0.004e	0.002e
D-D4		0.06n	0.07n	0.10n	0.09n	0.11n	0.06n	0.06n	0.06n	0.012n		0.04n	0.029n	0.03n
E-E5			0.15s	0.10s	0.09s	0.09s	0.03s	0.02s	0.05s	0.08s			0.07s	0.05s
		-0.08n	0.07n	0.06n	0.03n	0.05n			0.61s	0.62s	0.02s	0.02s	0.003s	0.006n

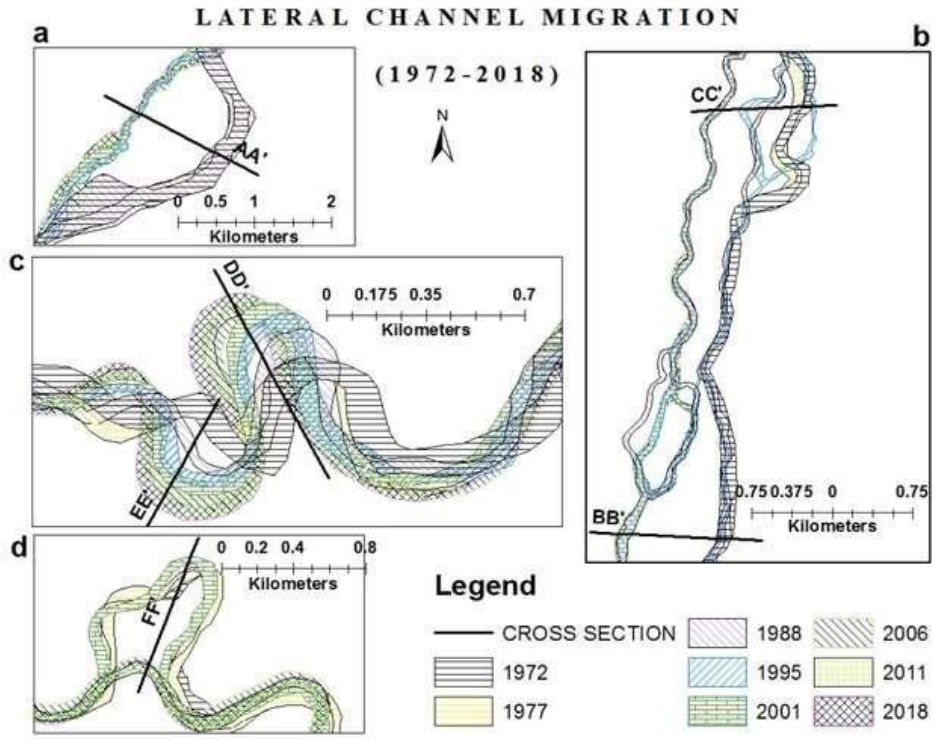

Figure 3: Spatio-temporal changes in river morphology. a) and b) shows new branching and cutting off the old through aggradations, c) shows lateral channel migration through the erosion of the meander bend, and d) shows channel avulsion through cutting off the meander neck.

In the years 1972, 1977, and 1988, the channel was in the right direction along cross-section AA' (Figure 3a), and in the early 1990s, the channel was shifted towards the left direction with an extent of about 1 km and till now the river flow in the same direction. The river discharge and rainfall data of the study area augments the channel avulsion. The higher rainfall (>2000 mm) at Boko rain gauge station was recorded in 1993, 1995, and 1996 (Figure 5), with recorded higher discharges in 1993 and 1995, above the yearly

average discharge of 80m^3/sec. In cross-sections BB' and CC', there is a quick diversion off the new channel along interconnecting wetlands because of high seasonal discharge and sedimentation of the main channel (Figure 3b). In 1972 and 1977, the channel was in the right direction, and the early 1980s, the channel shifted to the left with an extent of 0.8 km, and after that, the river flowed in the same direction. During 1972-2001, the channel was rapidly progressive in meander formation because of high discharge in the channel and/or continued flow of water currents that helped erode the sediment and lead to lateral erosion. Afterwards, the meander cut-off and oxbow lake formations were observed within the cross-sections DD' EE' and FF' (Figure 3c and 3d).

The rate of movement of the lateral migration of the channel is observed from 1972 to 2001 due to the river clip process. The rate of movement was 0.08 km (1972-1977), 0.06 km (1977-1988), and 0.054 km (1988-1995) on the right bank towards the north direction. However, the scenario changed in the early 2000s when the channel left its original course and drifted its direction towards the left. This is due to the river clip and slip-off slope process. The river drifts towards the left, about 0.61 km from 2001 to 2006. The river course formed a meander cut-off neck in 2002. The cross-section DD' is continually shifting towards the right (north) with the help of river clip process and moving at the rate 0.06 km from 1972 to 1977, it again shifts at same direction about 0.10 km (1977-1988), 0.11 km (1988-1995), 0.06 km (1995-2001), 0.012 km (2001-2006), 0.0497km (2006-2011), and 0.034 km (2011-2018). The cross-section EE' is also continually shifting towards left (south) at the rate of 0.15 km from 1977 to 1988; it continues to move towards south 0.092 km (1988-1995), 0.03 km (1995-2001), 0.05 km (2001-2006), and 0.069 km (2011-2018). However, from 2006 to 2011, there was no clear channel lateral movements.

4.2. Hydrogeomorphic Attributes

Longitudinal Profile and Channel Gradient

In the state of Meghalaya, the river originates at an altitude of 1700 m near Nonglyer (known as Khri River) and runs down for about 200 km. After reaching the alluvial plain of Assam, the river is known as the Kulsi River. The river has knick points due to the presence of the resistance rock, changes in slopes, high channel gradient, and high SL value in the upper courses. The knick points at 16 km and 54 km downstream from Nonglyer are presumed due to the Guwahati fault passing along the Kulsi River course (Yin et al., 2010), whereas the third knick point at about 10 km upstream of Ukium corresponds with the Banded Gneissic Complex of the Shillong Plateau. The alluvial plain associated with high stream length gradient indices in the upstream indicates tectonic activity (Imsong et al., 2018). The slope gradient and SL value of Kulsi River from Ukium (80m) to Nagerbera (35 m) abruptly fall by about 41 cm/km and 0.02, respectively, shown in Table 3. The Kukurmara site, about 34 km downstream from Ukium reach, has a slope gradient of about 0.98 m/km, indicating that the upstream's highly eroded materials are deposited downstream in the lower river courses (Figure 4).

Sinuosity Index (SI)

The Sinuosity index of the Kulsi River from the point Balijori to the confluence of the Brahmaputra near Nagarbera was found at 1.20 and 1.24 in the years 1972 and 2018, respectively. A river having a sinuosity index of 1.05 to 1.5 is called sinuous. It shows that the downstream Kulsi River is highly sinuous. From the point of Ukium to Balijora, the sinuosity index was found to be 1.10 in 1972 and 1.05 in 2018; the low Sinuosity index in this stretch specifies solid structural control and flows over the Kulsi fault line.

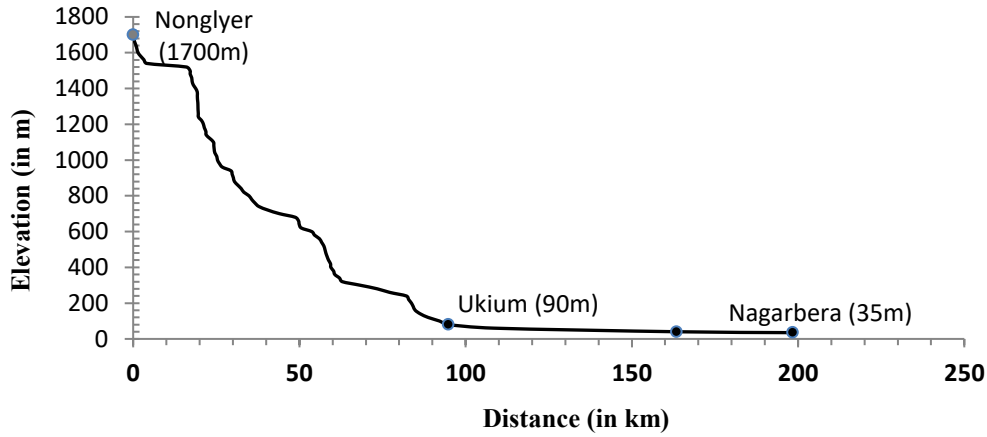

Figure 4: Longitudinal profile of the Kulsi River shows major knick points and high stream gradient in the upper course

Table 3: Relief characteristics of Kulsi River computed from the longitudinal profile

Name	Elevation (in m)	Stream length (in km)	Channel gradient, G (m/km)	Stream length Gradient index, SL
Nonglyer	1700	0	-	-
Ukium	80	101	16.02	3.185
Kukurmara	47	34	0.98	0.019
Chamaria	42	39	0.12	0.002
Nagarbera	35	25	1.38	0.005

Cross-Sectional Channel Characteristics

The cross-sectional channel characteristics play a significant role in lateral channel migration. Channel migration areas were surveyed from the Ukium to Nagarbera. Eight sample cross-sections were taken along the downstream direction of the Kulsi River for cross-sectional morphological measurements. Table 4 lists the characteristics of each cross-section: width, average and maximum depth, surface water, depth water velocity, and discharge. It is observed that the maximum channel width (90 meters) of the Kulsi River is

in the vicinity of the foothill. However, along with the downstream, it varies from 32 to 84 meters due to the bifurcation of the main channel after crossing Kulsi Point. The average depth of the channel varies from 0.32 meters at cross-section 1 to 1.83 m at cross-section 4. High sediment deposits in the Kulsi River are observed in the foothills bed, which lowers the channel depth. The velocity of the water depends on its depth - the surface velocity is increased with increasing depth. Therefore, maximum water discharge is found at cross-section 8 with a discharge rate of 613.41 cumecs.

Table 4: Cross-sectional channel characteristics at channel shifting points

Cross-section	Depth (in m)		Width (m)	Area (m^2)	Velocity (m/sec)		Discharge (m^3/sec)
	Maximum	Average			Depth water	Surface water	
1	0.75	0.32	90.1	28.83	0.007	2.51	72.36
2	1.10	0.56	36.5	20.69	0.346	12.2	252.42
3	2.00	1.50	32	48.19	0.220	5.6	269.86
4	3.26	1.83	35.2	64.41	0.350	6.81	438.63
5	2.14	1.17	51.6	60.37	0.325	4.97	300.03
6	2.88	1.75	54.8	95.90	0.339	4.05	388.39
7	2.80	1.13	84	95.42	0.366	5.6	534.35
8	2.70	1.31	67	87.63	0.410	7	613.41

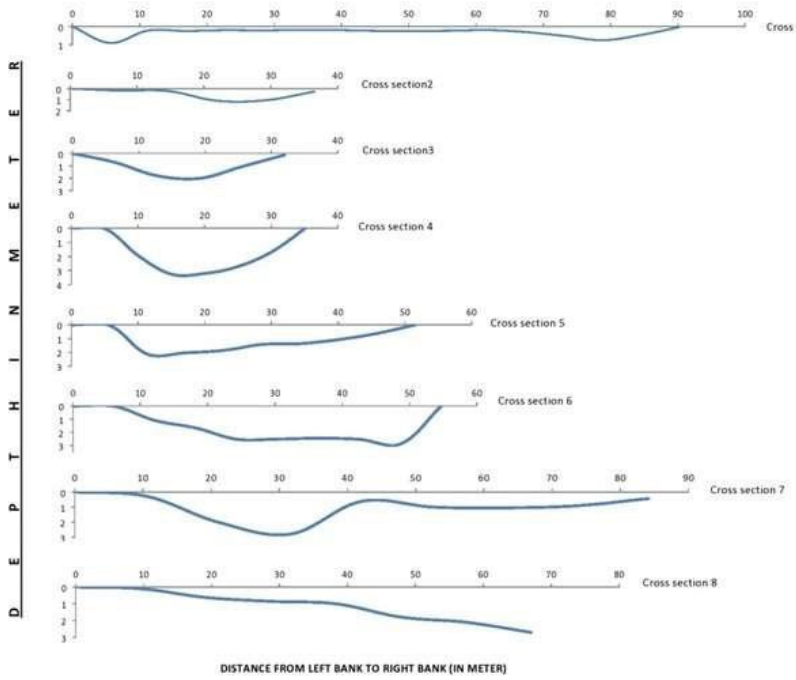

Figure 5: Cross-sectional morphology of the channel at selected sites. Cross-section 1 exhibits a wide valley with sediment deposits on the channel bed. A narrow V-shaped profile was developed in cross-sections 3 and 4; Cross-sections 2, 5, 6, and 7 developed a meander channel cross profile.

The cross-sectional morphology of the Kulsi River at selected sites is shown in Figure 5. It is observed that the width of the channel is found to be maximum with sedimentation along a river bed in cross-section 1, where the new channel was created after the 1988 flood. A narrow V-shaped profile was developed in cross-sections 3 and 4. Cross-sections 2, 5, 6, and 7 developed a meandering channel in the cross profile due to the erosion and deposition works of the river. The helical flow of the meander bend plays a vital role in sediment transport and deposition (Azpiroz-Zabala et al., 2017). On the inner bank, a slip-off slope is created due to the deposition of sediments. The river cliff slope is created due to the undercut by erosion on the outer bank. So, the maximum depth of the channel cross-sectional profile at the meander bend is formed along the concave bank due to the action of helical flow in the meander bend.

Flow Characteristics

The Kulsi River's flow regime mainly depends on the monsoon's seasonal rhythm. Northeast India experiences a southwest monsoon with high precipitation in the pre-monsoon period, and sometimes it is unpredictable. For instance, in the William Nagar rain gauge station of Meghalaya, located southwest of the Kulsi basin, rainfall intensity rose to 32.4 cm in an hour on 22 Sept 2014. Total and average hourly rainfalls for the same day are 191.2 cm and 7.96 cm, respectively. Similarly, the daily rainfall in the Guwahati Airport rain gauge station was recorded at 15.53 cm on 23 Sept 2014. This is the highest daily rainfall recorded during the present decade in Assam. The maximum annual rainfall of more than 2100 mm is recorded in 1977, 1988, and 1993.

The Kulsi River exhibits unique flow characteristics marked by significant seasonal variations in rainfall. Peak flow occurs during the monsoon, with more variable runoff patterns after each storm event. Current flows to a base flow characterise the inter-monsoon period reached just before the onset of the subsequent monsoon. The yearly average discharge of the Kulsi River varies from 38.541 cumecs in 1998 to 99.789 cumecs in 2014. From 1993 to 2018, the average annual discharge was 62.304 cumecs. Figure 6 represents the deviation of the annual discharge from the mean annual discharge from 1993 to 2018. The time cycle of these annual accumulations seems to be irregular in its period and amplitude. It is also observed that there has been a wide variation in annual flow characteristics since 1993, with sustained high discharges during 1993, 1995, and 2014. Figure 5 shows annual discharge data from 1993 to 2018, indicating a cyclic fluctuation with peaks in almost every alternative year. The pattern of variation of the annual peak flow of the river is also represented in the figure. It is observed from the annual hydrograph of the Kulsi River that the trend of peak flow decreased from 1996 to 2013.

5. DISCUSSION

The literature shows that the hydromorphological dynamics in low-lying alluvial channels may emerge due to floods. The peak discharge in the channel typically creates

new branches, cutting off the meanders and oxbow lakes (Struzynski et al., 2015). The floodplain characteristics include quick drains, those with high gradients, absence of vegetation cover or low vegetation, minor reliefs, and water table below the floodplain surface support channel avulsion by incision. The avulsions in the Kulsi channel after crossing the Ukium foothills (Figure 3a) fulfil all these conditions. Here, the interconnecting river wetland, locally known as Kendil Bill, along the Chikadonga tributary of the Kulsi River, plays a significant role in channel diversion.

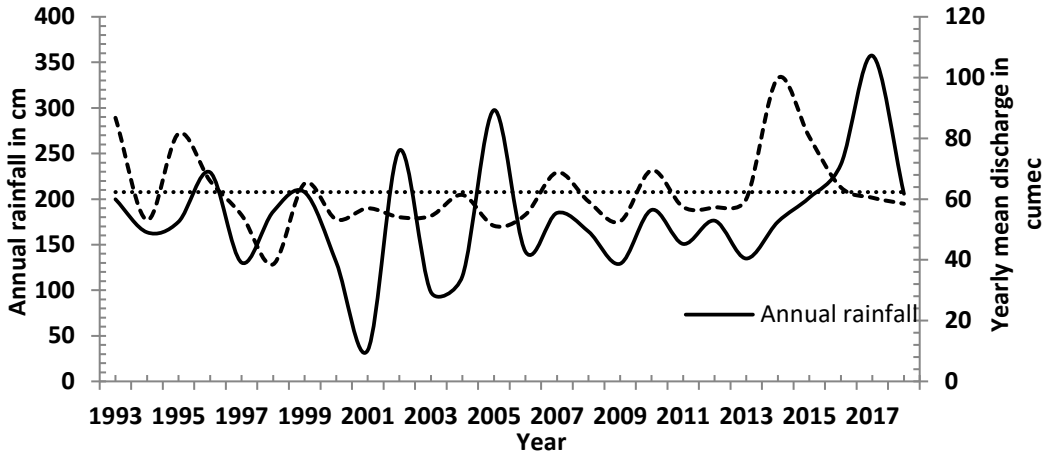

Figure 6 : Annual average discharge of Kulsi River at the point of Kukurmara and annual rainfall of Boko rain gauge station for the year 1993-2018.

Figure 8 illustrates the aerial view of channel change from 1972 to 2018 at the Chikadonga tributary. Here, the tributary flow is 2.80 km parallel to the main channel, and the spacing between them is about 80 meters near Lankhar village in 1967. The mainstream Kulsi diverted at this point by cutting the meander bend and joining with the Chikadonga River during bank-full discharge and floods after 1988. The rise of the channel bed through the sedimentation process cuts off the main channel after 1995 and creates a new pathway along the interconnecting wetlands, especially in the foothills of Kulsi (Figures 3a and 3b). Further downstream, the bank line is migrated through the cutting off of the meander neck (Figure 3d) and meander bend (Figure 3c). The tectonically active upstream of Kulsi River, as evidenced by the morphometric factors such as longitudinal profile, gradient, and stream length gradient index, proves faster erosion and excess sediment flux upstream leads to enormous sedimentation downstream, which is unable to carry through the meander bend and hence the channel form a new pathway for its flow. This variability of water discharge highly impacts bank erosion, especially during the bank-full stage (Dragicevic et al., 2017). Interestingly, the Lower Kulsi basin received 1800 mm to 2200 mm yearly mean rainfall during the last ten years (2009-2018), as shown in Figure 7. The extreme rainfalls in the upper catchment area cause massive flood situations in the low-lying areas that result in channel shifts and land loss on the bank of the Kulsi River.

For instance, a maximum annual rainfall of above 3500 mm was recorded in 2017 at the Boko rain gauge station, which is located within the study area. Due to this abnormal rainfall, the river experiences high discharges in the downstream plain regions with a high stream flow velocity in a short time span. The diversion of the river can be attributed to this increased sediment flux associated with the extreme rainfall event. It is identified that the river experienced an abandonment of a meandering loop due to this event by cut-offs. The high channel gradient of 16 m/km from the source to the foothills at Ukiam and the stream length gradient index of 3.185 indicate that the channel tends to have faster erosion and sediment flux downstream.

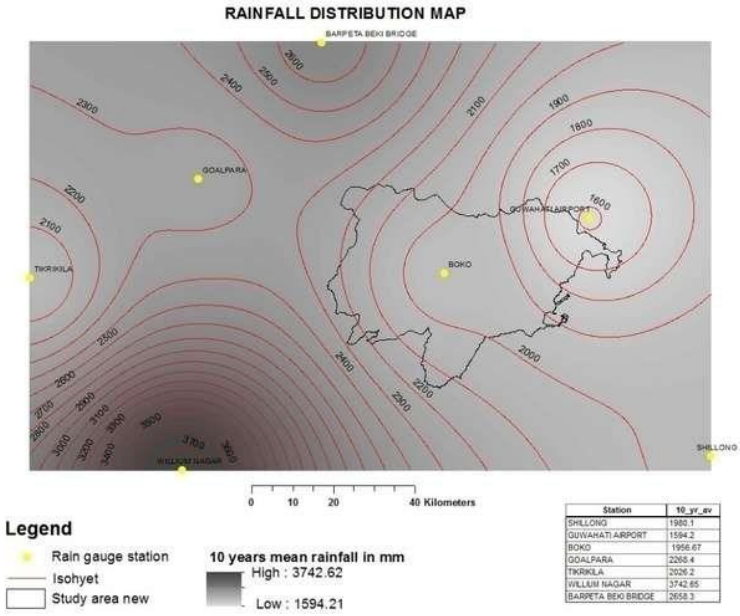

Figure 7 : Mean annual rainfall distribution in the study area

6. CONCLUSION

The paper is focused primarily on the spatio-temporal changes in Kulsi River using multi-temporal satellite data, topographic sheets with 20 m contour interval, structural and geological, hydrological attributes such as gauge rainfall, and water discharge, and cross-sectional channel geometry through field survey methods for the first time. Integrating multi-temporal satellite images and other hydrodynamic settings of the basin in GIS helps us detect lateral channel migration, the nature of their shifting, and its consequences on the landscapes. The morphotectonic character, extreme rainfall, and high discharge influence the channel migrations of the Kulsi River from the Ukium point to the confluence point near Nagerbera. There are five channel reaches that are identified as the most dynamic in their

lateral direction. They mainly belong to the young alluvial soil where progressive meandering, meander cut-off, and oxbow lake formation occur. Most of the bank line is migrated by cutting off the meander neck and meander bend. The river clip, slip-off slope, channel width, meander belt, and sediment supply are also responsible for channel diversion. The river's upper course stretch from Ukiam to Dumukh belongs to the active tectonic zone, and here, interconnecting riverine wetlands play a significant role in lateral channel migration during and after flood events. The highly erodible sediment of active tectonic catchments is deposited in the mainstream due to a sudden velocity drop in the foothills. Consequently, it changes its course along the riverine wetland during massive floods after 1988. The study offers in-depth information on channel avulsion in the Kulsi River, which helps to plan for constructing structural measures to mitigate the risks of flood hazards in future.

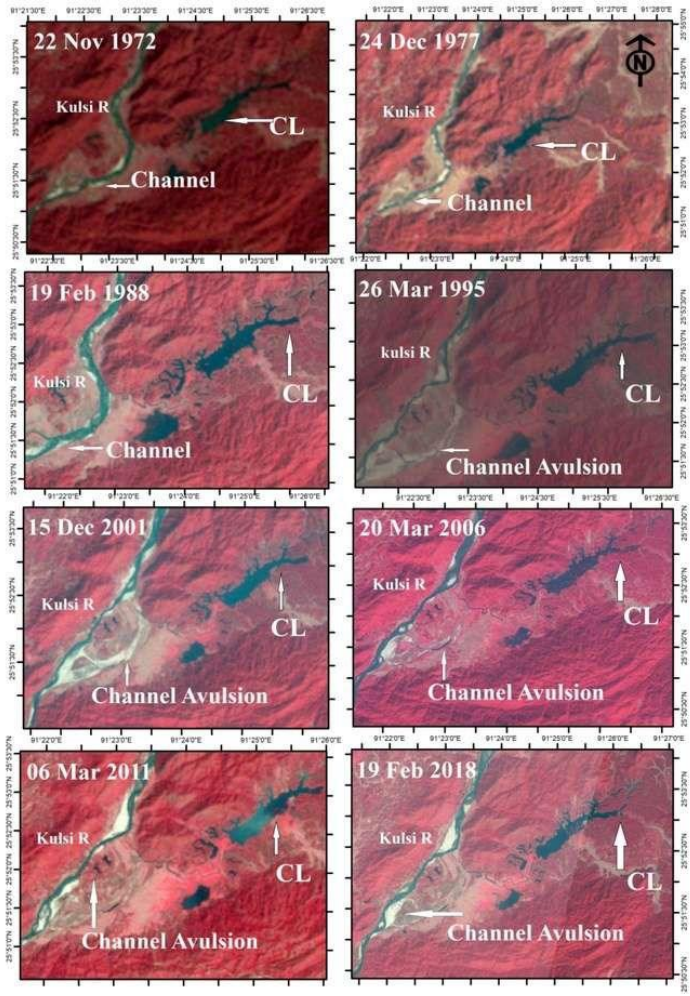

Figure 8: Satellites imagery showing channel avulsion (1972-2018) in Kulsi River

Acknowledgement

We are very much grateful to the funding agency Science and Engineering Research Board (SERB), the Department of Science and Technology, Government of India, for their financial support of this project (Grant No: EMR/2016/006422, 08 May 2018). Our special thanks to the scientists at the Regional Sericulture Research Station (RSRS), Boko, for providing rainfall and other meteorological data. We are also thankful to field assistants, research scholars, fishermen, and all who directly and indirectly contribute to this research work.

Availability of data and materials

The datasets used and analysed during the current study are available from the corresponding author upon reasonable request. The authors declare no conflict of interest in the completion of the work.

References

1. Azpiroz-zabala, M., Cartigny, M. J. B., Sumner, E. J., & Clare, M. A. (2017). A general model for the helical structure of geophysical flows in channel bends. *Geophysical Research Letters*, 44(11), 932–941. https://doi.org/10.1002/2017GL075721.
2. Baniya, S., Deshar, R., Chauhan, R., & Thakur, S. (2023). Assessment of channel migration of Koshi River in Nepal using remote sensing and GIS. *Environmental challenges,* 11(100692).
3. Brice, J.C. (1982). Stream channel stability assessment. Report FHW A/RD-82/021, US Department of Transportation Federal Highway Administration, Washington, DC 42.
4. Brizga, S.O., & Finlayson, B. L. (1990). Channel avulsion and river metamorphosis: The case of the Thomdon River, Victoria, Australia. *Earth Surface Processes and Landform*, 15, 391-404.
5. Bryant, M., Falk, P., & Paola, C. (1995). Experimental study of avulsion frequency and rate of deposition. The Geol. Soc. Ame., *Geology*, 23,365-368. https://doi.org/10.1130/0091-7613.
6. Dragicevic, S., Pripuzic, M., & Novkovic, I. (2017). Spatial and temporal Variability of Bank Erosion during the Period 1930-2016: Case Study- Kolubara River Basin (Serbia). *Water*, 9(10),748. https://doi.org/10.3390/w9100748.
7. Fisk, H. N. (1947). Fine grain alluvial deposits and their effects on Mississippi River activity, Vicksburg, Mississippi, Mississippi River Commission, 78.
8. Gole, C. V., & Chitale, S. V. (1996). Inland delta building activity of Kosi River, Journal of the Hydraulics Division. Proceedings of the American Society of Civil Engineers. 92, 111-126.
9. Hack, J. T. (1973). Stream profile analysis and stream gradient index. J. Res. *US Geol. The survey*, 1(4), 421-429.
10. Hassan, M., Ratna, S., Hassan, M., & Tamanna, S. (2017). Remote Sensing and GIS for the Spatio-Temporal Change Analysis of the East and the West River Bank Erosion

and Accretion of Jamuna River (1995-2015), Bangladesh. *Journal of Geoscience and Environment Protection*, 5, 79-92. https://doi.org/10.4236/gep.2017.59006.

11. Heller, P. L., & Paola, C. (1996). Downstream changes in alluvial architecture: an exploration of controls on channel-stacking patterns. *Journal of Sediment Research*, 66(2), 297-306.
12. Imsong, W., Choudhary, S., Phukan, S., & Duarah, B. P. (2018). Morphodynamics of the Kulsi River Basin in the northern front of Shillong Plateau: Exhibiting episodic inundation and channel migration. *J. Earth Syst. Sci, Indian Academy of Sciences*, 127(5), 1-15. https://doi.org/10.1007/s12040-017-0904-1.
13. Jones, L. S., & Schumm, S. A. (1999). Causes of avulsion: An overview. *Spec. Publ. Int. Assoc. Sedimental*, 28,171-178.
14. Mackin, H. J. (1948). Concept of the graded river. *Geol. Soc. Am*, 55, 463-512.
15. McCarty, T. S., Ellery, W. N., & Stainstreet, I. G. (1992). Avulsion mechanisms on the Okavango fan, Botswana: The control of a fluvial system by vegetation. *Sedimentology*, 39, 779-795.
16. Mohamad, N., Khanan, M.F.A., Musliman, I.A., Kadir, W.H.W., Ahmad, A., Rahman, M.Z.A., Jamal M.H., Zabidi, M., Suaib, N.M. & Zain, R.M. (2018). Spatio-temporal analysis of river morphological changes and erosion detection using very high-resolution satellite image, IOP Conf. Ser.: *Earth Environ. Sci,* 169 012020. https://doi.org/10.1088/1755-1315/169/1/012020.
17. Motta, D., Abad, J. D., Langendo, E. J., & Gracia, M. H. (2012). A simplified 2D model for meander migration with physically-based bank evolution. *Geomorphology*, 10, 163-164.
18. Petropoulos, G.P., Kalivas D. P., Griffiths, H. M., & Dimou, P. P. (2015). Remote sensing and GIS analysis for mapping spatio-temporal changes of erosion and deposition of two Mediterranean river deltas: The case of the Axios and Aliakmonas rivers, Greece. *International Journal of Applied Earth Observation and Geoinformation*, 35(B), 217-228. https://doi.org/10.1016/j.jag.2014.08.004.
19. Russell, R. J. (1954). Alluvial morphology of Anatolian river. *Annals of the Association of American Geographers*, 44, 363-391.
20. Smith, N. D., & Pérez-Arlucea, M. (1994). Fine-grain splay deposition in the avulsion belt of the lower Saskatchewan River, Canada. *Journal of Sedimentary Research*, B64, 159-168.
21. Sonowal, G., Thakuriah, G., & Hazarika, S. (2022). Role of Channel migration and influencing hydro-geomorphic attributes in Dibru river basin using remote sensing and GIS. *Nature environment and pollution technology*, 21(5), 2035-2054.
22. Strużyński, A., Ksiażek, L., & Bartnik, W. (2015). Wetland in River valleys as an effect of Fluvial Processes and Anthropopre, Wetland and Water Framwork Directive. *GeoPlanet: Earth and Planetary Sciences*, 69-90. https://doi.org/10.1007/978-3-319-13764-3_5.

23. Thakuriah, G. (2023a). Geospatial Tool-Based Geomorphological Mapping of The Lower Kulsi Basin, India. *Indonesian Journal on Geoscience*, 10 (2), 229-244. https://doi.org/10.17014/ijog.10.2.229-244.
24. Thakuriah, G. (2023b). GIS‑based revised universal soil loss equation for estimating annual soil erosion: a case of lower Kulsi basin, India. *SN Applied Sciences*, 5, 81. https://doi.org/10.1007/s42452-023-05303-0.
25. Thakuriah, G. (2023c). Geospatial and Analytical Hierarchical Process approach for potential sites of water harvesting in lower Kulsi basin, India. *Geoscape, 58-73.* https://doi.org/10.2478/geosc-2023-0005.

The Indian Geographical Journal
Volume 98 (1) June - 2023, pp 33-46
ISSN 0019-4824

STATUS OF AVAILABILITY AND ACCESSIBILITY OF SAFE GROUNDWATER SOURCES IN TRIPURA

Jimmi Debbarma[1*] Nibedita Das (Pan) [2]

[1] Department of Geography and Disaster Management, Tripura University, Suryamani Nagar, Tripura-West, Pin-799022, India India; E-mail: jimmigeo@tripurauniv.ac.in

[2] Department of Geography and Disaster Management, Tripura University, Suryamani Nagar, Tripura-West, Pin-799022, India; E-mail: nibeditadaspan@gmail.com

*Corresponding Author Email: jimmigeo@tripurauniv.ac.in

Abstract

The availability of clean and dependable water supplies is a necessary condition for long-term growth and development. Safe groundwater is water that is fit for consumption and other domestic purposes without having any significant risk to health in its long-term exposure. Safe water availability and accessibility are inextricably linked and vary spatially. The rationale behind this study lies in exploring the status of availability and accessibility of safe and reliable groundwater sources in the households of Tripura. The study area comprises hills and piedmonts, intermontane synclinal troughs, flood plains, terraces and tillas. The random sampling technique was used to gather primary data on the status and availability of groundwater sources. The results show that about 16% of households consume water from unprotected dug wells sources. In the research area, groundwater is highly enriched in iron content and manganese in some proportion due to the ferruginous nature of rocks containing aquifers. The households in the hills, piedmonts, terraces and tillas suffer from seasonal scarcities of safe groundwater. A greater number of wells dry up, especially during the dry season when there is a decline in the water table. Other notable problems observed in the study area include poor maintenance of tube wells/bore wells and broken water delivery points. The study prioritizes the physiographic regions in Tripura to draw plans for access to safe groundwater sources.

Keywords*:* Groundwater, Physiography, Water availability, Water accessibility, Health issues

Introduction

Groundwater is an integral part of the hydrological cycle and one of the most vital resources for millions of people's drinking, domestic, industrial, and agricultural requirements. About half of the world's drinking water is estimated to come from groundwater (Gronwall and Danert, 2020). About 85% of the population in India depends on

groundwater for drinking, and boreholes have become more prevalent over the past several decades for drinking water supplies. (Ali et al., 2019). Groundwater resource offers a dependable supply of drinking water to both rural and urban areas, but its utilization, availability and accessibility are hindered by a variety of factors (Wakode et al., 2014; Khan and Jharia, 2017; Mridha et al., 2020). The groundwater resources in India are shaped by both physical and socio-economic conditions (Kulkarni et al., 2015). Groundwater flow and occurrence are governed by various parameters, including rock type and structural attributes, topography, land use/land cover, drainage network and climatic conditions. The local physiographic features directly influence the groundwater's spatial availability (Kudamnya et al., 2021). Access to clean groundwater in rural areas is also restricted by physical constraints such as inadequate infrastructure, limited yield, and low groundwater quality. The political and social variables also affect people's ability to acquire water for daily needs (Mseli et al., 2019).

Groundwater is a vital resource that millions of people worldwide rely on for a range of water needs, but maintaining its safety and accessibility presents severe challenges in the face of rising demand, overexploitation, pollution, and climate change. Every community's socio-economic development heavily relies on sustainable water supply availability (Che et al., 2018). As a result, the availability of clean and dependable water supplies is necessary for long-term growth and development (Asonye et al., 2007). Safe groundwater is water that is fit for consumption and other domestic purposes without having any significant risk to health in its long-term exposure. Safe drinking water indicates an "improved water source" to households, which includes household connections, public standpipes, boreholes, protected dug wells, protected springs, and rainwater collectors. It is also important to note that "access to clean drinking water" is a provision of at least 20 litres per person per day from an "improved source" within one kilometre of the user's residence. According to WHO and UNICEF's estimates, in 2019, one in three people worldwide did not have access to clean drinking water; 79 per cent of people drink from unimproved sources, and 93 per cent drink from surface water residing in rural regions. More than 884 million people lack a source to secure consumable water, and as a result, poor drinking water is responsible for 72 per cent of diarrheal deaths. Safe drinking water can assist in decreasing or eliminating fatalities caused by water-borne diseases, as well as improve the quality of life all over the world (Lawson, 2011).

Groundwater is the most used resource in Tripura. Although there has been some research on groundwater quality in Tripura, no studies examine the differences in safe groundwater accessibility and availability sources across various physiographic regions. It is observed that the demand for safe water from the protected sources of groundwater, such as tube wells/bore wells, is a major issue in some regions of the state, particularly the hills and piedmonts, compared to other physiographic units. Access to clean and safe groundwater is also frequently hampered by these regions' malfunctioning water delivery points. Even when these sources are available, they are sometimes non-usable because of the poor quality due to heavy iron concentration in water.

In terms of groundwater accessibility, the people residing in the hilly areas have to travel further in order to fetch water as compared to the lesser travel time encountered by the residents of other physiographic units. During the dry period, households are compelled to obtain water from wherever it is found and mostly rely on unsafe dug wells in the hills and piedmonts, as well as terraces and tillas. Safeguarding groundwater supplies should be the top priority in terms of human health (Song et al., 2020). Therefore, this study was formulated to get comprehensive information about the availability and accessibility of safe groundwater sources to meet the needs of households inhabiting different physiographic areas in Tripura. The study seeks answers pertaining to (i) types of groundwater sources available in the major physiographic units and (ii) accessibility of groundwater in terms of the time and distance needed to get safe drinking water.

Study Area

Tripura is a landlocked state with a total population of 36,73,917 persons (350 persons/km^2) as per the 2011 census (Fig. 1) and 41,65,000 as per the projections in 2023 (Directorate of Economics and Statistics, 2024). The study area is located between 22º56' N to 24º32' N latitudes and 91º10' E to 92º21' E longitudes with a land area of 10,492 km^2. Geological formations, such as the Surma, Tipam, Dupitila, and Recent groups, are the main four types of formations found in the study area. Tripura has a varied topography, including hills and piedmonts, an intermontane synclinal trough, flood plains, terraces, and tillas (Fig. 1). The anticlinal hills in the research area run north-south parallel to one another, forming broad valleys with erratic rivers and streams and undulating hillocks. The landscape gets steeper as you move eastward from the west. The drainage pattern in the State is sub-parallel. The anticlinal hill ranges serve as watersheds from which different drainage channels develop, fill in valleys, and eventually empty into Bangladesh. Major rivers in the State are Juri, Longai, Fenny, Muhuri, Gumti, Haora, Khowai, Dhalai, Manu and Deo.

A humid subtropical climate characterizes Tripura, with an average temperature range from 10°C to 35°C. With an average annual rainfall of 2200 mm, the southwest monsoon provides the majority of the rain throughout the monsoon season, which begins in June and lasts until September. During the monsoon season, water swells in most of the major rivers of the state. Evergreen forests mostly dominate the study area. The study area also has several vegetation types, including bamboo, cane, savannah, moist deciduous, and grassland forests. The dense concentration of population is mainly observed in the city and towns of synclinal troughs, whereas in the hills and piedmonts, they are dispersed (Fig. 2).

In the study area, groundwater mainly occurs in the Tipam and Dupitila formations in rocks of sandstone and shale. The Tipam formation's sandstone, which has a far higher permeability than Surma or Dupitila sandstone, is the main source of water. Having abundant rainfall from the southwest monsoon, the geology, as well as the geomorphology of the State, is favourable for auto artesian conditions within synclinal valleys. Flood plains

with younger alluvial soil generally influence groundwater recharge due to high infiltration. Therefore, groundwater development occurs mostly in the synclinal trough, flood plains and adjacent anticlinal hills. However, there are issues with regard to the accessibility and availability of reliable and safe groundwater sources. In rural areas where groundwater treatment is not regular, it causes many waterborne diseases. Besides malfunctioning water delivery points, the lack of maintenance of tube wells and protected dug wells also hinders the household's access to safe water sources.

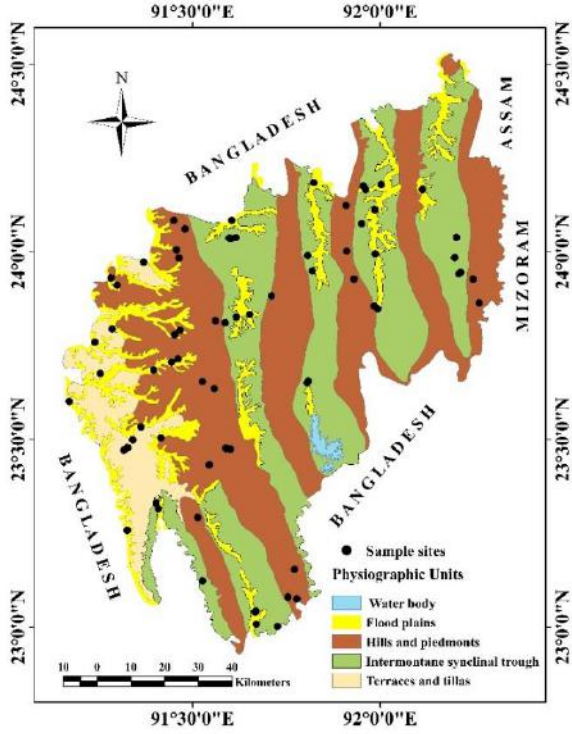

Fig. 1 Physiographic units and sample distributions in the study area

Materials and methods

This study used primary data to assess the availability and access to safe groundwater sources in Tripura. Questionnaires were used to generate primary data about the availability and accessibility of safe water sources from households of diverse physiographic units. The study employed a multi-stage sampling technique integrating both purposive and random sampling methods to ensure a representative and diverse sample. The prepared physiography map was superimposed over the district boundaries in the first stage. Secondly, the physiographic areas of the respective districts have been narrowed down to the blocks to locate the villages that fall within the maximum area dominated by each physiography. In the third stage, at least five villages from each physiographic unit were selected randomly. Unlike the administrative units, the physiographic units were not

defined by discrete boundaries; hence, selecting households within the diverse physiography was challenging. Therefore, finally, the sample size of households, i.e. 650, which forms the basic unit of study, was determined using Yamane's formula at a 95% confidence level and 5% margin of error to determine the minimum sample size needed to achieve a desired level of confidence and precision in the study's results. The Central Groundwater Board, Northeastern Region, Guwahati, was consulted as a secondary source to obtain information on the usage patterns of groundwater.

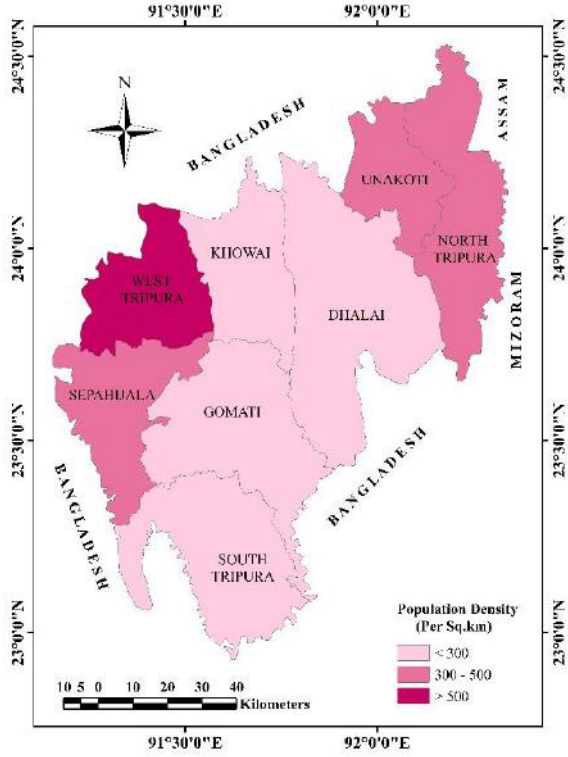

Fig. 2 Population density in Tripura

Results and Discussion

Pattern of Groundwater Utilization

Groundwater utilization pattern refers to the uses of water for different purposes. The socio-economic condition of households determines the pattern of groundwater utilization. Additionally, physiography also influences the consumption pattern of groundwater. The households that are far away from the water collection sources usually use groundwater for drinking purposes only. In the study area, the district-wise pattern of groundwater utilization reveals that groundwater is used mostly for domestic purposes,

such as drinking, cooking, washing clothes, bathing, animal use and house cleaning. The water requirements of individuals residing in rural areas are generally for these basic needs, whereas people living in urban areas use water in a variety of ways. The utilization of groundwater for irrigation is only observed in the plain areas of Khowai, West, Sepahijala and South Tripura districts (Fig. 3). Government-led irrigation projects and infrastructure development initiatives influenced groundwater utilization patterns in these districts. Due to the hilly terrain, the rest of the districts do not depend much on groundwater for irrigation.

The State benefits from ample groundwater resources, primarily due to the monsoonal rainfall, which helps recharge the aquifers. In hilly areas, the rugged terrain makes it challenging and expensive to access groundwater for irrigation purposes, leading to limited utilization of groundwater for domestic purposes. Areas adjacent to hills and piedmonts hold substantial potential for groundwater availability, and shallow aquifers in the plains and flood plains allow for relatively easy groundwater extraction.

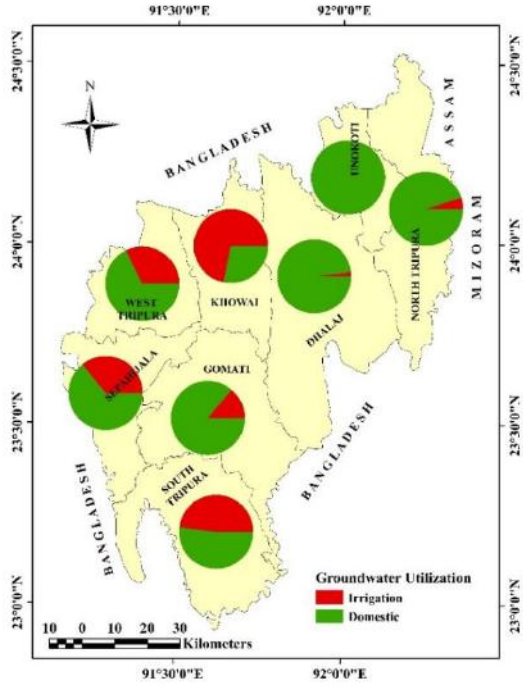

Fig. 3 District-wise groundwater utilization. Source: Central Groundwater Board, North Eastern Region, Guwahati

Sources of Safe Drinking Water

Availability of potable drinking water is a pressing need, as 30% of urban dwellers and 90% of rural dwellers still rely entirely on untreated surface or groundwater

(Palanisamy et al., 2007). Access to improved drinking water sources is a key requirement and a basic human right for everyone's health and hygiene. In the study area, tube wells, hand pumps, protected dug wells, protected spring water and piped water into the home offers an improved source of drinking water. Unimproved sources of water include unprotected dug wells, surface streams, ponds, reservoirs and water supplied through tankers.

Tube well/bore wells represent the primary water source in the flood plains, terraces and tillas. These groundwater sources were preferred due to their reliability and accessibility, especially in flat terrain where groundwater can be easily extracted. In the hills and piedmonts, and intermontane synclinal toughs, the major source of drinking water comes from public taps (Fig. 4). In hilly regions, the dispersed nature of households and the challenging terrain make it difficult and economically unfeasible to install deep tube wells or bore wells. Groundwater availability is also limited to specific areas along low-lying bordering anticlinal hills. Consequently, public tap water systems have become the more viable option for providing water to communities in these regions by the government. The dependence on public tap water in intermontane synclinal troughs and flood plains was caused by the extensive aquifers and groundwater reserves due to their relatively flat terrain and high permeability of soils. The dense concentration of the population also makes it more feasible and cost-effective to establish centralized water supply systems, such as public tap water networks, to serve a larger number of people. Shallow hand pumps, tube wells, and bore wells can also be installed relatively easily in the plains, allowing groundwater extraction to supply public tap water systems.

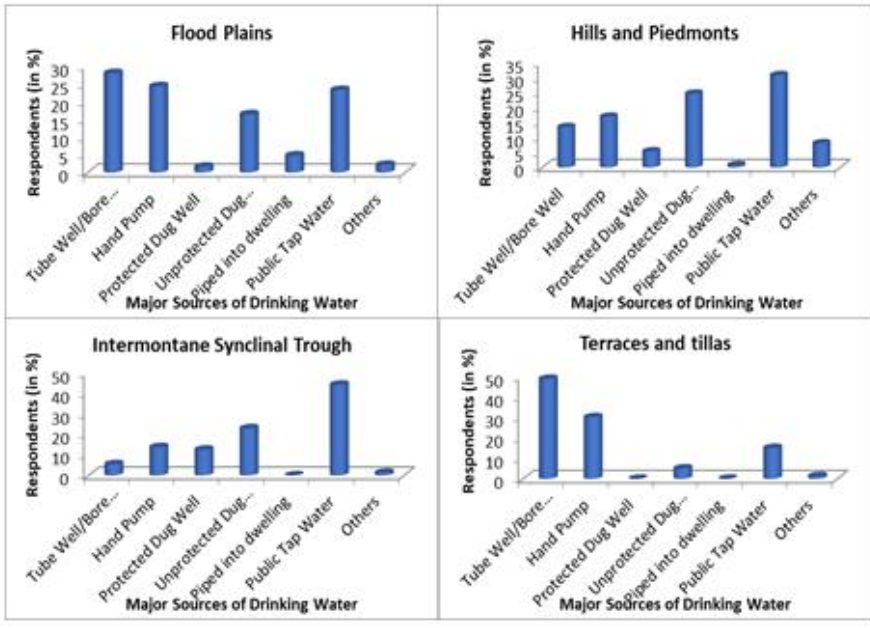

Fig. 4 Drinking water sources in different physiographic units in Tripura

It has been found that despite improved water sources in the State, there are still inequalities in accessing safe groundwater sources across the region. This indicates disparities in infrastructure development, economic factors, and geographical constraints that affect access to safe and reliable water sources. Furthermore, Fig. 4 illustrates that many households rely on unprotected dug wells for water consumption across all physiographic units. This reliance on unprotected sources poses potential health risks due to contamination and highlights the need for interventions to improve water quality and accessibility, particularly in areas where safer alternatives are less accessible.

Accessibility to Safe Drinking Water

Distance plays a critical role in terms of the collection and usage of water. It may also be indirectly linked to stress and burden associated with water collection. Water must be available when needed, and people who travel longer distances to get to a water source use less, negatively impacting consumption and hygienic standards (Manyanhaire et al., 2009). The study depicts that most households collect water within a travel distance of less than 100 m (Fig. 5). This shows the availability of water sources within a safe distance due to the government-operated tube wells, individually owned handpumps and public tap supply. However, the situation is slightly different in the hills and piedmonts, where a sizeable percentage of households, about 25%, is required to travel a distance of more than 100-200 m. Travelling a distance of more than 100 m in hilly terrain can be very tiring as well as challenging. It was also observed that about 2.31% of households travel beyond one km to fetch water. Groundwater sources, particularly the public tap supply in hilly terrain, were not uniformly distributed and were located at greater distances from residential areas than flat or plain regions. The terrain makes it challenging to install public taps in close proximity to all residents. As such, residents need to trek long distances, often uphill or downhill, to reach water sources. This prolonged travel time adds a burden to the overall time spent collecting water and impacts daily routines and productivity.

Seasonal Water Scarcity

Water scarcity is a seasonal phenomenon in the study area, particularly in the hills, piedmonts, terraces, and tillas. According to the respondents, water scarcity happens mostly during the dry season from the month of March till the onset of monsoon. Due to this seasonal scarcity, households in hilly areas endure a significant problem as they spend considerable time searching for water, while those in terraced regions face relatively less. However, households of the flood plains and intermontane synclinal troughs remain unaffected by such difficulties. Approximately 40% of the respondents mentioned that they have to spend lots of time in search of water, which becomes a severe problem during the dry season (Fig. 6). In hilly regions, terraces, and tillas, severe water shortages occur during the pre-monsoon season due to lack of rainfall to replenish the subsurface aquifers and limited water storage capacity. Without significant rainfall to recharge the groundwater sources, groundwater level declines, leading to shortages in water supply. Additionally, the public tap supply system faces significant strain during the dry season, leading to prolonged

waiting times for households to access water. Therefore, seasonal water scarcity-induced problems tend to increase the workload of the women in the hills, piedmonts, terraces and tillas (Fig. 7). In addition, the respondents are also exposed to the risk of consuming untreated water during seasonal water shortages as they are forced to rely on shallow groundwater sources (Fig. 8). About 30.61 and 31.25% of respondents from the hills and piedmonts, as well as terraces and tillas, agree that the risk of drinking untreated water is a severe issue.

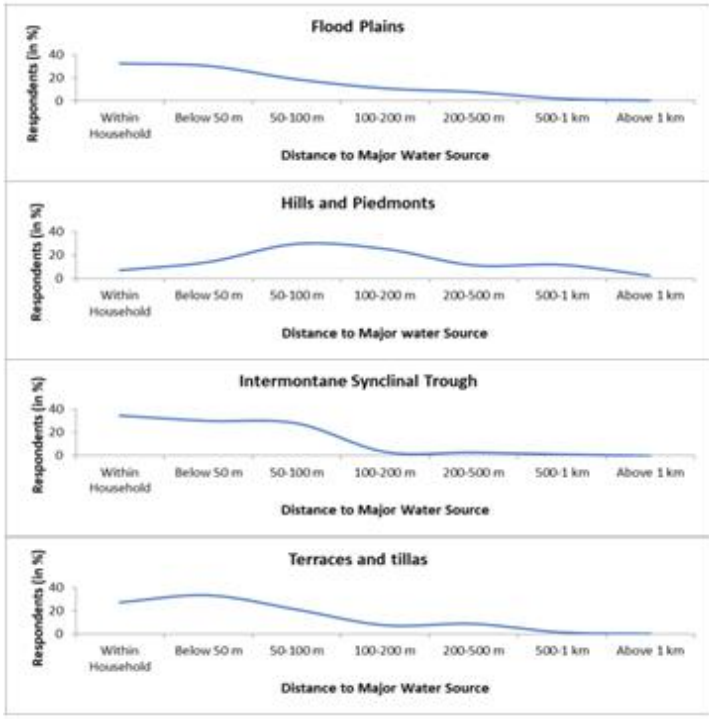

Fig. 5 Distance to access safe groundwater sources in Tripura

Water Collection and Quantity

According to the WHO, a person should have access to 50 to 100 litres of water daily to cover all of their basic requirements and prevent any health hazards. The amount of water available for improved hygiene practices depends significantly on how much time and effort goes into gathering water (Manyanhaire et al., 2009). The duration it takes to collect water, the time of day it is collected, the volume of water collected per trip/day, and the number of household members involved all have an impact on the quantity of water collected. In the study area, water collection by 47.79% of households is undertaken mostly at any time of the day as per their needs. Physiographic variations on time spent to collect water reveal that more than 70% of the households take 10-15 mins to collect water in the flood plains, terraces and tillas. The households in the intermontane synclinal troughs take about 15-20 mins to collect water (Fig. 9).

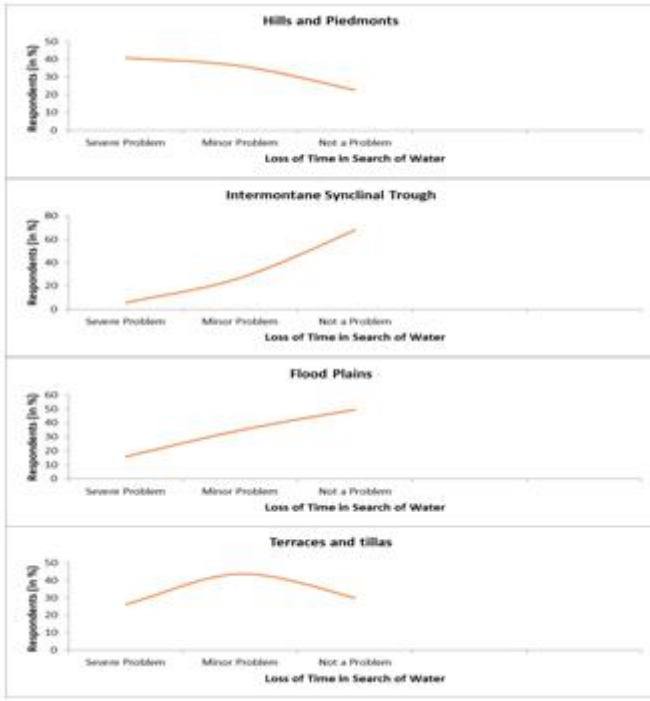

Fig. 6 Time spent to search for safe water resources in different physiographic units

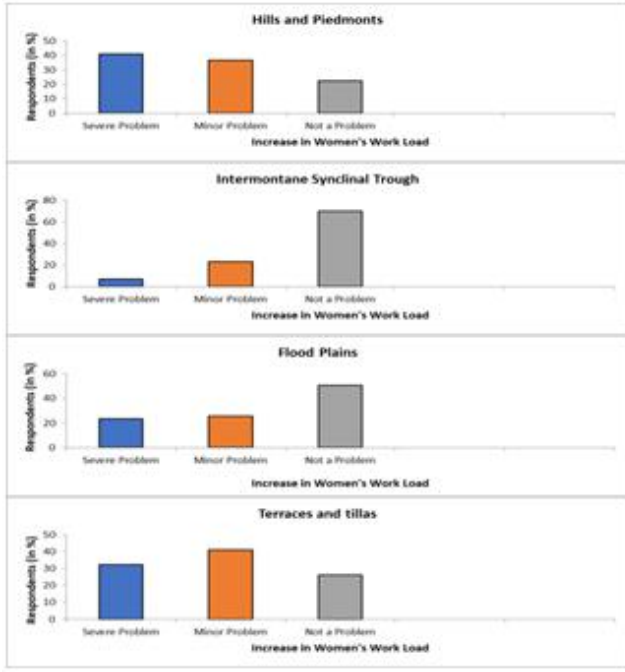

Fig. 7 Women's workload due to seasonal water scarcity in different physiographic units

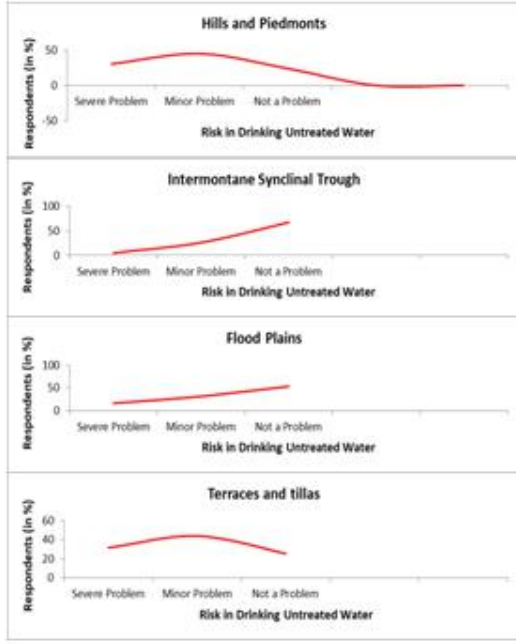

Fig. 8 Risk of drinking untreated water in different physiographic units

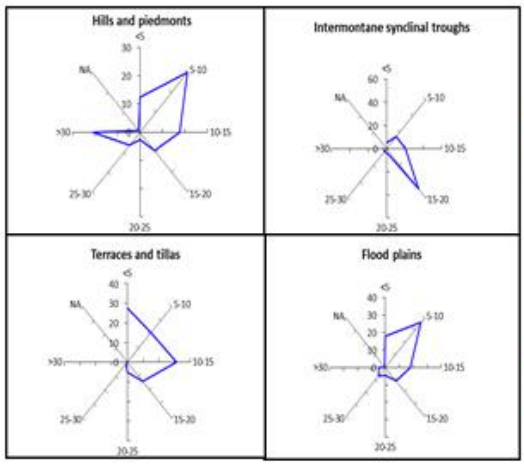

Fig. 9 Time taken to collect water (in min)

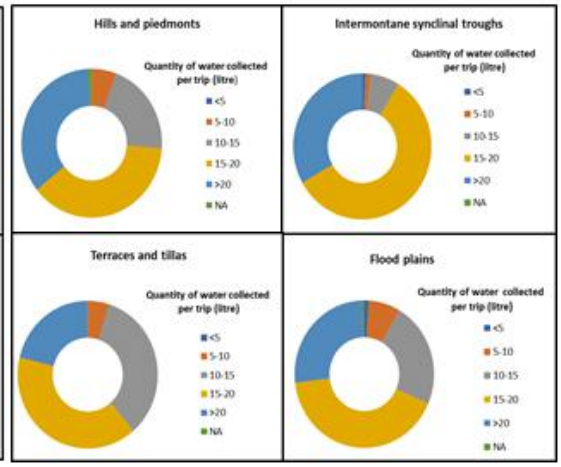

Fig. 10 Quantity of water gathered per visit

On average, the household members fetch 15-20 litres of water in a single trip, and more than 50 litres of water is collected by households in a day (Fig. 11). Among the units, the availability of government-provided wells and also privately owned groundwater sources in the terraces and floodplains results in less time consumption as well as a sufficient amount of water collected. In the hills and piedmonts, people have to travel significant distances to reach water collection points that are far away from residences, resulting in travel time exceeding 30 minutes.

Groundwater is predominantly used for domestic purposes in the State, indicating its importance for basic human needs such as drinking, cooking, and sanitation. The availability and accessibility of safe groundwater are of utmost importance since they determine an individual's well-being. Access to reliable and safe groundwater sources is, therefore, essential for the health and socio-economic status of a community. The provision of safe, reliable, and cheap water deprives a person of basic human rights, wreaking havoc on one's health, destroying opportunities and undermining one's dignity. As a result, the United Nations recognizes access to safe, sufficient, acceptable, cheap, and physically accessible water for personal and domestic use as a basic human right.

Conclusion

The study reveals disparities in the availability and accessibility of safe groundwater sources across different physiographic units in Tripura. The study indicates that the State's groundwater resources largely depend on physiography and the southwest monsoon. Different physiographic units utilize groundwater sources variably due to the availability of public and private water systems. Tube wells form the major source of drinking water in the flood plains, terraces, and tillas, whereas households in the hills, piedmonts, and intermontane synclinal troughs are found to be covered by public taps. Still, a significant percentage of households consuming water from unprotected dug wells can be noticed in all the physiographic units. Hills and piedmonts suffer from a lack of water availability due to seasonal water scarcity and poor aquifers. Women often bear the brunt of water scarcity in these regions, spending significant time and effort on water collection, especially during dry periods. Poor maintenance of water supply points, irregular water supply, and water contamination issues (e.g., high iron concentration) contribute to the challenge of ensuring safe water sources for households.

Seasonal variations in water availability exacerbate these challenges, with dry periods leading to declining water levels in wells and increased difficulty in accessing safe water sources. The findings suggest that a significant percentage of households, particularly those in hilly areas, lack access to safe, reliable, and physically accessible groundwater sources, thus being deprived of their basic human right to water. The study underscores the critical importance of addressing disparities in groundwater availability and accessibility, particularly in ensuring access to safe water sources for all segments of the population of the State, and highlights the need for targeted interventions to mitigate the challenges identified, especially in marginalized hilly areas.

References

1. Ali, S., Fakhri, Y., Golbini, M., Thakur, S.K., Alinejad, A., Parseh, I., Shekhar, S., & Bhattacharya, P. (2019). Concentration of fluoride in groundwater of India: A systematic review, meta-analysis and risk assessment. *Groundwater Sustainable Development*, 9.
2. Asonye, C.C., Okolie, N.P., Okenwa, E.E., & Iwuanyanwu, U.G. (2007). Some physico-chemical characteristics and heavy metal profiles of Nigerian rivers, streams and waterways. *African Journal of Biotechnology*, 6(5), 617-624.

3. Chen, T., Zhang, H., Sun C., Li, H., & Gao, Y. (2018). Multivariate statistical approaches to identify the major factors governing groundwater quality. *Applied Water Science*, 8(215), 1-6.
4. Directorate of Economics and Statistics, Government of Tripura (2024). Economic Review of Tripura 2022-2023. https://tripura.gov.in/sites/default/files/Economic_Review.pdf
5. Grönwall, J., & Danert, K. (2020). Regarding Groundwater and Drinking Water Access through A Human Rights Lens: Self-Supply as A Norm. *Water*, 12(419), 1-21.
6. Kudamnya, E.A., Edet, A., & Ekwere, A.S. (2021). Analysing principal components of physiographic factors affecting groundwater occurrences within Keffi, North-Central Nigeria. *The Egyptian Journal of Remote Sensing and Space Sciences,*24, 665-674.
7. Hoko, Z. (2005). An assessment of the water quality of drinking water in rural districts in Zimbabwe. The case of Gokwe South, Nkayi, Lupane and Mwenezi districts. *Physics and Chemistry of the Earth*, 301(11-16), 859-866.
8. Khan, R., & Jharia, D.C. (2017). Groundwater quality assessment for drinking purpose in Raipur City, Chhattisgarh, using Water Quality Index and Geographic Information System. *Journal of the Geological Society of India*, 90(1), 69-76.
9. Kulkarni, H., Shah, M., & Shankar, P.S.V. (2015). Shaping the contours of groundwater governance in India. *Journal of Hydrology: Regional Studies,*4,172-192.
10. Lawson, E.O. (2011). Physico-chemical parameters and heavy metal contents of water from the Mangrove Swamps of Lagos Lagoon, Lagos, Nigeria. *Advances in Biological Research*, 5(1), 8-21.
11. Manyanhaire; Offat, I., & Kamuzungu, T. (2009). Access to safe drinking water by rural communities in Zimbabwe: A case of Mundenda village in Mutasa District of Manicaland Province. *Journal of Sustainable Development in Africa*, 11(1), 113-127.
12. Mridha, G.C., Hossain, M.M., Uddin, M.S., & Masud, M.S. (2020). Study on availability of groundwater resources in Selangor state of Malaysia for an efficient planning and management of water resources. *Journal of water and climate Change*, 11.4, 1050-1066.
13. Mseli, Z.H., Goeller, D., Scharenberg, M., Mwegoha, W.J.S., Gianotti, R., Bongiorno, D., & Sawyer, A.H. (2019). Physical factors limiting access to clean groundwater in Tanzania villages. *Journal of Water, Sanitation and Hygiene for Development,* 09.3, 531-539.
14. Palanisamy, P.N., Geetha, A., Sujatha, M., Sivakumar, P., & Karunakaran, K. (2007). Assessment of groundwater quality in and around Gobichettipalayam town Erode District, Tamil Nadu, India. *E-Journal of Chemistry*, 4(3), 434-439.
15. Song, K., Ren, X., Mohamed, A.K., Liu, J., & Wang, F. (2020). Research on drinking‑groundwater source safety management based on numerical simulation. *Scientific Reports*, 10:15481.
16. UNDP (2006). Human Development Report. Beyond Scarcity: Power, Poverty and the Global Water Crisis. Retrieved from https://hdr.undp.org/system/files/documents/human-development-report-2006-english.human-development-report-2006-english

17. Wakode, H.B., Baier, K., Jha, R., Ahmed, S., & Azzam, R. (2014). Assessment of impact of urbanization on groundwater resources using GIS techniques-case study of Hyderabad, India. *International Journal of Environmental Research*, 8(4), 1145-1158.
18. WHO & UNICEF (2015). Progress on sanitation and drinking water-2015 update and MDG assessment. World Health Organization, Geneva, Switzerland. Retrieved from https://iris.who.int/bitstream/handle/10665/177752/9789241509145_eng.pdf?sequence=1&isAllowed=y
19. WHO & UNICEF (2019). Retrieved from https://www.who.int/news/item/18-06-2019-1-in-3-people-globally-do-not-have-access-to-safe-drinking-water-unicef-who
20. WHO (2017). Retrieved from https://www.who.int/news/item/06-03-2017-the-cost-of-a-polluted-environment-1-7-million-child-deaths-a-year-says-who

The Indian Geographical Journal
Volume 98 (1) June - 2023, pp 48-66
ISSN 0019-4824

MODELLING URBAN HEAT ISLAND USING REMOTE SENSING INDICES IN TIRUPPUR MUNICIPAL CORPORATION, TAMIL NADU

Masilamani Palanisamy, Prawin Balasubramaniam, Thilagaraj Periasamy

Department of Geography, Bharathidasan University, Tiruchirappalli,
Tamil Nadu, India - 620024.
Corresponding Author: masilamani@bdu.ac.in

Abstract

In the history of humankind, urbanization is one of the vibrant changing geographical phenomena. Almost 55% of the world's population lives in rapidly urban and surrounding areas. Urban heat island represents a significant environmental problem most urban centres face. Extreme heat in urban areas reflects substantial risks to the growing urban population. The increased surface temperature is due to the thermodynamic characteristics of the built-up in urban. The impact of land use/land cover (LULC) dynamics is closely related to urban heat islands (UHI). This study aims to identify the urban heat zones by utilising indicators such as the LULC, NDBI, LST and NDVI for Tiruppur Corporation. The study area Tiruppur is known as the knitwear capital of India, attracting thousands of migrants from all over the country and leading to a continuous accumulation of people. So, most of the migrant people settled in the Tiruppur belt. The present study analysed the spatio-temporal land-use patterns, NDBI, LST, NDVI and UTFVI for Tiruppur Corporation using Landsat and sentinel data sets for 1991, 2001, 2011 and 2021. The LULC were prepared by utilising the supervised classification algorithm of Support Vector Machine (SVM). On the other hand, the advanced technique of Google Earth Engine is utilised to map the LST and NDVI of the study area for the same year. All the results of four indicators, i.e., LULC, NDBI, LST, NDVI and UTFVI, are analysed with the temporal changes by segmenting them with six rings of each 2km. This will help to identify the changes and increase of urban heat from the core to the periphery areas of the Tiruppur Corporation. Thus, this study aids in improving future urban planning, including implementing green city technologies.

Keywords LULC, Tiruppur Corporation, LST, UHI, UTFVI.

Introduction

In recent decades, migration from rural to urban areas has drastically increased due to several factors (employment, education, economy, etc.), which has led to rapid urbanization and urban population growth (Kesavan et al., 2021). In 2016, the urban population reached 54.5% globally; if this continues, the urban population will be 60% of the

total world population by 2030 (U.N. 2016). This growth will convert the historical land use /land cover (LULC) pattern, which impacts the environmental and economic perspectives (Wang et al., 2018; Prakash et al., 2023). The change in LULC would cause changes not only in the landscape but also in the atmospheric conditions of the urban environment, such as the urban heat island (UHI) effect. The effect of the increased surface temperature in urban areas determines UHI (Weng et al. 2004). The growth of the impermeable surface and the decrease in the green space and water bodies are the leading causes of the temperature variation between urban and rural landscapes (Ranagalage et al., 2018). The growth of the city and its population are the indirect indicators of the UHI (Zhao et al. 2014); likewise, buildings, the nature of surfaces, including albedo, and heat capacity largely influence the UHI phenomena.

Highly populated countries like India and China are projected to occupy 35% of the total world urban population by the year 2050 (Bongaarts 2020). The UHI shows severe effects in these rapidly urbanizing countries (Peng et al., 2021). Hence, intensive research on diversified urban settings is needed to address the impacts of UHI (Zhou et al. 2019). The impacts of UHI are assessed through remote sensing (RS), vertical sensing, fixed stations, mobile traverses (Brandsma and Wolters 2012), and energy balances. Among these techniques, remote sensing is a more advanced and feasible method to measure both the air and surface temperature. The traditional methods like fixed station and mobile traverse are expensive and time-consuming (Padmanaban et al. 2017). The combination of remote sensing and Geographical Information System (GIS) techniques is considered to be the best method for observing environmental changes (Xiao et al., 2020). However, spatial and temporal resolution in remote sensing are the constraints in UHI assessments.

According to Weng et al. (2004), Land surface temperature (LST) is a fundamental indicator in UHI studies due to its capability to map temperature differences within urban areas, helping to pinpoint hotspots and assess their spatial extent. LST is the temperature measured on the earth's surface between land and atmosphere (Stow and Chen 2002). The changes in LULC play a significant role in the LST increase in the urban centres. The spatiotemporal changes of the LULC can be monitored using RS and GIS (Abdikan et al. 2014). The temporal LULC changes help to understand the land use types transformation, and it provides information about urban planning (Gordon et al. 2009), whereas improper urban planning is also one of the influencers of UHI (Sarvestani et al. 2011). LULC is an important component in the UHI study (Díaz and Blackburn 2003) along with LST, soil moisture and evapotranspiration of the surface, which are the leading factors for the high rise in UHI (Becerril-Piña et al. 2016).

Researchers also often utilize remote sensing-derived Normalized Difference Vegetation Index (NDVI) and Normalized Difference Built-up Index (NDBI) to evaluate UHI effectively (Zhang et al., 2022). NDVI is useful for examining the cooling effects of urban green spaces. Higher NDVI values indicate more vegetation, which typically corresponds to lower LST values, suggesting vegetation's role in mitigating UHI. Li et al. (2011) found that

urban areas with higher NDVI values generally exhibit reduced surface temperatures, underscoring the importance of green infrastructure in urban planning. NDBI is specifically designed to highlight built-up areas by using remote sensing data, making it a more suitable and efficient method for identifying urban features compared to Land Use/Land Cover (LULC) classification methods. LULC maps, while useful, may not always provide the same level of precision in distinguishing between different types of urban and non-urban land covers. For instance, Chen et al. (2023) demonstrated that using NDBI in UTFVI studies allows for a more detailed and precise analysis of the relationship between built-up areas and temperature variations, enhancing the understanding of how urbanization impacts thermal environments.

The effect of UHI can also be quantitatively computed using the Urban Thermal Field Variance Index (UTFVI). UTFVI provides a comprehensive view of the thermal conditions in urban areas by considering both temperature and vegetation cover. This index helps identify areas with high thermal stress, which are critical for targeting UHI mitigation efforts. Zhang et al. (2006) demonstrated that UTFVI could effectively assess thermal comfort levels in urban parks, highlighting areas needing intervention to improve urban living conditions. The results of UTFVI values are divided into six categories (Excellent, Good, Normal, Bad, Worse, Worst), and each category corresponds to a fixed Ecological Evaluation Index (EEI), which was used for evaluating thermal comfort (Ahmed, 2018). A previous study by Naim and Kafy (2021) assessed the UTFVI and defined the relationship between land cover and surface temperature in Chattogram City to identify the temporal changes of intensity of the UHI. Therefore, the combination of LST, UTFVI and NDVI is essential for identifying and analyzing heat patterns across urban landscapes, which are critical for understanding the intensity and distribution of UHI. Thus, the present case study for Tiruppur Corporation considered these indices in order to model the spatial distributions of UHI and thermal comfort. The study would help to improve future urban planning, including the implementation of green city technologies.

Study area

Tiruppur is considered to be the most urbanized developing district of Tamil Nadu state in recent times. Tiruppur corporation is the fifth most agglomerated urban Centre of Tamil Nadu based on census of India 2011. It is located at 10˚14' N to 77˚27' E and 11˚20' N and 77˚56' E on the banks of the Noyyal River (figure 1). It covers an area of 160 sq. km and is situated 450 kilometres southwest of the state capital Chennai and about 50 kilometres east of Coimbatore. The climate of Tiruppur is tropical, with the mean maximum and minimum temperatures varying between 35°C and 22 °C (95 to 72 °F). The total population of the corporation as of the 2011 census was 8,77,778 individuals. Tiruppur has experienced significant fluctuations in rainfall over the years. A study by Kaviya and Elango (2021) indicates that the region has seen variable monsoonal patterns, with periods of drought alternating with years of intense rainfall. Specifically, annual rainfall has ranged from 400 mm in drought years to over 1200 mm during years of good rainfall.

These fluctuations have had substantial impacts on water resources, agricultural productivity, and urban water supply. Temperature trends in Tiruppur show a clear upward trajectory over the past few decades. According to a recent study by Gnanasekaran et al. (2022), there has been a marked increase in both average maximum and minimum temperatures. The study reports that the average maximum temperature has increased by 1.5°C, and the average minimum temperature has increased by 1.2°C over the past 30 years. This rise in temperature has been attributed to global warming and increased urbanization, which exacerbate the urban heat island effect. Over the past few decades, the city has transformed into a major centre for textile manufacturing and export. The study by Balaji and Sundararajan (2020) highlights the rapid expansion of textile units, driven by both domestic and international demand.

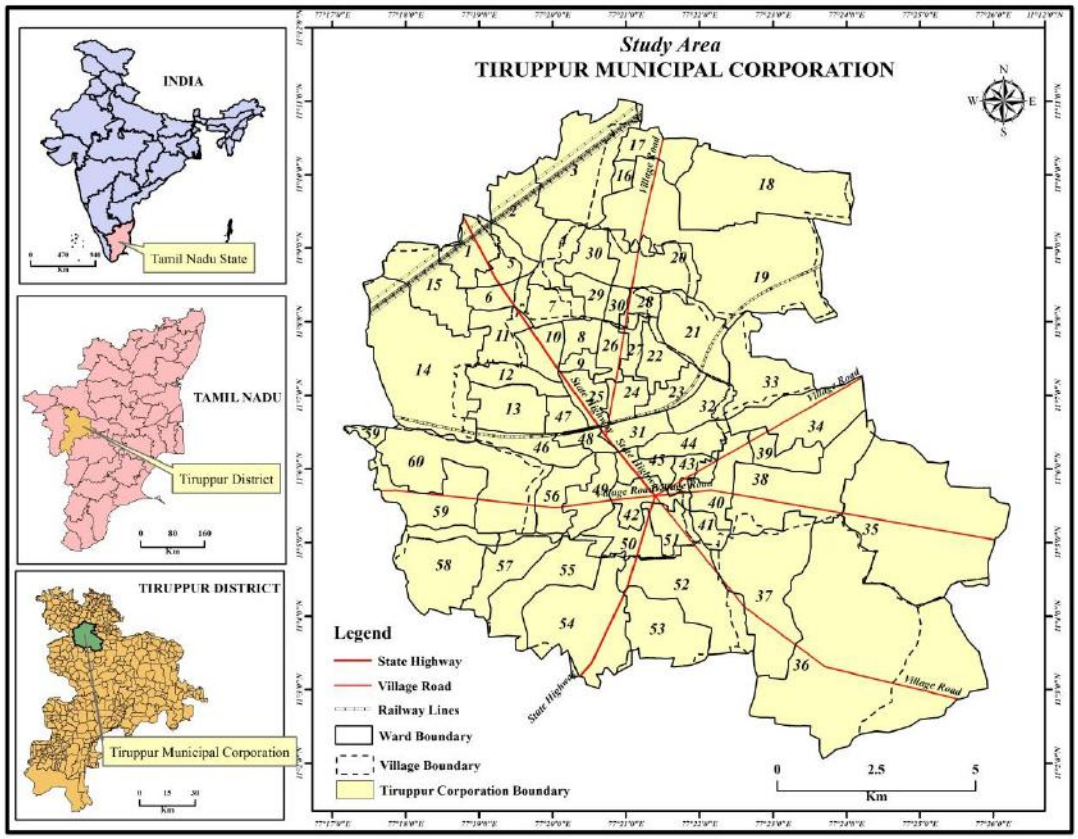

Figure 1: Location map of the Study Area with corporation and ward boundaries

Data Used and Methodology

The present study focused on modelling the Urban Heat Island of Tiruppur Municipal Corporation (TMC) using the Urban Thermal Field Variance Index for the years 1991, 2001, 2011 and 2021. The satellite images of Landsat 5 and 8 have been utilised from the Google Earth Engine Catalog for computing UTFVI. Computation of UTFVI

requires Normalised Difference Vegetation Index (NDVI) and Land Surface Temperature (LST), as shown in Figure 2. NDVI is calculated by utilising the red and near infrared (NIR) bands of Landsat data. Then, LST is calculated from the thermal bands of Landsat data through the mono-window algorithm (Li et al. 2022). The formulas for the calculation of LST and UTFVI are discussed below. The mean value of each season is considered for analysis and mapping.

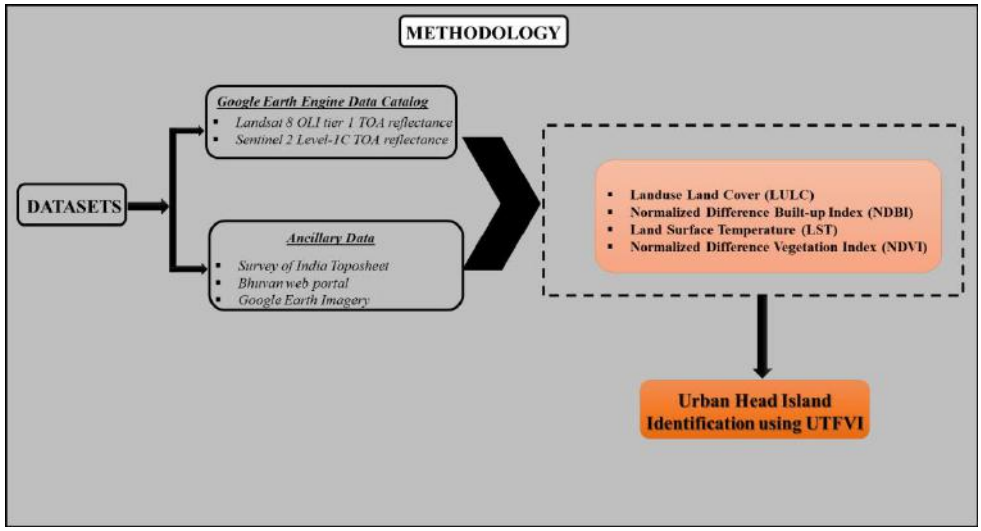

Figure 2: Methodological Framework

The radiance of the Landsat 5 image is calculated using the following equation (1):

$$L\lambda = LMIN\lambda + [(LMAX\lambda - LMIN\lambda) / QCALMAX] \times QCAL \quad \text{.....(1)}$$

Where, LMINλ = spectral radiance scales to QCALMIN (1.238), LMAXλ = spectral radiance scales to QCALMAX (15.303), QCALMIN = the minimum quantized calibrated pixel value (typically 1), QCALMAX = the maximum quantized calibrated pixel value (typically 255), QCAL = digital number.

The effective at-sensor brightness temperature (BT), also known as black body temperature, is obtained from the spectral radiance using Plank's inverse function (2).

$$BT = K2 / \ln (K1/L\lambda + 1) \quad \text{.....(2)}$$

Where, BT=Brightness temperature in Celsius, K1 (607.76) and K 2 = band-specific thermal conversion constant (Landsat 5 TM 1260.56), Lλ = Top of Atmospheric spectral radiance.

The final Land Surface Temperature (LST) is estimated by the equation (3),

$$BT = K2 / \ln (K1/L\lambda + 1) - 273.15 \quad \text{.....(3)}$$

Land Surface Temperature for Landsat 8 TIRS Sensor is calculated by conversion of DN values to at-sensor Radiance

$$L_{sensor\lambda} = M_\lambda * DN + A_\lambda \quad (4)$$

where, $L_{sensor\lambda}$ = spectral radiance (W/ (m2 * sr * μm)), M_λ = radiance multiplicative scaling factor for Band 10 = 0.0003342 (retrieved from Landsat 8 metadata file), A_λ = radiance additive scaling factor for Band 10 = 0.1 (retrieved from Landsat 8 metadata file) and DN = digital number.

Brightness temperature (TB) can be computed using the pre-launched calibration constants (K1 and K2) as expressed in the equation. Brightness temperature is the microwave radiation radiance travelling upward from the top of Earth's atmosphere. The calibration process has been done to convert thermal DN values of thermal bands to TB. Where, K_1= 774.8853, K_2 = 1321.0789 are retrieved from Landsat 8 metadata file.

$$T_B = \frac{K_2}{Ln(\frac{K_1}{L_\lambda}+1)} - 273.15 \quad (5)$$

The land surface emissivity values are obtained using equation (6).

$$\varepsilon = m.P_v + n \quad (6)$$

where, m = 0.004 and n = 0.986. PV is the proportion of vegetation extracted using equations 7 and 8.

$$P_v = \left[\frac{NDVI - NDVI_{min}}{NDVI_{max} - NDVI_{min}}\right]^2 \quad (7)$$

$$NDVI = \frac{NIR - RED}{NIR + RED} \quad (8)$$

where, NDVI is the normalized difference vegetation index. NDVI min and NDVI max are the minimum and maximum values of the NDVI, respectively. NDVI produces values in the range of -0.1 to +0.1, where vegetation areas will typically have values greater than zero, and the negative values indicate non-vegetative areas like urban, water, barren, ice, snow or clouds.

Emissivity corrected LST

Brightness temperatures assume that the Earth is a blackbody, which it is not, and this can lead to errors in surface temperature. In order to minimize these errors, emissivity correction is important and is done to retrieve the LST using an equation (9)

$$LST = {}^{T_B}\Big/_{1 + \left(\lambda * \frac{T_B}{C_2}\right) * Ln(\varepsilon)} \quad (9)$$

where, LST is the Land surface temperature (in degree Celsius ˚C), TB is the Brightness temperature, λ =10.8 μm is the effective wavelength of Landsat 8 OLI images, e is the land surface emissivity, which is equal to 1.438 x 10-2 mK in which σ is the Boltzmann constant (1.38 x 10-23 J/K), h is the Plank's constant (6.623 x 10-34 Js) and c is the velocity of light (3 x 108 m/s).

Land Use / Land Cover (LULC)

The LULC were prepared by utilizing the supervised classification algorithm of Support Vector Machine (SVM). SVM is very effective for LULC classification due to their high accuracy, ability to handle non-linear relationships through kernel functions, and robustness to overfitting. Recent research by Maxwell et al. (2023) highlights SVM's effectiveness in producing reliable and precise LULC maps compared to other machine-learning algorithms. SVM's adaptability to high-dimensional data and resistance to outliers make it an excellent choice for remote sensing applications. In this study, the accuracy assessment was done through the Confusion Matrix, and the overall accuracy was above 85% for all the years.

Urban Thermal Field Variance Index (UTFVI)

The UTFVI was estimated using equation (10) and subsequently was classified into six ecological evaluation indices (EEI) and urban heat Island phenomena, as shown in Table 1, which were used for evaluating the level of thermal comfort (Liu and Zhang 2011).

$$UTFVI = \frac{T_s - T_{mean}}{T_{mean}} \quad \text{.....(10)}$$

where TS is the LST (˚C) and Tmean is the mean LST (˚C).

Table 1. Threshold values of Urban Thermal Field Variance Index, Urban Heat Island Class and Ecological Evaluation Index

Urban Thermal Field Variance Index (UTFVI)	Urban Heat Island (UHI)	Ecological Evaluation Index
<0	None	Excellent
0.000 – 0.005	Weak	Good
0.005 – 0.010	Middle	Normal
0.010 – 0.015	Strong	Bad
0.015 – 0.020	Stronger	Worse
>0.020	Strongest	Worst

Results and Discussion

The factors such as the LULC, NDVI, LST, NDBI and UTFVI are computed to identify the UHI of the TMC and its surroundings. All the results are segmented with six rings of each 2km in order to analyse the surrounding scenario. The buffer rings are

selected based on the centroid of the study area boundary. The results and discussion of the following factors are given below.

Landuse Land Cover (LULC)

The LULC for the study region has been classified based on the NRSC level 1 classification, which includes water bodies, built-up, vegetation, agricultural land, and barren land for the temporal years 1991, 2001, 2011, and 2021. In 1991, the built-up of ring 1 was about 54.31% which is a constant decrease from ring 1 to ring 6 and is about 3.59 %. Similarly, the water bodies also constantly decrease from ring 1(4.60%) to ring 6 (0.90%). Then, the vegetation class is very low in ring 1, covering only 8.73% of the area, which has a sudden increase of 18.82% in ring 2, and its proportion increases to 20.44% in ring 6. Further, the barren and agricultural land has uneven distributions of variation between rings 1 and 6, as shown in Figure 3, in which the agricultural land shows a greater variation from 13.47% to 56.69% between rings 1 and 6.

In 2001, the built-up of ring 1 increased from 54.31 % to 82.62 % and in ring 6, 3.59% to 4.27 compared with the previous decade. The number of water bodies has also been reduced compared with the 1991 result. The vegetation also decreased from 8.73% to 2.37% in ring 1 and 20.44% to 11.87 % in ring 6. The barren land and agricultural land have a greater variation where the barren land decreased from 18.89% to 3.26 % in ring 1 and increased from 18.38 % to 19.41% in ring 6; in the case of agriculture, it decreased from 13.47% to 9.65 % in ring 1 and increased from 56.69% to 63.74% in ring 6 between the years of 1991 and 2001.

Compared with the year 2001, the built-up was increased in ring 1 from 82.62% to 84.25% and in ring 6 it increased to 4.27% to 5.43% in 2011. The water bodies were also reduced to 0.04% in 2011 compared to previous temporal years. The vegetation decreased from 2.37% to 1.02% in ring 1 and 11.87 % to 8.16% in ring 6 in 2011. The barren land has decreased from 3.26% to 2.38% in ring 1 and 19.41% to 15.37% in ring 6. However, in Agriculture it has increased from 9.65% to 12.30% in ring 1 and 63.74% to 70.93% in ring 6 in 2011.

In 2021, the built-up has slightly increased from 84.25% to 86.23% in ring 1 and 5.43% to 9.80% in ring 6 compared to 2011. In ring 1, water bodies are 0.04% in 2011 and 2021; in ring 6, it has increased from 0.10% to 1.20% in 2021. The vegetation has been increased from 1.02% to 8.17% in ring 1 and 8.16% to 16.16% in ring 6. The barren land has increased from 2.38% to 3.82% in ring 1 and 15.37% to 44.67% in ring 6 in 2021. Agriculture has been reduced from 12.30% to 1.74% in ring 1 and ring 6, and it has reduced to 70.93% to 28.16% in 2021.

Normalized Difference Vegetation Index (NDVI)

The values of NDVI are categorised into five classes as very low (<0.2), low (0.2 – 0.3), moderate (0.3 – 0.4), high (0.4 – 0.5) and very high (> 0.5) for all the four years of 1991, 2001, 2011 and 2021 (figure 4). It is interpreted from the results that the spatial distribution of the NDVI class is very low in ring 1 and is gradually increasing in the consequent rings towards ring 6 in almost all four years of 1991, 2001, 2011 and 2021. In ring 1 of 1991, the mean value of NDVI is marked as 0.253, which has decreased across the years 2001, 2011 and 2021 to 0.181, 0.176 and 0.174, respectively. Similarly, in ring 3, there was a marked decrease in mean values from 0.343 in 1991 to 0.207 in 2021. Further, in the 6th ring of 1991, it was noticed as 0.389 and decreased to 0.331 (2001), 0.257 (2011) and 0.238 (2021).

In ring 1 of 2001, the mean value of NDVI is marked as 0.181, which decreased across the years of 2011 and 2021 to 0.176 and 0.174, respectively. Similarly, in ring 4, there was a marked increase in mean values from 0.305 in 2001 to 0.211 in 2021. The following 5th ring gradually decreased in the mean values of 0.251 in 2011. Additionally, in the 6th ring of 2001, it was noticed as 0.331 and increased to 0.257 (2011) and 0.238 (2021).

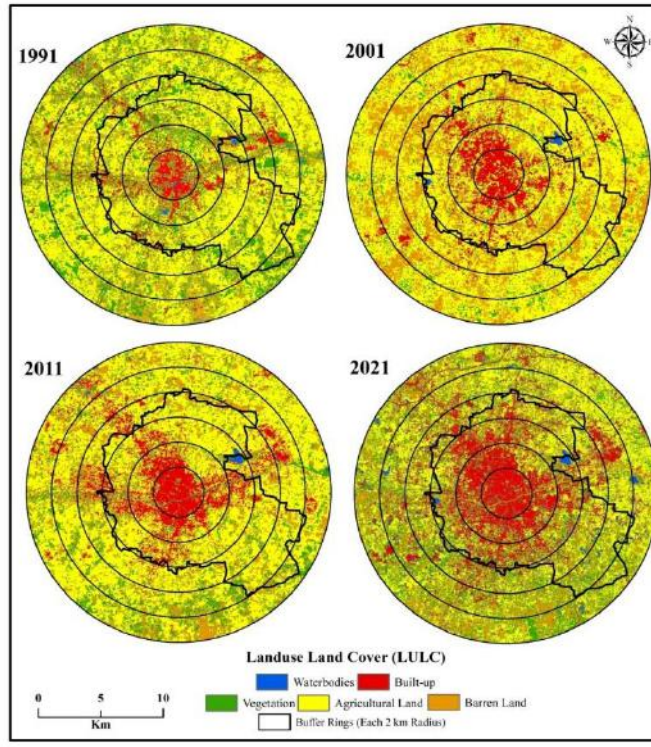

Figure 3: Spatial Distribution of Landuse and Land cover

In 2011, there was a decrease in NDVI values compared to 2001 across all rings, indicating potential changes in vegetation density over the decade. Despite this decrease, the general pattern of higher NDVI values in the inner rings persists, with ring 6 maintaining the highest value at 0.257. Similarly, in ring 1, there was also a marked increase in mean values from 0.176 in 2011 to 0.174 in 2021. The 3rd ring gradually decreased in the mean values of 0.217 in 2011. Further, in the 6th ring of 2011, it was noticed as 0.257 and decreased to 0.238 (2021). By 2021, NDVI values will continue to decline compared to 1991, 2001, and 2011. This decline suggests potential environmental changes affecting vegetation health. However, the inner rings consistently show lower NDVI values compared to the outer rings across all years. Ring 6 maintains the highest NDVI value in 2021, with lower values in previous years, such as ring 1 performing the lowest value in 2021 (0.174). In this study area, NDVI values significantly changed from 2011 to 2021, and the main reason for the growth of urbanization and increasing human activities.

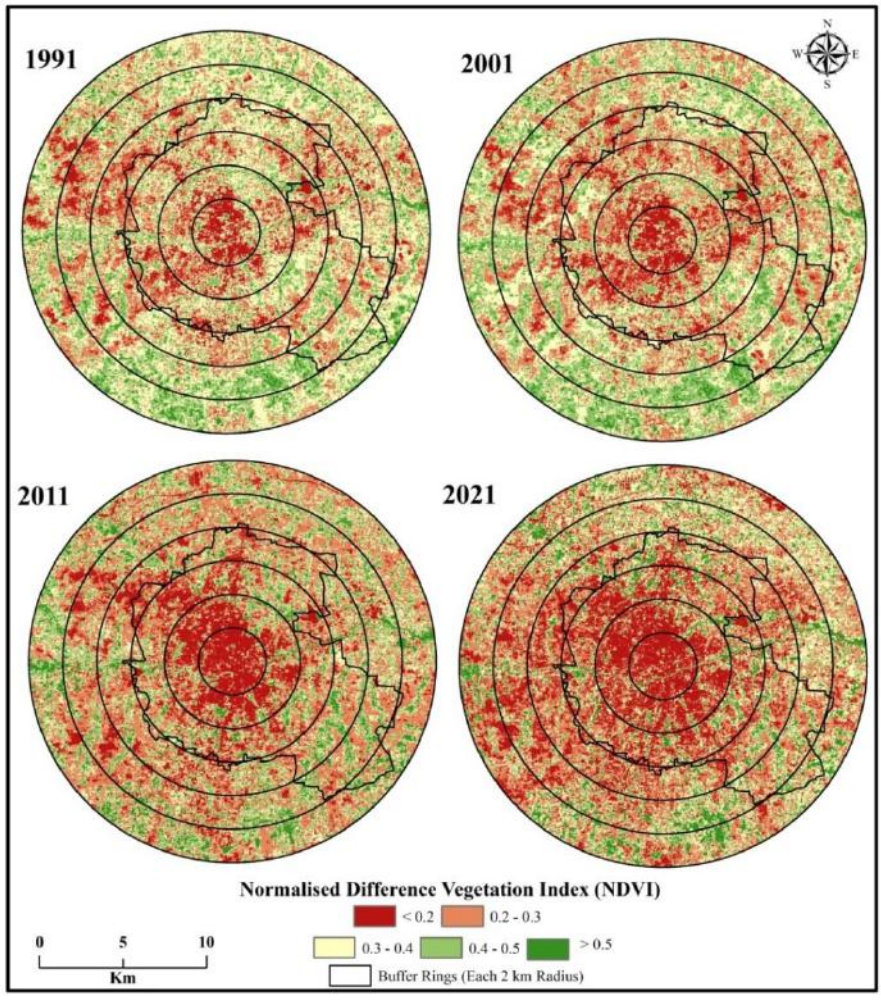

Figure 4: Spatial Distribution of Normalized Difference Vegetation Index

Land Surface Temperature (LST)

In 1991, the Land Surface Temperature (LST) values across all rings remained relatively stable over the decade, with minor anomalies observed. Rings 1 to 3 showed LST values ranging from 39.08 to 40.22, indicating a consistent temperature increase. Rings 4 to 6 also exhibited stable LST values, with temperatures ranging from 40.20 to 40.37 (figure 5).

By 2001, the LST values remained largely consistent compared to 1991, with minimal changes observed across all rings. Rings 1 to 4 maintained LST values of 40.22 to 40.27, indicating stable temperature patterns similar to the previous decade. Similarly, Rings 5 and 6 exhibited minor changes in LST values, ranging from 40.20 to 40.37. Here, in the year 2001, the outer region exhibited high LST values due to the distribution of a high amount of barren land without vegetation, which exhibits a larger amount of surface temperature than the core built-up areas.

In 2011, there was a noticeable increase in LST values across all rings compared to previous years. Rings 1 to 3 experienced a significant temperature rise, with LST values ranging from 45.91 to 43.33, indicating warmer conditions. Similarly, Rings 4 to 6 showed LST values ranging from 40.58 to 40.34. As a result, increasing temperatures across the study area in 2011 are potentially indicative of environmental changes or urban growth effects. By 2021, there was a slight decrease in LST values compared to 2011, although temperatures remained relatively high across all rings. Rings 2 to 4 exhibited LST values ranging from 42.19 to 41.21, indicating warm conditions. Similarly, Rings 5 to 6 maintained temperatures ranging from 39.68 to 40.31. Despite the slight decrease, the data suggests continued warmth across the study area in 2021, showing the processes of urbanization and some ongoing factors influence the surface temperature.

Normalized Difference Built-up Index (NDBI)

The purpose of the Normalized Difference Built-up Index (NDBI) in this study is to identify the Urban Thermal Field Variance Index (UTFVI) accurately to quantify and map urban built-up areas, which are critical in understanding the urban heat island (UHI) effect. The NDBI is calculated for the study region across the years of 1991, 2001, 2011 and 2021. These results are compared with Google Earth, and the threshold value for the built-up regions is identified as 0.36, by which the NDBI values are classified into two classes: built-up and non–built–up class. The results clearly illustrate the spatial distribution and development of built-up across the rings in each year and also the development across the temporal years (figure 6).

In 1991, the intensity of built-up was only marked in ring 1 and ring 2, whereas in other rings the distribution of built-up was very dispersed and scattered. However, during the year 2001, the concentration of built-up extended towards ring 3 and also the intensity in rings 1 and 2 increased when compared to the previous decade. The condition in 2011

is almost similar to that of the distribution in 2001, since the extension of built-up concentration is absent in the fourth ring; instead, the intensity of built-up is increased in the rings 1, 2, and 3. Further, in 2021, a larger increase of built-up was noticed in all the rings, and the intensity of the built-up was extended to ring 4 of the study region. In addition, it is noticed that the intensity of built-up has attained its maximum extent in the rings 1 and 2.

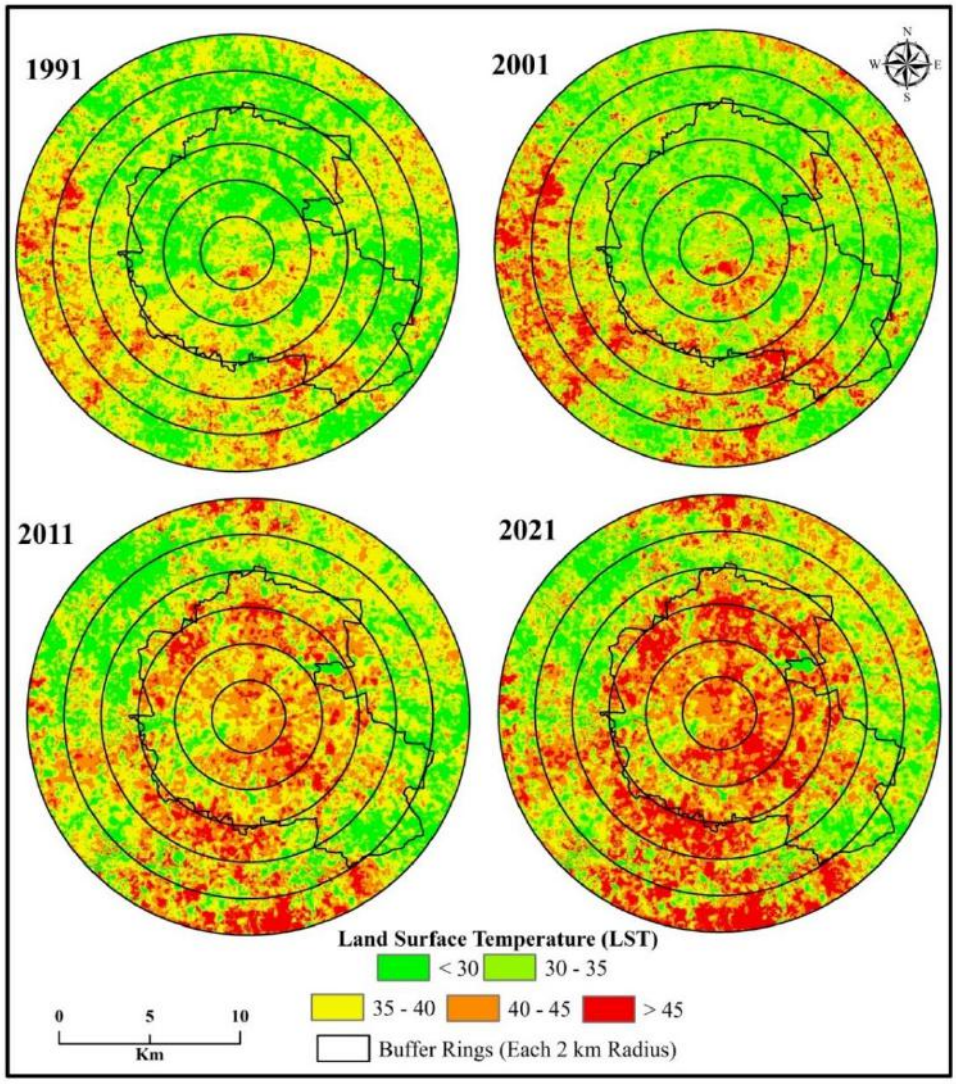

Figure 5: Spatial Distribution of Land Surface Temperature

Urban Thermal Field Variance Index (UTFVI)

The urban thermal field variance index is basically a conceptual factor based on surface temperature, which also defines urban heat islands. The Urban thermal field is

classified into six classes based on the Urban Heat Island aspect such as none (<0), weak (0.000 -0.005), middle (0.005-0.010), strong (0.010-0.015), stronger (0.015-0.020), strongest (>0.020) for 1991, 2001, 2011, and 2021. As per the results of UTFVI, the temperature gradually increases from 1991 to 2021 (figure 7).

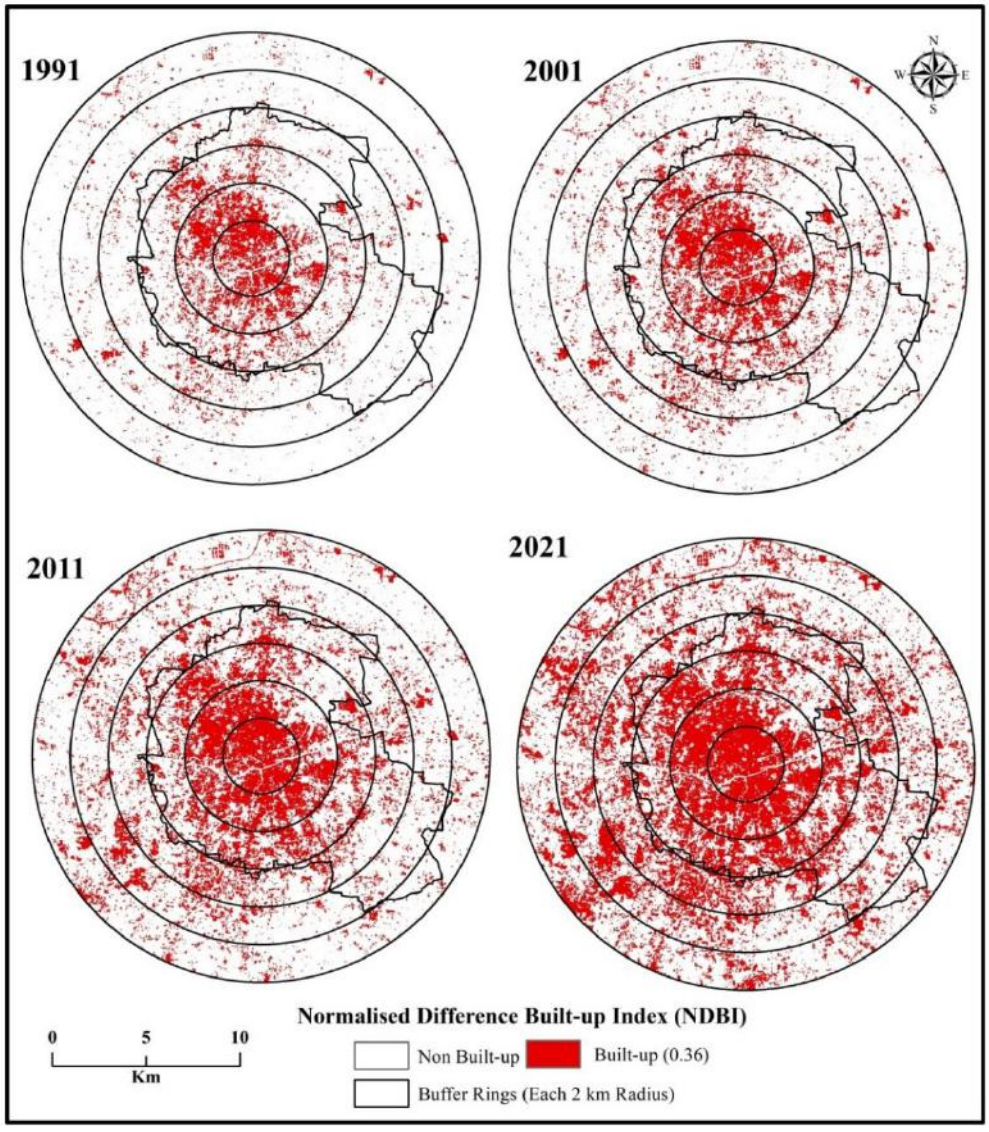

Figure 6: Spatial Distribution of Normalized Difference Built-up Index

In 1991, the structural distribution of thermal variance was relatively low compared to the respective years. In ring 1 there is only a distribution of strong and stronger classes where it is changed to a high distribution of stronger and a low distribution of strong classes

in the same ring during the year 2001. This condition is even more different in 2011, when some of the stronger UHI conditions are changed to the strongest UHI conditions. Thus, in the year 2021, most of the parts of ring 1 fall under the strongest UHI condition. This is the similar condition in the ring 2 as well in all the observed years. However, in ring 3, during 1991, there is a maximum distribution of strong UHI conditions along with the distribution of none, weak and middle class. However, this distribution has tremendously changed across the years 2001, 2011 and 2021 as the none-to-middle UHI class is reduced, and most of the portions of ring 3 are increased with the strong to strongest class condition. Moreover, as mentioned in the LST, here in the year 2001, the UTFVI value is higher in the outer ring than in the core rings due to the abundant distribution of barren land in the outer rings. It is noticed from the result of UTFVI that the Tiruppur Municipal Corporation is highly affected by the heat stress that is from ring 1 to ring 4 of 2021 is falls under the stronger and strongest UHI class. In addition, the northwest portion of the study region is also affected by the strong to strongest UHI condition in all four years.

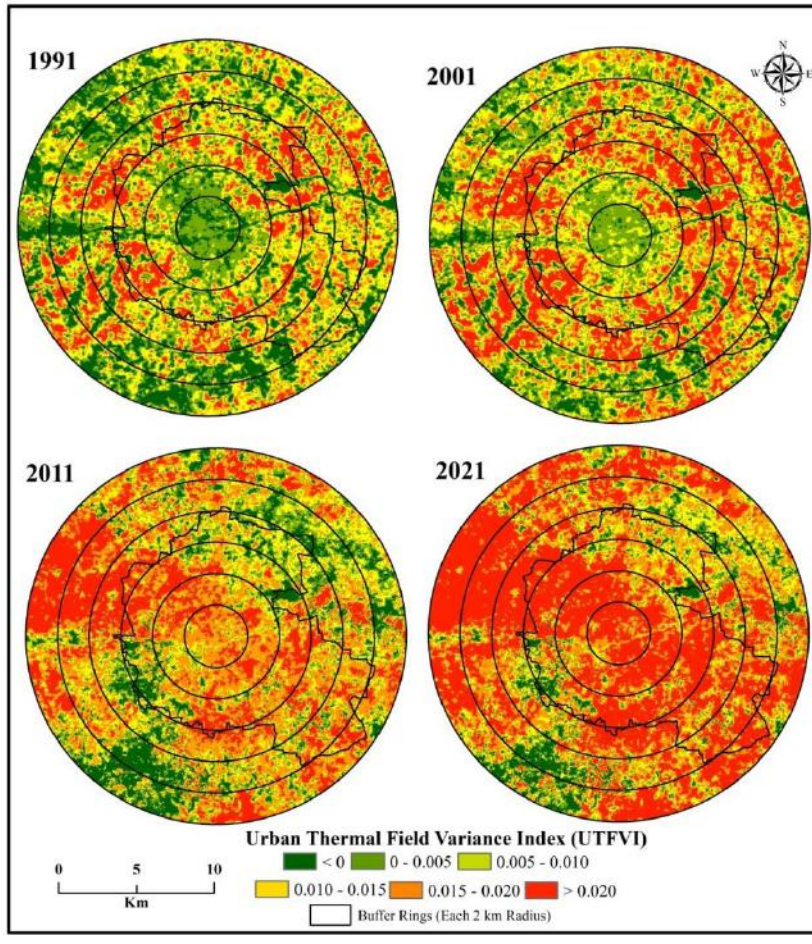

Figure 7: Spatial Distribution of Urban Thermal Field Variance Index

Identifying the trend of UHI is very helpful in designing appropriate adaptation methods for sustainable urban growth. A previous study by Moisa et al. (2022) found that the urban thermal environment is highly influenced by changes in LULC. In this present study, the temporal changes of the LULC along with the LST, NDVI, NDBI, and UTFVI were identified to determine the influence of urbanization on UHI phenomena in the study area. A similar study by Moisa and Gemeda (2022) assesses the urban thermal field variance index and thermal comfort level of Addis Ababa metropolitan city, Ethiopia. Their study categorised them into six zones to identify the UHI.

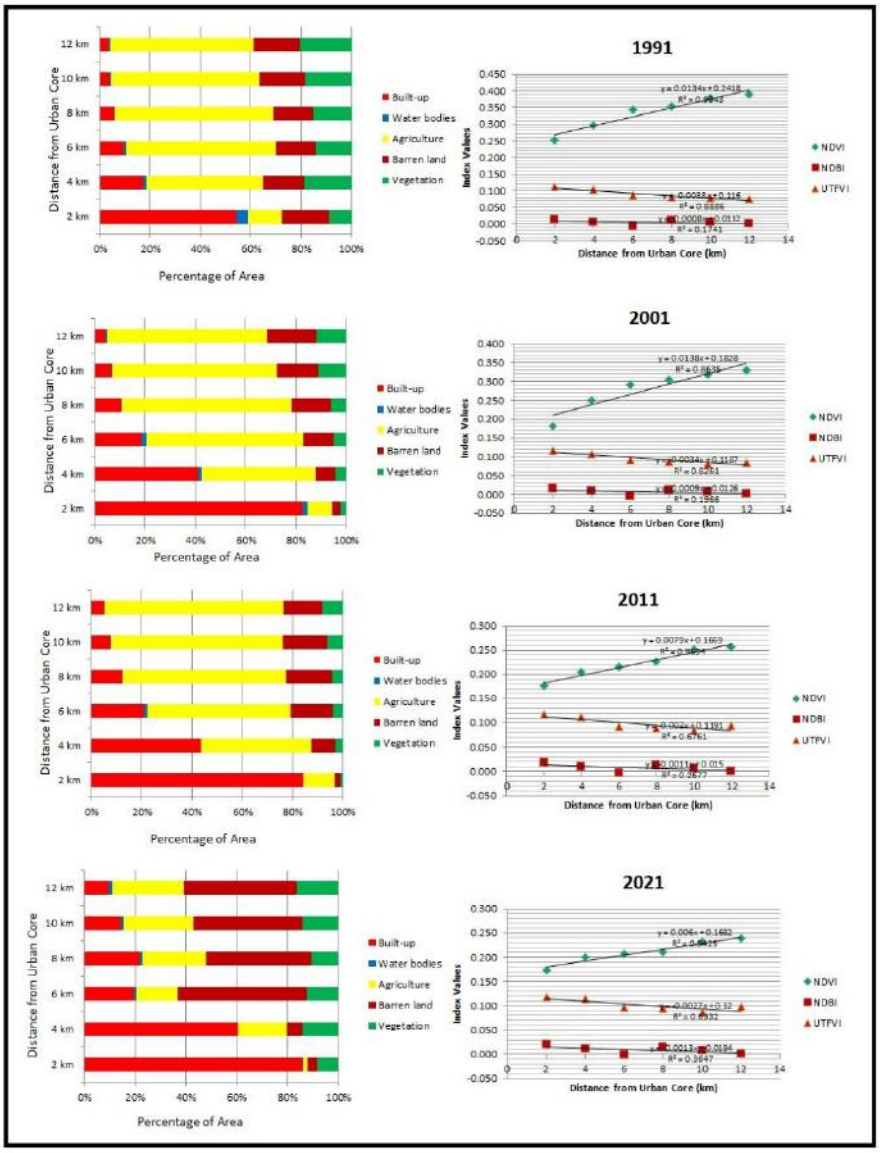

Figure 8: Graphical Representation of land use / Land cover, NDBI and UTFVI

In the present study, during 1991, the structural distribution of thermal variance was relatively low compared to the recent years. In ring 1, there is only a distribution of strong classes, which is changed to stronger classes in the year 2001. This condition became even more intense in 2011, when some of the stronger UHI conditions were changed to the strongest UHI conditions. Thus, in the year 2021, most of the parts of ring 1 fall under the strongest UHI condition. This condition is supported by the other factors where the NDVI values are very low, indicating very low vegetation; the LST values are high, indicating very high temperature; and the NDBI values are also very high, indicating high intensity of built-up distribution. The result of LULC also supports the UTFVI result with the higher distribution of built-up in the same ring. Accordingly, the strong to strongest classes are increasing exponentially during these years (1991 to 2021) and are mostly concentrated over the core in the central rings 1 and 2 and also in the northwestern portions of the study region (rings 4, 5, 6) during the year 2011 and 2021. However, it is observed that during the years 1991 and 2001, the core areas exhibited less LST and UTFVI than the outer rings, which have a high distribution of barren land without vegetation, which poses a higher surface temperature than the built-up (figure 8). This condition is also supported by the higher decrease of vegetation (NDVI), increase of temperature (LST) and the increase of built-up (NDBI and LULC). By identifying the areas most affected by UHI, this research provides a clear spatial understanding of heat distribution within the city. The findings can be leveraged to prioritize cooling measures in the most vulnerable neighbourhoods. Incorporating more green spaces and implementing green roofing and cool roofing technologies can foster a more resilient urban environment in Tiruppur city.

Conclusion

The present study aims to identify the impact of urbanization on the increasing temperature and development of urban heat islands in Tiruppur city. The urban expansion and distribution are inferred by analysing the LULC, NDVI, and NDBI changes from 1991 to 2021 at a decade interval. These spatio-temporal changes were compared with temperature analysis by computing LST and UTFVI. The result infers that the strong to strongest classes are increasing exponentially from 1991 to 2021 and are mainly concentrated over the city core, such as rings 1 and 2, and in the northwestern portions of the study region, in rings 4, 5 and 6. This inference is supported by the decrease of vegetation (NDVI), increase of temperature (LST) and the increase of built-up (NDBI and LULC). Thus, in the near future, this urban heat island will increase enormously to the outer rings and affect all the life forms. The findings of this study offer crucial insights that can significantly aid governance in devising effective strategies to combat urban heat and improve the overall quality of life for residents in TMC. Policymakers can use these insights to enforce stricter regulations on building materials and urban designs that contribute to heat retention, ensuring that resources are allocated efficiently and effectively.

Competing Interests

The authors declare that there are no competing interests.

Acknowledgement

Masilamani Palanisamy is the awardee of ICSSR minor research project (File No. 02/3/SC/2021-22/ICSSR/RP/MN). This paper is largely an outcome of the Research project sponsored by the Indian Council of Social Science Research (ICSSR). However, the responsibility for the facts stated, opinions expressed, and the conclusions drawn is entirely that of the author. The authors would like to thank the Department of Geography (SAP DRS-II, RUSA 2.0) Bharathidasan University for letting to utilize the lab facilities and their support. All authors would like to thank Prof. K. Kumaraswamy and Prof. R. Jegankumar for their support. The authors extend their thanks to Dr. S. Abdul Rahaman, Mr. K. Prakash, Mr. J. Killivalavan and Ms. Thanuja Krishnan R for their support.

References

1. Abdikan, S., Balik Sanli, F., Sunar, F., & Ehlers, M. (2014). A comparative data-fusion analysis of multi-sensor satellite images. International Journal of Digital Earth, 7(8), 671-687.
2. Ahmed, S. (2018). Assessment of urban heat islands and impact of climate change on socioeconomic over Suez Governorate using remote sensing and GIS techniques. The Egyptian Journal of Remote Sensing and Space Science, 21(1), 15-25.
3. Balaji, P., & Sundararajan, M. (2020). Their study provides insights into the growth of the textile industry in Tiruppur, discussing its economic significance and the factors driving this expansion.
4. Becerril-Piña, R., Díaz-Delgado, C., Mastachi-Loza, C. A., & González-Sosa, E. (2016). Integration of remote sensing techniques for monitoring desertification in Mexico. Human and Ecological Risk Assessment: An International Journal, 22(6), 1323-1340.
5. Bongaarts, J. (2020). United Nations Department of Economic and Social Affairs, Population Division World Family Planning 2020: Highlights, United Nations Publications, 2020. 46 p.
6. Brandsma, T., & Wolters, D. (2012). Measurement and statistical modelling of the urban heat island of the city of Utrecht (the Netherlands). Journal of Applied Meteorology and Climatology, 51(6), 1046-1060.
7. Chen, J., Li, X., Zhao, W., & Wu, J. (2023). Integration of NDBI and other remote sensing indices for comprehensive analysis of urban heat island effects: A case study in Beijing, China. Remote Sensing of Environment, 280, 113247. doi:10.1016/j.rse.2022.113247
8. Díaz, BM., & Blackburn, GA. (2003). Remote sensing of mangrove biophysical properties: evidence from a laboratory simulation of the possible effects of background variation on spectral vegetation indices. Int JRemote Sens 24:53–73.
9. Gnanasekaran, M., Rajendran, V., & Prakash, K. (2022). The research documents the increasing temperature trends in Tiruppur, exploring the contributing factors and potential impacts on urban life.

10. Gordon, A., Simondson, D., White, M., Moilanen, A., & Bekessy, S. A. (2009). Integrating conservation planning and landuse planning in urban landscapes. Landscape and urban planning, 91(4), 183-194.
11. Kaviya, R., & Elango, L. (2021). This study examines the variability in rainfall patterns in Tiruppur, highlighting the implications of these changes on water resources and urban planning.
12. Kesavan, R., Muthian, M., Sudalaimuthu, K., Sundarsingh, S., & Krishnan, S. (2021). ARIMA modeling for forecasting land surface temperature and determination of urban heat island using remote sensing techniques for Chennai city, India. Arabian Journal of Geosciences, 14(11), 1-14.
13. Li, J., Wang, X., Wang, X., Ma, W., & Zhang, H. (2011). Remote sensing evaluation of urban heat island and its spatial pattern of the Shanghai metropolitan area, China. Ecological Complexity, 8(2), 177-183.
14. Li, X., Zhang, X., Wang, Y., & Liu, Q. (2022). Improved split-window algorithm for land surface temperature retrieval from MODIS data. Remote Sensing of Environment, 265, 112660. https://doi.org/10.1016/j.rse.2021.112660
15. Liu, L., & Zhang, Y. (2011) Urban heat island analysis using the Landsat TM data and ASTER data: a case study in Hong Kong. Remote Sensing 3(7), 1535–1552. https:// doi. org/ 10. 3390/ rs307 1535
16. Maxwell, A. E., Warner, T. A., & Fang, F. (2023). Implementation of support vector machines in remote sensing: Recent advances and applications. Remote Sensing, 15(3), 456-472.
17. Moisa, M. B., & Gemeda, D. O. (2022). Assessment of urban thermal field variance index and thermal comfort level of Addis Ababa metropolitan city, Ethiopia. Heliyon, 8(8).
18. Moisa, M. B., Merga, B. B., & Gemeda, D. O. (2022). Urban heat island dynamics in response to land use land cover change: a case of Jimma city, southwestern Ethiopia. Theoretical and Applied Climatology, 149(1-2), 413-423.
19. Naim, M. N. H., & Kafy, A. A. (2021). Assessment of urban thermal field variance index and defining the relationship between land cover and surface temperature in Chattogram city: a remote sensing and statistical approach. Environmental Challenges, 4, 100107.
20. Padmanaban, R., Bhowmik, A. K., & Cabral, P. (2017). A remote sensing approach to environmental monitoring in a reclaimed mine area. ISPRS international journal of geo-information, 6(12), 401.
21. Prakash., Rajagopal, Jegankumar., & Libina, Rs. (2023). Analysing spatial and geometrical patterns of urbanization using spatial metrics – A case study of Tiruchirappalli urban, India. 10.21203/rs.3.rs-2726357/v1.
22. Ranagalage, M., Estoque, R. C., Handayani, H. H., Zhang, X., Morimoto, T., Tadono, T., & Murayama, Y. (2018). Relation between urban volume and land surface temperature: A comparative study of planned and traditional cities in Japan. Sustainability, 10(7), 2366.

23. Sabet Sarvestani, M., Ab Latif Ibrahim., & Pavlos Kanaroglou. (2011).“Three Decades of Urban Growth in the City of Shiraz, Iran: A Remote Sensing and Geographic Information Systems Application.”. Cities, 28(4), 320-329.
24. Stow, D. A., & Chen, D. M. (2002). Sensitivity of multitemporal NOAA AVHRR data of an urbanizing region to land-use/land-cover changes and misregistration. Remote sensing of Environment, 80(2), 297-307.
25. The World’s Cities in 2016. T. W. C. in 2016—D. B. (ST/ESA/S.A.), Population Deprtment, Department of Economic and Social Affairs, United Nations. 2016.
26. Wang, R., Derdouri, A., & Murayama, Y. (2018). Spatiotemporal simulation of future land use/cover change scenarios in the Tokyo metropolitan area. Sustainability, 10(6), 2056.
27. Weng, Q., Lu, D., & Schubring, J. (2004). Estimation of land surface temperature–vegetation abundance relationship for urban heat island studies. Remote sensing of Environment, 89(4), 467-483.
28. Zhang, H., Wang, Y., & Zhang, Y. (2006). Assessing the thermal field of urban parks using remote sensing data. International Journal of Remote Sensing, 27(19), 4199-4214.
29. Zhao, L., Lee, X., Smith, R. B., & Oleson, K. (2014). Strong contributions of local background climate to urban heat islands. Nature, 511(7508), 216-219.
30. Zhou, B., Erell, E., Hough, I., Rosenblatt, J., Just, A. C., Novack, V., & Kloog, I. (2020). Estimating near-surface air temperature across Israel using a machine learning based hybrid approach. International Journal of Climatology, 40(14), 6106-6121.
31. United Nations. (2018). World Urbanization Prospects: The 2018 Revision. Department of Economic and Social Affairs, Population Division. Retrieved from https://population.un.org/wup/Publications/
32. Peng, S., Piao, S., Zeng, Z., Ciais, P., Zhou, L., Li, L. Z. X., Myneni, R. B., Yin, Y., & Zeng, H. (2021). Urban heat island impacts on land surface temperature trends in a rapidly urbanizing region. International Journal of Climatology, 41(3), 1710-1720. doi:10.1002/joc.6915
33. Xiao, J., Shen, Y., Ge, J., Tateishi, R., Tang, C., Liang, Y., & Huang, Z. (2020). Evaluating urban expansion and land use change in Shijiazhuang, China, using GIS and remote sensing. Remote Sensing, 12(8), 1334. doi:10.3390/rs12081334
34. Zhang, Y., Balzter, H., Liu, B., Chen, Y., & Zhang, X. (2022). A comprehensive analysis of urban heat island dynamics using multi-sensor remote sensing data: A case study of the Yangtze River Delta, China. Remote Sensing of Environment, 271, 112890. doi:10.1016/j.rse.2021.112890

The Indian Geographical Journal
Volume 98 (1) June - 2023, pp 68-86
ISSN 0019-4824

PATTERNS AND DETERMINANTS OF SHORT-TERM YOUTH MIGRATION IN UTTAR PRADESH

Saumya Chauhan, E. Venkatesham

Department of Geography, Central University of Tamil Nadu, Thiruvarur, Tamil Nadu
Corresponding author: venkatepl@cutn.ac.in

Abstract

This study investigates short-term internal migration patterns among young adults in Uttar Pradesh, focusing on age-sex wise reasons and migration streams in the state. The research specifically targets migrants aged 15-34, identified based on their last residence, with durations less than one year. This age bracket has been chosen for its heightened likelihood of engaging in migration, forming the core demographic base under investigation. The analysis has been categorised into four migration streams– Rural to Rural, Rural to Urban, Urban to Rural and Urban to Urban. Utilising 2011 Census data, the research identifies rural-to-rural migration as dominant, mostly led by marriage-induced movements. The analysis reveals distinct gender disparities, with male migrants more prevalent, especially in rural-to-urban and urban-to-urban streams. Work/employment emerges as a significant factor in migration decisions, while education-related migration remains low. The results have been validated by the latest data available for migration from PLFS for 2020. The findings shed light on societal dynamics, emphasizing the pivotal role of marriage and employment in shaping migration trends among Uttar Pradesh's young population.

Keywords: Short-term migration, Migration streams, Intra-state migration, Gender disparities

Introduction

Migration serves as a catalyst for social transformation within societies (Mahapatro, 2020). Despite international migration garnering more attention, internal migration significantly surpasses it, with a four-fold greater volume, as highlighted by the UNDP (2009) and Bhagat (2011). The decision to migrate plays a pivotal role for individuals and groups, influenced by factors such as community, gender, age, educational attainment, socioeconomic background, environmental considerations, and marriage (Khan et al., 2016). These variations lead to behavioural changes, prompting individuals to either move to or depart from a particular location (Clarke,1980), indicating distinctions between migrants and non-migrants (Khan et al., 2016).

Historical census data, starting from 1881, reveals the evolution of migration-related inquiries in India. The focus shifted from the place of birth to the location of the last home, providing insights into return migration dynamics. In 1981, "reasons for migration" were introduced, categorized into employment, education, family relocation, marriage, and

others. The 2001 Census added, "moved after birth," and natural calamities were merged into "others" (Census of India, 2001). Short-term migration, defined as residing in a place for three months to less than 12 months (Global Migration Indicators 2021), or less than 1 year (Census quest., 2011), is a noteworthy aspect.

Motivations for migration, as theorized by Premi (1984), encompass factors in the origin place, destination area, intervening obstacles, and individual factors. Census data from India identifies seven major reasons for migration, with marriage alone accounting for 49% of total migration nationally, followed by household relocation, other reasons, post-birth relocation, and work and education (Tumbe, 2012). Internal migration is predominantly observed in the rural-to-rural stream, dominated by male migrants aged 15-34 due to work and employment reasons, while female migration is primarily induced by marriage (Khan et al., 2016). Internal migration is also linked to internal brain drain and correlates strongly with livelihood options among rural poor communities, particularly from Scheduled Castes (SCs) and Scheduled Tribes (STs) (Bhagat & Keshri, 2021).

Several studies highlight the multifaceted impact of internal migration. While some argue that short-term migration reduces young migrants' engagement in labour activities, enhancing the educational quality and delaying the age of migration (Lahiri, 2020), others approach it from the perspective of seasonal migrants, directly connecting it to socio-economic variations. Viewing internal migration as stepwise migration from rural areas is another perspective (Majumdar & Taukeer, 2019).

Social status plays a pivotal role in migration (singhatana, 2017), with evidence from rural Uttar Pradesh suggesting that male migrants from upper castes possess more skills and educational attainment, while those from lower castes often lack in these areas, leading to engagement in informal sectors with fewer degrees and skills (Singh, 2018). Narrowing the focus, studies explore the experiences of Dalits in the new market-oriented economic model in Uttar Pradesh, shedding light on opportunities and needs within this community (Kapur et al., 2010).

It is noticeable that even after identifying the most prone migrating population are young (15-34 years), as pointed out by Wankhede, (2021), they have not been approached minutely through different migration streams. Being among the top three contributors of migration, Uttar Pradesh has been studied seldom from the point of view of young adult migrants (UN, 2009 and Khan, 2016) and this paper tries to fill this gap. The study of UP needs to be explored as it has a huge population to supply in the migration streams, and the reasons hidden behind migrations may vary over time. The paper traces the volume of short-term migrants, categorising them by gender and different age groups across all migration streams and analyse the gender-specific reasons for internal short-term migration within the age group of 15 to 34 years across diverse migration streams in the state.

Study Area

Uttar Pradesh has been selected for this study due to its rich abundance of natural

resources capable of sustaining a significant population. The state spans latitudes 23° 52'N to 31° 02'N and longitudes 77° 04'E to 84° 03'E. Bordered by Nepal and Uttarakhand to the north, Bihar and Jharkhand to the east, Madhya Pradesh and Chhattisgarh to the south, Rajasthan to the southwest, Haryana and Delhi to the west, and Himachal Pradesh to the northwest, Uttar Pradesh is strategically located. Administrative divisions are organized into 18 divisions and 75 districts. Covering an area of 240,928 sq. km, Uttar Pradesh ranks fourth among all states, yet it claims the top spot in population with 199.58 million people according to the 2011 Census. The male population constitutes 104.48 million, and the female population is 95.33 million, contributing to 16.5% of the national population. Uttar Pradesh holds the third position in population density, with 829 persons per sq. km. The sex ratio stands at 912 females per 1000 males, and literacy rates indicate 77.3% for males and 57.2% for females. Despite its vast expanse, the state is predominantly agrarian, with 77.7% of the population residing in rural areas as of 2011. The state's topography is dominated by the fertile soil irrigated by the extensive river system, particularly the plains of the mighty Ganga River and its tributaries, which support primary activities and rural populations. Urban areas account for only 22.2% of the total population.

Based on the place of the last residence, it is identified that the state recorded 8.8 million people engaged in short-term migration (residence less than 1 year), while durations of 1-4 years and 5-6 years contributed 47 million and 42 million individuals, respectively, at the national level in 2001. Notably, rural areas in Uttar Pradesh serve as emigration zones, primarily inhabited by female migrants across various migration streams.

Methodology

The study utilizes secondary data from the Registrar General of India, Census 2011, to investigate internal migration patterns in Uttar Pradesh. The paper focuses on migrants based on the place of their last residence. Data from the D series of the Census, specifying migration reasons for various age groups and durations of residence, is analyzed. The study concentrates on individuals with a residence duration of less than 1 year, indicative of short-term migration, within the age group of 15-34 years, a demographic more prone to migration. Further categorization is done for ages 15-19, 20-24, 25-29, and 30-34. The analytical approach involves applying the simple percentage method to comprehensively analyze migration patterns within the specified parameters.

The datasheet for the D-05 series concludes with a description of the data that states, *"The place of last residence unclassifiable as "Rural" or "Urban" is included in "total"* (D series, Census, 2011). The crucial element for additional computation is this description. The total number of migrants for a given age-specific duration of residence should equal the sum of all rural and urban migrants for the same age-specific duration of residence; yet, this description leads to a finding that the two are not equal. This can be understood from equation (1) which is provided below.

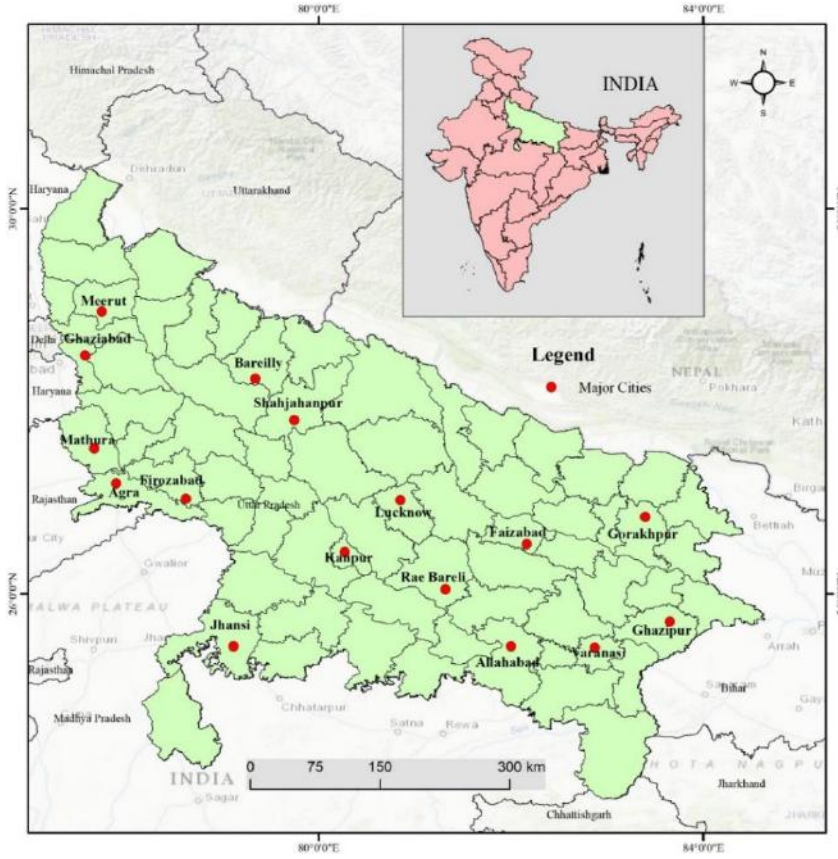

Fig 1: Map of Uttar Pradesh and its neighbour states. Major cities act as a hotspot of migration.

Rural migrants residing less than 1 year of age group 15-19 (964818) + Urban migrants residing less than 1 year of age group 15-19 (431688) ≠ Total migrants residing less than 1 year of age group 15-19 (1489848) (1)

The real number of migrants is shown on the left side of the equation, while the people whose residence cannot be classified as rural or urban are included on the right side of the equation. Therefore, determining the real number of migrants in both rural and urban areas is the first stage in the computation. The further steps are:

1. Determine the exact number of migrants across all migration streams.
2. The percentage of migrants in each stream, calculated as (age and the number of migrants in that stream ÷ the age and the actual number of migrants in that stream) * 100

The results from the 2011 Census have been supported by the latest data on migration released by NSSO/PLFS in their report “Migration in India 2020-21”.

As the work is focused on 2011 data, the literature has been taken back from 2007 to 2023 related to internal migration and short-term migration in India and Uttar Pradesh and run the bibliometric analysis to identify the reasons for migration. The metadata for bibliometric analysis has been manually taken from Google Scholar between 2008 and 2023 and filtered out 124 articles meeting with the interest area of internal migration and short-term migration in India and Uttar Pradesh (Fig.2).

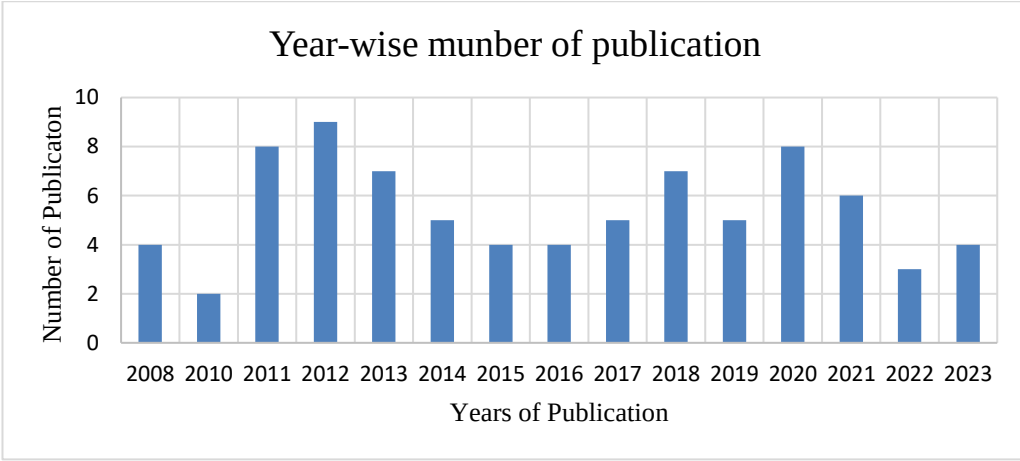

Fig 2: Year-wise publications (2008-2023) related to internal migration and short-term migration in India and Uttar Pradesh

Results

This study explores migration dynamics in Uttar Pradesh, focusing on migrations lasting less than 1 year and homing in on the 15-34 age group, renowned for its heightened mobility, the analysis unveils intricate patterns across different internal migration streams. Fig 3 displays the percentage distribution of short-term internal migrants (less than 1 year) across various streams in Uttar Pradesh, with data sourced from the Registrar General of India's Census of India 2011 (Series D 05). The study focuses on young adults aged 15-34, divided into four age groups: 15-19, 20-24, 25-29, and 30-34, considering their heightened propensity for migration according to existing research (Internal Migration in India, 2011).

Data source: RGI, Census of India,2011

Upon examining the data presented in Table 1, noteworthy trends become apparent. Rural-to-rural migration takes precedence across all age brackets, reaching its zenith in the 15-19 age group at an impressive rate of 69.51%. Particularly noteworthy is the predominantly female composition within this age cohort, accounting for 77.27% of the total rural-to-rural migrants. In contrast, rural-to-urban migration contributes a comparatively lower share, ranging from 7-8% for all age groups. Urban migration, encompassing both urban-to-rural and urban-to-urban streams, collectively averages around 20% for all age groups. The 15-19 age group, however, has the lowest urban migration share at 11.5%.

Examining gender distribution, male migrants dominate the rural-to-urban, urban-to-rural, and urban-to-urban streams, as indicated by the data from the 2011 Census. The 15-19 age group stands out, with female migrants surpassing males in the rural-to-rural stream, illustrating the unique mobility patterns of this demographic.

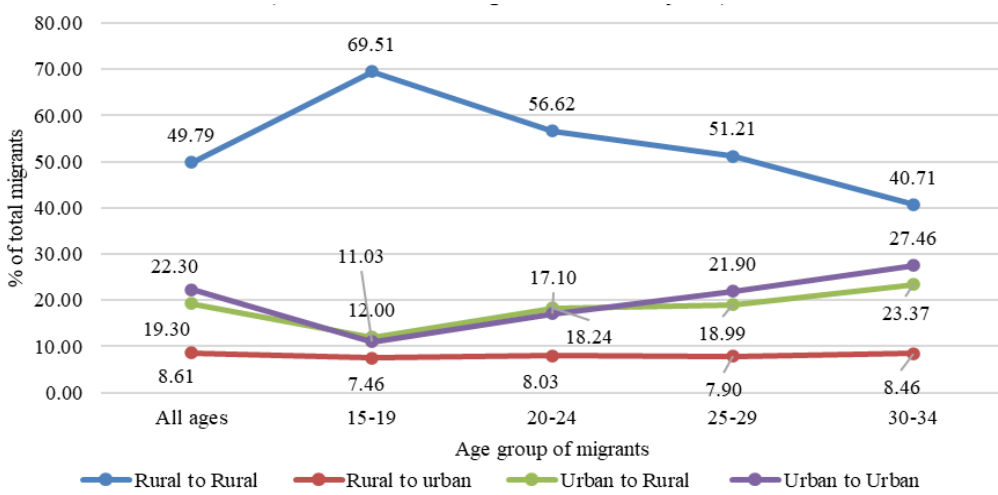

Fig 3: Total internal short-term migrants (%) of different streams in Uttar Pradesh.

Table 1: Gender composition of internal short-term migrants (%) of different streams in UP

	Rural to Rural		Rural to urban		Urban to Rural		Urban to Urban	
age group	M	F	M	F	M	F	M	F
All ages	32.86	59.22	10.01	7.83	27.81	14.56	29.32	18.39
15-19	34.98	77.27	11.39	6.58	26.99	8.63	26.63	7.52
20-24	29.97	64.52	9.83	7.50	34.08	13.55	26.13	14.43
25-29	31.00	59.50	9.56	7.22	31.28	13.94	28.16	19.33
30-34	30.47	48.38	9.04	8.02	30.15	18.29	30.34	25.30

Data source: RGI, Census of India,2011

The study identifies young adults aged 15-34 as the most mobile demographic, reacting swiftly to external opportunities. The 15-19 age group, in particular, experiences high mobility, marked by female dominance in rural-to-rural migration. This age bracket encounters significant life changes, such as independence, career initiation, and family formation. The consistent prevalence of rural-to-rural migration across all age groups suggests that economic transformations from rural to urban and vice versa are limited. Individual decisions and intervening obstacles, in line with push and pull factors, play crucial roles in shaping migration patterns. The detailed gender-wise distribution presented in Table 1 emphasizes that, for the rural-to-rural stream, female migrants consistently contribute a substantial portion across all age groups, although their share is lower compared to male migrants in other streams.

Gender and age-wise reasons for short-term migration in the age group of 15 to 34 years have been calculated (residence less than 1 year) to identify the age and sex-specific reasons responsible for migration and see their variation among all the streams. This estimation gives valuable information about the specific reasons for specific age and sex and will be helpful to understand social circles in society to formulate policies.

1. Rural to rural

A prominent trend evident from Fig 4 is the dominance of marriage as a primary reason for migration across all age groups. Marriage accounts for a substantial share, with figures peaking at 81% for the 15-19 age group, gradually decreasing to 43.86% for the 30-34 age group. Notably, this trend is more pronounced among female migrants, reaching as high as 88% in the 15-19 age group. The persistence of high percentages of female migrants across all age groups underlines societal norms where women typically move to their husband's residences after marriage.

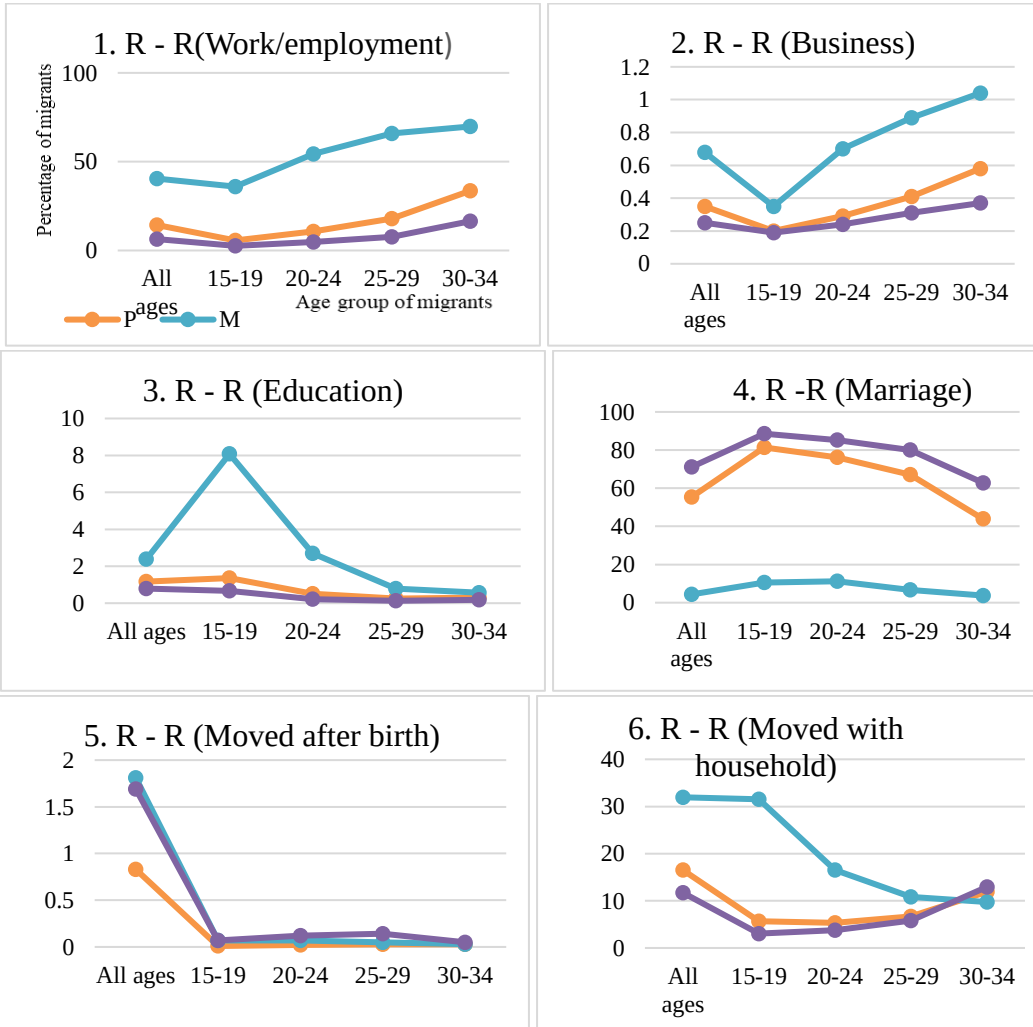

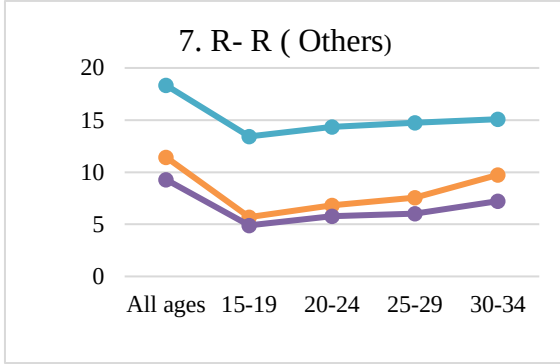

Fig 4: Age – Sex wise seven reasons for short-term migration in the Rural-to-Rural stream in UP (in percentage) (where, the X-axis = age group of migrants, Y axis = Percentage of migrants, the Green line = Persons, the Blue line = Males, Yellow line = Female)

Data source: RGI, Census of India,2011

Beyond marriage, economic factors, particularly work and employment, emerge as influential drivers of migration, especially for male migrants. The 15-19 age group sees the least contribution to work-related migration at 35%, but this figure rises significantly for subsequent age groups, reaching 69% for the 30-34 age group. Female participation in work-related migration remains comparatively low, ranging from 2-16% across age groups. The reasons "moved with household" and "other" display relatively stable patterns across total persons and female migrants. Those opting to move with their households often make this decision early in life to seek improved living conditions.

Education-related migration, while crucial for societal development, registers a low percentage, ranging from 1% to 0.25%. This could be attributed to changing perceptions and a preference for urban educational institutions. The rural-to-rural stream reflects a larger societal trend, wherein urbanization plays a pivotal role in shaping migration patterns.

It can be derived from the data that female migration in the rural-to-rural stream is primarily driven by marriage, followed by work and moving with the household. The increasing share of female migrants in the work category suggests a positive shift in societal acceptance of working women. However, the limited educational migration among women, particularly in age groups beyond 25, underscores persistent challenges in this regard.

2. Rural to Urban

Fig 5 provides a detailed breakdown of age and sex-wise reasons for short-term migration in the rural-to-urban stream in Uttar Pradesh. It reveals several significant observations about the drivers and patterns of migration in this particular context. In the rural-to-urban stream, marriage and moving with the household emerge as the dominant

reasons for migration, accounting for 27.31% and 32.26% respectively across all age groups. This underscores the strong influence of familial and domestic considerations in motivating individuals to migrate from rural to urban areas. The prevalence of these reasons suggests that family-related factors play a crucial role in shaping migration dynamics, emphasizing the importance of familial ties and household arrangements in relocation decisions.

Contrary to expectations, the "business" category appears to be the least influential in inducing rural-to-urban migration, with percentages ranging from 1% to 0.5%. This unexpected finding suggests that economic drivers, specifically business opportunities, may not be strong enough to compel individuals to leave their rural homes and relocate to urban settings. This could reflect a certain level of attachment to one's native place despite perceived economic challenges.

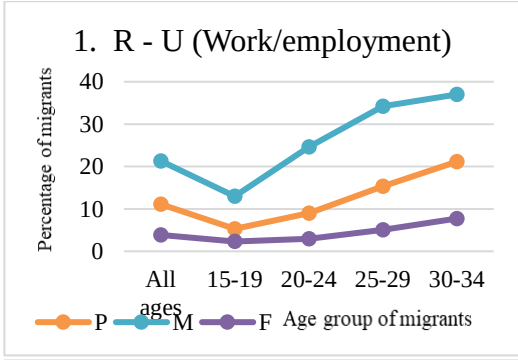

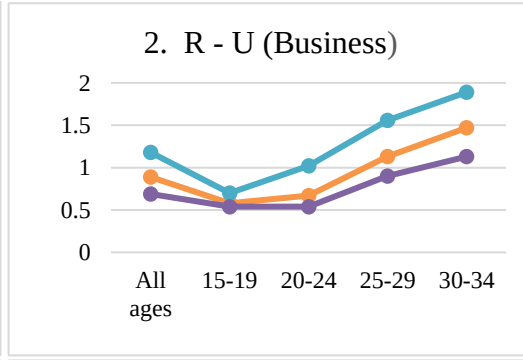

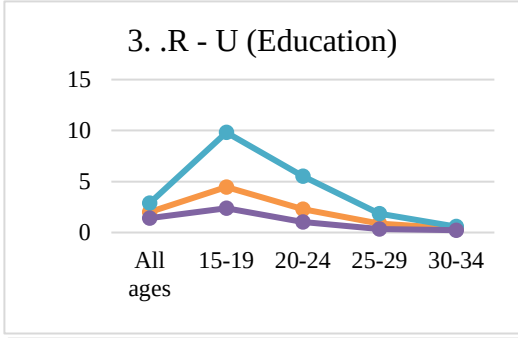

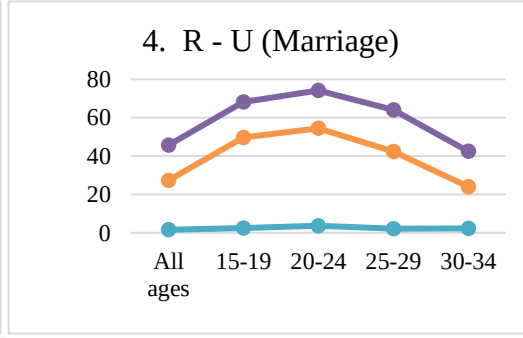

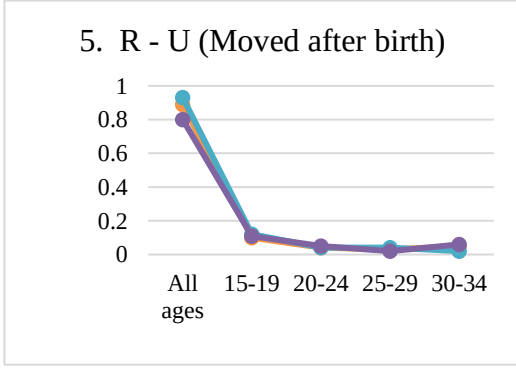

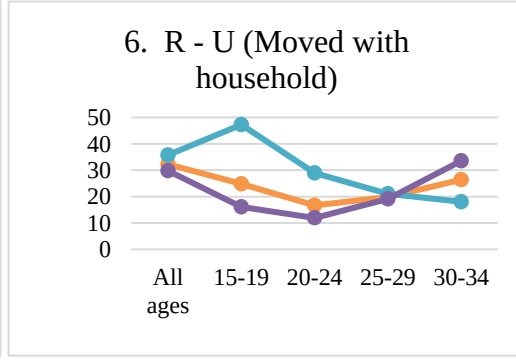

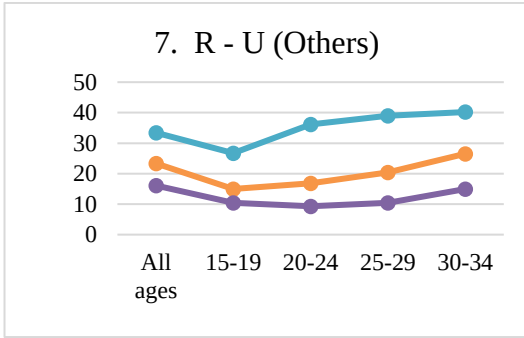

Fig 5: Age – Sex wise seven reasons for short-term migration in Rural to Urban stream in UP (in percentage) (where, X-axis = age group of migrants Y-axis = Percentage of migrants, and Green line = Persons, Blue line = Males, Yellow line = Female)

Data source: RGI, Census of India,2011

Education-related migration contributes to a total of 2%, with a higher concentration among individuals aged 15-19. However, this percentage diminishes to less than 1% among those above 25 years of age. This trend may indicate that younger individuals are more inclined to migrate for educational purposes, possibly seeking better opportunities in urban educational institutions. The decreasing contribution in older age groups could be influenced by various factors such as established careers or familial responsibilities. The gender dynamics suggest that female migrants constitute less than half of their male counterparts in the rural-to-urban stream. However, marriage-induced migration stands out as the highest among the reasons, and female migrants play a significant role in this category. The data aligns with societal norms where marriage, especially between the ages of 15-25, is considered ideal.

The analysis reveals that the rural-to-urban migration pattern is heavily influenced by familial ties, particularly marriage and moving with the household. Surprisingly, economic factors, as represented by the "business" category, appear to have a minimal impact. Educational migration is more prevalent among younger age groups, and despite an overall low percentage, it highlights the potential influence of educational pursuits on migration decisions. The gender dynamics, with female migrants being prominent in marriage-induced migration, reflect traditional societal norms and expectations.

3. Urban to Rural

In the context of urban-rural migration, as shown in Fig 6, the key determinants influencing relocation patterns are "moved with household" and "work," standing out as primary motivators, succeeded by "others" and "marriage." Noteworthy is the prominence of "moved with household," constituting 35% of migrants across all age cohorts. This category exhibits a distinct gender distribution, with females contributing 43%, surpassing males at 28%. Particularly in the 15-19 age group, a distinctive pattern emerges, with male migrants

(43%) outnumbering their female counterparts (28%), suggesting unique dynamics associated with familial and caregiving responsibilities.

The second most prevalent reason for migration is work/employment, attracting 27% of urban migrants to rural areas in search of job opportunities. Remarkably, 47% of these migrants are male, reflecting entrenched societal norms in a patriarchal context where males are traditionally designated as primary breadwinners. This phenomenon is further linked to the preference for government employment, with males, upon securing such positions, often experiencing rural postings. The data demonstrates a clear trend, with 54% of male migrants in the 20-24 age group, 66% in the 25-29 age group, and 71% in the 30-34 age group transitioning from urban to rural areas.

Educational migration constitutes 4% of the overall migration across all age groups, with a notable impact in the 15-19 age group, contributing to 11% of the total migrants. This suggests a deliberate strategy for rural development, as evidenced by the intentional establishment of high-ranking educational institutions in rural areas. Gender-wise analysis within the 15-19 years age group reveals participation of 21% of male migrants and 5% of female migrants in educational migration.

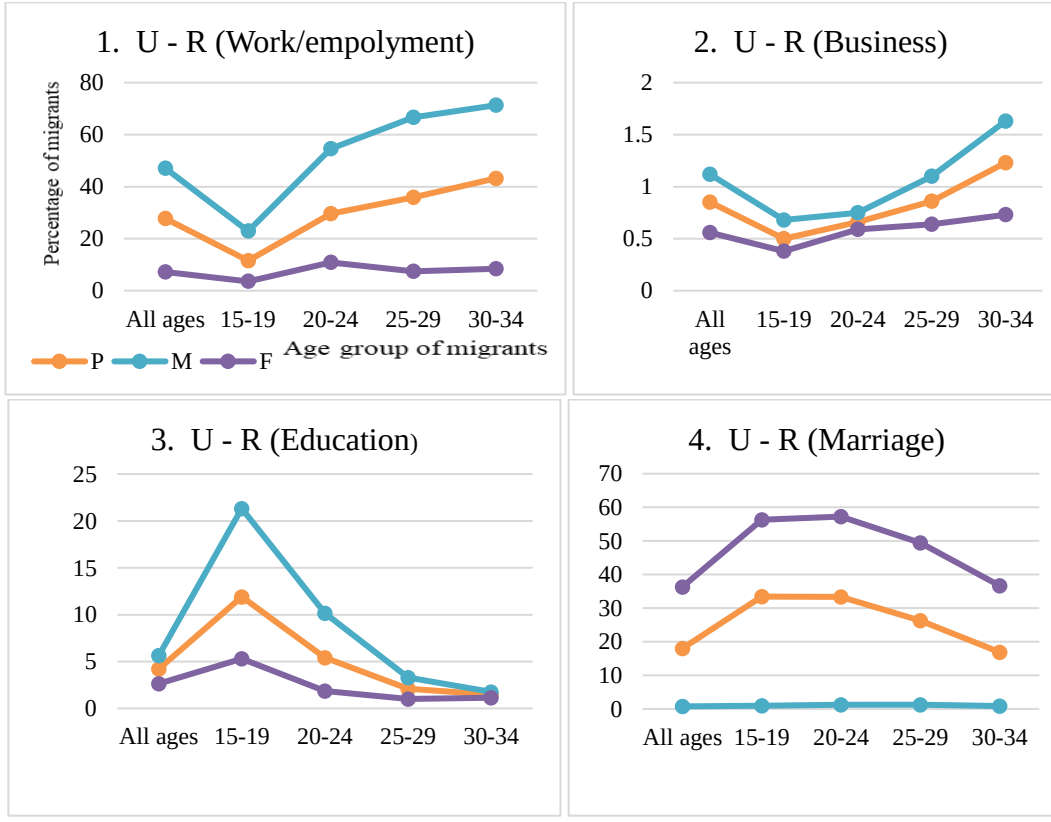

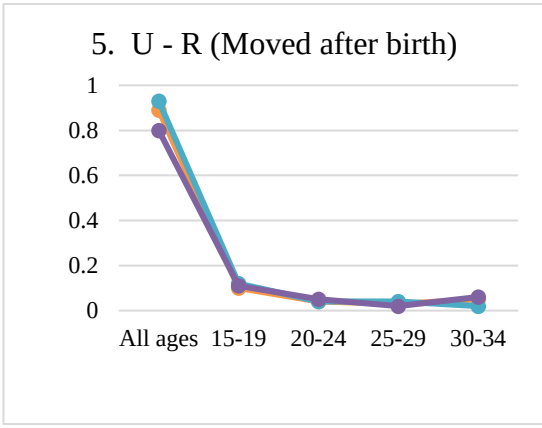

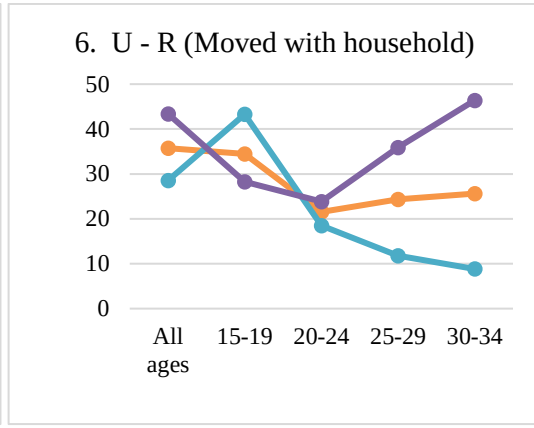

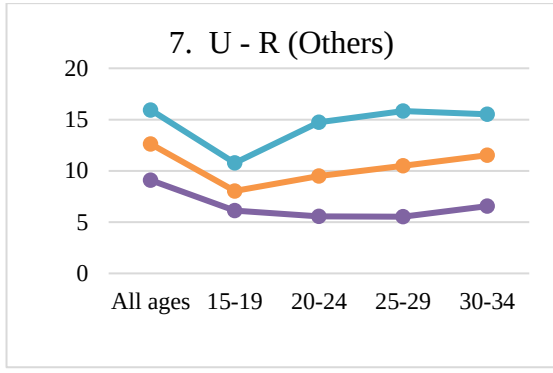

Fig 6: Age – Sex wise seven reasons for short-term migration in Urban to Rural stream in UP (where, X-axis = age group of migrants Y-axis = Percentage of migrants, and Green line = Persons, Blue line = Males, Yellow line = Female)

The Urban to Rural migration in UP is characterized by a dual influence of familial ties, particularly "moved with household," and economic factors, with "work" playing a pivotal role. Gender dynamics underscore traditional expectations, with males primarily migrating for employment opportunities. The strategic placement of educational institutions in rural areas reflects a thoughtful approach to rural development through educational initiatives. This research provides insightful perspectives into the intricate interplay of societal norms, economic considerations, and educational pursuits shaping migration trends in this specific stream.

The 15-19 age group reveals distinct patterns in migration reasons. Work (5%) and business (1%) show minimal contribution, while education constitutes 13% of total migrants, with higher involvement from males (21%) compared to females (6%). Notably, "Marriage" emerges as the second most prevalent reason in this age group, encompassing 23% of total migrants, primarily driven by 41% of female migrants. The "Moved after birth" category holds minimal significance, contributing only 3% to the overall migrants, with slight variations across age groups ranging from 0.11% to 0.27%.

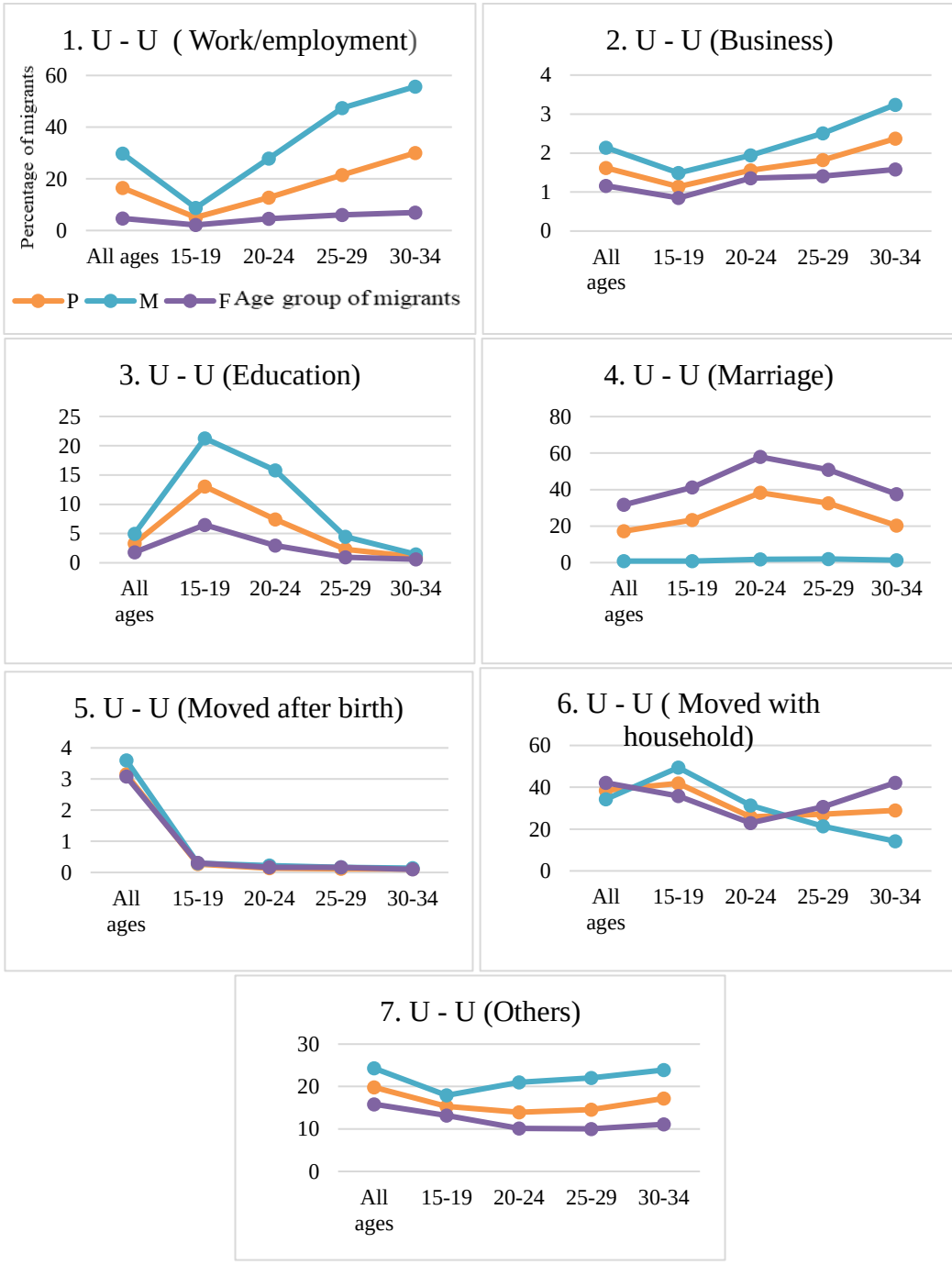

Fig 7: Age – Sex wise seven reasons for short-term migration in the Urban-to-Urban stream in UP (where, X-axis = age group of migrants Y-axis = Percentage of migrants, and Green line = Persons, Blue line = Males, Yellow line = Female)

Data source: RGI, Census of India,2011

Discussion

A careful examination of migration patterns in Uttar Pradesh, as presented in the table and figures, uncovers noteworthy trends and offers profound insights into the factors steering short-term migration across various streams. This discussion will succinctly summarize key findings and draw connections to pertinent literature.

The prevalence of rural-to-rural migration across all age brackets, particularly peaking in the 15-19 age group, aligns with existing literature emphasizing the significance of internal rural migration (Mitra & Murayama, 2009; Raman & Bhagat, 2021). The dominance of marriage as a driving factor, especially among females, underscores societal norms and the high percentage of female migrants in the 15-19 age group raises concerns about potential instances of child marriage (Bhagat et al., 2018). Work-related migration is substantial, predominantly among males, highlighting the economic aspect of rural-to-rural mobility (Panchamukhi, 2013). However, limited female participation in work-related migration suggests persistent challenges for women in this context. Educational migration remains relatively low, reflecting broader trends of lower educational attainment in rural areas (Premi, 1984).

In rural-to-urban migration, familial ties, particularly marriage and moving with the household, take precedence over economic factors (Korra,2012). Surprisingly, the minimal role of business opportunities suggests a strong influence of traditional and familial considerations (Bhagat, 2012). Educational migration is more pronounced among younger age groups, indicating a potential inclination towards urban educational institutions. However, the decreasing contribution in older age groups suggests other factors influencing migration decisions. Gender dynamics in this stream reflect traditional expectations, with females playing a significant role in marriage-induced migration (Piplai, & Majumdar,1969)

Key motivators for the urban-to-rural migration stream can be highlighted in the figure are "moved with household" and "work/employment." The higher percentage of females in the "moved with household" category highlights unique dynamics associated with familial and caregiving responsibilities (Rajan & Bhagat, 2021). Economic factors, particularly job opportunities, drive a significant number of male migrants, aligning with patriarchal norms and a preference for government employment (Bhagat et al., 2018). In the Urban-to-urban migration stream, factors such as "moved with household" and "Others" emphasize the importance of family and indicate group migration with fewer risk factors associated with migration (Clarke,1980) and unspecified reasons in relocation decisions (Ozden & Sewadeh,2010). Gender dynamics in this stream highlight traditional expectations, with females more inclined towards family-related reasons. The overall low percentage of educational migration suggests that factors beyond education play a more significant role in urban-to-urban migration (Mahapatro, 2020).

It can be inferred from the above figures and supported by literature that educational migration contributes to rural development, with intentional efforts to establish educational institutions in rural areas. However, it is visible that, gender disparities persist, with a higher percentage of male migrants participating in educational migration.

Recent evidence from PLFS survey

The limitation of the paper is the latest available migration data. The last census was conducted in 2011, and the next census is still in process. Therefore, by comparing the 2011 census data with the recently available report on migration 2020 issued by MOSPI, PLFS series, one can understand the trend of migration. Data in the report showed that internal migration is highly dominated by females both in rural and urban areas. It also provides evidence that the rural migration stream prevailed by females while in the other three streams, the share of female migrants is lower than that of males (Fig 8). Be it rural or urban areas both receive the higher share of migrants from rural areas. The recent data also gives a similar trend that most females migrate due to "marriage" followed by "moving with household" in rural areas while on the other hand, urban female migrants show some variation: marriage still being the first reason followed by moving with household and then comes employment and studies. Figure 9 and 10 give a valid comparative idea about the trending reasons for migration among males and females. The only difference between these two datasets is that PLFs do not give any data on "moved after birth" and "moved with household" Apart from these, the rest of the variables are the same; hence, they can be compared from the above analysis derived from Census 2011.

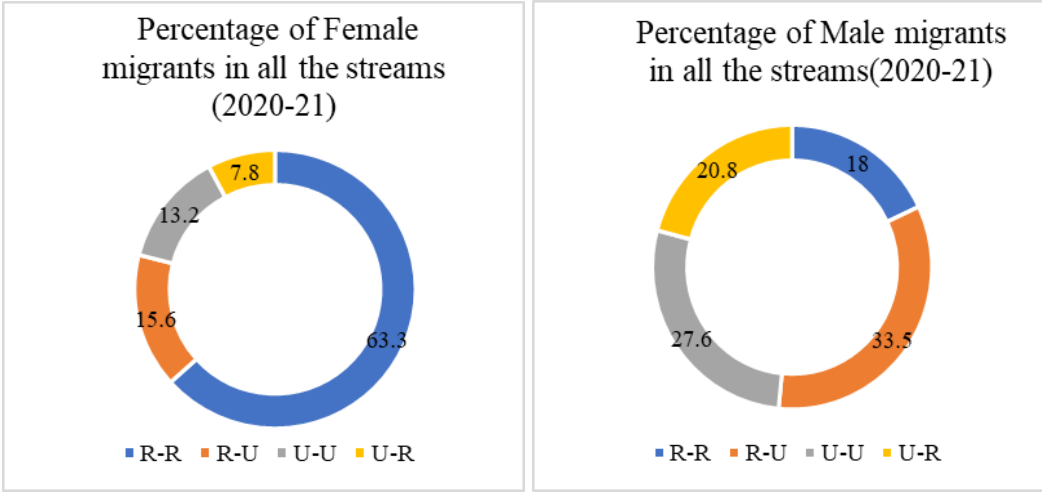

Fig 8: Percentage of Male and female migrants in all the streams, recent trend.

Source: Migration In India, 2020-2021

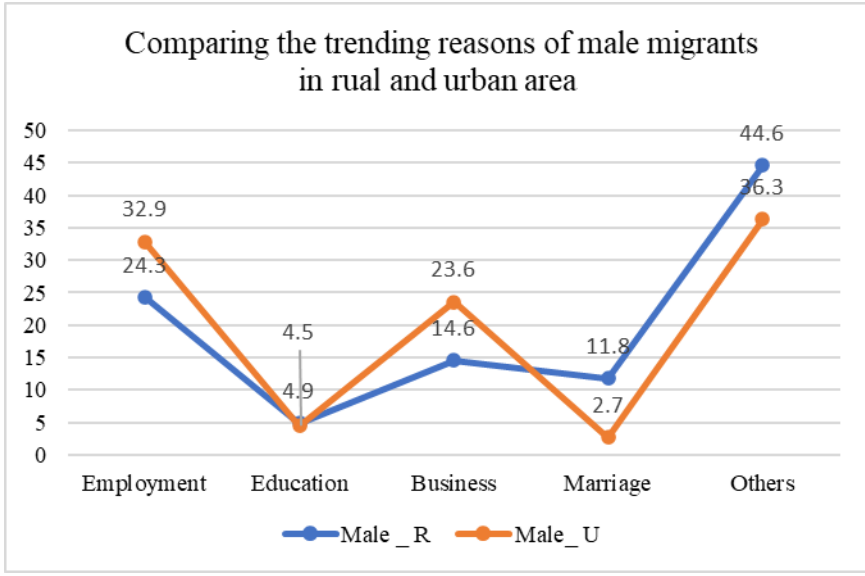

Fig 9: Reasons of male migration in rural and urban area (2020-21)

Source: Migration In India, 2020-2021

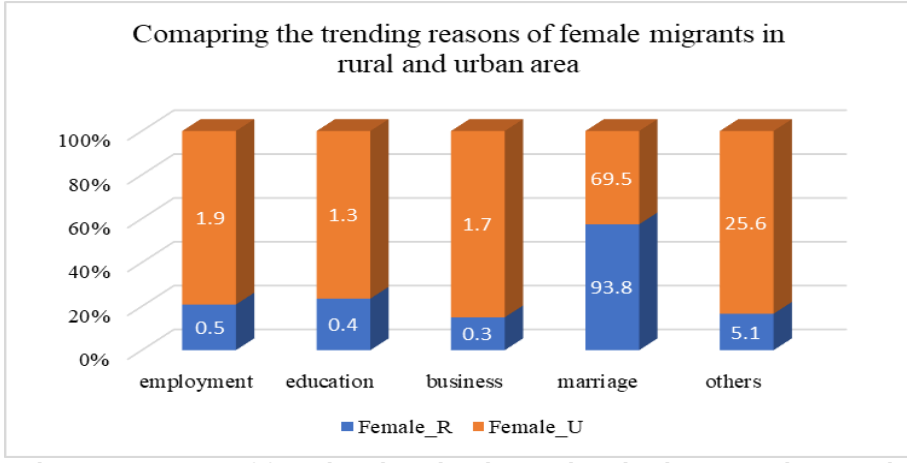

Fig 10: Reasons of female migration in rural and urban area (2020-21)

Source: Migration In India, 2020-2021

Conclusion

The comprehensive analysis of short-term migration patterns in Uttar Pradesh illuminates the intricate dynamics in the mobility of the population. The prevalent rural-to-rural migration, especially in the 15-19 age group, underscores the profound impact of societal norms, economic motivations, and familial ties on migration decisions. The dominance of marriage, particularly among females, raises concerns about early marriages,

emphasizing the need for addressing associated social challenges. Persistent gender disparities and the limited participation of females in work-related migration highlight existing obstacles hindering women's mobility and educational attainment. Younger age groups exhibit a higher inclination towards educational migration, diminishing in older age brackets, indicating the influence of established careers and familial responsibilities. Though the primary work is based on census data, similar trends have been noted in the latest migration survey of 2020 as well. Policy implications stress the necessity for targeted interventions addressing traditional norms, promoting gender equality, and facilitating educational opportunities to foster inclusive growth and societal development in Uttar Pradesh.

Acknowledgement:

SC would like to express my sincere gratitude to EV (Co-author) for his invaluable guidance, support, and encouragement throughout this research. His expertise and insight were instrumental in shaping this work. I am also grateful to UGC for providing the financial support necessary for this research. Without their funding, this project would not have been possible. My thanks extend to my colleagues, Ashish and Simran, for their collaborative efforts and constructive feedback. Additionally, I wish to thank the editor team of the Indian Geographical Journal for always being so supportive. Their contributions significantly enhanced the quality of this study. Finally, I deeply appreciate my family and friends for their unwavering support and understanding throughout this endeavor.

References:

1. Annual Report (2022). *Periodic Labour Force Survey (PLFS) Ministry of Statistics and Programme Implementation* (pp.2022–2045). https://mospi.gov.in/sites/default/files/publication_reports/AR_PLFS_2022_23N.pdf
2. Bhagat B. R. (2011). Migrants' (Denied) Right to the City. Internal migration in India initiative: National Workshop on Internal Migration and Human Development in India: 6-7 December 2011: workshop compendium. (2011). *United Nations Educational, Scientific and Cultural Organization: UNICEF*
3. Bhagat B.R. and Keshri K. (2021), "Internal migration and Labour Circulation in India", *International Union for the Scientific Study of population, International Population conference 2021*. https://ipc2021.popconf.org/.
4. Bhagat, R. B. (2012). Internal migration in India: are the underclass more mobile? In *India Migration Report 2011* (pp. 7-24). Routledge India.
5. Bhagat, R. B., Keshri, K., & Ansary, R. (2018). Internal migration in India: Intensity, flows and impact. In Comparing Internal Migration in the Countries of Asia" Conference, *Asian Demographic Research Institute, Shanghai University, Shanghai, China, July.*
6. Census Quest / Government of India. (2011). Censusindia.gov.in. https://censusindia.gov.in/census.website/CENSUS_ques.

7. Clarke, J. I. (1980). Population Geography. Progress in Human Geography, 4(3), 385–391. https://doi.org/10.1177/030913258000400305
8. Global migration indicators (2021). International Organization for Migration.
9. Government of India. (2001). *Census tables / Government of India.* https://censusindia.gov.in/census.website/data/census-tables
10. Government of India. (2011). *Census tables / Government of India.* https://censusindia.gov.in/census.website/data/census-tables-migration
11. Global Migration Indicator 2021. https://www.iom.int/resources/global-migration-indicators-2021
12. Kapur, D., Prasad, C. B., Pritchett, L., & Babu, D. S. (2010). Rethinking Inequality: Dalits in Uttar Pradesh in the Market Reform Era*. Economic and Political Weekly,* 45(35), 39–49. http://www.jstor.org/stable/25742020
13. Khan, J. H. (2016). Age-Sex Wise Reasons of Internal Migration in Uttar Pradesh, India. *The Global Journal of Multidisciplinary Studies*.
14. Korra, V. (2012). Short-duration migration in India*. India Migration Report 2011: Migration, Identity and Conflict,* 52.
15. Lahiri S. (2020). Impact of internal migration on left behind youth's labor force participation in India. *Economics Bulletin.*Vol,40. Issue,3.
16. Mahapatro, S. R. (2020). Internal migration: Emerging patterns. *Handbook of internal migration in India,* 80-92.
17. Majumder, B., & Taukeer, M. (2019). Dual-Step Migration from a Village in Uttar Pradesh: Causes, Processes and Consequences. *Productivity,* 60(2).
18. Mitra, A., & Murayama, M. (2009). Rural to urban migration: A district-level analysis for India. *International Journal of Migration, Health, and Social Care,* 5(2), 35-52.
19. U.N. (2009). Human Development Report 2009. https://hdr.undp.org/content/human-development-report-2009
20. Ozden, C., & Sewadeh, M. (2010). How important is migration? The poor half million in South Asia: What is holding back lagging regions, 294-322.
21. Panchamukhi, V. R. (2013). Changing pattern of Internal Migration in India 1999/00-2007/08: Issues and Challenges. *The Indian Economic Journal*, 61(1), 129-148.
22. Piplai, T., & Majumdar, N. (1969). Internal migration in India: some socio-economic implications. *Sankhyā: The Indian Journal of Statistics,* Series B, 509-522.
23. Premi, M. K. (1984). A case for microlevel studies on internal migration in India. Canberra: Australian National University. IUSSP Seminar on micro-approaches to demographic research. http://hdl.handle.net/1885/266300
24. Rajan, S. I., & Bhagat, R. B. (2021). Internal migration in India: integrating migration with development and urbanization policies. *Policy Brief*, 12, 59.
25. Raman, L., & Bhagat, R. B. (2021). Trend and Pattern of Internal Migration in India 1971-2011. *Paper Presented at IIPS International Seminar 2021 on Pandemic and Population Dynamics,* 18-20 March 2021.
26. Singh, R. (2018). Impact of male out-migration on women left behind: A study of two villages in Uttar Pradesh. *Remittances Review, 3(1), 75-92.*

27. Tumbe, C. (2012). India Migration Bibliography. *SSRN Electronic Journal.* https://doi.org/10.2139/ssrn.2117805
28. Wankhede, P. et.al. (2021). The Impact of COVID-19 on India's Internal Migration. *Across the Spectrum of Socioeconomics.* Papers.ssrn.com.
29. Wimalaratana, W. (2017). International migration and migration theories. https://www.researchgate.net/publication/312211237

The Indian Geographical Journal
Volume 98 (1) June - 2023, pp 87-90
ISSN 0019-4824

Archives - 1

NEWS AND NOTES

from The Indian Geographical Journal Formerly Known as The Journal of The Madras Geographical Association

(Volume XIX, 1944, pp.91-93)

PROCEEDINGS OF THE INDIAN GEOGRAPHICAL CONFERENCE HELD AT ANNAMALAI UNIVERSITY, ANNAMALAINAGAR, ON THE 9TH & 10TH MAY 1944

The Annual Conference of the Indian Geographical Society was held at the Annamalai University, Annamalainagar, on the 9th and 10th May 1944, conjointly with the Provincial Educational Conference.

The Conference was opened by M. Ruthnaswamy Esq., C.I.E., Vice-Chancellor, Annamalai University. Dr. M. S. Krishnan the President-elect was then proposed to the Chair by Miss A. R. Irawathy. After the Presidential address on the 'Mineral Resources of South India' was delivered by Dr. M. S. Krishnan, the first day's session concluded with a vote of thanks by the Secretary.

On Wednesday the 10th May, the following papers were read:-

(1) Historical Geography of the South Arcot District by Sri Rao Bahadur Prof. C. S. Srinivasachari.

(2) Some Aspects of Drainage in South Arcot by Janab A. Ghulam Mahomad Bahadur, District Agricultural Officer, South Arcot.

(3) Communication Lines in South Arcot by Sri M. P. Rajagopalan.

(4) Population in South Arcot District by Mr. George Kuriyan.

Then followed a discussion on the following topics:-

(1) Place of A-Group Geography in the S.S.L.C. syllabus.

(2) Question papers in A-Group Geography for the S.S.L.C.

The following resolutions were passed:-

(1) Resolved that the Conference expresses its thanks to the Director of Public Instruction for having arranged the time table for the S.S.L.C. Examination in such a way that the paper on Geography is held as the first test for the day and not the last, as was hitherto conducted.

(2) Resolved that A-Group Geography be given equal status with the other similar subjects like History in the S.S.L.C. syllabus by increasing (i) the duration of the Geography paper from 1 to at least 1½ hours and (ii) the maximum marks from 40 to 50.

(3) This Conference feels that the question paper in A-Group Geography for the S.S.L.C., for 1944, is in many ways unsatisfactory and the translations of the paper into Tamil and Telugu still more so. As examples of inaccuracies and wrong statements the following are cited:-

(a) Question 2 (d):-As it is worded, this is not quite correct, since the towns mentioned are not exactly at the river mouths.

(b) Question 8 (b):-This is wrong in two respects. Darjeeling and Calcutta are in different latitudes and the difference in temperature between these stations does not depend upon the altitude alone. Secondly the question involves the relationship between the mean temperature at different latitudes and absolute altitude. There is no known law by which the mean temperature falls with the absolute altitude at different latitudes. If the question merely resolves itself to an arithmetical division, then it is certainly out of place in a paper on Geography and should be relegated to one in Elementary Arithmetic.

(c) Question 8 (b): -The paper in English refers to tributaries while the Tamil translation denotes distributaries: -These are fundamentally different.

(d) Question 8 (a):-The Tamil translation conveys a meaning of determining the average of the rainfall measures during the year instead of annual rainfall and is therefore misleading to the students.

Further, the Conference feels that the question paper is too long for the time allotted and that it is undesirable to ask only questions which require one-word answers, or filling up of blanks by a single word, or group of words.

The Conference therefore recommends that questions on general principles testing the knowledge of the candidates instead of their memory, requiring answers in short paragraphs, be set in future. Further, this Conference requests the Director of Public Instruction to be pleased to issue a new model paper in A-Group Geography based on these suggestions.

(4) Resolved that the Secretary be authorised to forward a copy of all these proceedings of the Conference together with the Resolutions to the Director of Public Instruction for his favourable consideration.

The Secretary Mr. George Kuriyan then made an appeal for liberal contributions towards the N. Subrahmanyam Memorial Fund.

With the President's concluding remarks and vote of thanks by the Secretary the session concluded.

GEORGE KURIYAN,

Hon. Secretary

Archives - 2

NEWS AND NOTES

from The Indian Geographical Journal Formerly Known as The Journal of The Madras Geographical Association

(Volume XIX, 1944, p - 165)

N. Subramanyam Memorial

In aid of the N. Subramanyam Memorial Fund, a Variety Entertainment was staged at the Lady Willingdon Training College Hall, Triplicane, Madras, on the 28th October 1944 with Lt. Col. Diwan Bahadur Dr. A. Lakshmanaswami Mudaliar, B.A., M.D., LL.D., D.Sc., Vice-Chancellor, University of Madras, in the chair.

Sri P. Nagaraja Rao and party enacted a few seenes from the tamil drama SARASA, which was followed by a Bharata Natyam and Abhinayam by two young and talented artistes, Srimathi Yogam and Srimathi Mangalam. They kept the whole audience spell bound for an hour by a most exquisite display of the art of Indian Dancing. This was followed by Prof. C. S. Kamalapati and his troupe staging a few scenes from Shakespeare's Merchant of Venice and Macbeth.

Miss J. M. Gerrard, Principal, Lady Willingdon Training College and President of the Indian Geographical Society welcomed the Vice-Chancellor and proposed him to the chair. The Vice- Chancellor gave a short account of the life and work of the late Mr. N. Subramanyam and laid stress upon the enormously important role which Geography plays in the life of man. He was glad that although it has been a Cindrella in the curricula of studies in this University, recent changes tend to suggest that in the years to come, it is likely to become one of the most important subjects of study in the University Classes.

Mr. George Kuriyan, Hony. Secretary, N. Subramanyam Memorial Committee and the Indian Geographical Society proposed a vote of thanks, in which he made a special mention of the voluntary co-operation which he received from all the artistes who enacted the shows and in particular from Srimathies Yogam and Mangalam for their performance at very short notice, owing to Srimathi Kalanidhi Ganapathi having disappointed at the last

moment. The success of this entertainment was entirely due to the Entertainment Sub-Committee and Mr. Kuriyan took the opportunity of thanking Miss A. R. Irawathy, Convenor, and her Entertainment Committee

Further, he desires to express here his thanks to Sri G. Srinivasachari of the G. S. PRESS, for so ably doing all the printing work in connection with the Memorial and that free of all cost- a generous help given most willingly and sometimes under very exacting conditions.

The Secretary N. Subramanyam Memorial Committee reports that the entertainment brought in a gross receipt of Rs. 822 which has been credited to the Memorial Fund.

The Indian Geographical Journal
Volume 98 (1) June - 2023, pp 87-87
ISSN 0019-4824

THE INDIAN GEOGRAPHICAL SOCIETY

Department of Geography, University of Madras, Chennai - 600 025

13th IGS Online Talent Test – 2023

Date: 24.11.2023 Time: 11.00 a.m. - 12.00 Noon

WINNERS

Young Geographer (Under Graduate Programme)

The IGS Founder Prof. N. Subrahmanyam Award

Name of the Student	Name of the Institution	Total Score	Marks Scored	Rank
Ginshibha Singh R	Department of Geography, Nirmala College for Women (Autonomous), Coimbatore 641 018.	75	71	I
Kaviya S	Department of Geography, Queen Mary's College (Autonomous), Chennai - 600 004.	75	71	I
Akash V	Department of Geography, Government Arts College (Autonomous), Coimbatore 641 018.	75	70	II
Sindhuja V	Department of Geography, Nirmala College for Women (Autonomous), Coimbatore 641 018.	75	70	II
Tamilarasi A	Department of Geography, Queen Mary's College (Autonomous), Chennai - 600 004.	75	69	III

Young Geographer (Post Graduate Programme)
Prof. A. Ramesh Award

Name of the Student	Name of the Institution	Total Score	Marks Scored	Rank
Sabarinath D	Department of Geography, Madurai Kamaraj University, Madurai - 625 021	75	68	I
Ajith S	Department of Geography, University of Madras 600 025	75	66	II
Divya S	Department of Geography, University of Madras 600 025	75	64	III
Kavin M	Department of Geography, Government Arts College (Autonomous), Karur – 639 005	75	64	III
Mala K	Department of Geography, Government Arts College (Autonomous), Coimbatore – 641 018	75	64	III
Tamilarasan P	Department of Geography, Government Arts College (Autonomous), Namakkal 637 002	75	64	III

The Indian Geographical Journal
Volume 98 (2) December - 2023, pp 91-117
ISSN 0019-4824

SPATIAL VARIATIONS OF TECTONIC QUIESCENCE AND RESURGENCE CONSTRAINTS FROM THE LONGITUDINAL PROFILES AND CONFLUENCE ANGLES OF THE CAUVERY RIVER BASIN

AL Fathima[1*], Mu. Ramkumar[1], V. Thirukumaran[2], Athira Pramod[1], Juni K.J[1]

[1] Department of Geology, Periyar University, Salem-11, India
[2] Department of Geology, Government Arts College (Autonomous), Salem-7, India

Corresponding Author Mail ID: alfathima28@gmail.com

Abstract

Cauvery River, an east-flowing river, originates at about 1345 m elevation in the Western Ghat hill ranges in the southern part of the Indian Peninsula. The study focused on geomorphic aspects of this river by examining longitudinal profiles, knickpoints and confluence angles to understand the interactions between geology, tectonics, and fluvial processes in shaping river landscapes. Cauvery and tributaries display uneven longitudinal profiles with numerous knickpoints along the profiles. High R^2 values in longitudinal profiles indicate a strong correlation between stream slope and distance, suggesting equilibrium conditions and consistent erosional processes. Conversely, variability in R^2 values highlights the dynamic nature of these systems. Field investigations were conducted at selected knickpoints and knickzones to validate the extracted data. Each sub-basin within the Cauvery Basin exhibits unique topographic and geomorphic characteristics, reflecting diverse geological settings and regional influences. The study emphasizes the distinctiveness of sub-basins such as Hemavathi, Shimsha, Arkavati, and Kabini, highlighting their varied dynamics. The presence of knickpoints, especially at lithologic boundaries and structural features underscores the influence of geological factors such as erosion, base-level fluctuations, and tectonic activities. Associations between factors and abrupt changes in elevation along river profiles illustrate the complex interplay between geological processes and fluvial geomorphology, underscoring the multidimensional nature of landscape evolution. This research contributes to understanding neotectonic activity and its impact on river morphology, providing insights into the intricate interactions between geological processes and fluvial dynamics in the Cauvery River Basin.

Keywords: Cauvery River Basin; Confluence angle; Knickpoints; Longitudinal profile; Tectonic activity

Introduction

The drainage system within a region serves as a chronicle of tectonic transformations (Schumm, 1986). Tectonic activities alter stream flow characteristics

primarily by reshaping the base level of erosion, adjusting incision rates, or inducing diversions. Analyzing stream features can unveil the tectonic disturbances responsible for incisions, provided there hasn't been a diversion forced by tectonic activity (Larue, 2008a). Erosion rates across landscapes are believed to be influenced by tectonic uplift. Thus, deriving erosion rate indicators from topographic data offers innovative avenues for pinpointing areas of tectonic movement (e.g., Wobus et al., 2006a) and may even reveal potentially active faults (e.g., Kirby and Whipple, 2012). The analysis of channel networks holds particular significance in discerning external influences from the topographic configuration, as fluvial networks establish boundary conditions for adjacent hillslopes, thereby serving as conduits for transmitting climatic and tectonic cues throughout the landscape (e.g., Burbank et al., 1996).

Longitudinal profiles of channels arise from a complex interplay involving fluvial incision, lithological characteristics, tectonic forces, and shifts in base-level conditions (Larue, 2008b). The evolution of these profiles is heavily influenced by lithological diversity and by analyzing the river profile's geometry, one can spatially identify patterns of rock uplift. Notably, the presence of knickpoints, where river gradients abruptly change, signifies ongoing tectonic processes. River profiles in equilibrium typically exhibit a concave upward shape, indicating a balance between fluvial incision and base-level changes (Keller and Pinter, 2002). Conversely, if fluvial incision outpaces base-level changes, a smooth downstream concavity develops (Larue, 2008b), attributed to increased discharge and reduced grain size. Convex profiles suggest higher uplifting rates relative to denudation. Knickpoints, often caused by resistant lithology or increased shear stress, denote stream disequilibrium and signal adjustments in base level (Bishop et al., 2005; Larue, 2008b). Additionally, lateral tilting and vertical tectonic movements contribute to profile anomalies, offering insights into the tectonic history of a drainage basin. Thus, longitudinal profiles serve as valuable indicators of a basin's tectonic evolution.

Understanding the impact of tectonic forces on the evolution of channel networks and longitudinal profiles is crucial for identifying and analyzing neotectonic activity. The dynamic interplay between fluvial processes, lithological variations, and tectonic influences shapes the morphology of river channels over time. However, despite significant advancements in our understanding of these processes, there remains a need to accurately distinguish between tectonically induced changes and those driven by other factors such as climatic variations. Moreover, the identification of key indicators, such as knickpoints and profile anomalies, can provide valuable insights into the extent and nature of tectonic movements within a drainage basin. Therefore, the development of robust methodologies and analytical frameworks that leverage channel morphology data to detect and characterize neotectonic activity is essential for advancing our understanding of landscape evolution and terrain stability in tectonically active regions. The primary objectives of the present study entail characterizing neotectonic activity and examining the fluvial response to terrain stability within the Cauvery River Basin. This will be achieved through a comprehensive quantitative analysis of longitudinal profiles, coupled with an investigation into the influence of confluence angles of tributaries on the main river channel.

Geological Setting

The Cauvery River is one of the perennial rivers of south India draining over the states of Karnataka, Kerala and Tamil Nadu and its catchment lies between 10°7'N and 13°28'N, 75°28'E and 79°52'E. Cauvery River Basin trends NW-SE in direction and has an areal extent of 81155 sq. km. and a delta of 8800 sq. km. The tributaries are Amaravati, Arkavati, Bhavani, Shimsha, Thirumanimutharu, Thoppayaru, Sarabanga, Chinnar, Palar, Suvarnavati, Lakshmantirtha, Hemavati, Kaveri, Kabini, Kudamarutti, Aiyaru, Noyyal and distributatries are Arasalar, Coleroon, Kaveri, Vettar, Vennar. The river Cauvery originates from the Talakavery at the Brahmagiri hills of Western Ghats, the river has a total length of 760 km. A major part of the catchment zone lies in Karnataka state. The Cauvery Basin is peninsular India's fifth-largest drainage area (Kale et al. 2014).

The Delta head of this river is located at Mukkombu, Tiruchirapalli, from where the river branches off into the Cauvery and Coleroon. At Kallanai (Grand Anicut—Tiruchirappalli), it further branches off into two distributary channels, namely, the Cauvery and the Vennar. They branch further into 36 channels, whose total length is 1,607 km. These in turn branch off into 2,988 channels running to a length of 18,395 km (Kandaswamy 1986).

The mean annual temperature of the Cauvery River Basin is 25° C, however, in summer the maximum temperature reaches up to 43°C. The average rainfall of the basin is 110 cm, which has an average elevation of about 630 m. The Southwest monsoon is responsible for the rain in the basin, 75% of the annual rainfall, 85% of the annual sediment transport and 73% of annual water discharge acquired for the three months (June- August) (Vaithiyanathan et al., 1992; Sharma and Rajamani, 2001). Figure 1 shows the map of the location study area prepared in ArcGIS software.

The river originates in the Brahamagiri Range of the Western Ghats at an elevation of 1345 m above mean sea level and extends approximately 800 kilometers to the Bay of Bengal. The river's initial route is eastward through the Mysore Plateau (average elevation 1000 m). The river's eventual course in the state of Tamil Nadu, where it has created flood plains and a delta, is also eastward. A series of block mountains lie between the Mysore Plateau and the Tamil Nadu lowlands, believed to have been created after the Indian and Asian continents collided (Radhakrishna 1993). The river's drainage pattern becomes trellis-like in this steep section, resulting in an overall southern flow for the main channel. According to Radhakrishna (1993), the river in the Mysore Plateau has been revitalized by the region's uplift. Two important streams, the Bhavani and Amravati, enter the Cauvery River in its lower reaches in the south. The raised sections of the Nilgiri, Cardamom and Anaimalai hills also feed these two important tributaries. The Palghat–Kaveri gap, which separates two continental blocks, is assumed to be followed by the two major tributaries and the main canal (Radhakrishna 1993).

The Cauvery River Basin is dominated by Archean (>2500 Ma) gneissic, charnockitic, and granitic rocks (Figure 2). The region is separated into two major terranes:

the Dharwar Craton in the north and the granulite terrane in the south. The two terranes are separated by a transition zone to the north, where granitic rocks with supracrustal belts (schist belts) are metamorphosed to grades lower than the amphibolite facies. Both granitic and supracrustal rocks transform to granulite grade south of the transition zone, resulting in charnockite, pyroxene granulite, and high-grade amphibolite assemblages. The higher reaches' transition zone gneisses and charnockites have been dated to be between 3000 and 2500 Ma. (Friend and Nutman, 1991). The craton-southern granulitic belt boundary has been well-defined as a zone of strong faulting and thrusting in which the charnockite terrane has been raised and overthrusted onto the craton (Radhakrishna, 1968). The Himalayan orogeny, according to Radhakrishna (1993), caused the uplift and construction of many block mountains by reactivating the shear and fault systems (Sharma and Rajamani, 2001).

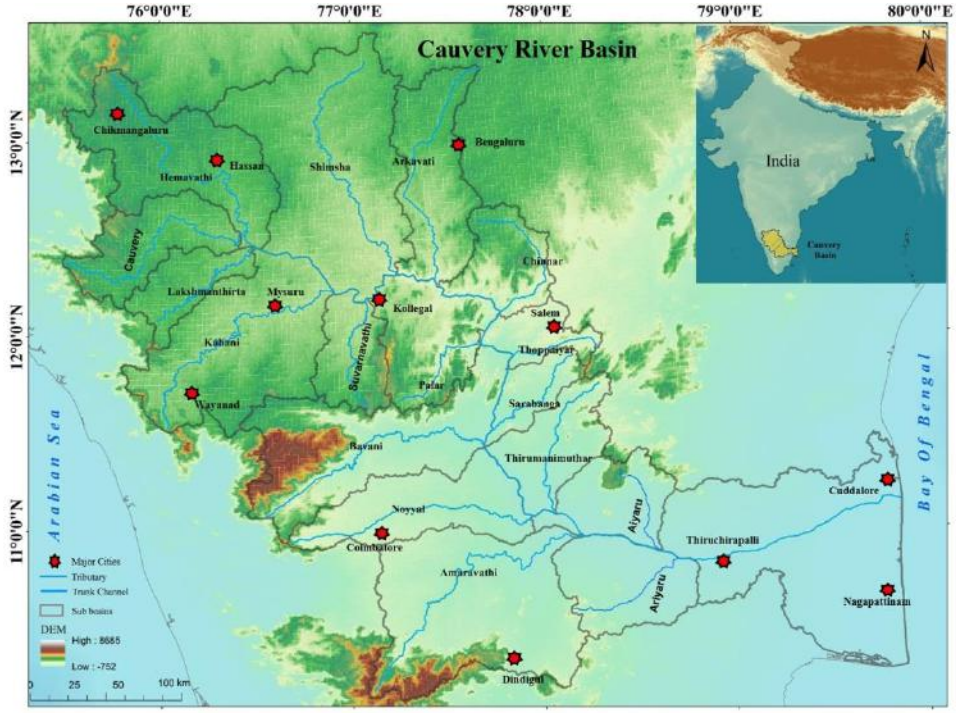

Figure 1: Cauvery River Basin shows the location of the study area. The inset map shows the location of the Cauvery Basin in India. SRTM DEM is downloaded from USGS Earth Explorer (https://earthexplorer.usgs.gov/).

Materials and Methods

Documentation and Analysis of Longitudinal Profile

Google Earth Pro, provides a user-friendly interface that allows researchers to easily access and visualize elevation data and is a widely utilized tool for observing our planet. The software primarily used the Shuttle Radar Topography Mission (SRTM) dataset for its elevation data, which has a resolution of 30 meters. Various features within Google

Earth contribute to the advancement of geomorphological concepts. The platform allows users to tilt scenes and view landscapes in three dimensions, enabling enhanced visualization. Additionally, functionalities such as measurement tools and elevation profile construction greatly aid in the identification and characterization of landscapes (Dolliver, 2012). The simplicity of accessing data through Google Earth Pro may outweigh the potential benefits from other datasets that require more technical expertise to acquire and process.

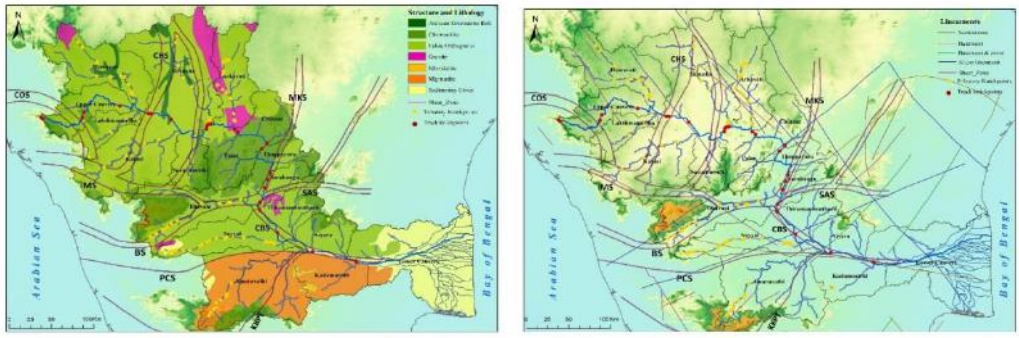

Figure 2: Shows the lithology and structure of the Cauvery River Basin (Geological Survey of India Map), drainage (source: mapped from toposheets from SOI https://www.surveyofindia.gov.in/). Figure 3: The knickpoint distribution along the trunk river and immediate tributaries with the major faults of the Cauvery River Basin (source: lineaments from atlas of Geological Survey of India), SRTM DEM (source: https://earthexplorer.usgs.gov/).

To generate the longitudinal profile of the Cauvery River and tributaries first, the main channel and tributaries are digitized in Google Earth Pro. Later, elevation values at an interval of 1 kilometre were entered in Excel⁞ from the elevation profile provided in Google Earth Pro. The distortion of data due to the vegetation cover is avoided by the use of multi-temporal satellite images available in the software. Longitudinal profiles were made in Excel⁞ with distance in meters as x-axis values and elevation in meters as y-axis values. The convex reaches or sudden falls in the longitudinal profile are marked and verified again in Google Earth Pro. These locations are saved and extracted as *kml* file format followed by the ground truth verification of the work with field survey. In this study, we conducted a longitudinal profiles analysis of the channels of 16 main tributary rivers and the trunk channel within the Cauvery Basin. Comprehensive observations were made along each river channel, spanning from their respective origins to their confluences. Anomalous points were identified through the detection of flow patterns contrary to the prevailing slope conditions.

The metric known as "Goodness of Fitness" (R^2) serves as a crucial indicator of a drainage basin's level of maturity. During a phase of equilibrium in the stream, the slope typically exhibits a linear relationship, reflected by a high R^2 value in the concave longitudinal profile, particularly evident in the primary stream profile of the basin (Ramkumar 2019). However, the dynamic interplay between intrinsic and extrinsic factors can cause the

longitudinal profile's knickpoint to shift from downstream to upstream as a transient response. This phenomenon disrupts the linear fit observed in the slope-area profile, leading to a decrease in the R2 value, particularly noticeable in the primary stream's longitudinal profile within the basin. In longitudinal profile analysis of rivers, the R-squared (R^2) value is calculated using excel. The collected data is organized into pairs of values, typically representing distance along the river's course (independent variable, x) and corresponding stream slope (dependent variable, y). A linear regression model is fitted to the data. This model aims to find the best-fitting line that describes the relationship between distance and stream slope. The equation of the line is typically of the form $y = mx + b$, where m is the slope of the line (which represents the rate of change of stream slope with distance) and b is the y-intercept. n longitudinal profile analysis, R^2 is significant because it provides a quantitative measure of how well the linear model represents the relationship between variables along the stream's course.

A high R^2 value indicates that the linear model fits the data well, suggesting a strong correlation between stream slope and distance. This implies that the stream is likely in an equilibrium state, with consistent erosion and sediment transport processes along its course. Conversely, a low R^2 value suggests that the linear model does not fit the data well, indicating variability or non-linearity in the relationship between stream slope and distance. This variability could be due to factors such as changes in geological substrate, tectonic activity, or human disturbances (Leopold et, al., 1964) The longitudinal profile graph slope, expressed as $mx + b$ of a river channel is significant in terms of landscape and channel evolution for several reasons. The gradient (m) of the longitudinal profile represents the rate of change of elevation (or slope) with respect to distance along the river's course. A steeper gradient indicates a faster rate of descent, which typically corresponds to areas of rapid erosion, such as waterfalls or steep rapids. In terms of landscape evolution, steep gradients suggest active erosion and rapid channel incision, which can shape the overall landscape over time.

The y-intercept (b) of the longitudinal profile represents the elevation of the river channel at a specific reference point along its course. This point may correspond to the source of the river, where it originates from higher elevations, or to a base level, such as a lake or the ocean, where the river eventually flows into. The y-intercept provides important information about the overall elevation profile of the river and its relationship to the surrounding topography. Changes in the slope (m) and y-intercept (b) of the longitudinal profile over time reflect the evolutionary trajectory of the river channel. For example, a decrease in slope may indicate a decrease in the rate of erosion or sediment transport, possibly due to changes in discharge, substrate, or tectonic activity. Conversely, an increase in slope may suggest rejuvenation of the river channel, often associated with increased erosional activity and channel incision. Longitudinal profile slope can also indicate the response of the river channel to tectonic uplift, climate change, or other external forces. For instance, a steepening of the slope may result from tectonic uplift, which increases the river's erosive power and leads to greater incision. Similarly, changes in slope and y-intercept can reflect variations in climate, such as increased precipitation

leading to higher discharge and more rapid erosion (Montgomery and Buffington, 1997; Howard, 1994).

Identification of Confluence Angle

To find out the actual angle theta between the mainstream and tributaries at the confluences, we have used a graphical technique adopted from Mosley's momentum equation (Figure 4) with the help of Google Earth Maps and the digitized stream networks. The streams were digitized using the Survey of India toposheets of 1:50000 scale. 154 topographic maps were downloaded from the SOI website (https://www.surveyofindia.gov.in/) and the images were geometrically rectified with respect to the WGS 1984 data frame. The drainages were digitized using the ArcGIS 10.8 software for morphometric analysis. The channel segments have been ranked according to Strahler's (1964) stream ordering system. The technique for angle measurement of each confluence is, a straight line has been drawn from each confluence between the tributary and main upstream which is parallel to the main downstream towards the reverse of the flow direction, considering an acute angle with respect to the main downstream. The confluence angles of tributaries are shown in Figures 10 and 11.

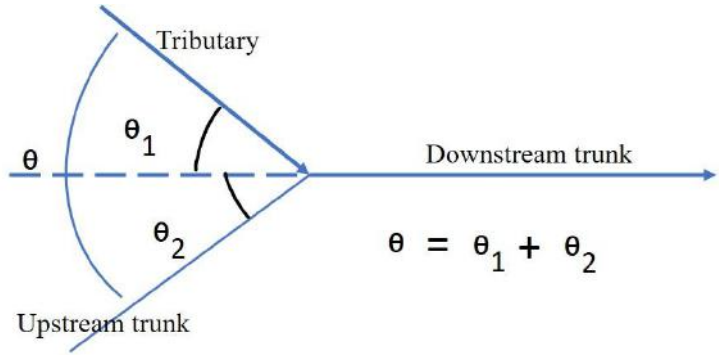

Figure 4: Sketch for confluence angle measurement (After Mosley 1976)

Results

Knickpoints recorded in the longitudinal profiles of the Cauvery River (Figure 5) and its 16 tributaries (Figure 6). The comparison profile of all tributaries is also shown in Figure 9. The 760-km-long Cauvery River shows convex and concave shapes upstream and downstream, respectively, and has an R2 (goodness of fit) value of 0.9345. These changes in stream profile shapes are separated by eight major knickpoints. However, there are several other minor knickpoints and knickzones along the river's course.

The longitudinal profile of Hemavathi has an R^2 value of 0.9682, 11 knickpoints in the downstream course and an average slope of y = -1.2729x + 997.57 (Figure 6a). The river confluences to the trunk river at an angle of 70° (Figure 10a). Shimsha has an R^2 value of 0.8871, has 8 knickpoints in the downstream course and an average slope of y = -

1.4307x + 822.08 (Figure 6b). The river confluences to the trunk river at an angle of 50° (Figure 10b). The R^2 value of Arkavathi is 0.9013, has 7 knickpoints in the downstream course and an average slope of y = - 2.8092x + 975.3 (Figure 6c). The river confluences to the trunk river at an angle of 85° (Figure 10c). The longitudinal profile of Kabini has an R^2 value of 0.9475, has 4 knickpoints in the downstream course and an average slope of y = -0.44x + 733.03 (Figure 6d). The river confluences to the trunk river at an angle of 50° (Figure 10e). Lakshmantirtha has an R^2 value of 0.9598 and has only 3 knickpoints, one in the catchment region in Wayanad district, Kerala and the river has an average slope of y = -0.4837x + 810.63 (Figure 6e). The river confluences to the trunk river at an angle of 50° (Figure 10d).

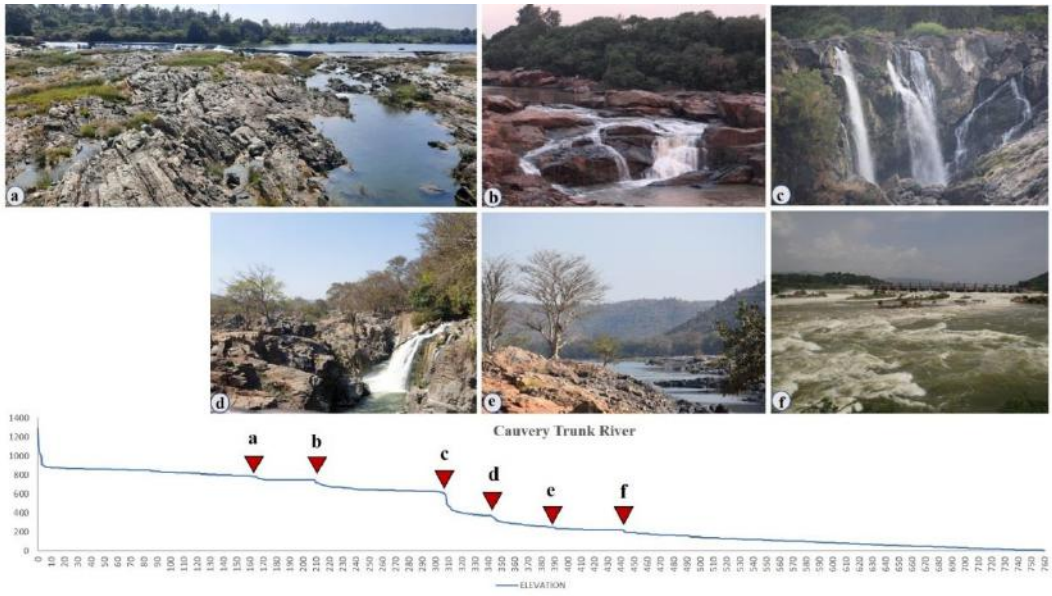

Figure 5: Knickpoints recorded in the longitudinal profiles of the Cauvery River. (a) step fault controlled waterfall in the upstream, which is the first prominent knickpoint along the course of the Cauvery River showing the bedrock channel (b) Balachukki Falls in the Sivanasamudra Falls which is the highest magnitude of knickpoint along the Cauvery, (c) Chunchunakate falls, which is the fault-controlled knickpoint (d) Hogenekkal falls, NE-SW fault controlled major knickpoint, (e) knickzones and bedrock channel in the downstream of Hogenekkal, (f) Downstream of Mettur Stanley reservoir which is the anthropogenically altered major knickpoint in the Middle Cauvery River Basin

Suvarnavati has an R^2 value of 0.6284, has only 2 knickpoints in the catchment and the river has an average slope of y = -3.136x + 828.75 (Figure 6f). The river confluences to the trunk river at an angle of 75° (Figure 10f). The R^2 value of Chinnar is 0.8725, has 5 knickpoints in the course and the river has an average slope of y = -4.3053x + 414.06 (Figure 6g). The river confluences to the trunk river at an angle of 90° (Figure 11b). The longitudinal profile of Palar has an R^2 value of 0.9763, has only a knickpoint in the

catchment and the river has an average slope of y = -6.5071x + 718.64 (Figure 6h). The river confluences to the trunk river at an angle of 125° (Figure 10h). The longitudinal profile of Bhavani has an R^2 value of 0.8648, has 12 knickpoints in the downstream course and the river has an average slope of y = -1.8192x + 473.69 (Figure 6i). The river confluences to the trunk river at an angle of 85° (Figure 11a). Thoppaiyaru has an R^2 value of 0.753, has six knickpoints in the downstream course and the river has an average slope of y = -5.2861x + 549.29 (Figure 6j).

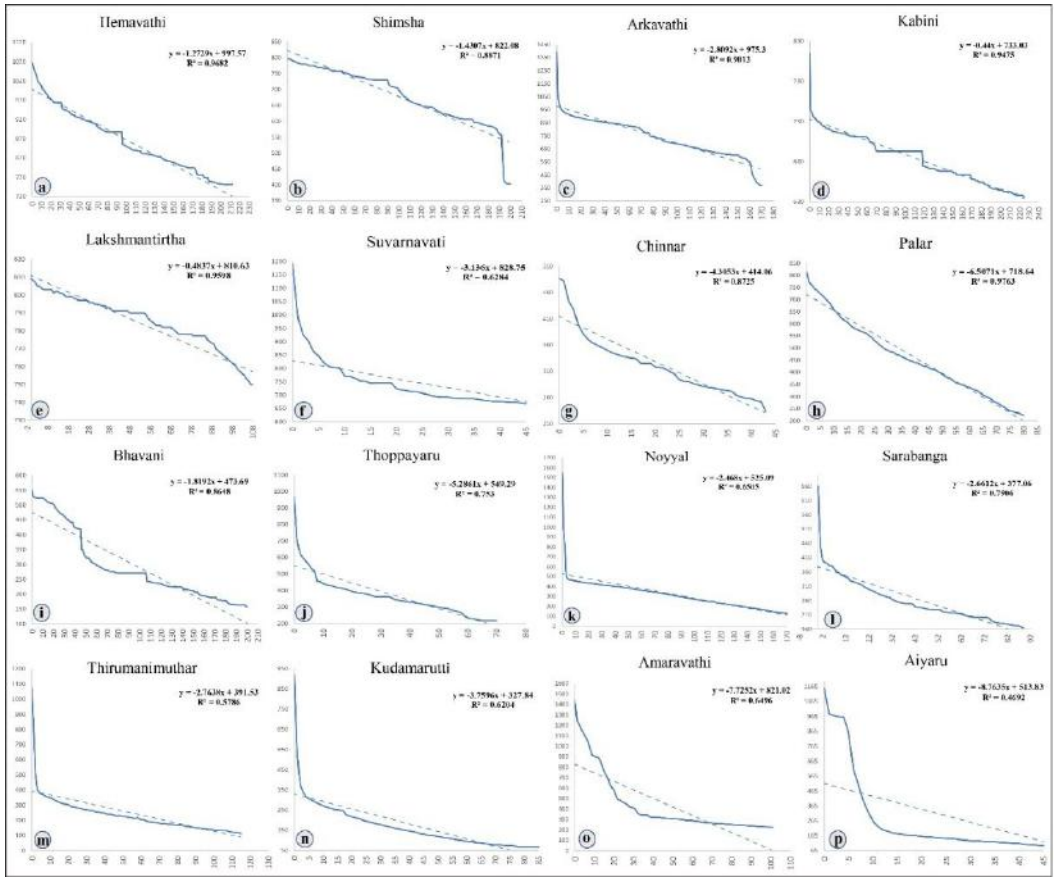

Figure 6: Longitudinal profiles of (a) Hemavati with subsequent breaks in the profile, (b) convex-up profile of Shimsha, (c) Arkavati shows concave-convex-concave nature, (d) Kabini shows prominent successive breaks in the profile, (e) convex-up nature in Lakshmantirtha, (f) concave profile in Suvarnavati, (g) concave profile of Chinnar, (h) Palar shows a highest slope of 9.763 with steep channel gradient, (i) Bhavani shows highly concave nature followed by a sudden fall in the course, (j) Thoppaiyaru, (k) Noyyal, (l) Sarabanga, (m) Thirumanimuthar, (n) Kudamarutti showing gradual slope in the channel (o) Amaravati shows steep slope followed by the gradual course in the channel (p) Aiyaru has the lowest slope/R^2 value and have a significant knickpoint in its upstream.

Figure 7: (a) Thoovanam waterfalls in Amaravati River Basin, is a prominent knickpoint, (b) knickzone in bedrock channel of Amaravati, (c) cobble-boulder deposited at the upstream courses of Amaravati, (d) channel flowing in knickzones of Arkavati River, also shows uplifted rocks in the right bank of the river, (e) Chunchi falls, which is highest magnitude knickpoint/knickzone in the in the downstream of Arkavati and flows into the narrow gorges in the Biligirirangan terrain, (f) pothole development in the riffle and chute structure in the downstream of Kodiveri waterfalls of Bhavani River, (g) gradual elevation difference in the knickzone in the Bhavani River shows the deposition of cobbles in the bedrock channel bed, (h) channel shows low energy condition in Noyyal River, (i) remnants of riffle and chute structure in the anthropogenically altered knickpoint in the Hemavati (j) Iruppu waterfalls in the upstream of Lakshmantirtha, which is the highest knickpoint in the upstream, (k) pebble deposited channel bed in the Kabini, (k) knickzone in the upstream of Hemavati River shows steep channel gradient, (l) gentle channel gradient in Bhavani, boundary hills of Bhavani sub-basin is also visible in the backdrop, (m) gradual and gentle downstream course of channel in Thirumanimuthar

Figure 8: (a & b) Knickpoint in the Sarabanga River shows bedrock channel with minor vertical drops in the course of the channel, (c) Agayagangai Falls, single and prominent knickpoint in the Aiyaru River (d) rocky channel bed along the knickzone in Shimsha with no sediment deposition indicating steep slope and high energy of the river, (e) boundary hill and bedrock channel in the vicinity of knickzone in Palar River, boundary hills of the sub-basin can be seen at the backdrop, (f) knickzone and the bedrock channel with sand deposition in the Palar River, (g & h) knickpoint and knickzones at Thirumanimuthar River, (i) Anaimadavu waterfalls at the upstream of Toppaiyaru River, (j) downstream flow of Aiyaru with no significant changes in the channel gradient, altered banks are also visible, (k) bedrock channel at the downstream of knickpoint in the Thoppaiyaru River, (l) minor knickpoint in the Hemavathi River in the bedrock channel, (m) knickpoint at the Suvarnavati River (Suvarnavati Dam), (n & o) shear zone and knickzone development in the Chinnar River.

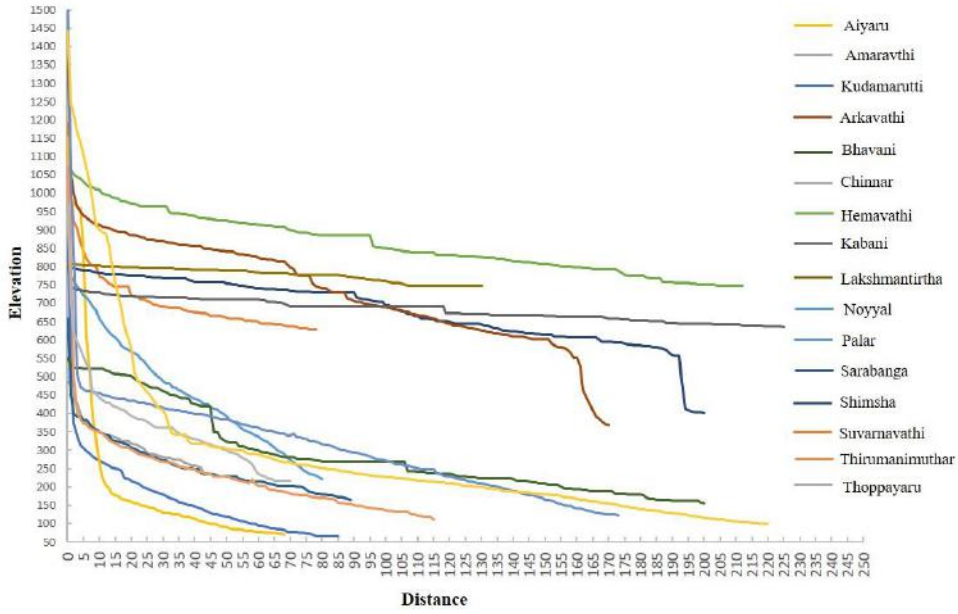

Figure 9: Comparison profile with the result of plots of longitudinal profiles of 16 tributaries of the Cauvery River, Hemavathi flows in an elevated terrain compared to the other tributary rivers in the basin, where Noyyal and Kudamarutti have the lowest base level.

The river confluences parallel to the trunk river at 180° (Figure 10g). The R2 value of the longitudinal profile of Noyyal is 0.6505, there are 12 knickpoints in the course, and the river has an average slope of y = -2.468x + 525.09 (Figure 6k). The river confluences-to the trunk river at an angle of 50° (Figure 10h). The R^2 value of Sarabanga is 0.7906, has 9 knickpoints in the course and the river has an average slope of y = -2.6612x + 377.06 (Figure 6l). The river confluences–with the trunk river at an angle of 35° (Figure 11g). Thirumanimuthar has an R^2 value of 0.5786, has 8 knickpoints in its course and the river has an average slope of y = -2.7638x + 391.53 (Figure 6m). The river confluences to the trunk river at an angle of 60° (Figure 11c). The R2 value of the longitudinal profile of Kudamarutti is 0.6204, there is only 1 knickpoint in the catchment, and the river has an average slope of y = -3.7596x + 327.84 (Figure 6n). The river confluences with the trunk river at an angle of 65° (Figure 11d). The R2 value of Amaravathi is 0.6496, there are nine knickpoints in the downstream course, and the river has an average slope of y = -7.7252x + 821.02 (Figure 6o). The river confluences with the trunk river at an angle of 65° (Figure 11e). Kudamarutti has an R^2 value of 0.4692 and has only 1 knickpoint in the catchment, which is Agayagangai Falls located in Kolli hills and the river has an average slope of y = -8.7635x + 513.83 (Figure 6p). The river confluences to the trunk river at an angle of 45° (Figure 11f).

Discussion

Behavioural Patterns of Major Sub-basins

The behavioural patterns of sub-basins within the Cauvery River Basin have been comprehensively investigated through extensive field surveys. The inclusion of selected field photographs in Figures 7 and 8 enriches the understanding of these patterns.

Hemavathi's catchment exhibits highly undulating topography with lateritic soil. Additionally, the Basin features a pediment-pediplain complex characterized by red soil. Knickpoints located upstream manifest within an incised channel with bedrock rapids, while flood plains commence in the upstream course itself. The Basin's geomorphology is significantly influenced by regional structural controls, evidenced by the N-S trending strike directions of bedrock reflections (Figure 8l). Downstream, well-developed terraces with pebbles and cobbles on old terraces and fine to medium sand on recent terraces are observed. Knickpoints are accompanied by observations of Mylonites, indicating a shear zone. Mid-channel bars, spanning 170 kilometers, exhibit flourishing vegetation cover, with the channel assuming meandering patterns downstream. Flood plain formation followed by natural levees becomes noticeable. As the channel progresses towards the confluence, a shift in channel morphology, characterized by riffle-chute structures and pebble gravel deposition, signifies active channel dynamics influenced by regional tectonics (Figure 7i).

Shimsha originates and traverses low-relief surfaces devoid of undulations, with ferrous/red soil dominating the Pedi plain amidst dense plantations. Despite this, the channel generates flood plains upstream and exhibits sand deposition within the channel bed. Structural controls become prominent as the channel nears the confluence, marked by Shimsha Falls, a major 76-meter cascade. Notably, the bedrock channel features a prominent N-S trending strike direction (Figure 8d). Downstream reactivation occurs approximately 130 kilometers from the source, characterized by increased velocity and riffle-chute structures in the channel bed (Figure 8d). Subsequent channel downcutting leaves paleo-terraces on either bank, ultimately leading to the channel's descent into deep gorges en route to its confluence.

Arkavati encounters numerous structural control points, or knickpoints, as it progresses downstream. The initial knickpoint, situated 68 kilometres from the channel's origin, occurs within an incised channel bed comprised of granitic gneiss (Figure 7d). Erosive activity results in the absence of material deposition such as gravel and sand downstream. This erosional signature persists throughout the Basin's knickpoints. Near the downstream region, boundary hills shape an L-shaped topography with valleys, exhibiting highly weathered and jointed rocks with minimal soil cover. Chunchi Falls downstream represents a point of structural activity, leading to a 90-degree turn in the channel's flow path towards the confluence.

Kabini demonstrates an early propensity for floodplain formation, with the first knickpoint occurring at 69 kilometers, marked by successive elevation breaks downstream.

The Basin's peculiarities include a bedrock channel alongside cobble, pebble, gravel, and coarse sand deposition across a 50-meter channel width. The catchment region's undulating topography transitions to slightly undulating terrain downstream, with stable banks, old terraces, and well-developed flood plains near Mysore's plateau region. The channel width peaks near the confluence, reaching approximately 180 meters.

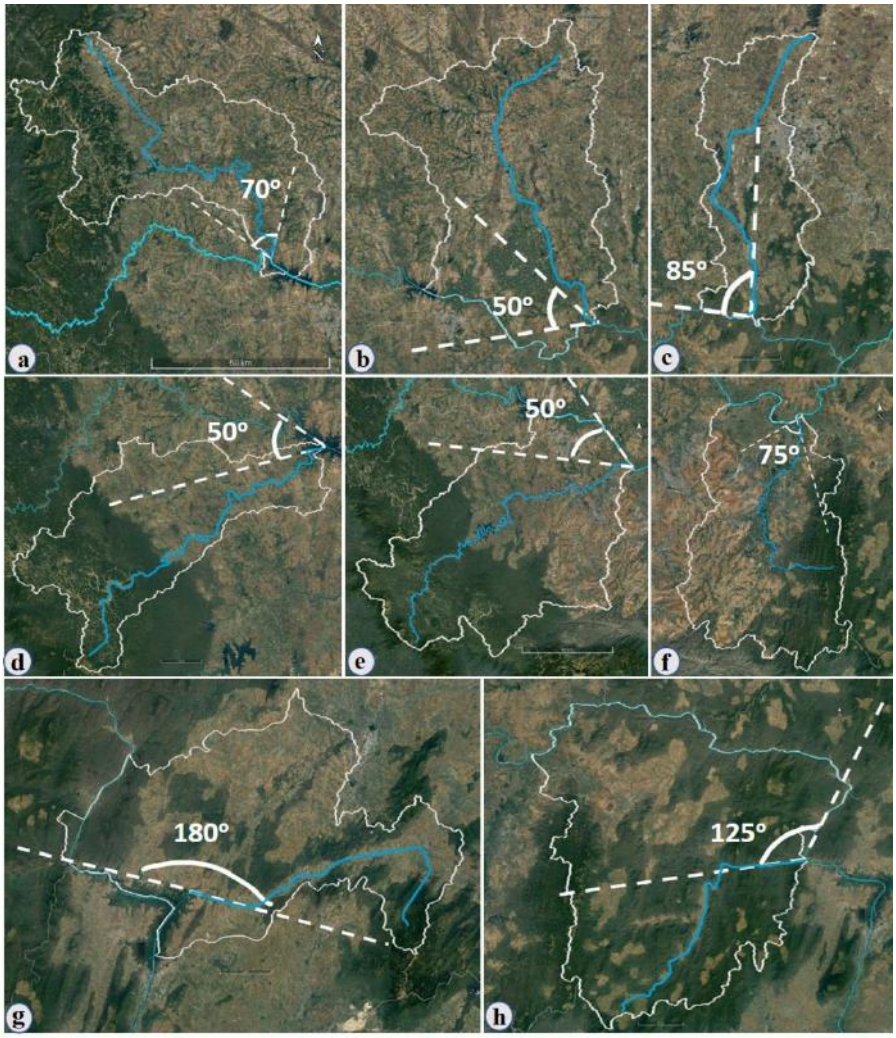

Figure 10: Confluence of (a) Hemavati shows an acute angle of 70°, the river shows straight course and successive two 90° turns in the upstream (b) Shimsha has an acute angle of 50°, (c) Arkavati has successive three near ninety degree turns in the course and an 85° confluence, (d) Lakshmantirtha shows 50° and a meandering channel course, (e) Kabini shows an acute angle of 50°, (f) Suvarnavati has an acute angle of 75°, (g) Thoppayaru has an obtuse/zero degrees angle of 180°, (h) Palar has an obtuse angle of 125° and a ninety-degree turn in the course.

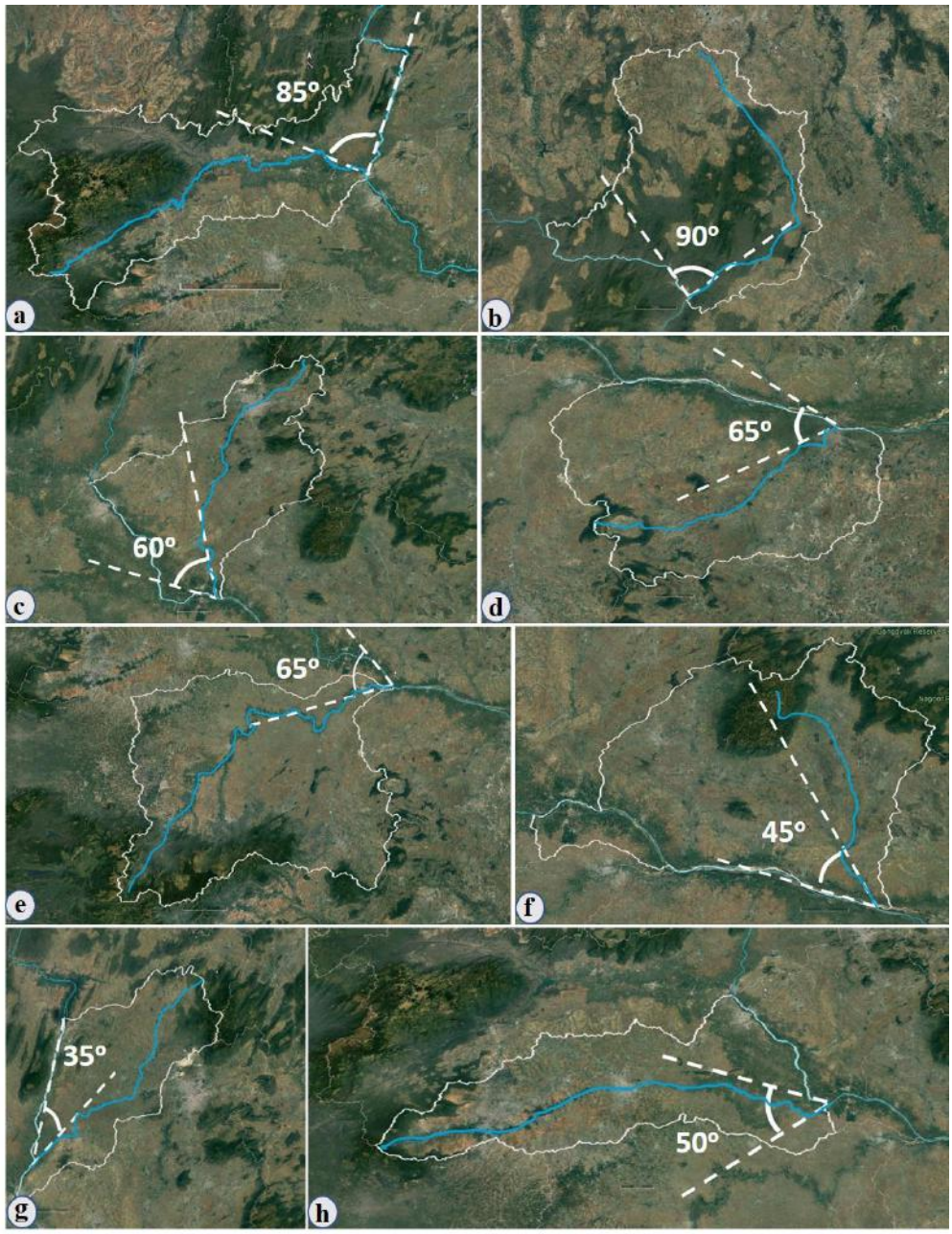

Figure 11: Confluence of (a) Bhavani is an 85° angle, (b) Chinnar has a perpendicular/90° angle and almost straight channel and a ninety-degree turn in the course, (c) Thirumanimuthar has an acute angle of 60°, (d) Kudamarutti has an acute angle of 65°, (e) Amaravati has 65° (f) Aiyaru has 45°, (g) Sarabanga has an acute angle of 35° and the channel shows obtuse angle turn in its course, (h) acute angle of 50° of Noyyal.

Lakshmantirtha's catchment is characterized by lateritic soil and dense forest cover. The undulating terrain features high elevation low relief surfaces and flood plain formation extending up to 100 meters upstream. Notably, the Basin's lone knickpoint, Iruppu Falls, is a cascade with a strike direction of N 45º E (Figure 7j). Pebble deposition characterizes the downstream course, while calcrete formations are ubiquitous. The channel, reaching base level, incises valleys and forms paleo-terraces, with a bedrock strike direction of N 150º E and a maximum channel width of 15-20 meters.

The Palar and Suvarnavati rivers, which originate in the charnockitic terrain of the Biligirirangan Hills, exhibit distinctive geomorphological characteristics. These watercourses flow through bedrock channels characterized by the presence of knickzones rather than discrete knickpoints (Figure 8e and f). This geomorphic feature suggests a complex interplay between lithology, tectonics, and fluvial processes in shaping the river profiles. In contrast, the Chinnar River displays two notable morphological features along its downstream course. Firstly, it develops extensive floodplains in its upper reaches, extending to the point where the river intersects a major fault line (Figure 3). Secondly, in its lower reaches, the river's course is marked by narrow gorges (Figure 8 n and o), persisting until its confluence point. This transition from broad floodplains to confined gorges likely reflects the river's response to structural controls and variations in bedrock erodibility.

Bhavani's catchment boasts numerous first-order streams with dendritic drainage patterns. Neo-tectonic activity is evident in boundary hills, which feature cliff faces and rocky barren surfaces. Knickpoints exhibit a consistent N 237º E strike direction in the riffle and chute structure (Figure 7f), indicating an NE-SW bedrock trend. The absence of V-shaped valleys results in the lack of terrace and floodplain formations along the channel banks. Cobble deposition persists downstream, indicating active sediment transport and selective erosion (Figure 7g).

The catchment hills surrounding Thoppaiyaru give rise to distinctive L-shaped valleys, characterized by brown-colored soil and coconut plantations. These hills are densely covered with forests and exhibit an abundance of rolled-down boulders extending up to the pediment region. Along the channel's bed and banks, numerous boulders are scattered. Upon leaving the pediment, the left bank of the channel subsides, resulting in extensive floodplain deposits, paddy fields, and natural levees. Conversely, the right bank also experiences subsidence, featuring similar floodplain deposits, paddy fields, and natural levees. Notably, a section of the channel is exposed by 3 meters en route to Anaimadaavu waterfalls, the sole cascade along the Thoppaiyaru River (Figure 8i), formed by a cascade of two successive faults of 2 meters each. Boulders from surrounding hill slopes are deposited within the narrow stream channel (5-8m), alongside sand in the channel bed. As the channel reaches its base level, it carves incised valleys and paleoterraces, with the bedrock exhibiting a strike direction of N 150º E and a maximum channel width of 15-20 meters.

The boundary hills and valleys within the Noyyal Basin display an L-shaped topography, notable for the absence of foothills and residual hillocks across the entire

basin. The terrain remains relatively flat, with minimal undulations, and the channel gradient is notably low (Figure 7h). Knickpoints in the upstream section have been transformed into check dams. Upstream, the channel width measures less than 30 meters, with negligible transport of sediment load within the channel bed. Calcretized natural levees are a prominent feature of the Noyyal River, owing to the channel's operation at base level. Downstream, natural levees and flood plains extend over a wide area, maintaining consistent channel width. Near the confluence, fluvial paleo-terraces are prevalent, with incised channels reaching the bedrock. Structural controls become prominent in the vicinity of the confluence, with the channel's strike direction transitioning from N 260º W to an exact N-S orientation. Despite similarities in riverine characteristics with upstream regions, structural influences play a significant role in transforming basin characteristics to a rocky channel near the confluence of the Cauvery.

The boundary hills of Sarabanga resemble those of adjacent river basins, such as Thoppaiyaru, featuring an L-shaped topography. These hills are characterized by thin soil cover and exposed, intensely weathered rocky surfaces. Along the basin boundary, sharp peaks and cliff faces are prominent features. Upstream, the stream width is less than 10 meters, with a low water discharge rate compared to other left bank tributaries of the Cauvery. However, near the confluence, the channel widens to a maximum of 40 meters, creating vast flood plains extending up to 1 kilometer. As the channel progresses downstream, it encounters significant structural control points, including falls, cascades, and rapids (Figures 8 a&b), with a strike direction of N 45º E, aligning with the regional trending of hill ranges as observed in Google Earth Pro satellite images.

Anthropogenic interventions have altered all knickpoints along the Thirumanimuthar, resulting in the river no longer exhibiting fluvial downstream characteristics in terms of deposition and water quality. The channel's incision rate is minimal, with well-developed flood plains on either bank (Figure 8g). Despite consistent anthropogenic interventions downstream, the channel is experiencing reactivation due to tributary stream discharges and knickzone influences. Approximately 50 kilometers downstream, the right bank becomes raised, resulting in the formation of an erosional bank on the left and old terraces on the right. Cobble deposition begins at this point, coinciding with the channel's departure from the pediment region of surrounding hillocks. Aside from fault zone or knickzone interventions within the channel course, the basin exhibits minimal undulations as it progresses downstream, culminating in a sudden fall marked by structural evidence such as abrupt topographic breaks and large-scale granulite gneiss bedrock exposure. The bedrock's strike direction trends from NE-SW to E-W in the downstream course of the river.

The Amaravathi basin features a topographic arrangement of hills and foothills at its source, with the first orders originating from boundary hills as well as foothills upstream (Figure 7b). V-shaped valleys are a common feature between the hills and foothills, with thick vegetation covering the boundary hills. The terrain is characterized by undulations, structural controls, and a high density of knickpoints spanning the entire 40-kilometer river

course. The most significant knickpoint is a 30-meter drop known as Thoovanam Waterfall (Figure 7a), located at Marayoor near Munnar, with bedrock orientation set at N-S. Pambar, a tributary of Amaravathi, exhibits minimal deposition up to 20 kilometers of its course. As the stream gradient decreases with the onset of pediment characteristics, cobble-boulder deposition begins on the left bank (Figure 7c). Downstream, the channel is recharged by residual hillocks with thin or no soil cover. Flat-topped hills become prominent features of the downstream course. Despite transitioning to a rocky nature due to knickzone development, the Amaravati River begins depositing sand and forming floodplains after 38

kilometers of flow. Notably, the left bank of the Amaravati River rises towards the river's downslope course.

Longitudinal profile and knickpoints

The longitudinal profile is a cross-sectional representation of the channel reach and its measurement in a linear direction downstream. It is a measure of elevation and distance covered by the stream along the geomorphic features. The profile aids in detecting knickpoints along the stream to define the transient response of the stream to variation in lithology, climate, and rock uplift and/or subsidence (Kirby et al., 2003) The link between tectonic processes and stream longitudinal profile shape has been the subject of several types of research (Ambili & Narayana, 2014). When semi-logarithmically plotted, the equilibrium stream profile on a single lithology is a straight line (Tucker & Whipple, 2002).

A more resistant lithology, an increase in shear stress, or surface uplift can all contribute to knickpoints, or the sharp reaches in the longitudinal profile (Bishop et al., 2005). A stream in equilibrium has a concave-up longitudinal profile, whereas a disruption in the gentle curve usually characterized by a “convex reach” is known as a knickpoint. Knickpoints delineate the transition between the steady state and changing landscape in each catchment. These anomalies in profiles may point to an equilibrium stream (Bishop et al., 2005) or, in some instances, a dynamic equilibrium between fluvial processes and tectonic movements, where the upstream retreat reflects changes in base-level in the upstream valley. Knickzones should respond to changes in the local lithology or the base level. Rapid river incision caused by upstream movement of knickzones creates terraces and makes valley side slopes unstable (Hayakawa and Matsukura, 2002).

The high values of R^2 for Hemavati, Shimsha, Arkavati, Kabini, Lakshmantirtha, and Palar rivers indicate that the linear model fits the data well, suggesting a strong correlation between stream slope and distance. This implies that the stream is likely in an equilibrium state, with consistent erosion and sediment transport processes along its course (Leopold et, al., 1964). Conversely, a low to very low R^2 value of Suvarnavati, Thoppaiyaru, Noyyal, Sarabanga, Thirumanimuthar, Kudamarutti, Amaravathi and Aiyaru suggests that the linear model does not fit the data well, indicating variability or non-linearity in the relationship between stream slope and distance (Figure 6). The longitudinal profiles of the Aiyaru and Kudamarutti catchments exhibit notable geomorphological characteristics,

particularly in the form of a single prominent knickpoint followed by a gradual downstream course (Figure 8c and j). This distinctive profile configuration demonstrates significant variability in the fluvial system's longitudinal development. The presence of an isolated knickpoint in each of these catchments suggests a localized perturbation in the river's equilibrium profile. Such features often arise from various factors, including lithological boundaries, tectonic activity, or base-level changes. The singular nature of these knickpoints implies a discrete event or threshold in the catchment's geomorphic evolution rather than a series of ongoing disturbances. Longitudinal profiles of sixteen tributaries of the Cauvery show variable curves and gradients (Figure 6). While the Upper Cauvery Basins and the Cauvery trunk river have steep slopes along the spatial distribution of longitudinal profiles, differential uplift could be due to the high gradient of stream profiles.

In the process of discerning knickpoints within longitudinal profiles, the utilization of spatial maps, including those depicting geology, structure, and lithology, emerges as a crucial factor. These maps facilitate an understanding of the underlying terrain and its geological characteristics. The occurrence of knickpoints at lithologic boundaries can be attributed to various factors, including but not limited to differential erosion, fluctuations in base levels, and tectonic activities. These mechanisms collectively contribute to the formation and evolution of knickpoints along river longitudinal profiles, highlighting the multidimensional nature of landscape dynamics influenced by geological processes.

Knickpoints can form at lithologic boundaries due to base-level changes. A base level is the lowest point to which a river can erode its bed. When a lithologic boundary is encountered, the base level might change abruptly due to differences in rock resistance. This change can lead to the formation of a knickpoint as the river adjusts to the new base-level. (Howard, 1994) When a river encounters a lithologic boundary, such as a transition from softer to harder rock or from resistant to less resistant rock, it can also create a knickpoint where the erosion rate suddenly increases. This happens because the river's erosive power may vary depending on the type of rock it's eroding. For instance, softer rocks might erode more quickly, leading to the formation of a steeper section in the channel, while harder rocks might resist erosion, resulting in a relatively flat section. In the examination of the longitudinal profile of the trunk, a total of 24 knickpoints were identified. Notably, five of these knickpoints were found to coincide with lithologic boundaries delineating gneiss and charnockite formations. Further investigation revealed the presence of litho-boundary controlled knickpoints along prominent river systems, including the Arkavati, Hemavathi, Shimsha, and Thirumanimutharu (Figure 2). Remarkably, singular instances of knickpoints were observed at the (Suvarnavati Figure 8m) and Aiyaru (Figure 8c) rivers, suggestive of potential correlation with the underlying lithologic composition, particularly the formation of charnockite. These findings underscore the significance of lithologic boundaries in influencing the morphological characteristics of river profiles, thus warranting deeper exploration into the mechanisms governing fluvial geomorphological evolution within such contexts.

Lithologic boundaries are often associated with geological structures such as faults or folds, which can influence the course and behavior of rivers. Tectonic activity can create

uplift or subsidence along these boundaries, leading to the formation of knickpoints as rivers respond to changes in topography and rock structure (Crosby et. al., 2010) These factors potentially account for the presence of knickpoints identified along the Bhavani and Sarabanga rivers. Notably, these abrupt changes in elevation are consistently observed along the Bhavani Shear Zone (BS) and Salem Arthur Shear Zone (SAS), as depicted in Figure 2. Furthermore, knickpoints dispersed throughout the Cauvery trunk stream predominantly align with shear zones or fault boundaries, as illustrated in Figures 2 and 3. These observations underscore the significance of structural features such as shear zones and faults in influencing the formation and distribution of knickpoints within fluvial networks, indicative of their role in shaping regional geomorphological landscapes.

Confluence angle and its impact on channel morphology

The upstream and downstream sections of the mainstream vary in width and depth, and these differences are related to variances in the confluence morphology. (Roy and Woldenberg 1986). In general, at a cross-section, the downstream reach is wider and deeper. It is quite challenging to perform a scientific investigation into the complexity and variations of both local and downstream features of river channel confluences because they are the crucial interfaces where two streams with different characteristics meet. River channel confluences represent a critical component of drainage system geometry, and are points at which river morphology and hydrology can change drastically (Mosley 1976). Rezaur et al. (1999) have estimated that the angle of incidence of 15°–75° has been associated with the rapid increase of the scour depth and that it occurs slowly up to 120°. Upper reaches of the basin have confluence angles between 50° and 85° which indicates an increase in the scouring capacity of the channel. The Thoppayaru River in the middle Cauvery Basin confluences at an angle of 180° to the mainstream (Figure 10g) and the Palar has a confluence angle of 125°. These two obtuse angles of confluence show anomalous characteristics within the basin while the lower tributaries have less scoring capacity since the confluence angle is less.

The obtuse angle of Thoppaiyaru and Palar suggests (Figure 12a) a relatively gentle merging of these two watercourses. Such an angle could be indicative of low sediment load or relatively equal flow rates between the tributaries, resulting in a smoother confluence. Additionally, the surrounding topography may influence the angle, with wider valleys or flatter terrain encouraging a more gradual merging of rivers. Conversely, the perpendicular angle of confluence (Figure 11b) noted at Chinnar suggests a sharper meeting point between the tributaries. This could arise from varying flow rates or sediment loads, causing one tributary to intersect the other more abruptly. It's also possible that the topography at this confluence point is characterized by steeper slopes or narrower channels, promoting a more abrupt merging of the rivers. The observation that all other tributaries exhibit acute angles of confluence implies a consistent trend in their merging patterns. Acute angles typically indicate a more forceful convergence, which could be driven by factors such as high flow rates, significant differences in water volume between the tributaries, or the presence of obstructions that force a sharper merging angle.

Furthermore, these observations could be influenced by anthropogenic factors such as human interventions like dams or diversions, which can alter natural river flow patterns and confluence angles. The confluence angles observed among the tributaries likely reflect a complex interplay of geological, hydrological, and anthropogenic factors, each contributing to the unique merging patterns observed in this study. Further analysis incorporating detailed topographic and hydrological data could provide deeper insights into the underlying processes shaping these confluence angles.

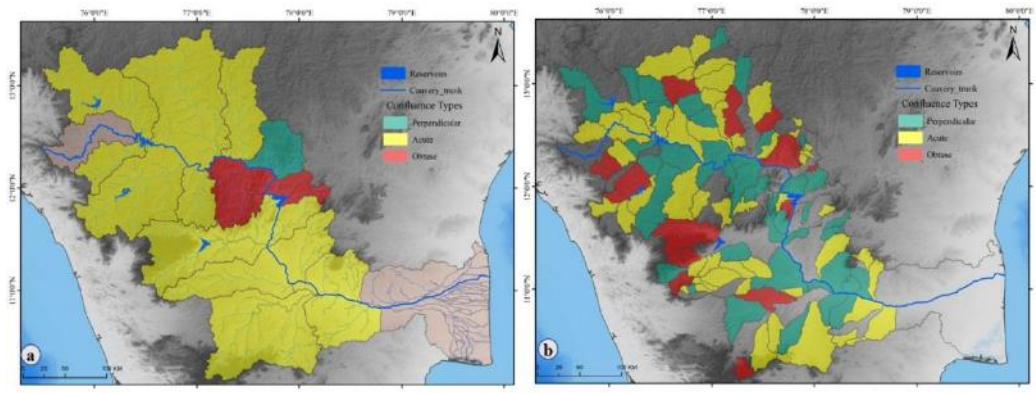

Figure 12 a: Confluence angle map for the first level tributaries, shows obtuse confluence angle in Palar and Thoppaiyaru rivers and perpendicular confluence of Chinnar River b: second level tributaries of the basin show random confluences in the Cauvery River Basin.

In examining the second-level tributaries within each subbasin, our study reveals distinct confluence angles that offer insights into the geomorphic and hydrological dynamics of the basin. It is observed that 19 smaller basins exhibit obtuse confluence angles as they join the main tributary (Figure 12b). Notably, these confluences predominantly occur in proximity to dam/reservoir installations or within flat terrain regions. This observation suggests a correlation between the obtuse angles and specific environmental conditions, notably the presence of hydraulic controls/ structures or regions characterized by gentle gradients. Such conditions likely facilitate a more gradual merging of smaller basins into the main tributary. Conversely, tributaries characterized by acute confluence angles tend to be situated in areas with steeper slopes within the basin's topography. This observation suggests a relationship between acute angles and the geomorphic features of the basin, particularly areas with pronounced elevation differentials. The sharper merging angles in these instances likely reflect the hydraulic forces generated by the rapid descent of watercourses down steep gradients. These findings underscore the influence of both topographical characteristics and anthropogenic interventions on confluence angles within the basin.

The determination of tectonic activity solely based on the confluence angle of a single tributary may lack conclusive evidence. This is because stream junction angles are susceptible to various influences beyond crustal deformation. Factors such as topographic

slope at the junctions, flow discharge, sediment load within channels, sediment transport dynamics at confluences, channel bed morphology, flow velocity, turbulence, scour depth, bar size variations in channels, debris flow occurrences, groundwater seepage, instances of stream capture, channel instability, lateral migration, and channel meandering collectively contribute to the observed confluence angles. Therefore, interpreting tectonic activity based solely on a single tributary's confluence angle necessitates a thorough consideration of these multifaceted environmental dynamics Montgomery et., al 2001; Church and Zimmermann, 2007).

Conclusion

The morphometric analysis of stream profiles in the Cauvery River basin has yielded significant insights into the complex interplay between geomorphological processes and geological factors that shape fluvial landscapes. The tributaries of the Cauvery River exhibit non-uniform concave profiles, characterized by the presence of numerous knickpoints. These discontinuities in the longitudinal profiles can be primarily attributed to structural and lithological controls, as the majority of the streams traverse diverse lithologies and intersect shear zones and faults along their courses. Notable exceptions to this pattern include the Kabini, Noyyal, and Amaravathi tributaries, which flow through relatively homogeneous lithology, and the Amaravathi, Aiyaru, Kudamarutti, and Noyyal tributaries, which do not intersect major structural features. Arkavati, Shimsha, Hemavati, Chinnar, and Bhavani, demonstrate elevated slope values, suggesting that the rate of tectonic uplift exceeds the rate of fluvial incision in these sub-basins. This observation underscores the significant influence of lithological variations and structural controls on channel gradient and overall river profile morphology. Statistical analysis of the relationship between stream slope and distance reveals varying degrees of correlation across the tributary network. High R^2 values observed for the Hemavathi, Arkavati, Kabini, Palar, and Lakshmantirtha rivers indicate a strong linear correlation between these parameters, suggesting equilibrium conditions and consistent erosional processes along their courses. Conversely, the lower and more variable R^2 values obtained for the Aiyaru, Thirumanimuthar, and Kudamarutti rivers imply non-linear relationships between stream slope and distance, highlighting the dynamic and potentially disequilibrium nature of these fluvial systems. Furthermore, the presence of obtuse and right-angle confluences, particularly evident in the cases of Thoppaiyaru, Chinnar, and Palar tributaries, provides additional evidence of structural control on the river network configuration. These angular junctions reflect the influence of underlying geological structures, such as faults or joint systems, on the drainage pattern development.

This comprehensive analysis of stream profiles in the Cauvery River basin elucidates the complex interactions between tectonic, lithological, and fluvial processes in shaping the regional geomorphology, offering valuable insights into the evolution of this drainage system. Knickpoints at lithologic boundaries are influenced by factors like differential erosion and tectonic activities. Geological structures such as faults and folds determine river course and behavior, with tectonic activity leading to uplift or subsidence

and the formation of knickpoints. Structural features like shear zones and faults shape knickpoint distribution in fluvial networks. Tributary river basins of Cauvery River Basin have unique topographic features and geomorphic processes, reflecting diverse geological settings. Longitudinal profiles indicate stream responses to geomorphic and tectonic processes, with knickpoints marking transitions between steady-state and evolving landscapes. Lithologic boundaries significantly influence knickpoint formation, with associations between structural features and abrupt elevation changes along river profiles. The complex interplay between geological processes and fluvial geomorphology is highlighted, underscoring the multidimensional nature of landscape evolution. Further research using detailed spatial mapping and modeling is needed to elucidate relationships between lithology, tectonics, and river morphology, advancing the understanding of fluvial geomorphological evolution in diverse landscapes.

Acknowledgment

ALF expresses gratitude to Periyar University for granting a University Research Fellowship to support the doctoral program. Thanks are extended to the anonymous reviewers whose critical feedback significantly enhanced the quality of the manuscript. The author also appreciates the editors for their encouragement and support throughout the process.

References

1. Ambili, V., & Narayana, A. C. (2014). Tectonic effects on the longitudinal profiles of the Chaliyar River and its tributaries, southwest India. *Geomorphology*, *217*, 37-47.

2. Bishop, P., Hoey, T.B., Jansen, J.D., & Artza, I.L. (2005). Knickpoint recession rate and catchment area: the case of uplifted rivers in eastern Scotland. *Earth Surface Processes and Landforms*. 30 (6), 767–778

3. Burbank, D.W., Leland, J., Fielding, E., Anderson, R.S., Brozovic, N., Reid, M.R., & Duncan, C. (1996) Bedrock incision, rock uplift and threshold hillslopes in the northwestern Himalayas: *Nature*, v. 379, p. 505–510

4. Church, M., & Zimmermann, A. (2007). Advances in fluvial dynamics and sediment transport. *John Wiley & Sons*.

5. Crosby, B. T., Whipple, K. X., & Gasparini, N. M. (2010). Bedrock channel adjustment to tectonic forcing: Implications for predicting river incision rates. *American Journal of Science,* 310(10), 1106-1146.

6. Dolliver, H. A. (2012). Using Google Earth to teach geomorphology. Google Earth and virtual visualizations in geoscience education and research. *Geological Society of America Special Paper*, 492, 419-429.

7. Friend, C. R. L., & Nutman, A. P. (1991). SHRIMP U-Pb geochronology of the Closepet granite and Peninsular gneiss, Karnataka, South India. *Journal of the Geological Society of India*, *38*(4), 357-368.

8. Hayakawa, Y., & Matsukura, Y. (2002). Recession rates of waterfalls in Bosco Peninsula, Japan: a predictive equation. *Earth Surfaces and Landforms*. 28, 675–684.

9. Howard, A.D. (1994). A detachment-limited model of drainage basin evolution. *Water Resources Research*, 30(7), 2261-2285.
10. Kale, V. S. (2014). Geomorphic history and landscapes of India. In V. Kale (Ed.), Landscapes and landforms of India. *World Geomorphological Landscapes*. (pp. 25–37). Dordrecht: Springer. https://doi.org/ 10.1007/978-94-017-8029-2_3.
11. Kandaswamy, P.K. (1986) Irrigation development in Tamil Nadu, Bhagirath, vol 22. pp 67–73.
12. Keller, E.A, & Pinter, N. (2002) Active tectonics: earthquakes, uplift, and landscape, 2nd edn. Prentice Hall, Upper Saddle River.
13. Kirby, E., Whipple, K. X., Tang, W., & Chen, Z. (2003). Distribution of active rock uplift along the eastern margin of the Tibetan Plateau: Inferences from bedrock channel longitudinal profiles. *Journal of Geophysical Research: Solid Earth*, *108*(B4).
14. Kirby, E., & Whipple, K. X. (2012). Expression of active tectonics in erosional landscapes. *Journal of Structural Geology*, 44, 54–75. https:// doi.org/10.1016/j.jsg.2012.07.009
15. Larue, J.P. (2008a). Effects of tectonics and lithology on long profiles of 16 rivers of the southern Central Massif border between the Aude and the Orb (France). *Geomorphology*. 93, 343–367.
16. Larue, J.P. (2008b). Tectonic influence on the Quaternary drainage evolution on the northwestern margin of the French Central Massif: the Cruese valley example. *Geomorphology.* 93, 398–420.
17. Leopold, L. B., Wolman, M. G., & Miller, J. P. (1964). Fluvial processes in geomorphology: San Francisco, W. H. Freeman and Co., 552 p.
18. Mosley, M. P. (1976). An experimental study of channel confluences. *The journal of geology*, 84(5), 535-562.
19. Montgomery, D.R., & Buffington, J.M. (1997). Channel-reach morphology in mountain drainage basins. *Geological Society of America Bulletin*, 109(5), 596-611.
20. Montgomery, D. R., & Gran, K. B. (2001). Downstream changes in river channel geometry. *Geology*, 29(2), 139-142.
21. Radhakrishna, B. P. (1968). Geomorphological approach to the charnockite problem. *Geological Society of India*, *9*(1), 67-74.
22. Radhakrishna, B. P. (1993). Neogene uplift and geomorphic rejuvenation of the Indian Peninsula. *Current Science*, 787-793.
23. Ramkumar, M., Santosh, M., Rahaman, S. M. A., Balasundareshwaran, A., Balasubramani, K., Mathew, M. J., & Kumaraswamy, K. (2019). Tectono-morphological evolution of the Cauvery, Vaigai, and Thamirabarani River basins: Implications on timing, stratigraphic markers, relative roles of intrinsic and extrinsic factors, and transience of Southern Indian landscape. *Geological Journal*, *54*(5), 2870-2911.
24. Rezaur, R.B., Jayawardena, A.W., Hossain, M.M. (1999). Factors affecting confluence scour. In: Jayawardena AW, Lee JHW, Wang ZY (eds) *River sedimentation*. Balkema, Rotterdam, pp 187–192.

25. Roy, A. G., & Woldenberg, M. J. (1986). A model for changes in channel form at a river confluence. *The Journal of Geology*, *94*(3), 402-411.Schumm, S.A., 1986. Alluvial river response to active tectonics. *Studies in Geophysics*.
26. Sharma, Anupam., & Rajamani, V. (2001). Weathering of charnockites and sediment production in the catchment area of the Cauvery River, southern India. *Sedimentary geology*, *143*(1-2), 169-184.
27. Strahler, A. N. (1964). Quantitative geomorphology of drainage basin and channel networks. *Handbook of applied hydrology*.
28. Tucker, G. E., & Whipple, K. X. (2002). Topographic outcomes predicted by stream erosion models: Sensitivity analysis and intermodel comparison. *Journal of Geophysical Research: Solid Earth*, *107*(B9), ETG-1.
29. Vaithiyanathan, P., Ramanathan, A. L., & Subramanian, V. (1992). Sediment transport in the Cauvery River basin: sediment characteristics and controlling factors. *Journal of Hydrology*, *139*(1-4), 197-210.
30. Wobus, C. W., Whipple, K. X., Kirby, E., Snyder, N. P., Johnson, J., Spyropolou, K., & Sheehan, D. (2006). Tectonics from topography: Procedures, promise and pitfalls. In S. D. Willett, N. Hovius, M. T. Brandon, & D. M. Fisher (Eds.), *Tectonics, climate and landscape evolution: Geological Society of America* Special 398, Penrose Conference Series (pp. 55–74).

The Indian Geographical Journal
Volume 98 (2) December - 2023, pp 118-134
ISSN 0019-4824

MEASUREMENT OF CHANNEL PLANFORM IN PARTS OF THE UPPER GANGA PLAINS OF UTTAR PRADESH USING REMOTE SENSING AND GIS TECHNIQUES

K. Nageswara Rao, Anurag Singh

Geography Discipline, School of Sciences, Indira Gandhi National Open University
New Delhi-110068.
Corresponding author mail: knrao@ignou.ac.in

Abstract

The dynamic channel planforms of river systems must be understood in order to regulate the impacts of river channels on neighbouring ecosystems. The present research used remote sensing and GIS methods to examine the morphological characteristics of channels and their changing patterns in the Ganga River and its tributaries, including the Ramganga, Kali, and Garra channels from 1975 to 2018. Earth observation data, topographic maps, and GPS field surveys were used to conduct geomorphic mapping, sinuosity changes, and large-scale river channel dynamics. The river's phenomenal oscillation is accentuated by its movement across four decades. To assess the meandering of the river, the sinuosity of the river channels was calculated. The length of the channel varies from 55.1 to 58.9 with a sinuosity (SSI) of 1.02 to 1.11 for Ganga, 27.3-32.4 (SSI: 1-1.07) for Ramganga, 57.5-64.3 (SSI: 1-1.02) for Kali, and it is 26.9-32.9 (SSI: 1-1.08) for Garra. Twenty-six cross-sections were taken into consideration to determine the pace of river movement. The results indicate that the migration of both banks of the river channels varied between 30 and 2900 m in the Ganga, 5 and 649 m in Kali, 134 and 2849 m in the Ramganga, and 25 and 805 m in the Garra. The river channels have continuously moved from their previous positions as a result of hydrological processes and the region's terrain. The aim of carrying out this particular study is to enable the authorities/stakeholders to identify the location-wise erosion and accretion-impacted regions towards implementing constructive steps for managing the river channel shifting activity. The study provides baseline data for addressing river management challenges related to river dynamics, floods, droughts, and environmental sustainability.

Keywords*:* Geomorphic mapping, Sinuosity Index, River Dynamics, Ganga Plains, Uttar Pradesh, Remote Sensing and GIS

Introduction

Running water is a dynamic geomorphic agent that erodes materials and transports them to different locations on the earth's surface. Form and processes are intertwined, and both must be examined to understand the genesis and evolution of landforms. The shape may be measured by analysing its geometric and hydrological parameters, which include discharge and flow rate. The processes may be river function, such as erosion, deposition,

and transportation. Alluvial channels are dynamic and vulnerable to change, yet they change in a variety of ways and at extremely variable rates. River course change is a natural phenomenon caused mostly by bankline erosion, accretion, and downcutting. The changing behaviour of the river channel regulates channel pattern, indicating channel form adjustment with the underlying topography and human activities (Charlton, 2008; Verma et al., 2021). During turbulent flow conditions, lateral migration is invariably linked with bank erosion of the stream bed or channel wall.

The three major Himalayan rivers, the Ganga, Brahmaputra, and Indus, are the world's most sediment-loaded rivers, carrying an estimated 599, 650, and 291 Mt/year, respectively, sediments every year. It accounts for approximately 9% of the entire yearly load transported from continents to seas globally (Meybeck, 1976; Hasnain & Thayyen, 1999; Sinha and Tandon, 2014). The Ganga Plains provide the greatest examples for learning the major issues of river dynamics. The river course of Ganga has changed over time, especially in its seaward stretches before entering the Bay of Bengal (Gupta, 2012). Several scientists have studied fluvial dynamics in terms of tectonics, sedimentology, and hydrological variability (Jain and Sinha, 2004; Thakur and Aggarwal, 2012; Mukherjee and Pal, 2018; Agnihotri et al. 2020). Pati et al. (2008) analysed the western bank of the Ganga in Allahabad to detect the course shift on a spatiotemporal scale. Sarif et al. (2021) investigated the river course changes and morphometric features of the Ganga upstream and downstream of the Farakka Barrage from 1794 to 2017 using historical maps, aerial photographs, satellite imagery and geospatial techniques to understand the river dynamics. Satellite-based remote sensing and GIS tools are utilised to monitor the dynamic environmental changes in river channels. The measurement of a river's channel sinuosity is an important aspect of morphometric analysis since it indicates channel flow and morphological features (Karki and Nakagawa, 2019; Jodhani, 2023).

Accurate knowledge of the physical properties of alluvial channels through quantitative analysis is required for alluvial plain regions because they play a significant role in human subsistence. Alluvial channels have a natural propensity to deviate from a straight path, increasing their sinuosity (Mittal, et al., 2023). Over time, meanders migrate downstream and cause issues at the local level. As a result, rivers with varied patterns behave differently, as do other physical properties such as channel slope and gradient. Therefore, pattern identification might be the initial step in assessing river stability and possible threats. Fluvial processes are primarily caused by natural causes such as discharge, terrain, soils, geological structure, and anthropogenic like deforestation, channelization and construction of dams, etc. Flooding occurs regularly in the upper Ganga plains as a result of the construction of reservoirs and dams on the upper course, the alteration of channels and canals, deforestation and changing agricultural practices, and other human activities. These operations may cause differences in river processes, such as channel course shifting and river bedload destabilisation. Excavation of fertile soils, unauthorised sand and gravel mining, and change of plant cover have all been prevalent in recent days, resulting in flash floods and increased water velocity, all of which have an impact on river processes. Keeping this in mind, the study of shifting courses and fluvial

processes, with a focus on the river Ganga and its tributaries running between Farrukhabad and Hardoi in Uttar Pradesh, has been undertaken as a problem for understanding river form and process. The following objectives were set: (i) explore various morphological aspects, (ii) establish geometric properties of channels and their changing pattern, and (iii) analyse the likely reasons for the changing pattern of river processes.

Description of the Study Area

The river Ganga and its tributaries, namely the Ramganga, the Kali and the Garra, are draining through this study area. The river Ganga originates at a height of 3892 meters from the Gangotri glacier in the Himalayas and flows 2525 km through vast alluvial plains. It Develops one of the biggest delta systems in the world and finally debouches into the Bay of Bengal. The river Ganga gains its name at Devprayag in the Uttaranchal Himalaya, where the Bhagirathi and Alaknanda river meets to form the main channel of this river. The total drainage area is more than a million square kilometres, and it supports nearly 40% of India's total population. Physiographically, the river plains are divided into three categories, namely, Upper, Central and Lower plains, covering various states, i.e. Uttarakhand, Uttar Pradesh, Bihar, Jharkhand and West Bengal.

The study area is a part of the Upper Ganga Plains located between Farrukhabad, Kannuaj and Hardoi region of Uttar Pradesh (UP) State in India. This region is bounded by the districts of Badaun, Shahjahanpur in the north; Kheri, Sitapur in the East; Kanpur Dehat, Kanpur Nagar, Unnao, Lucknow in the South; and Auraiya, Etawah, Manipuri in the West. It lies between latitudes 27°01' - 27°18' N and longitudes 79°38' - 80°00' E covering an area of about 1121 sq. km (Figure 1). In the present study region, the river Ganga is the trunk stream flowing with a stretch of 60 km in length and varying distance from 2 to 5 km in width. The Ramganga, Garra and Kali rivers are the three main tributaries of the river Ganga passing through the study area. The tributary Ramganga joins the Ganga at a distance of 10 km north of Kannauj and the Ganga-Garra confluence is located further 10 km downstream. The river Ramganga originally emanates from Doodhatoli ranges in Uttarakhand at a height of 3600 m. It flows through the Corbett National Park of Uttarakhand and it descends upon the plains near Ramnagar of Nainital district. Bijnor, Moradabad, Bareilly, Badaun, Shahjahanpur and Hardoi cities of Uttar Pradesh are situated on its banks. The river Garra is another tributary of the river Ganga and it originates from the Nandhaur range in Nainital District of Uttarakhand, Kaumon Himalaya. It flows through the three districts of Uttar Pradesh namely Pilibhit, Shahjahanpur and Hardoi. The total length of the river from its origin to the merging point at Hardoi is about 200 km. In the present study, the river Garra flows about 30 km in length and varies from a width of 0.5 to 1 km. It merges with the river Ganga more than 12 km distance to the Kannauj area. Another important tributary of the river Ganga is the Kali River originated in the Doon valley of Uttarakhand and passes through the Saharanpur, Muzaffarnagar and Bagpat districts of Uttar Pradesh. In the present study, the river Kali flows through the districts of Kannauj and Hardoi and it merges with the river Ganga after flowing about 60 km distance.

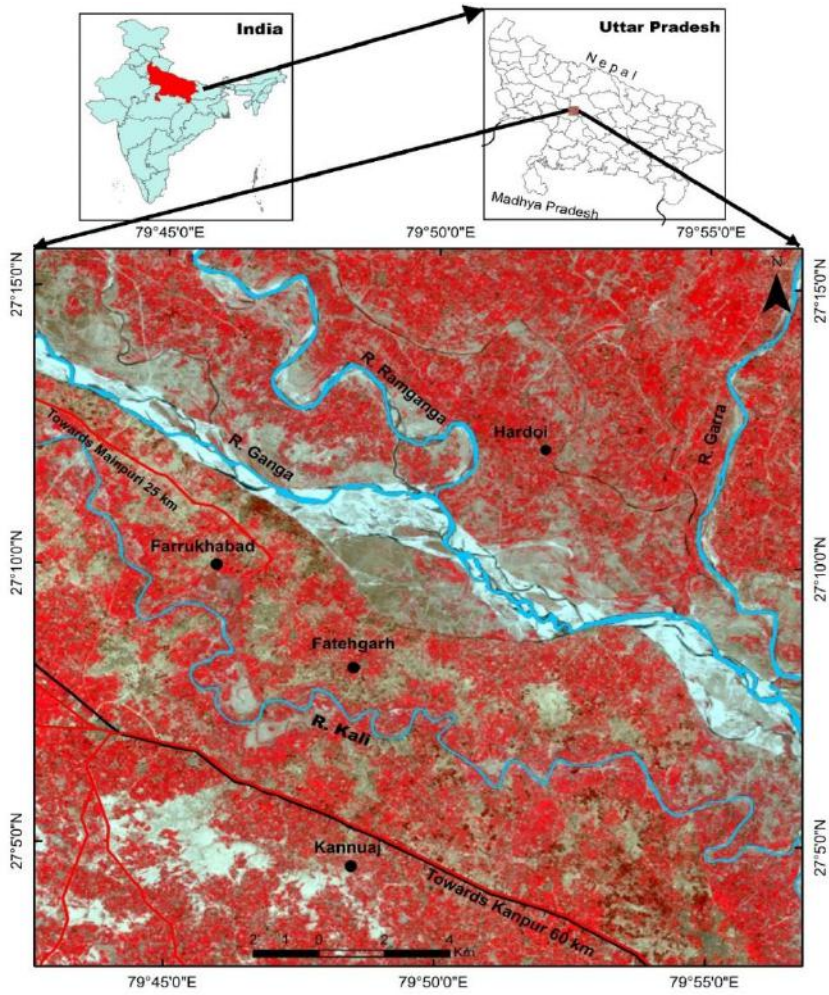

Figure 1. Location of the study area

Climatic variables such as temperature and rainfall play an important role in studying the environmental behaviour of a particular region. The study area is characterized by a sub-tropical humid type of climate. The lowest temperature is 8°C recorded in the month of January and the maximum temperature reaches up to 41°C in the month of May (IMD 2018). The dry winds called *Loo*, which blow at a greater speed, causing heat-related stress and sometimes leading to death. The area receives more than 95% of total rainfall during the southwest monsoon season (June to September). The average annual rainfall received by the study area is 881 mm.

Quaternary alluvium is divided into two types of alluvium i.e. older alluvium and newer alluvium. The major portion of the study area is occupied by older alluvium (Bhagar) of middle to upper Pleistocene age. Newer alluvium (Khadar) is restricted to the paleo bank of the river represented by terraces consisting of fine to medium-grained, gray, micaceous,

unconsolidated sand with grey silt and clay sediments. Lithologically, the surface is characterized by sand flats and elongated mounds. The silty clayey surface hosts a number of paleochannels and oxbow lakes and supports multiple crops.

The region supports nearly 0.9 million population, with a major portion of rural accounting for 77%. The advantage of fertile plains, along with the water accessibility from the Ganga and its tributaries, is the density of the study area is 900 persons per sq. km (Census 2011). The literacy rate is 69.6% of which female are 55.2% and male are 57.5%.

Materials and Methods

The Survey of India topo maps numbered 54 M/11, M/12, M/15, and M/16 on a 1:50,000 scale was utilized to prepare a base map for the study region. LANDSAT satellite data MSS, TM, ETM+ and Sentinel-2 for the years 1975, 1988, 2002, and 2018, respectively, was used for the purpose of research. The date of acquisition of the datasets during the month of November 21-29 for all the years. The digital elevation map of the study area is generated from the Shuttle Radar Topography Mission (SRTM) DEM. The image data is geo-rectified with WGS-1984-UTM (Zone 44) projection. Image enhancement techniques have been applied to enhance the image quality for a better understanding of feature extraction. The colour composite technique has been applied to creating false colour composite (FCC) maps (Figure 1). The base map and satellite data were utilised to analyse the historical river channel changing of the Ganga and its tributaries, including the Ramganga, Garra, and Kali. ERDAS Imagine 14 and ArcGIS 10.5 software were used to analyse digital images and conduct statistical analyses. In addition, a GPS field survey was carried out to identify distinct landforms and landscape characteristics.

The river channels were delineated through on-screen digitization using a base map (1975) and satellite data (1988, 2002, and 2018) to calculate various sinuosity indexes in a GIS environment. The topographic sinuosity index (TSI), hydraulic sinuosity index (HSI) and standard sinuosity index (SSI) were calculated by using the following formulae (Muller, 1968).

HSI = Percent equivalent of CI-VI/ CI-1
TSI = Percent equivalent of VI-1/CI-1
SSI = CL/VL

Where CL is the channel length, VL is the valley length along the stream, CI (channel index) is the ratio of CL to Areal distance, and VI (valley index) is the ratio of VL to Areal distance.

Further, the river courses have been categorized as straight (SSI =1.0), sinuous (SSI =1.0-1.5) and meandering (SSI > 1.5).

We have also investigated the river course changes of the river Ganga and its tributaries the Ramganga, the Kali and the Garra rivers. The spectral band (B4) micro meter

(μm) was utilised to delineate the river bankline since it is suited for water detection. The shifting courses of the river channels were studied during a forty-three-year period from 1975 to 2018. Based on the basemap (1975), 26 fixed cross-sections were chosen. The 2018 image was used as a reference to determine the current location of the Ganga and its tributaries. To better comprehend the river's morphological variations, cross-sections of uneven distances were chosen at several sites along the river's flow from north to south. These cross-section locations were chosen based on the visual assessment of temporal satellite images and significant morphological changes in the river. All cross-sections were labelled with alphabetical letters ranging from A to Z. The cross-sections were labelled A-J for the Ganga, K-O for Kali, P-T for the Ramganga, and U-Z for the Garra. Positive numbers indicate a right-side shift, while negative values suggest a left-side shift from the baseline year. The distance between the left and right banks of the river channel, as well as the direction of migration of the river bank line throughout the research period, were estimated at all cross-sections.

Results and Discussion

Mapping of Fluvial Landforms

The research region has a variety of fluvial landforms, including alluvial plains, abandoned channels, oxbow lakes, sandbars, meander scars, paleochannels, active channels, islands, and floodplains (Figure 2). These geomorphic features were mapped using satellite data by adopting visual interpretation techniques in a GIS environment. To evaluate landform characteristics, we carried out extensive fieldwork and employed high-resolution Google Earth images. Geologic influences such as tectonic history, lithology, structure, and denudation, as well as river flow and sediment transport mechanisms, can all influence valley formation and landform morphology (Goodbred, 2003). Alluvial channels are susceptible to change of pattern and shifting in their position as the alluvium or sediment load is eroded, transported and deposited.

Alluvial plain: This geomorphic unit occupies around 810 square kilometres, accounting for 73% of the overall area. These plains have flat or level slopes and are surrounded by flat-lying regions such as flood plains and water bodies. The alluvial plain is considered the most fertile terrain, and it provides a variety of economic and livelihood activities for the inhabitants.

Flood plain: It is distinguished by the presence of many oxbow lakes, abandoned channels, mender scars, and sparse plant cover. Flood plains form on both sides of river channels when the river overflows its banks during flooding. The Ganga floodplain is substantially larger than the other streams that run through the study region. A wide flood plain is observed between the Fatehgarh and Kannauj regions. Sediment and mud are deposited on the floodplain at regular intervals, making the soil rich and suitable for agricultural activity.

Paleochannels: Paleochannels have been noticed as stretch, lobate, or sinuous alluvial landforms spanning around 22.4 square kilometres. These are plotted using

variable geometry, breadth, and orientation, demonstrating the river's fluctuating migratory distances from the present path. These geomorphic features are found in groups and contain high moisture in low-lying locations, making them useful for reconstructing an area's morphological past. They are made up of fine to extremely fine grey to yellowish-brown clay, with sand and silt mixed together. During drier periods, these paleochannels, which are potential aquifers for groundwater, might be profitably utilised.

Active channel: This geomorphic unit has constant water flow throughout the year. The rivers Ganga, Garra, Ramganga, and Kali flow through the region of approximately 20.4 sq. km. All rivers are sinuous in character. Sand deposition is easily distinguished by its light tone and smooth texture.

Sand Bars and Islands: These accretion features of the alluvial channel are typically associated with the meandering channel. The channel bars located near the point where rivers join the plain are characterised by coarser deposits, whereas the point bars found downstream are produced with clay and silt. Islands are inner morphological features of a river channel that might impact the river's shape and dynamics. Sand bars and islands occupy approximately 15.5 and 5.5 square kilometres of the study area, respectively.

Meander scar: Scars are the remnants of meandering active channels made of sand and silt that formed during the formation of the oxbow lake. When the oxbow lake entirely fills with sediments, it forms meander scars. They disconnect from the current channel and eventually become a distinct feature.

Ox-bow lakes: These are recognised as independent, but during floods, they became joined to the main river channel.

Abandoned channel: These are linked to the shifting channel of the Ramganga and Garra rivers. The channels are distinguished by their dry bed.

Sinuosity Analysis

The most important indications in hydrologic geometry are the pattern and size of meanders in river channels. Engineers and geoscientists can use it to build bridges or dams. Table 1 shows the findings of sinuosity indices for the Ganga, Ramganga, Garra, and Kali River systems. From 1975 to 2018, the channel index of Ganga ranged between 1.26 and 1.38. Similarly, the valley index varies from 1.2 to 1.29. It represents how the river spreads in its valley and forms bars inside its meander path. The SSI indicates a sinuous (<1.05) to braided river pattern (>1.11), while the HSI shows an alternating increasing and reducing pattern, and the TSI shows a declining and growing pattern. The Ramganga River is the Ganga's right bank tributary, and its merger point varies from year to year. As a result, the confluence point is also changing. The high CI (1.79) and SSI (1.07) indicate that the river is sinuous, although the HSI is less impacted than the TSI. The Garra river channel is influenced by terrain, with HSI ranging from 2.13 (1988) to 27.31 (2002). TSI ranges from 72.68 to 97.86, demonstrating a significant impact on terrain. The CI of the river Kali, a left-

bank Ganga tributary, fluctuated from 1.76 (1972) to 1.99 (2018). The high measurements for VI-1.97 (2018), TSI-97.86 (1988), and SSI-1.08 (2002) indicate sinuous. The investigation found that the Ganga and its tributaries belong to the sinuous channel (1 to 1.11) group, which represents the river's mature stage. Alluvial channels regularly change their pattern in response to the rate of water discharge and sediment load. The sinuosity values range from 1.0 (straight) to 3.0 (Brice and Blodgett, 1978). The HSI is relatively low in the studied area, indicating that the valley is at the constriction stage. The high TSI value affects sinuosity, indicating that the research region is dominated by topography, whereas deposited material from flood plains reduces HSI.

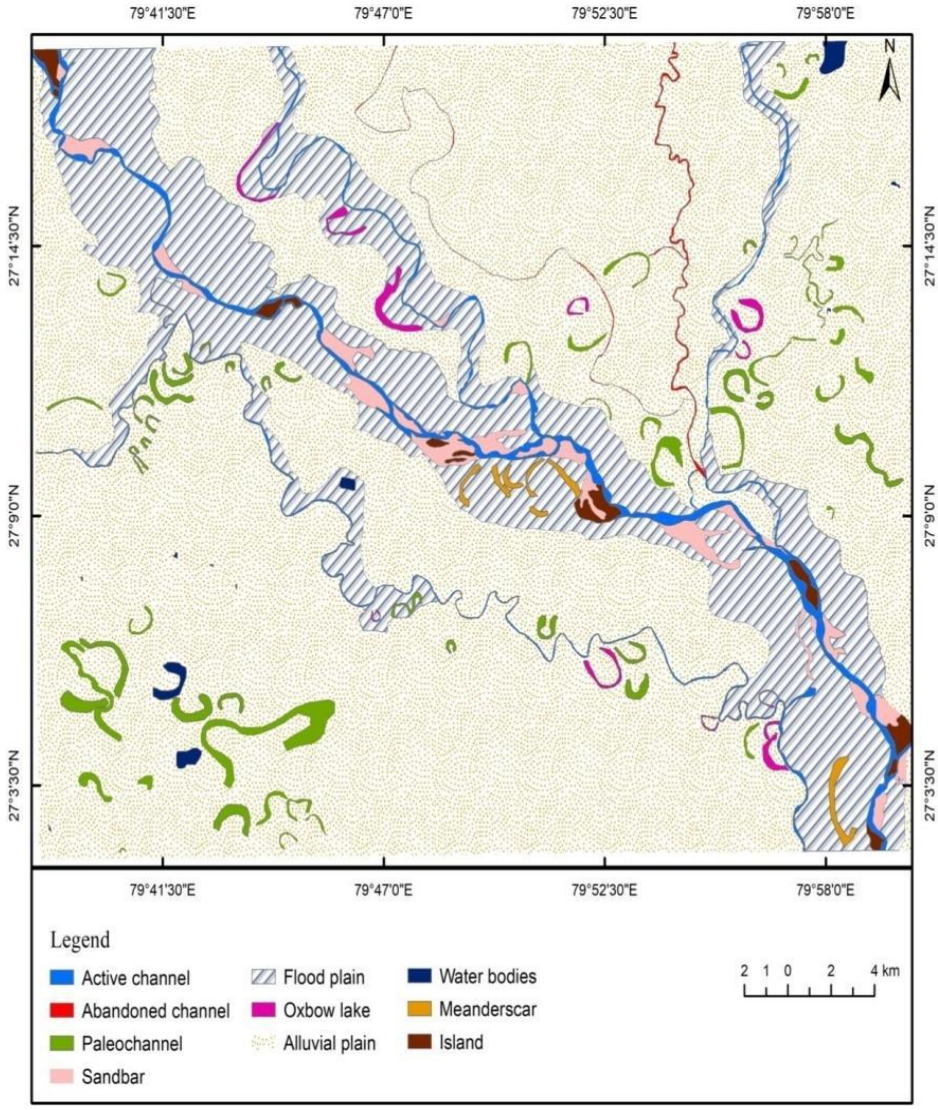

Figure Figure 2. Fluvial landforms identified in the study area

Table 1: Sinuosity index of river channels of the study area.

River	Year	CL	VL	AL	CI	VI	HSI (%)	TSI (%)	SSI
Ganga	1975	55.11	53.68	41.6	1.32	1.29	10.58	89.41	1.02
	1988	58.89	52.82	42.48	1.38	1.24	36.98	63.01	1.11
	2002	56.89	55.47	44.75	1.27	1.23	11.69	88.3	1.02
	2018	58.37	55.66	46.15	1.26	1.2	22.17	77.82	1.04
Ramganga	1975	27.31	27.07	15.92	1.71	1.7	2.1	97.89	1.00
	1988	28.51	27.03	15.92	1.79	1.69	11.75	88.24	1.05
	2002	29	26.94	17.84	1.62	1.51	18.45	81.54	1.07
	2018	32.45	28.87	18.25	1.77	1.58	25.21	74.78	1.00
Kali	1975	57.48	56.97	32.18	1.78	1.77	2.01	97.98	1.00
	1988	60.7	60.17	37.67	1.61	1.59	2.3	97.69	1.00
	2002	62.49	61.02	31.65	1.97	1.92	4.76	95.23	1.02
	2018	64.36	63.66	32.26	1.99	1.97	2.18	97.87	1.01
Garra	1975	32.91	31.41	23.07	1.42	1.36	15.24	84.75	1.04
	1988	29.28	29.13	22.25	1.31	1.3	2.13	97.86	1.00
	2002	25.67	23.69	18.42	1.39	1.28	27.31	72.68	1.08
	2018	26.92	26.61	19.38	1.38	1.37	4.11	95.88	1.01

(Note: CL- the length of the channel in the stream, VL- the valley length along a stream, CI- (Channel Index) = CL/ Air, an index of total sinuosity, both hydraulic and topographic, VI- (Valley Index) = VL/ Air, an index of total topographic sinuosity, TSI- topographic sinuosity index, HSI- hydraulic sinuosity index and SSI- standard sinuosity index)

River Dynamics

River Dynamics of the Ganga Reach: The width of the river channel in several cross-sections (A to J) varied between 1975 and 2018. Proper channel constructing suggests that the Ganga River is gradually migrating to the north and northeast (Table 2). The river's breadth ranged from 130 m to 2200 m in 1975 and 150 m to 680 m in 2018. The maximum and minimum shifts of erosion were -1891.8 m (A) and -30.6 (H) on the right bank, and -2506.6 m (A) and -576.5 m (E) on the left bank. Deposition shift rates were 1722.9 m (J) and 30.7 m (C) on the right bank, and 2888.5 m (J) and 41.7 m (C) on the left. Overall, eight migration erosional sites (05-right bank and 03-left bank) and twelve

depositional shift sites (05-right bank and 07-left bank) were found (Figure 3). At cross-section A, both banks experienced significant erosion of -1891.8 m and -2506.6 m towards the south-west. The large-scale deposition shift occurred on the right bank of the channel, between 1722.9 m and 2888.5 m at cross-section J towards the north. Following the cross-section F, the river divides into two branches and eventually unites in the channel around H. Between F and H, erosion and depositional processes dominate (Figure 3). There is a significant difference in river width between these two places. Industrial plants, notably those producing glass, have been developed in this region for business purposes. Sand mining operations are affecting the Ganga River and its tributaries. These unauthorised and illegal operations take place in the villages of Behta Ballu, Samchipur Tarai, Raipur Chihatpur, Katri Sota, Sinoli, and Katri Naampur. During the research period, the river course moved significantly on the right bank, and channel migration occurred mostly in the south-west direction. In 1975, the river channel between cross-sections I and J was separated into two branches, however, it is still running as a single channel in 2018.

Figure 3 a) Meandering of river Ganga b) River islands c & d) Severe erosion occurred at left and right bank of the river Ganga e) Thick alluvium deposits (terrace) f) River depositional process.

Table 2: Width of river and its bankline at various cross-sections during 1975-2018.

River	Cross-Section	River Width (m)		Right Bank (m)	Left Bank (m)	Direction of Migration
		1975	2018			
Ganga	A	130	680	-1891.8	-2506.6	South-west
	B	150	190	906.8	865.8	North-east
	C	150	180	30.7	41.7	Southward
	D	150	200	699.1	656.5	North
	E	340	180	-747.5	-576.5	South-west
	F	210	320	-681.8	-848.1	South-west
	G	2200	150	-159.4	1932.9	North
	H	920	270	-30.6	588	North
	I	320	410	1035.2	957.1	North
	J	1540	260	1722.9	2888.5	North
Kali	K	170	40	-68.4	89.6	North
	L	170	110	5	170.1	North
	M	280	50	-66.9	34.5	North
	N	210	50	539.5	645.7	North
	O	190	100	28.1	164	North
Ramganga	P	180	70	160	235.9	North-east
	Q	160	100	-1209.5	-1153.3	South-west
	R	340	50	-134.1	154.7	North
	S	300	50	-653.8	-404.1	South-west
	T	290	60	-2848.9	-2609.5	South-west
Garra	U	190	100	56.0	150	North-east
	V	200	90	-25.6	93.8	North-east
	W	170	70	-390.1	-288.2	South-west
	X	160	20	-66.1	73.8	North
	Y	150	30	-805.7	-612.8	South-west
	Z	160	-	-	-	-

(Note: Positive values indicate the right-side shift and negative values show a left-side shift from the base year)

River Dynamics of the Kali Reach: The channel width of Kali reach ranged from 170 m to 280 m in 1975 and 40 m to 110 m in 2018. At cross-section N, there is a massive migration lead to deposition of 539.5 m on the right bank and 645.7 m on the left bank of the river channel heading north. This is the location where the greatest amount of shifting occurs. Only K (68.4 m) and M (66.9 m) on the right bank showed erosion, while the remaining locations were identified as depositional sites. Both bank lines of the Kali River contain the highest number of positive values, indicating a northward movement.

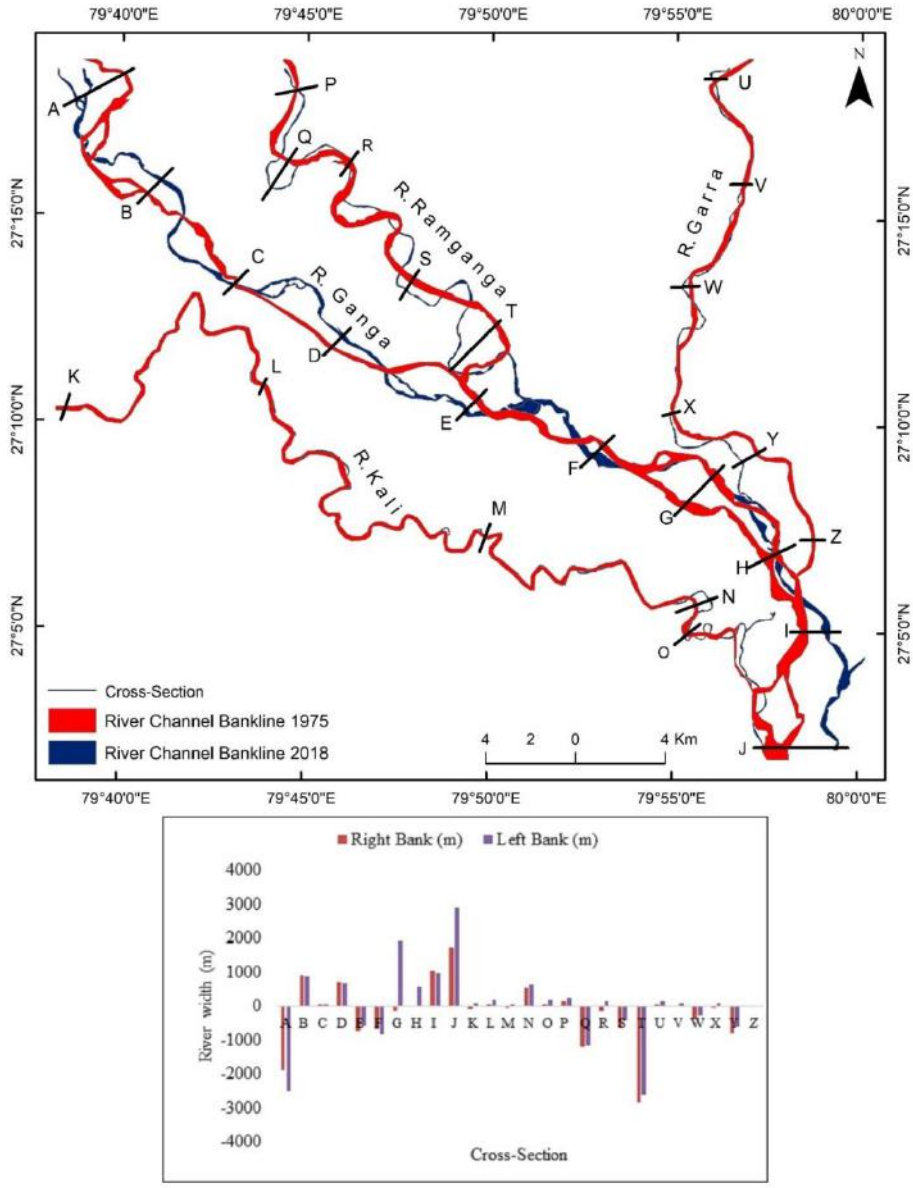

Figure 4. Channel position of the river Ganga and its tributaries in the study area.

River Dynamics of the Ramganga Reach: In cross-sections from P to T, the river bank line was shifted to the left, primarily in the south-west direction. In 1975, the maximum river width was reported at R (340 m), while the minimum was at Q (160 m). In 2018, the river's breadth ranged from 50 to 100 metres. During the research period, erosion was the most common occurrence, followed by deposition. The right and left banks have shifted maximums at T, which are -2848.9 m and -2609.5, respectively. The river's path was altered to the southwest. Accretion is greater at P on the left bank at 235.9 m and 160 m on the right bank. Overall, this river runs in a meandering manner, as seen in Figure 4.

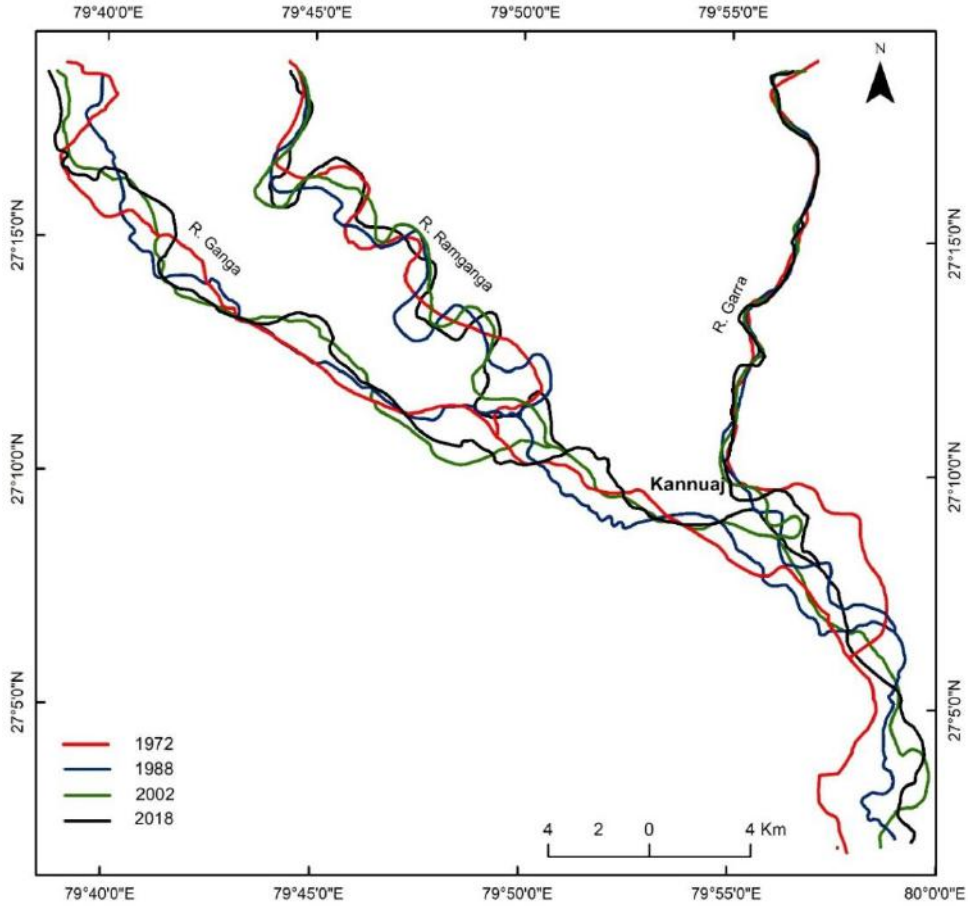

Figure 5. Change of confluence of river channels Ganga-Ramganga and Ganga-Garra.

River Dynamics of the Garra Reach: The width of the river channel in U-Z cross-sections ranged from 150 m to 200 m in 1975 and 20 m to 100 m in 2018. The Garra's channel positions suggest a progressive migration northward and northeastward. The maximum and minimum shift of channel erosion was -805.7 m (Y) and -25.6 m (V) on the right bank, and -612.8 m (Y) and -288.2 m (W) on the left bank. The deposition was only

seen in the right bank 56 m at U. The left bank had a maximum of 150 m (U) and a minimum of 73.8 m at the cross-section X. After this point, the region is prone to active floods, which may result in channel relocation. Overall, this reach had a considerable number of erosional sites. In 1975, the river channel was combined with the Ganga at 1500 metres south of the Z cross-section, then at 1830 metres south of the Y in 2018. The change occurred at the confluence site between Y and Z, which is connected to local channel shifting at the confluence point caused by silt and water discharge variations in the active river channel (Figure 5). The river's course reveals lateral bank erosion. Between 1975 and 2018, all cross-sections preserved the U-right bank line relocated to the left side of the river. Maximum migration occurred at the Y cross-section, which measured -805.71 m and -612.82 m along its right and left bank lines, respectively, in the south-west direction. The river channel width at the cross-section Z was 160 m in 1975, but it has not reached this point in 2018 since it merged with the Ganga above this cross-section.

Conclusions

Alluvial rivers are characterised by channel erosion and accretion. Variations in water flow and sediment discharge rate cause the river channel to shift location. Channel shifting is primarily determined by a variety of hydrological and morphological features, including erosion, deposition, and discharge. Alluvial rivers meander naturally and are characterised by lateral erosion. It produces a shifting pattern throughout time. The present study examines the river channel movement and sinuosity of the Ganga and its tributaries, the Ramganga, Kali, and Garra rivers, from 1975 to 2018. Alluvial plains are occupied nearly 75% of the total area. River sinuosity index varies between 1.00 and 1.11 in the study area indicating sinuous to braided pattern. The Ganga River migrated as little as 30 m and as far as 2900 m at various cross-sections. Maximum and minimum changes were noted at different cross-sections of other river channels as follows: 5 to 649 m for Kali, 134 to 2849 m for Ramganga, and 25 to 805 m for Garra. The river channels have continuously moved from their previous positions as a result of hydrological processes and the region's terrain. Erosion was widespread along the Ganga and its tributaries. Except for the Kali River, all channels are constantly changing as they go from north to southeast. River channel movement or migration is caused by dynamic physical processes such as water and sediment movement over time. Aside from natural causes, manmade influences also contribute to changes in the river's location. Several significant activities were noted in the study area, including unauthorised farming, illicit sand mining, and the building of artificial dams to control river flow. When combined with river flow data, high-resolution satellite data collected at regular intervals during the monsoon and non-monsoon seasons might be very helpful in accurately determining river dynamics. The shifting location or movement of river channels across time and geography is crucial for resolving management issues. Time-sequential images from different times, as well as GIS assistance for mapping and measuring channel position, can be employed in a variety of geographic regions, notably in fluvial environments. It has been demonstrated that GIS techniques, together with fieldwork, play a vital role in fluvial morphology and riverbank erosion studies.

Acknowledgement

Anurag Singh is grateful to the University Grants Commission for providing Junior Research Fellowship for conducting the present research work. The authors also thank anonymous reviewers and editor for providing constructive suggestions to improve the manuscript.

References

1. Agnihotri, A. K., Ohri, A., & Mishra, S. (2020). Channel planform dynamics of lower Ramganga River, Ganga basin, GIS and remote sensing analyses. Geocarto International, *35*(9), pp. 934–953.
2. Brice, J.C. & Blodgett, J.C. (1978). Countermeasures for hydraulic problems at bridges. Federal Highway Administration, 1 and 2, pp.78-162.
3. Census. (2011). District Census Report, Govt. of India, New Delhi.
4. Charlton, R. (2008). Fundamentals of fluvial geomorphology. London: Routledge.
5. Gupta, N. (2012). Channel Plan form Dynamics of the Ganga-Padma System, India, Faculty of Social and Human Sciences, University of Southampton.
6. Goodbred, S., Kuehl, S., Steckler, M.S. & Sarkar, M.H. (2003). Controls on facie distribution and stratigraphic preservation in the Ganges- Brahmaputra delta sequence. Sedimentary Geology, 155(3-4), pp. 301-316.
7. Hasnain, S.I. & Thayyen R.J., (1999). Discharge and suspended-sediment concentration of meltwaters, draining from the Dokriani glacier, Garhwal Himalaya, India. Journal of Hydrology, 218, pp. 191-198.
8. IMD. (2018). Annual Report, 2018. Information Science & Knowledge Resource Development Division (IS&KRDD), India Meteorological Department, New Delhi.
9. Jain, V. & Sinha, R. (2004). Fluvial dynamics of an anabranching river system in Himalayan foreland basin, Baghmati River, north Bihar plains, India. Geomorphology, 60, pp. 147- 170.
10. Jodhani, K. H., Patel, D. & Madhavan, N. (2023). A review on analysis of flood modelling using different numerical models. Materials Today: Proceedings, 80(3), pp. 3867–3876.
11. Karki, S. & Nakagawa, H. (2019). Meandering channels response to a series of Permeable and impermeable. Journal of Japan Society of Civil Engineers, 75, pp. 1021-1026.
12. Mukherjee, K. & Pal, S. (2018). Channel migration zone mapping of the River Ganga in the Diara surrounding region of Eastern India. Environment, Development and Sustainability, 20, pp. 2181-2203.
13. Mueller, J.E. (1968). An introduction to the hydraulic and topographic sinuosity indexes. Annals of Association of American Geographer, 58(2) pp. 371-385.
14. Mittal, R., Said, S. & Beg, Mubeen. (2023). Assessment of Changes in Planform Morphology of the Upper Yamuna River Segment, India, Using Remote Sensing and GIS. Physical Geography, 44(4), pp. 446-477.

15. Meybeck, M. (1976). Total mineral dissolved transport by world major rivers. Hydrological Sciences Journal, 21, pp. 265–284.
16. Pati, K.P., Lal, J., Prakash, K. & Bhusan, R. (2008). Spatio-temporal shift of Western bank of the Ganga River Allahabad City and its Implications. Journal of the Indian Society of Remote Sensing, 36, pp. 289-297.
17. Sarif, N.M., Siddiqui, L., Islam, S.M., Praveen, N. & Saha, Monojit. (2021). Evolution of river course and morphometric features of the River Ganga: A case study of up and downstream of Farakka Barrage. International Soil and Water Conservation Research, 9(4), pp. 578-590.
18. Sinha, R., & Tandon, S. K. (2014). Indus-Ganga-Brahmaputra plains: the alluvial landscape. Landscapes and landforms of India, pp. 53-63. DOI: 10.1007/978-94-017-8029-2_5
19. Thakur, P.K., Laha, C. & Aggarwal, S.P. (2012). River bank erosion hazard study of river Ganga, upstream of Farakka barrage using remote sensing and GIS. Natural Hazards, 61, pp. 967–987.

The Indian Geographical Journal
Volume 98 (2) December - 2023, pp 135-154
ISSN 0019-4824

IMPACT OF LAND USE LAND COVER DYNAMICS ON ECOSYSTEM SERVICE VALUES: A STUDY ON EASTERN HIMALAYAN REGION

Shrabanti Dutta and Narender Verma

Department of Geography, Banaras Hindu University, Varanasi – 221005
Corresponding author mail id: nverma1972@gmail.com

Abstract

In recent decades, researchers worldwide have been paying closer attention to biodiversity in terms of the economic valuation of ecosystem services (ESVs). Eastern Himalayan region, spanning across the Darjeeling district of West Bengal, Sikkim, NE India, and Bhutan, offers valuable ecosystem services. However, the assessment of ESVs in this region remains limited. Therefore, the present study evaluated the land use land cover (LULC) changes and their impact on the ecosystem services values (ESVs) in the Eastern Himalayan Region for the years 1992, 2002, 2012, and 2020. Using ESA CCI Land cover products (300-meter resolution), LULC maps were prepared, and ESVs were calculated based on global value coefficients adopted from the study by Costanza et al. (2014). The results reveal an increase in urban areas, wetlands, forest cover, croplands, and barren lands; with urban areas experiencing the most significant expansion (265.81%). Conversely, grasslands and water bodies decreased, indicating growing anthropogenic influences. Sensitivity analysis also confirmed the validity of assessing ESVs over time. These findings underscore the importance of integrating ESVs into decision-making processes affecting the natural world.

Keywords : Ecosystem services, Ecosystem Service Values (ESVs), Land use land cover change, Eastern Himalayan Region

Introduction

Ecosystem services encompass the numerous advantages bestowed upon society by nature. It enables human existence through the provision of healthy food, clean water, disease and climate regulation, crop pollination, soil formation, and various cultural and recreational benefits. Humans derive these services from ecosystem functions, the underlying processes within ecosystems. So, the interdependence of ecosystem functions and services is essential for supporting human welfare. Human capital (people), social capital (society), and built capital (built environment) are crucial for the flow of ecosystem services. Interactions between natural capital and its yield benefits contribute to human well-being. While ecosystem services hold significant economic value globally, they are often overlooked in decision-making due to the need for more monetary quantification in the economy. This necessitates periodic evaluation of ecosystem service (Costanza et al., 1997).

The concept of ecosystem services received greater attention from researchers after the publication of the 'Ecosystem Service Valuation Model' by Robert Costanza et al. in 1997 and the 'Millennium Ecosystem Assessment (MEA)' Report by the United Nations in 2005. The report titled 'The Economics of Ecosystems and Biodiversity (TEEB)' published by the UN Environment Program in 2010 further aroused interest in this issue among mass audiences. (Costanza et al., 2014a). Although Costanza's model was criticized for the uncertainties of the coefficients and limitations regarding their application at the local level. However, these efforts are considered fruitful and valuable for understanding various benefits arising from ecosystem functions necessary to estimate the value of ESs.

Ecosystem services evaluation connects ecology with the economy by considering additional value beyond market values. It aims to assess trade-offs associated with the ecosystem's 'relative' contribution to sustainable human well-being goals (Costanza et al., 2014a). There are several methods to quantify ecosystem services viz. market-based methods, revealed preference methods, stated preference methods, or benefit transfer methodologies. Among these, the benefit transfer is the most frequented method for its simplicity and effectiveness. Several studies have applied this method to analyze the relation of ESV of a region with LULC changes (Kindu et al., 2016; Li et al., 2019; Jiang et al., 2020; Sharma et al., 2020; Das et al., 2023). The method infers the economic values of environmental goods and services at a place by using information about the same goods at another place. It helps to estimate the economic values in monetary units of those goods and services that are not traded in markets. However, the accuracy of this method depends on the accuracy or measurement errors in the original studies (Wilson & Hoehn, 2006).

The LULC type governs the provision of ecosystem services in a given area. It creates the bridge between natural ecological processes and human socio-economic activities. It influences the supply of ecosystem services by altering the structure and composition of ecosystems (Li et al., 2019). Therefore, tracking alterations in Land Use/Land Cover (LULC) develops an understanding of shifts in ecosystem services (ESs) related to the growth of human-influenced landscapes (Sharma et al., 2020). However, the quantum of LULC change is not uniform across the regions. For instance, in their study on the Qinghai-Tibetan Plateau Jiang et al., 2020 found that total ecosystem service values (ESVs) increased between 1990 and 2015; while Gashaw et al., 2018 in their study of the Andassa watershed, Upper Blue Nile basin revealed that the ESV had declined between 1985 and 2015. Therefore, it can be said that the studies are very location-specific due to the dependency of ESV on LULC dynamics.

Among different landscapes in the world, mountains are recognized as important ecosystems by the Convention on Biological Diversity (CBD) (ICIMOD Report, 2010). The Eastern Himalayan Region has a complex and diverse physiography characterized by mountains, hills, valleys, and flood plains. They are rich in natural and crop-related biodiversity. It provides multiple essential ecosystem services like water resources, climate regulation, soil retention, carbon sequestration, and so on. However, past literature reveals that there is a dearth of studies on ecosystem services as compared to Western and

Central Himalayan regions (Rana et al., 2021). The biological diversity of the region is threatened by deforestation, degradation, forest encroachment, jhum cultivation, forest fire, illegal extraction of forest products, infrastructural development, etc. (Chatterjee et al., 2006). The region's economy is heavily reliant on forestry and agriculture and struggles with issues like unsustainable resource use and poverty (Chettri & Sharma, 2006). So, without assessing the impact of these land use changes on the ecosystems, the quantitative knowledge about ESV would be limited. Therefore, the present study aims to study the impact of land use/land cover change on Ecosystem Service Value over the region with the following objectives (1) To evaluate Land Use Land Cover changes during 1992, 2002, 2012, and 2020 over the Eastern Himalayan Region, (2) Examine the distribution of Ecosystem Service Values, and their changes over the reference years and (3) Analyse the sensitivity of ESV in response to LULC change. The findings from this study could give insights into the importance of these services and their effective management in policy and decision-making.

Study area

The Eastern Himalayan Region, the area of interest for the present study extends between 21°58' N to 29°30' N latitudes and 87°59' E to 97°30' E longitudes. It consists of Sikkim, parts of West Bengal (Darjeeling District), Arunachal Pradesh, Assam, Meghalaya, Nagaland, Manipur, Mizoram, Tripura and the entire Bhutan (Figure 1). It covers an area of about 2,80,157 sq. km. The climatic characteristics of this region are pre-humid to humid, with approximately 2,450 mm of rainfall per year. The topography of Meghalaya, Manipur, Nagaland, and Sikkim are characterized by steep to very steep slopes, whereas Assam valley has very gentle slopes. Due to variations in topography, climate, and vegetation varies considerably. The soil is red sandy to lateritic type, characterized by old and recent alluvial and terai soils.

Situated at the juncture between Asia and the Indian subcontinent, this region has a relatively young geological structure and extreme altitudinal variations and is recognized as one of the rich biodiversity regions at the global scale. The region provides multiple ecosystem services (provisioning, regulating, cultural, and supporting services); which helps to study the distribution of different ecosystem services. The ecological diversity of this region is attributed to diverse topography, soil, and climate. The region comes under the major biome of alpine, temperate, and sub-tropical forests; and lies at the intersection of multiple biogeographic regions, i.e., the Indo-Malayan Realm, Palearctic Realm, and the Sino-Japanese Region. Also, the region is classified as a part of Indo-Burma biodiversity hotspots and Himalayan hotspots.

The human population is not evenly distributed over the region. Population density is high in the Terai regions of Nepal and West Bengal; Dooars region of Assam and the population is scattered in the regions of Meghalaya, Manipur, Tripura, and Brahmaputra basin. The livelihood of a major portion of the population depends upon agriculture and allied activities. In the last three decades, the population in this region has gone up by

about 2.1% annually. So, the current status regarding the impact of human influence on the biodiversity of the region needs to be understood because the Eastern Himalaya, as a unique and responsive ecosystem, demands focused consideration, especially given its vital life support functions for the conservation and sustainable development of mountain environments.

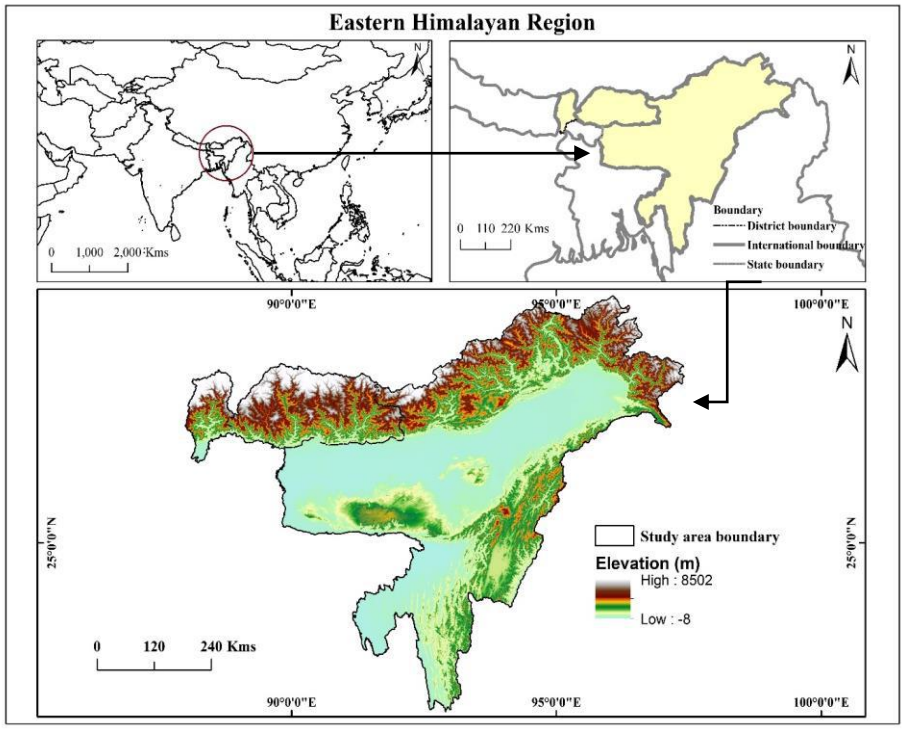

Figure 1: Location map of the study area

Materials and Methods

Database

The current research utilized annual European Space Agency Climate Change Initiative land cover (ESA CCI-LC) maps to examine changes in land use and land cover across the study area. Global land cover maps were generated from 1992 to 2020, with a resolution of 300 meters, focusing on three 5-year periods centred around the years 2010 (2008-2012), 2005 (2003-2007), and 2000 (1998-2002). Until 2015 (version 2.0.7), the land cover maps were produced within the framework of the ESA CCI initiative. Starting from 2016, the maps were operationally generated under the EC Copernicus Climate Change Service. These maps categorized land cover into 22 Level-1 classes (providing information at the global scale) and 14 Level-2 classes (offering more detailed information at the regional scale). To validate the classification results, the GlobCover 2009 dataset was employed to evaluate the accuracy of the CCI-LC map for the 2010 period, yielding a total accuracy of 73.2%. LULC maps of 1992, 2002, 2012, and 2020 are selected for the present

study (*http://maps.elie.ucl.ac.be/CCI/viewer*) with eight major land cover classes viz. Forests, Cropland, Grassland, Wetland, Urban areas, Barren land, Waterbodies, and Permanent snow and ice are chosen to synchronize with the biomes mentioned in Constanza et al. (1997) and Constanza et al. (2014).

Methods used

Valuation of ecosystem services is a process of assessing their contribution to human welfare. Ecosystem Service Values (ESV) help to take into account the natural capital along with physical and social capital, which are equally important in sustainable human well-being. (Kubiszewski et al., 2013). Analyzing social well-being through ecosystem service valuation using monetary metrics allows for a meaningful comparison of the social benefits offered by distinct management approaches.

Numerous approaches are prevalent to aggregate both market and non-market components of ESV. The benefit Transfer method is employed to estimate the ESVs for the study area. This method estimates the Ecosystem Service Values at one location based on the existing data related to similar valuation studies and transfers those values of Ecosystem Services and other information to a similar location (Kubiszewski et al., 2013). Thus, the method works by assuming a constant unit value for each hectare of a specific ecosystem type and then calculates the total value by multiplying that constant value by the area of each type (Costanza et al., 2014a).

Estimation of Ecosystem Service Values

We have estimated Ecosystem Service Values (ESVs) for the 1992, 2002, 2012, and 2020 reference periods, and computed their changes over the years. For this purpose, those Land use/land cover types which though not exactly similar have close semblance to the biomes mentioned in Costanza et al., 2014 (Table 1) are used as proxies to estimate the ESVs of different land use/land cover types for each reference year (Kindu et al., 2016; Gashaw et al., 2018; Li et al., 2019).

Table 1: Global Value coefficients of different LULC types corresponding to equivalent biome

LULC type	Equivalent biome	Value coefficients (US$/ha/yr)
		2011
Cropland	Cropland	5567
Forest land	Forest	3800
Grassland	Grass/rangelands	4166
Wetland	Wetlands	140174
Urban area	Urban	6661
Barren land	Desert	0
Waterbodies	Lakes/rivers	12512
Permanent snow and ice	Ice/rock	0

Source: (adopted from Costanza et al., 2014)

The ESV (in US dollars) of different LULC types is calculated using Equation 1. The value coefficients (VC) adopted from Costanza et al., 2014 corresponding to different LULC types are multiplied by the area (in hectares) under each LULC type. The total ESV for a particular reference year is obtained by summing up the ESVs from each LULC type. In this way, individual and total ESVs for all the reference periods are calculated (Tables 2 and 3).

$$ESVi = \Sigma\,(Ai * VCi) \qquad \text{Equation (1)}$$

$ESVi$ is the Ecosystem Service Value of a particular LULC type 'i', Ai is the area (in ha) of that LULC type 'i' and VCi is Value Coefficient for that LULC type 'i' (US Dollar/ha/year)

Table 2: Area under each LULC type from 1992 to 2020

LULC types	1992		2002		2012		2020	
	Hectares	%	Hectares	%	Hectares	%	Hectares	%
Cropland	6601284	21.83	6948432	22.97	7017102	23.2	6776136	22.4
Forest land	18520245	61.23	19106919	63.17	19339065	63.94	19651482	64.97
Grassland	4329783	14.32	3381174	11.18	3049794	10.08	2948571	9.75
Wetland	8361	0.03	8982	0.03	11754	0.04	14724	0.05
Urban area	20349	0.07	26946	0.09	50886	0.17	74439	0.25
Barren land	133236	0.44	136557	0.45	161361	0.53	160389	0.53
Waterbodies	364617	1.21	368865	1.22	347913	1.15	352359	1.16
Permanent snow and ice	267930	0.89	267930	0.89	267930	0.89	268398	0.89

Source: Computed by authors

Rate of ESV change

The Changes in ESVs are obtained by taking differences in Ecosystem Service Values in each reference year. Here, we have assessed the percent change of ESVs across different periods (1992-2002, 2002-2012, 2012-2020, and 1992-2020) using the Equation 2 (Table 4).

$$C = \frac{(ESV present\ year - ESV initial\ year)}{ESV initial\ year} * 100 \qquad \text{Equation (2)}$$

Ecosystem Service Values for Individual Ecosystem Functions

Further, the ESVs provided by individual Ecosystem Functions are estimated using Equation 3. For these, 13 ecosystem services (4 provisioning services, 5 regulating services, 3 supporting services, and 1 cultural service) are considered, and the value of each Ecosystem Function is calculated by multiplying the area of each LULC type with the value coefficients of each function of each LULC type (Table 5).

$$ESVj = \Sigma\,(Ai * VCij) \qquad \text{Equation (3)}$$

$ESVj$ is the Ecosystem Service Value of individual ecosystem functions 'j' provided by all the LULC types, Ai is the area (in ha) of LULC type 'i' and $VCij$ is the Value Coefficient of that function 'j' for LULC type 'i' (US Dollar/ha/year)

Elasticity of the ESVs in response to LULC change

Elasticity or sensitivity analysis is performed to determine the dependency of changes in ESVs with the changes of different LULC categories using Equation 4. If a small change in LULC reflects significant ESV changes, then the elasticity will be large, which means it has high sensitivity, and vice versa. The value of elasticity is divided into three classes (Jiang et al., 2020); where an elasticity value less than 0.5 represents inelastic, between 0.5 to 1, elastic, and a value > 1, is highly elastic (Table 6).

$$E = \left\{\frac{ESVend - ESVstart}{ESVstart}\right\} / \left(\frac{\Sigma \Delta Li}{\Sigma Li}\right) \quad \text{Equation (4)}$$

E is the elasticity of ESV, $ESVend$ is the ESV at the end of the research period and $ESVstart$ ESV at the beginning of research period, ΔLi is area converted from one LULC type to the other 'i' and Li is the area of LULC type 'i'.

Results

Analysis of LULC Dynamics

The LULC dynamics of the Eastern Himalayan Region are shown in Table 2 and Figure 2. The spatio-temporal distribution of LULC shows heterogeneity over the region (Figure 3). Throughout the decades, this region has been dominated by forest cover, followed by cropland and grassland. The other land use types are sparsely distributed in some particular areas. In 1990, the forests covered 61.23% of the total area, which increased to 64.97% in 2020. More than 70% area is covered with forest lands and grasslands in the states of Sikkim, Arunachal Pradesh, Darjeeling hills in West Bengal, Meghalaya, Manipur, and Mizoram. The increase of both open and dense forest cover and the implementation of afforestation programs is attributed to the increase in forest area in the region. Cropland has increased from 21.83% in 1992 to 23.2% in 2012 and then decreased to 22.4% in 2020. The major distribution of cropland is concentrated in the state of Assam, covering the central part of the region. In the case of grassland, it has decreased from 14.32% in 1992 to 9.75% in 2020. The area of waterbodies has decreased from 1.21% in 1992 to 1.16% in 2020, but wetlands have shown a slight increase from 0.03% in 1992 to 0.05% in 2020. A positive change was noticed for urban areas, which was 0.07% in 1992 and reached 0.25% in 2020. Urban centers like Darjeeling, Siliguri in Darjeeling District of West Bengal; Gangtok, Peling in Sikkim; Thimpu, Phuntsholing, Paro in Bhutan; Tawang, Itanagar, Ziro in Arunachal Pradesh; Dimapur, Kohima in Nagaland; Imphal in Manipur; Aizawl in Mizoram; Agartala in Tripura, etc are scattered over the region and expanded in their areas over time. Barren lands are sparsely distributed throughout the area, which have gradually increased from 0.44% in 1992 to 0.53% in 2020. In contrast, permanent snow and

ice cover is mainly distributed in the northernmost part of Sikkim, Bhutan, and Arunachal Pradesh, which remained unchanged for the last 28 years (0.89%). More detailed change metrics of each LULC type are given in Figure 3.

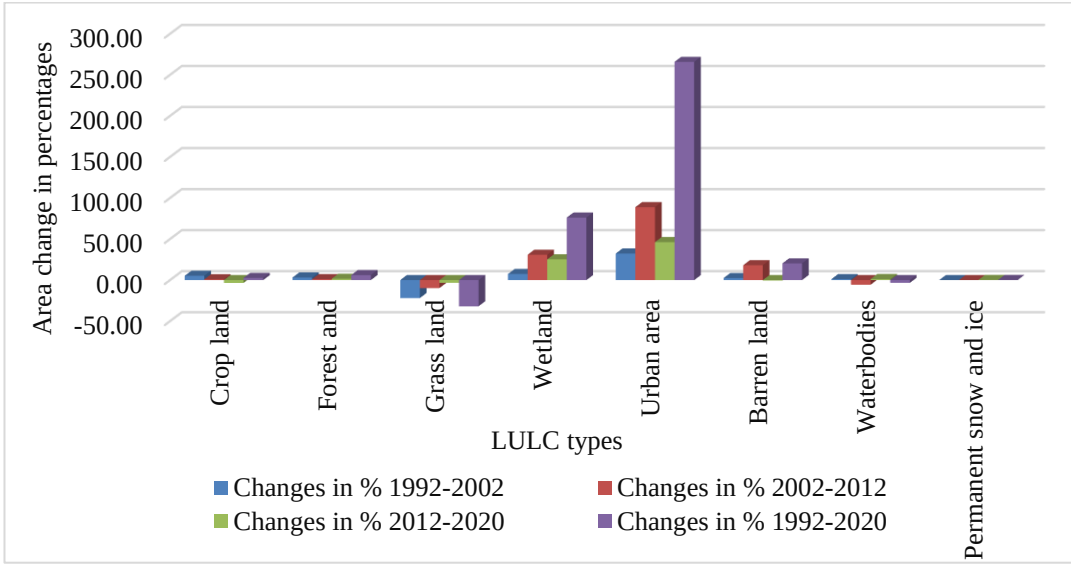

Figure 2: Spatial distribution of LULC in (a) 1992, (b) 2002, (c) 2012, and (d) 2020 over the Eastern Himalayan region

Status and changes of estimated ESVs

Table 3 shows the calculated Ecosystem Service Values (ESVs) of each LULC type during the study period. The total ESV of the region has shown a positive change from 131.034 billion US$ in 1992, 131.427 billion US$ in 2002, 131.597 billion US$ in 2012 to 131.652 billion US$ in 2020. In particular, forest land is found to be the major contributor to total ESV followed by cropland and grassland. In 1992, forest, cropland, and grassland had the ESV of 70.38, 36.75 and 18.04 billion US$ respectively. Waterbodies, wetlands, and urban areas shared very little proportion of the total ESV, i.e. 4.56, 1.17, and 0.14 billion US$, respectively. In 2002, ESVs increased for forest and cropland to 72.61 and 38.68 billion US$, respectively. However, the value (ESV) of grassland decreased to 14.09 billion US$. ESV of waterbodies, wetlands, and urban areas have increased to 4.62, 1.26, and 0.18 billion US$, respectively. In 2012, ESVs of the forest, cropland, wetland, and urban areas showed a gradual increase to 73.49, 39.06, 1.65, and 0.34 billion US$, respectively. In contrast, ESVs of grassland and waterbodies have decreased to 12.71 and 4.35 billion US$, respectively. Forest land, wetlands, urban areas, and waterbodies positively contributed to ESVs in 2020 with values of 74.68, 2.06, 0.50, and 4.41 billion US$, respectively. However, the ESVs of cropland and grassland have decreased in this period to 37.72 and 12.28 billion US$, respectively. Throughout the years, barren land and permanent snow and ice cover had an ESV of 0. Therefore, it can be said that although the

Ecosystem Service Values have differed through each LULC type within the study period, there is a total estimated gain of 618 million US$ from 1992 to 2020.

Table 3: Estimated Ecosystem Service Value of each LULC type

LULC type	Ecosystem Service Value (in billion US$)			
	1992	2002	2012	2020
Cropland	36.749	38.682	39.064	37.723
Forest land	70.377	72.606	73.488	74.676
Grassland	18.038	14.086	12.705	12.284
Wetland	1.172	1.259	1.648	2.064
Urban area	0.136	0.179	0.339	0.496
Barren land	0	0	0	0
Waterbodies	4.562	4.615	4.353	4.409
Permanent snow and ice	0	0	0	0
Total	131.034	131.427	131.597	131.652

Source: Computed by authors

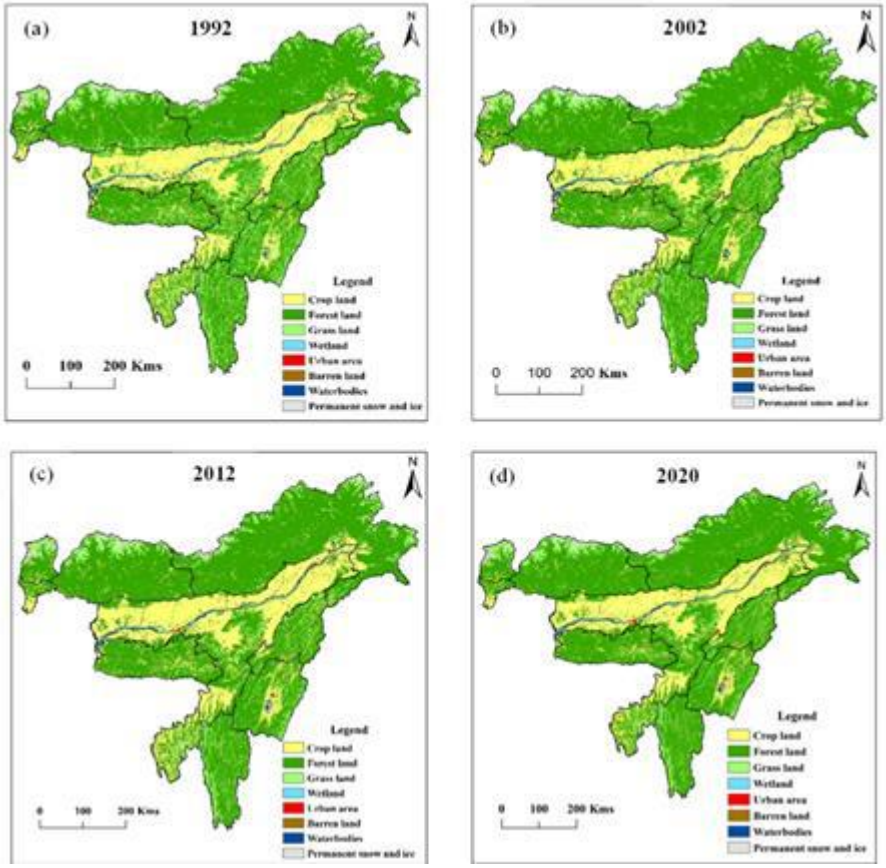

Figure 3: Area changes of LULC in Eastern Himalaya (in hectares) from 1992 to 2020

Table 4: Percentage change of total ecosystem service values under each LULC type

LULC types	ESV change (in percent)			
	1992-2002	2002-2012	2012-2020	1992-2020
Cropland	5.260	0.988	-3.433	2.650
Forest land	3.167	1.215	1.617	6.109
Grassland	-21.909	-9.804	-3.314	-31.899
Wetland	7.423	30.898	25.243	76.109
Urban area	31.618	89.385	46.313	264.706
Barren land	0.000	0.000	0.000	0.000
Waterbodies	1.162	-5.677	1.286	-3.354
Permanent snow and ice	0.000	0.000	0.000	0.000
Total	0.300	0.129	0.042	0.472

Source: Computed by authors

Changes in ESV show a gradual increase in total values in the last three decades (1992-2002, 2002-2012, and 2012-2020) from 1992 to 2020 (Table 4). In the first decade (1992-2002), total ESV increased by 393 million (0.30%), in the second decade (2002-2012) it increased by 170 million (0.13%), and in the last decade (2012-2020) it increased by 55 million (0.042%) There was a constant positive change in ESVs for forest land (6.11% in 1992-2020), wetland (76.11% in 1992-2020) and urban areas (264.71% in 1992-2020), while significant reduction of ESVs was noticed for grassland (31.90% in 1992-2020). In the case of cropland, ESV increased by 5.26% in 1992-2002 and 0.98% in 2002-2012; and then decreased by 3.43% in 2012-2020. ESV of waterbodies increased by 1.16% in 1992-2002 but decreased by 5.68% in 2002-2012 and then again increased by 1.29% in 2012-2020. Figure 4 shows the heterogeneity in the spatial distribution of resources providing ecosystem services.

Changes in estimated individual ESFs

The contribution of different ecosystem services (ESs) provided by all the LULC types toward the total ESV is presented in Table 5. During the entire study period, the prime ESs provided by major LULC types were found to be water regulation, waste treatment, water supply, etc. (waterbodies); food production, raw materials, etc. (cropland); food production, genetic resources, erosion control, gas regulation, etc. (vegetation cover). The value of Ecosystem Service Functions (ESFs) varied significantly during the study period. Among all services, the contribution of Provisioning Services to the total ESV was the highest (44%), followed by Regulating Services (24%), Supporting Services (17%), and Cultural Services (15%) in 1992. After three decades, in 2020 their contribution to total ESV has changed to 42%, 26%, 16%, and 16% respectively. In aggregate, the value of both Provisioning and Supporting services has declined by 1.65 billion US$ and 0.71 billion US$ from 1992 to 2020, while the value of Regulating and Cultural services has increased by 1.84 billion US$ and 1.35 billion US$ during the same time frame. Among them, the highest

decrease is noticed for genetic resources (0.99 billion US$), followed by food production (0.93 billion US$) and habitat (0.90 billion US$) during 1992-2020. Recreational values have shown the highest increase of 1.35 billion US$ from 19.23 billion US$ in 1992 to 20.58 billion US$ in 2020.

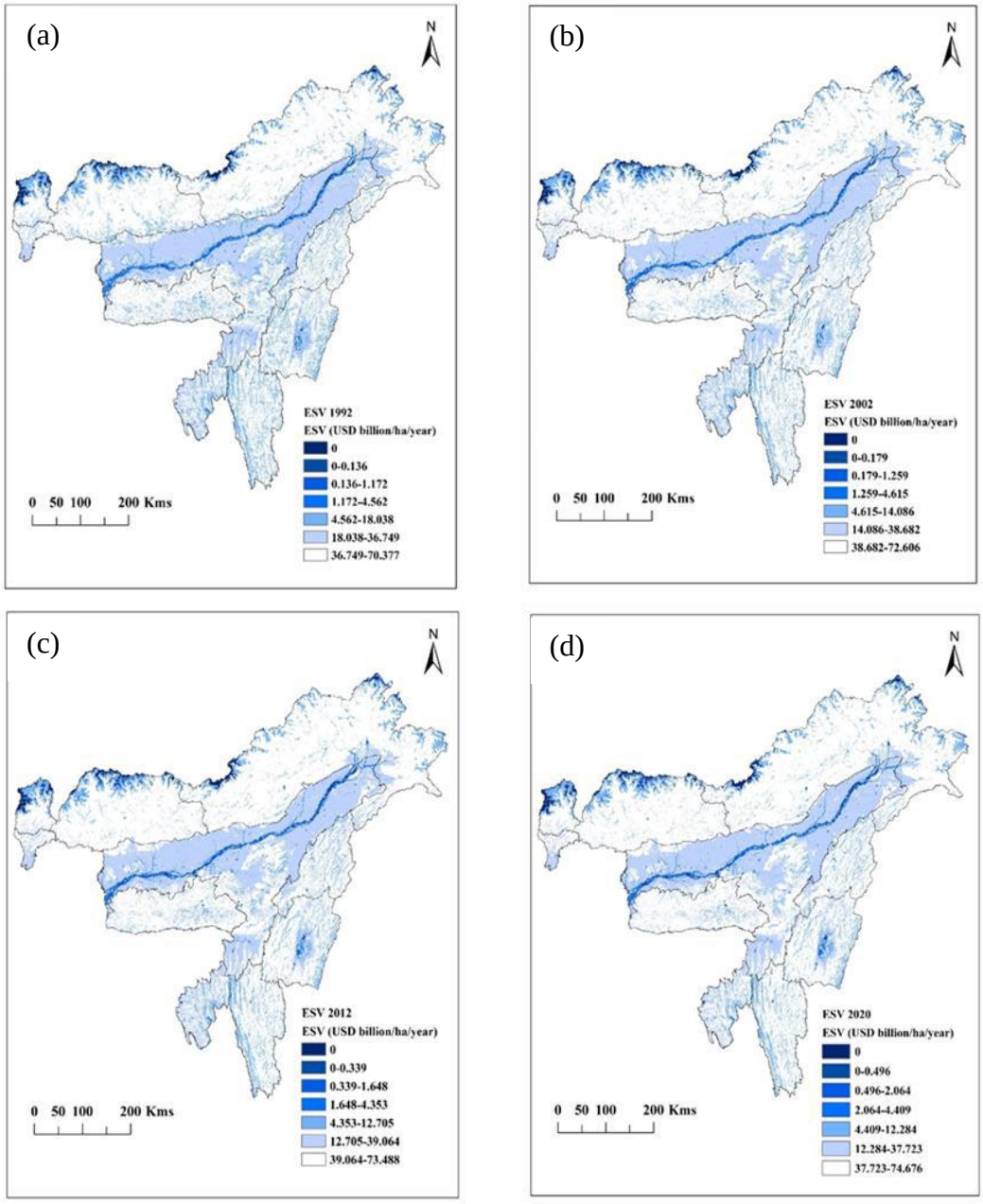

Figure 4: Spatial distribution of Ecosystem Service Values (USD billions) for (a) 1992, (b) 2002, (c) 2012 and (d) 2020

Table 5: Estimated Ecosystem Service Values of each Ecosystem Service Function in Billion US Dollars per year using Global Coefficients (adopted from Costanza et al., 2014)

Types of ecosystem services	Sub-types (f)	Ecosystem Service Functions (ESVf) provided by LULC classes in billion US$			
		1992	2002	2012	2020
Regulating Services	Climate regulation	16.074	16.602	16.804	16.945
	Water regulation	2.824	2.856	2.703	2.743
	Erosion control	2.778	2.834	2.86	2.872
	Waste treatment	6.434	6.644	6.963	7.232
	Biological control	3.485	3.566	3.598	3.641
Total R Services		31.595	32.502	32.928	33.433
Provisioning Services	Water Supply	6.216	6.39	6.396	6.349
	Food Production	25.543	25.378	25.206	24.613
	Raw materials	4.498	4.612	4.646	4.636
	Genetic resources	20.434	19.907	19.681	19.448
Total P Services		56.691	56.287	55.929	55.046
Supporting Services	Soil formation	3.780	3.971	4.01	3.886
	Nutrient cycling	1.227	1.266	1.283	1.305
	Habitat	16.824	16.044	15.82	15.927
Total S Services		21.831	21.281	21.113	21.118
Cultural Services	Recreation	19.229	19.84	20.156	20.583
Total C Services		19.229	19.840	20.156	20.583
Total		129.346	129.910	130.126	130.180

Source: Computed by authors

From 1992 to 2002, ESVs of Regulating services increased by 907 million US$, within which the value of climate regulation services showed the highest increase (528 million US$) during this period. In the case of Provisioning services, total ESV has declined by 404 million US$ due to the decreased value of food production and genetic resources (165 million US$ and 527 million US$ respectively). The value of Supporting services also declined by 550 million US$ because of the habitat quality decline by 780 million US$. The value of Cultural services has increased due to the increase in recreation values (611 million US$) during the time. For the period 2002-2012, ESV of Regulating services and Cultural services have increased by 426 and 216 million US$ respectively, whereas ESV of Provisioning services and Supporting services have decreased by 358 and 168 million US$ respectively. Within the Regulating services, the value of all the ES functions has increased except water regulation services. For the other three ecosystem services, the same pattern of changes in ESVs has been noticed in the previous decade. During 2012-2020, ESV of Regulating services, Cultural services, and Supporting services have increased by 505, 427, and 5 million US$ respectively. On the contrary, the ESV of Provisioning Services has decreased by 883 million US$. In this period, all ES function's values under Regulating services have increased, while the value of all the ES functions under Provisioning services has decreased. The value of habitat quality from Supporting services and recreational

values from Cultural services has increased by 107 and 427 million US$ respectively. In summary, most of the values of ES functions have increased from 1992 to 2020 with a net increase of 0.834 billion US$ except for some ESs like water regulation (Regulating services); genetic resources and food production (Provisioning services) and habitat (Supporting services).

Sensitivity Analysis

Data from LULC changes and their relation with changes in ESVs are combined to perform the sensitivity analysis over the study area (Table 6). During 1992-2002, 2002-2012, and 2012-2020, 2.27%, 2.33%, and 6.27% were converted from one LULC type to the others, respectively, within the total geographic area. Correspondingly, the ESVs also changed by 393, 170, and 55 million US$, respectively, during the consecutive study periods. Results indicate that all the Elasticity values are less than "1", indicating that the total estimated ecosystem values are inelastic to LULC changes. Therefore, this sensitivity analysis indicates that the ESV estimation is robust despite uncertainties on the value coefficients.

Table 6: Summary of changes in LULC and estimated total ESV with the value of Elasticity

	Total area	Change in area		in billion US$			
Period	(hect)	(hect)	%	ESV_{start}	ESV_{end}	ESV_{change}	Elasticity
1992-2002	30245805	687015	2.27	131.034	131.427	0.393	0.132041
2002-2012	30245805	704664	2.33	131.427	131.597	0.17	0.05552
2012-2020	30245805	1897218	6.27	131.597	131.652	0.055	0.006663

Source: Computed by the authors

Discussion

Impact of LULC change on ESVs

The present study evaluated the monetary value of ecosystem services (ESV) over the Eastern Himalayan Region using the LULC datasets as a proxy biome and equivalent value coefficients proposed by Costanza et al., 2014a. Here, the relation of LULC changes with changes in Ecosystem Service Values varied differently for different LULC types in the study period. In some cases, it has increased while reduced for others. For instance, the area of forest lands has increased from 61.23% in 1992 to 64.97% in 2020. Croplands have increased from 21.83% in 1992 to 22.4% in 2020. The area of wetlands has also shown a slight increase from 0.03% in 1992 to 0.05% in 2020. Urban areas increased from 0.07% to 0.25% within the period 1992-2020. Similarly, the percentage share of ESV of forest lands in the total ESV has increased from 53.71% in 1992 to 56.72% in 2020. ESV of croplands also has increased from 28.04% in 1992 to 28.65% in 2020. ESV of wetlands and urban areas have shown an increase from 0.89% to 1.57% and 0.10% to 0.38%, respectively, from 1992 to 2020. On the contrary, the decline in areas of grasslands and waterbodies has led to a decrease in the percentage of ESVs for the same LULC types. For instance, the

reduction of grassland area from 14.32% (in 1992) to 9.75% (in 2020) has resulted in a decline of ESVs from 13.77% (in 1992) to 9.33% (in 2020). Likewise, the area of waterbodies has decreased from 1.21% to 1.16% and its corresponding ESV has also declined from 3.48% in 1992 to 3.35% in 2020.

Factors affecting spatial distribution of ESV

As forest land is the major contributor to the total ESV, changes in the forest ecosystem greatly affected the changes in the total ecosystem service values in the study area (Figure 5). The total increase in forest cover in the Eastern Himalayan Region played a significant role in increasing ESV during 1992-2020. Although some North-Eastern States experienced a decline due to forest encroachments for agricultural purposes. Notably, Nagaland, Arunachal Pradesh, and Assam's Hills witnessed a decrease in total forest cover, primarily driven by increased wood usage in construction. Arunachal Pradesh faced challenges like the diversion of forested land for development and shifting cultivation. Nevertheless, some species exhibited positive changes, particularly in bamboo regeneration. Arunachal Pradesh and Assam Hills witnessed the disappearance of dense forest cover, an increase in open forest, and a decrease in moderate forest from 2001 to 2015. In Mizoram, while open forest cover increased due to plantation, thin density, and dense forest canopy consistently decreased due to biomass removal; therefore, total forest cover has shown a decreasing trend. However, in Nagaland, the open forest may have disappeared, with biotic pressure emerging as a significant factor in forest decline (Sain et al., 2019).

Positive trends in forest cover are evident in Meghalaya, attributed to effective conservation policies fostering regeneration and afforestation. In Sikkim, Tripura, and Manipur, there is also an encouraging rise in dense forest cover. Meghalaya and Tripura experienced a conversion of open forest cover into dense forest, possibly facilitated by fast-growing species in the Northeast Himalayas (Sain et al., 2019). Also, the hill district (Darjeeling) of West Bengal has shown an increase in both open and dense forest cover during 2001-2021 as per the State Forest Report, India. Bhutan has also experienced an increase in forest cover during the last three decades (1990-2020) due to the implementation of annual campaigns for plantation, and social forestry by the Bhutan Ministry of Agriculture and Forest, while reduction is noticed for grassland. Deforestation was also observed in the region, but afforestation overpowered the forest cover loss during the study period (Yangchen et al., 2015; Gilani et al., 2015).

Further assessment of individual ecosystem functions of LULC classes executed that provisioning and regulating services make a comparatively larger contribution (over 60%) than supporting and cultural services across all reference years to the total ESV. Similar findings were estimated by Pradhan & Khaling (2023), who examined the economic valuation of ecosystem services over 31 sample villages of Darjeeling-Sikkim Himalaya using choice experiments from the field survey and found that local communities expressed a higher willingness to pay for regulating services (freshwater regulation). Provisioning and

regulating services are more highly valued than the other two. Also, they have identified the perception of local people about the decreasing trend of provisioning services, especially freshwater availability. A gradual decrease of waterbodies has affected the ESV of water regulation, showing a reduction during 1992-2020. The increase (1992-2012) and decline (2012-2020) of croplands have impacted the decreased ESV of food production. Gradual decrease of grasslands has affected the ESV of genetic resources, and habitat as well, which has shown a negative change during the study period. On the other hand, forest land, urban areas, and wetlands have contributed to an increase in ESV of recreation by enhancing the aesthetic value of the landscape. Therefore, a thorough evaluation of ecosystem services serves as a valuable resource for comprehending and producing pertinent information for decision-making concerning the sustainable management of ecosystem services.

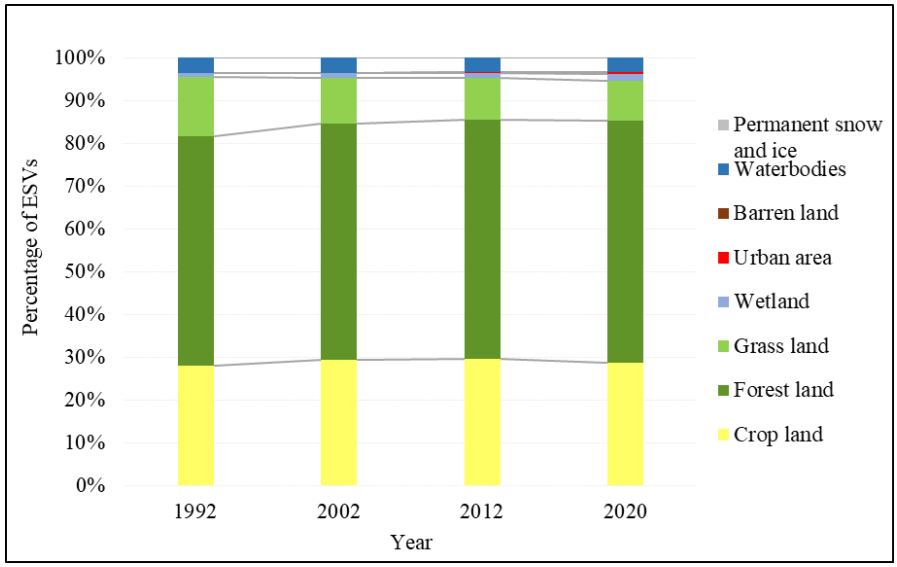

Figure 5: Contribution of different LULC types to total ESV during the study period (1992, 2002, 2012, and 2020)

Limitations and Future Perspectives

The present study has contributed to understanding ESV distribution and the impact of LULC changes on the ESVs over the Eastern Himalayan Region. Several studies have used LULC as a proxy biome to estimate the ESVs over different regions in the world (Jiang et al., 2020; Hu et al., 2020; Sharma et al., 2020; Das et al., 2023), but there is still a lack of long-term assessment of spatial heterogeneity in the Eastern Himalayan Region. There are uncertainties regarding the unit value coefficients proposed by Costanza et al., 2014a. For instance, the study doesn't consider spatial heterogeneity of ecosystem services within the ecosystems (LULC classes); which may lead to fluctuations in the result of ESVs. If we take the example of forest cover, this study has assumed the same value coefficient for all types of forest cover, therefore, providing the same ESV for all of them. In

reality, tropical and temperate forests provide different ecosystem services in terms of provisioning or regulating services; which will reflect some kind of variation in the ESVs for both cases. The analysis employed global land cover data to evaluate Ecosystem Service Values (ESVs) at a relatively low resolution (300*300 m per pixel). This coarse resolution may lead to inaccuracies in quantifying the spatial extent of Land Use and Land Cover (LULC) categories. Also, the study has not taken into account the inflation in current market prices, which may impact the ESVs over time. Therefore, the inclusion of these factors in future studies will enhance the efficiency and applicability of the research.

Conclusion

A combination of LULC proxy and unit value transfer is the simplest and most effective approach for evaluating ESV in vast regions, especially where fieldwork is challenging and expensive due to harsh natural conditions, resulting in limited primary data. We have applied this approach to the Eastern Himalayan Region which emerges as a crucial provider of multiple essential ecosystem services. The study sheds light on ESV changes in response to LULC dynamics in the Eastern Himalayan Region, revealing an improvement in total and individual ecosystem services. The total ESV has increased by 618 million US$ from 131.034 billion US$ in 1992 to 131.652 billion US$ in 2020. Forests, followed by cropland and grassland, emerge as primary contributors to the total ESV in the region. Therefore, the increase in ESVs was mainly linked to the increase in forest cover as a result of afforestation, which is identified to be the main provider of ecosystem services. Among individual ecosystem service functions (ESV) provisioning and regulating services make a comparatively larger contribution (over 60%) than supporting and cultural services across all reference years to the total ESV. The contribution of individual ecosystem functions increased throughout the study period. Significant declines have occurred in the values of specific ecosystem service functions such as water regulation (Regulating services); genetic resources and food production (Provisioning services) and habitat (Supporting services). Sensitivity analysis reveals all elasticity values to be considerably below “1”, affirming the validity of assessing ESVs over the study periods to understand their responsiveness to LULC dynamics. These initial assessments underscore the importance of ecosystem services in the region, setting the stage for more thorough and precise estimations in subsequent analyses.

Acknowledgement:

The authors are grateful to the Hon’ble Vice Chancellor and Head, Department of Geography, Banaras Hindu University, Varanasi for providing the necessary infrastructure for carrying out this research work. The first author is grateful to the University Grants Commission, New Delhi for providing a Junior Research Fellowship for this research.

References:

1. Chatterjee, S., Dutta, P. K., Saikia, A., Dutta, P., Ghosh, D., Pangging, G., & Goswami, A. K. (2006). Biodiversity Significance of North East India Biodiversity Significance of North East India for the study on Natural Resources, Water and Environment Nexus for

Development and Growth in North Eastern India. https://www.researchgate.net/publication/272362960
2. Chettri, N., & Sharma, E. (2006). Prospective For Developing A Transboundary Conservation Landscape In The Eastern Himalayas (J. A. , T. M. M. A. S. L. O.-W. and E. D. W. McNeely, Ed.). Society for Conservation Biology Asia Section and Resources Himalaya, Kathmandu, Nepal.
3. Costanza, R., de Groot, R., Sutton, P., van der Ploeg, S., Anderson, S. J., Kubiszewski, I., Farber, S., & Turner, R. K. (2014a). Changes in the global value of ecosystem services. Global Environmental Change, 26(1), 152–158. https://doi.org/10.1016/j.gloenvcha.2014.04.002
4. Costanza, R., de Groot, R., Sutton, P., van der Ploeg, S., Anderson, S. J., Kubiszewski, I., Farber, S., & Turner, R. K. (2014b). Changes in the global value of ecosystem services. Global Environmental Change, 26(1), 152–158. https://doi.org/10.1016/j.gloenvcha.2014.04.002
5. Das, A., Das, M., Houqe, R., & Pereira, P. (2023). Mapping ecosystem services for ecological planning and management: a case from a tropical planning region, Eastern India. Environmental Science and Pollution Research, 30(3), 7543–7560. https://doi.org/10.1007/s11356-022-22732-3
6. Sain, K., Dr. Goel, M. K., Dr. Kuniyal, J. C., Dr. Mathur, V. B., & Prof Garkoti, S. C. (2019). Status of Ecosystem Health in the Indian Himalayan Region. A Report under National Mission for Sustaining the Himalayan Ecosystem. Climate Change Programme. Department of Science and Technology. Govt of India.
7. Gashaw, T., Tulu, T., Argaw, M., Worqlul, A. W., Tolessa, T., & Kindu, M. (2018). Estimating the impacts of land use/land cover changes on Ecosystem Service Values: The case of the Andassa watershed in the Upper Blue Nile basin of Ethiopia. Ecosystem Services, 31, 219–228. https://doi.org/10.1016/j.ecoser.2018.05.001
8. Gilani, H., Shrestha, H. L., Murthy, M. S. R., Phuntso, P., Pradhan, S., Bajracharya, B., & Shrestha, B. (2015). Decadal land cover change dynamics in Bhutan. Journal of Environmental Management, 148, 91–100. https://doi.org/10.1016/j.jenvman.2014.02.014
9. Hu, Z., Wang, S., Bai, X., Luo, G., Li, Q., Wu, L., Yang, Y., Tian, S., Li, C., & Deng, Y. (2020). Changes in ecosystem service values in karst areas of China. Agriculture, Ecosystems and Environment, 301. https://doi.org/10.1016/j.agee.2020.107026
10. Jiang, W., Lü, Y., Liu, Y., & Gao, W. (2020). Ecosystem service value of the Qinghai-Tibet Plateau significantly increased during 25 years. Ecosystem Services, 44. https://doi.org/10.1016/j.ecoser.2020.101146
11. Kindu, M., Schneider, T., Teketay, D., & Knoke, T. (2016). Changes of ecosystem service values in response to land use/land cover dynamics in Munessa-Shashemene landscape of the Ethiopian highlands. Science of the Total Environment, 547, 137–147. https://doi.org/10.1016/j.scitotenv.2015.12.127
12. Kreuter, U. P., Harris, H. G., Matlock, M. D., & Lacey, R. E. (2001). Change in ecosystem service values in the San Antonio area, Texas. In Ecological Economics (Vol. 39). www.elsevier.com/locate/ecolecon

13. Kubiszewski, I., Costanza, R., Dorji, L., Thoennes, P., & Tshering, K. (2013). An initial estimate of the value of ecosystem services in Bhutan. Ecosystem Services, 3. https://doi.org/10.1016/j.ecoser.2012.11.004
14. Land Cover Cci Product User Guide Version 2 Document Ref: Cci-Lc-Pug Deliverable Ref: D3.4-PUG Version: 2.4. (2012).
15. Li, J., Chen, H., Zhang, C., & Pan, T. (2019). Variations in ecosystem service value in response to land use/land cover changes in Central Asia from 1995-2035. PeerJ, 2019(9). https://doi.org/10.7717/peerj.7665
16. Pradhan, A., & Khaling, S. (2023). Community priorities, values, and perceptions associated with ecosystem services provided by the socio-ecological landscapes of Darjeeling-Sikkim Himalaya. Regional Environmental Change, 23(1). https://doi.org/10.1007/s10113-023-02028-z
17. Rana, S. K., Rawal, R. S., Dangwal, B., Bhatt, I. D., & Price, T. D. (2021). 200 Years of Research on Himalayan Biodiversity: Trends, Gaps, and Policy Implications. In Frontiers in Ecology and Evolution (Vol. 8). Frontiers Media S.A. https://doi.org/10.3389/fevo.2020.603422
18. Robert Costanza, by, de Groot, R., Farber, S., Grasso, M., Hannon, B., Limburg, K., Naeem, S., & O, R. V. (1997). The Value of the World's Ecosystem Services and Natural Capital (Vol. 387).
19. Schägner, J. P., Brander, L., Maes, J., & Hartje, V. (2013). Mapping ecosystem services' values: Current practice and future prospects. In Ecosystem Services (Vol. 4, pp. 33–46). https://doi.org/10.1016/j.ecoser.2013.02.003
20. Schild, A., Chettri, N., Sharma, E., Shakya, B., Thapa, R., Bajracharya, B., Uddin, K., Oli, K. P., Choudhury -Icimod, D., & Kathmandu, N. (2010). Biodiversity in the Eastern Himalayas: Status, Trends and Vulnerability to Climate Change Climate Change Impact and Vulnerability in the Eastern Himalayas-Technical Report 2 Biodiversity in the Eastern Himalayas: Status, Trends and Vulnerability to Climate Change.
21. Sharma, S., Nahid, S., Sharma, M., Sannigrahi, S., Anees, M. M., Sharma, R., Shekhar, R., Basu, A. S., Pilla, F., Basu, B., & Joshi, P. K. (2020). A long-term and comprehensive assessment of urbanization-induced impacts on ecosystem services in the capital city of India. City and Environment Interactions, 7. https://doi.org/10.1016/j.cacint.2020.100047
22. Troy, A., & Wilson, M. A. (2006). Mapping ecosystem services: Practical challenges and opportunities in linking GIS and value transfer. Ecological Economics, 60(2), 435–449. https://doi.org/10.1016/j.ecolecon.2006.04.007
23. Wilson, M. A., & Hoehn, J. P. (2006). Valuing environmental goods and services using benefit transfer: The state-of-the art and science. In Ecological Economics (Vol. 60, Issue 2, pp. 335–342). https://doi.org/10.1016/j.ecolecon.2006.08.015
24. Yangchen, U., Thinley, U., & Wallentin, G. (2015). Land Use Land Cover Changes in Bhutan: 2000-2013. https://www.researchgate.net/publication/288181926

The Indian Geographical Journal
Volume 98 (2) December - 2023, pp 60-79
ISSN 0019-4824

A GEO-SPATIAL APPROACH TO RAINFALL VARIABILITY AND TIME SERIES TREND ANALYSIS IN THE MAYURAKSHI BASIN, EASTERN INDIA

David Durjoy Lal Soren, **Jonmenjoy Barman**, **Brototi Biswas**

Department of Geography & RM, Mizoram (Central) University, Aizawl, Mizoram-India
Corresponding author*: devid.dls.king@gmail.com

Abstract

The primary driving forces behind this investigation were the trend in rainfall, variability in change point identification, and forecasting for the Mayurakshi basin, located in eastern India, using the data from 1991 to 2020. Sen's Slope was employed to determine the slope's magnitude, and Mann-Kendall (mMK) statistics were utilized to assess the long-term trend of rainfall. The trend's conclusion showed that the rainfall trend fluctuated throughout time, and then experienced a negative magnitude. The Pettitt Test, the Standard Normal Homogeneity Test (SNHT), and Buishand's U test statistics were used to determine the change point of rainfall during a 30-year long-term period. The results of the change point analysis showed that the significance level was lower than the p-value ($\propto = 0.05$), indicating a plausible change point in rainfall occurring in the year 2008. To gain insights into the seasonal nature of rainfall, the Rainfall Seasonality Index (RSI) was computed for all rainfall stations in the basin. The RSI indicated equitable rainfall distribution, primarily during the monsoonal season. The assessment of wet and drought conditions in the basin was performed using the Rainfall Anomaly Index (RAI). The RAI revealed that the basin experienced drought in 50% of the years during the 30 years. The outcomes of this study hold practical implications for future planning, including crop and environmental management.

Keywords: Trend; Change point detection; Seasonality; Anomaly.

Introduction

Rainfall is one of the important parameters that directly control water resources and agriculture. For effective management of water resources, accurate quantification of climatic parameters such as rainfall changes is crucial. Water resources are immediately impacted by changes in rainfall patterns, which are directly related to changes in the hydrological cycle (Gajbhiye et al. 2015). The southwest monsoon, which brings copious amounts of precipitation, is extremely important to the Indian subcontinent. However, there has been a rise in precipitation variability and uncertainty in recent decades (Das et al. 2021). Significant spatiotemporal variability and uncertainty in rainfall have been observed across the Indian subcontinent. In contrast to the northeastern region of India, Rajasthan in

western India receives barely 100mm of rain on average each year. Stream flow patterns, soil moisture content, and groundwater recharge are all being impacted by changing climatic conditions, particularly the frequency and amount of rainfall (Srivastava et al. 2014).

The variability and erratic character of rainfall events, which cause longer dry seasons, less runoff, and food insecurity, are the main effects of climate change. As a result, agriculture is greatly impacted by climate change and its effect on rainfall variability in many different places around the world (Gajbhiye et al. 2015). Numerous climate factors have changed as a result of the ongoing increase in fossil fuel use and greenhouse gas emissions. Change points are sudden shifts in climate behaviour. Therefore, it is essential for agricultural planning, and efficient water resource management in any location to analyze climatic factors, notably rainfall patterns, variations, and trends. Understanding precipitation patterns on the Indian subcontinent requires a thorough understanding of climate change.

Numerous studies (Karmeshu et al. 2012) have focused on the evaluation of change points at both global and regional scales. The Mann-Kendall test, Sen's slope non-parametric test, and Pettit's test are frequently used by researchers to evaluate trends, estimate trend magnitudes, and identify change points when they examine historical time series data (Das et al. 2021). To assess the consistency of long-term time series data and spot potential changes, the standard normal homogeneity test is also used (Dhorde et al., 2013).

Various statistical strategies have been utilized for change point detection in the context of parametric methods under the assumption that the data have a normal distribution. According to Chargui et al. (2018), these methods include Buishand U, Buishand range, standard normal homogeneity, and log-likelihood-based approaches. For one to understand climate anomalies and put into practice efficient management techniques, one must have a solid understanding of change detection and trend analysis (Fischer et al. 2012). As a result, understanding rainfall patterns depends heavily on the research of temporal and spatial changes in rainfall as well as the analysis of long-term rainfall time series

The ability to identify trends in climatic variables has been demonstrated by several indexes. The Precipitation Concentration Index (PCI), Rainfall Seasonality Index (RSI), and Rainfall Anomaly Index (RAI) (Walsh and Lawler 1981) are a few examples, these are powerful indicators to understand the behaviour of drought condition seasonal variation in such agrarian Mayurakshi basin. In this study, we concentrate on evaluating rainfall trends and the amplitude of linear changes using Sen's slope and Mann-Kendall statistics. Statistical tests are preferred for determining absolute homogeneity and change points in areas under study that have diverse topographical features or a wide distribution of stations. This is crucial since critical connections might not be readily apparent (Ahmed et al. 2020). Thus, we employed the Pettitt Test, Buishand U Statistic, and Standard Normal Homogeneity Test to identify significant changes in the time series rainfall data.

Additionally, we applied two widely recognized indexes, RSI and RAI, to evaluate the spatio-temporal variability and seasonality of rainfall.

The Mayurakshi River is essential for irrigation, drinking water supply, fishing, and the important agricultural region of eastern India (Ghosh et al. 2022). There are numerous dams and multifunctional projects in the Mayurakshi basin. Several studies conducted on this basin on different aspects such as hydro-geomorphological modification of the Mayurakshi River, and the impact of the Tillpara barrage on the tributary of Mayurakshi (Pal 2016, 2017), spatiotemporal analysis of the regional agricultural disparity of Mayurakshi basin (Chakraborty et al, 2016). The study aims to explore how precipitation affects the Mayurakshi basin. A thorough understanding of rainfall variability and trends will give a comprehensive insight into future patterns, enabling the river basin to plan more efficiently and enhance both agricultural and water resource management planning.

Study area

Mayurakshi is one of the most important river systems in eastern India. The river originates from Trikut Hill in the Chota Nagpur plateau of Jharkhand state. The basin extends from 23° 63′ 12″ to 24° 51′ 3″ N latitude and 86° 84′ 38″ to 88° 16′ 12″ E longitude in the states of Jharkhand and West Bengal and covers an area of 8805.06 km^2. Geologically, the whole area of the upper part of the basin is dated back to the Proterozoic and Phanerozoic eon formations of undivided Precambrian rock. The middle catchment of the basin is most dominantly deposited by laterite and lateritic soil, and the lower catchment of the basin is mostly covered by young and old alluvial soil. The relief of the upper catchment of the Mayurakshi basin is very undulating and covered with flat-topped isolated hills, most of which are >300 meters. The basin's middle catchment area is part of West Bengal's Birbhum district. It is also known as the Rarh region, and it is part of the undulating eastward-extended fringing portion of the Chotonagpur plateau that ranges from 71m to 120m in height. The lower catchment is mostly covered by the lower-laying flood plain.

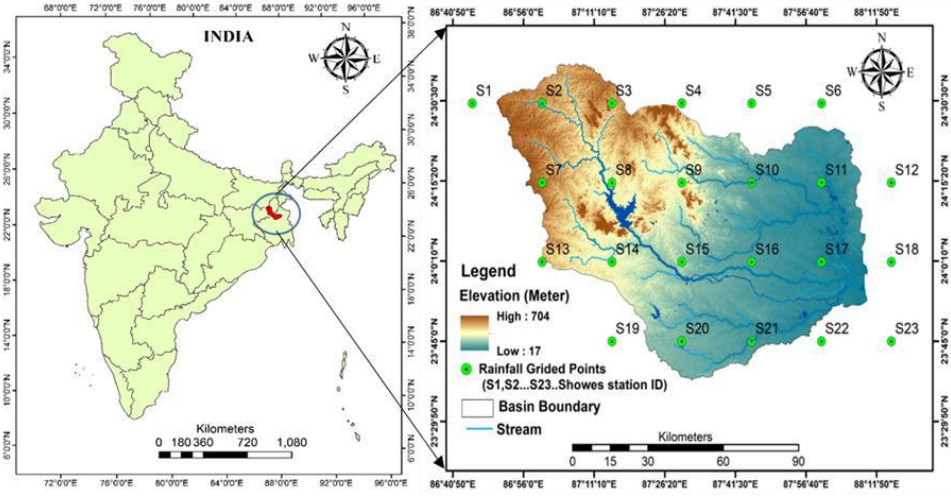

Fig. 1: Location of the study area and distribution of rainfall grid points

Methodology

Data Source

The rainfall data from 1991 to 2020 was collected from the India Meteorological Department (IMD), Pune (https://www.imdpune.gov.in/cmpg/Griddata/Rainfall_25_Bin.html). The obtained daily gridded rainfall data (in millimetres) has a high spatial resolution of 0.25 × 0.25 degrees. After collecting the rainfall data, the row data set was exported to MS Excel, where it was corrected for missing values, and the stations were filtered to get the required rainfall stations for the study area. A total of 23 stations covering the entire study area were assigned names as - S1, S2, S3... S23 (Table 1). The rainfall data was arranged on a daily, monthly, and annual basis for subsequent analysis.

Mann-Kendall Statistic

The Mann-Kendall, a non-parametric test, is a suitable measure for analyzing the trends in time series data, both for long and short-term periods. It assesses consistent increasing or decreasing trends effectively. Due to its non-parametric nature, the MK test can be applied to various data distributions, making it widely used compared to other statistical methods for studying long-term trends in time series data.

The Kendall's statistics (S) in the long-term time series data, denoted as m1, m2, m3, ..., and mn, is estimated using the following equation:

$$S = \sum_{k=1}^{n-1} \sum_{j=k=1}^{n} sgn(\mathrm{x_J} - \mathrm{x_k}) \qquad \text{(EQ-1)}$$

where sgn (x_J - x_k) is defined as:

$$\left\{ \begin{array}{l} +1 \text{ --------} (\mathrm{x_J} - \mathrm{x_k}) > 0 \\ 0 \text{ ---------} (\mathrm{x_J} - \mathrm{x_k}) = 0 \\ -1 \text{---------} (\mathrm{x_J} - \mathrm{x_k}) < 0 \end{array} \right\} \qquad \text{(EQ-2)}$$

In the equation, x1, x2, ..., xn is the data points at different time intervals, where n is the total time period. If the value of n is equal to or greater than 10, a Z-transformation is applied to approximate a normal distribution known as the Kendall Z-value. The Z statistics is obtained by adapting the variance of VAR(S).

$$VAR(S) = 1/18\left[n(n-1)(2n+5) - \sum_{p-1}^{g} (t_p - 1)(2t_p - 5) \right] \qquad \text{(EQ-3)}$$

Here, n is the number of observations, g is the equal trend values, p represents the value of tide groups in the data set, and tp indicates the number of data values. The symbol Σ represents the summation of all tide groups.

The calculated VAR(S) is employed to compute the Z transformation for the MK test statistics Z-value:

$$Z = \begin{cases} \frac{S-1}{VAR(S)} S > 1 \\ 0, S = 0 \\ \frac{S-1}{VAR(S)} S < 0 \end{cases} \quad \text{(EQ-4)}$$

The Z-value follows a standard normal distribution, where the negative value represents a downward trend and the positive value indicates an upward trend. The significance level α is used for testing, typically using a two-tailed test.

Modified Mann–Kendall Test

The statistical test conducted by Kendell can produce inaccurate results when the time series data have a significant autocorrelation. To address this issue, researchers are using the modified Mann-Kendall test. Therefore, before proceeding with the analysis of any time series data, initially the data is tested for serial dependency at the lag-1 significance level. If the data follows a significant autocorrelation in such conditions, modified Mann-Kendall (mMK) statistics were employed.

The mMK VAR (S) is estimated using the following equation:

$$\mathrm{VAR}(S) = \left(\frac{n(n-1)(2n+5)}{18}\right) \cdot \left(\frac{n}{n_e^*}\right) \quad \text{(EQ-5)}$$

The correction factor $\left(\frac{n}{n_e^*}\right)$is calculated to adjust the autocorrelation data:

$$\left(\frac{n}{n_e^*}\right) = 1 + \left(\frac{2}{n^3-3n^2+2n}\right) \sum_{\mathrm{f}=1}^{n-1} (n-f)(n-f-1)(n-f-2)\rho_e(f) \quad \text{(EQ-6)}$$

The value of $\rho_e(f)$ represents the auto-correlation among the rank of observations and is computed as follows:

$$\rho(f) = 2\sin\left(\frac{\pi}{6}\rho_e(f)\right) \quad \text{(EQ-7)}$$

Sen's Slope

The MK or mMK Statistic is employed to determine the direction (positive or negative) of a given attribute, while Sen's Slope is commonly applied to assess the magnitude of the inclination. Sen (1968) proposed a non-parametric statistic to quantify the slope and measure the linear change. This method, widely employed to compute trend

magnitude (Kamal and Pachauri 2019), utilizes Sen's slope estimates, which can be either positive or negative.

The slope is calculated as described by Hirsch et al. (1982), the equation is as follows:

$$F(t) = Qt+B \quad \text{(EQ-8)}$$

Here, F(t) represents a time series that can increase or decrease, here Q is the slope and B is a constant. The slope Q can be computed using the formula:

$$Q_i = \frac{xj-xk}{j-k} \; i = 1,2,3,4,5 \ldots n \; j > k \quad \text{(EQ-9)}$$

In this equation, x_j and xk is the data values at time j and k, consecutively, with j > k. The median of the n values of Qi is determined by the following formula:

$$Qi = \begin{cases} \left[\frac{Qn+1}{2}\right] \ldots\ldots\ldots\ldots\ldots\ldots\ldots\ldots\ldots n \text{ odd} \\ \frac{1}{2}\left[\frac{Qn}{2}\right] + \left[\frac{Qn+2}{2}\right] \ldots\ldots\ldots\ldots n \text{ even} \end{cases} \quad \text{(EQ-10)}$$

The positive Qi represents an increasing trend, whereas a negative Qi represents a decreasing trend, and a value of zero indicates no trend.

Pettitt Test

Pettitt (1997) developed a technique called single change point detection, this statistical analysis is used to identify abrupt changes in time series data. This method has been widely utilized by researchers such as Bryson et al. (2012), and others.

$$U_k = 2\sum_{i=0}^{n} m_i - k(n+1) \quad \text{(EQ-11)}$$

In Equation 11, m_i presents the order of the ith observation, while x1, x2, x3, ..., xn represent the data points organized in ascending order. The variable k can take values from 1 to n.

$$K = \max\left|U_k\right| \quad \text{(EQ-12)}$$

$$U_k = \sum_{i=1}^{t} \sum_{1j=t+1}^{n} sign\left(x_i - x_j\right) \quad \text{(EQ-13)}$$

U_k is calculated as the sum of sign (x_i - x_j) for all i from 1 to t, and j from t+1 to n, as shown in Equation 13.

$$K\alpha=[-1n\alpha(n^3+n^2)/6]^{1/2} \quad \text{(EQ-14)}$$

To determine the change point in the time series, the value of K come to its maximum at U_k. The critical value, denoted as Kα, is obtained using Equation 14. Here, α represents the desired level of significance for determining the critical value, and n is the sum of the observations.

Buishand U Statistic

Ndione et al. (2017) employed the Buishand's U test to calculate the change point. This statistical test, proposed by Buishand in 1984, was specifically utilized for detecting a single change point. The formulation of the Buishand U test is expressed as follows:

$$U = \frac{\sum_{k=1}^{n-1} (S_K / D_X)^2}{n(n+1)} \quad \text{(EQ-15)}$$

In this equation, S_k represents the cumulative deducted value from the mean, and D^2_x corresponds to the standard deviation presented in equations EQ-13 and EQ-14.

$$S_k = \sum_{i=1}^{k} (X_i - \bar{X}) \quad \text{(EQ-16)}$$

$$D_x^2 = 1/n \sum_{i=1}^{n} (X_i - \bar{X})^2 \quad \text{(EQ-17)}$$

Standard Normal Homogeneity Test

The standard normal homogeneity (SNH) tests, developed by Alexandersson in 1986, serve as a statistical approach to determine a change point in time-series data. The equations presented by Alexandersson in 1986 are as follows:

$$Ty = y\bar{z}_1 + (n-y)\bar{z}_2, Y = 1.2, 3.....n \quad \text{(EQ-18)}$$

In Equation 18, the $T(_y)$ statistic is computed to compare the mean value of the first year (y) and the last year (n-y). The computation of Z1 and Z2 can be expressed as follows:

$$\bar{Z}_1 = 1/y \sum_{i=1}^{n} (y_1 - \bar{y} / S_q) \text{ and } \bar{Z}_2 = 1/n - y \sum_{i=y+1}^{n} (y_1 - \bar{y} / S_q) \quad \text{(EQ-19)}$$

In Equation 19, represents the arithmetic mean of the ratio S_q, while represents the standard deviation of the series. A breaking point within the time series is identified when the *T* value reaches its maximum. The homogeneity critical value is computed to determine the homogeneity.

$$T_o = \max T_y \quad \text{(EQ-20)}$$

Rainfall Seasonality Index

The Rainfall Seasonality Index (RSI) is a measurement which conveys the relative seasonality of the rainfall pattern. RSI is the statistical representation of the annual discrepancy in monthly rainfall. RSI helps in understanding the seasonal characteristics of rainfall and its pattern. The RSI is calculated using the following formula (Walsh and Lawler, 1981):

$$RSI = \frac{1}{\overline{R}} \sum_{n=1}^{n=12} \left| \overline{x}_{ny} - \overline{R}_{y} / 12 \right| \quad \text{(EQ-21)}$$

n the formula, $\bar{x}_{ny}$ indicates the calculated rainfall in month n of a given year y, while $\overline{R_y} / 12$ indicates the average yearly rainfall for that particular year $_y$.

Rainfall Anomaly Index

This study computed the precipitation abnormalities using the statistical method known as the Rainfall Anomaly Index (RAI). Indicating deviations from typical rainfall quantities, anomalies can be either positive (+) or negative (-). Following the method suggested by Van-Rooy (Van-Rooy 1965), the ten highest and lowest precipitation measurements are ordered and averaged to create thresholds for positive and negative anomalies.

The RAI is computed using the following equations:

$$RAI = 3 * (Pi - \overline{P}) / (\overline{r} - \overline{P}) \quad \text{(EQ-22)}$$

$$RAI = -3 * (Pi - \overline{P}) / (\overline{r} - \overline{P}) \quad \text{(EQ-23)}$$

Here, Pi stands for the annual precipitation in millimeters, P for the time series' average rainfall, and (r, P) for the average of the ten highest and lowest annual precipitation values. The prefix ±3 is used to calculate positive and negative anomalies, respectively.

Results and Discussion

Rainfall Dynamics

To examine the evolving patterns and spatial-temporal fluctuations of rainfall, an analysis was conducted using the comprehensive rainfall data of the Mayurakshi basin spanning from 1991 to 2020. The study encompassed 23 rainfall stations situated within the basin. Below is a summary of the decadal annual and seasonal variations in rainfall as well as the long-term trend in rainfall variability.

Decadal and long-term variation of rainfall

The focus of the study was a 30-year span of rainfall variations, examining spatial and seasonal patterns at a micro-level scale. In the first decade (1991–2000), rainfall

exhibited a consistent upward trend (Fig. 3). The characteristics of rainfall in this period varied, ranging from a maximum and minimum of 1964.86 mm and 1288.99 mm to an average of 1557.10 ± 174.44 mm. The upper part of the basin experienced a significant concentration of rainfall. Moving into the second decade, the mean annual rainfall was 1430.30 ± 155.26 mm, displaying lower variability (CVR 10.85) compared to the first and third decades (Table 1). Between 2001 and 2010, the northeast region of the upper and middle basin areas observed a high concentration of rainfall (Fig. 4b). However, in the third decade, the basin received lower rainfall (1438.68 mm) compared to the first and second decades. During this period, the maximum and minimum rainfall were recorded as 1438.68 mm and 989.27 mm, respectively, with an average of 1207.24 ± 138.41 mm. Rainfall in the third decade displayed a decreasing trend from the upper to the middle and lower basin areas (Fig. 2c). Overall, in the long-term rainfall pattern, the maximum and minimum rainfall of the basin were 1717.37 mm and 1172.51 mm, respectively, with an average annual rainfall of 1398.21 ± 139.95 mm. The northeastern regions of the upper and middle basin areas consistently experienced a high concentration of rainfall, while the lower parts of the basin generally recorded low rainfall over the study period (Table 1, Fig. 2d). Geographically, the upper part of the basin is located in a plateau region, with plateau mountains contributing to favourable conditions for monsoonal rainfall. This explains the higher rainfall that occurred in the upper basin than in the lower basin area.

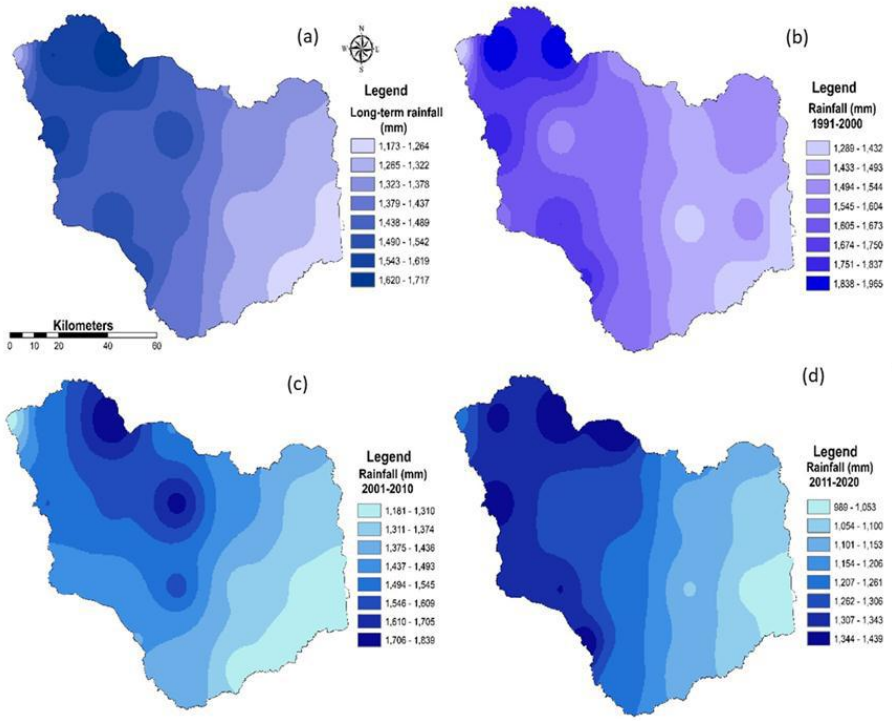

Fig. 2: Decadal and long-term spatial rainfall variation (a) 1st decade, (b) 2nd decade, (c) 3rd decade, (d) long-term basin average

Table 1: Decadal and long-term rainfall variation

Latitude	Longitude	Station	Rainfall (mm)			
			1991-2000	2001-2010	2011-2020	Long-term
24.5	86.75	**S1**	1366.99	1281.24	1243.97	1297.40
24.5	87.00	**S2**	1964.86	1539.25	1355.59	1619.90
24.5	87.25	**S3**	1932.73	1838.98	1380.41	1717.37
24.5	87.50	**S4**	1517.00	1490.56	1438.68	1482.08
24.5	87.75	**S5**	1473.01	1463.85	1188.43	1375.10
24.5	88.00	**S6**	1531.51	1405.81	1152.86	1363.39
24.25	87.00	**S7**	1803.64	1544.97	1369.27	1572.63
24.25	87.25	**S8**	1503.83	1553.95	1297.35	1451.71
24.25	87.50	**S9**	1577.24	1744.03	1305.31	1542.20
24.25	87.75	**S10**	1456.03	1459.32	1117.93	1344.42
24.25	88.00	**S11**	1533.84	1336.77	1058.22	1309.61
24.25	88.25	**S12**	1485.60	1320.04	1061.23	1288.96
24.00	87.00	**S13**	1589.06	1446.53	1340.73	1458.77
24.00	87.25	**S14**	1750.35	1465.52	1344.43	1520.10
24.00	87.50	**S15**	1550.16	1566.56	1237.19	1451.30
24.00	87.75	**S16**	1391.20	1345.04	1095.81	1277.35
24.00	88.00	**S17**	1541.70	1287.93	1028.08	1285.90
24.00	88.25	**S18**	1288.99	1232.09	996.44	1172.51
23.75	87.25	**S19**	1770.11	1435.10	1377.65	1527.62
23.75	87.50	**S20**	1583.93	1413.80	1220.77	1406.16
23.75	87.75	**S21**	1459.81	1271.42	1106.56	1279.26
23.75	88.00	**S22**	1325.02	1180.60	1060.33	1188.65
23.75	88.25	**S23**	1416.67	1273.55	989.27	1226.49
maximum			1964.86	1838.98	1438.68	1717.37
minimum			1288.99	1180.60	989.27	1172.51
average			1557.10	1430.30	1207.24	1398.21
SD			174.44	155.26	138.41	139.95
CVR			11.20	10.85	11.46	10.00

Trend of rainfall

The modified Mann-Kendall (mMK) statistic was employed to assess the trend over a 30-year period within the basin. The comprehensive analysis of the entire basin using the mMK indicated variations in rainfall and the impact of climate change throughout the study period. The p-value was computed to determine the overall rainfall variation, and it was

found to be less than the significance level alpha (0.05), suggesting a plausible change in the basin's rainfall series during the 30-year period. Additionally, the trend exhibited temporal variability.

In general, the negative Kendall's Z value (-1.67) and normalized Kendall's tau (-0.218) indicated a decreasing trend in rainfall (Fig 3 and Table 2). Furthermore, Sen's slope, which provides a measure of the trend's magnitude, showed a strongly negative value (-10.40), indicating a downward trend in rainfall (Fig 3). The basin comprised 23 rainfall stations, and except for station S8, all stations exhibited negative rainfall trends throughout the sampled period. Among them, stations S2, S17, S11, S12, S23, and S24 demonstrated the highest negative Sen's slope values (Q = -25.77, -21.30, -19.48, -18.20, -18.15, and -17.20), signifying a significant decline in rainfall trends. Correspondingly, these stations also exhibited negative Z statistics of -2.18, -5.00, -4.02, -3.39, -2.85, and -2.00, respectively.

Within the study area, significant negative rainfall trends were recorded at S2, S6, S10, S11, S12, S17, S20, and S23, with consistent patterns of negative normalized Kendall's Z and Sen's slope Q values (Fig 4 and Table 2).

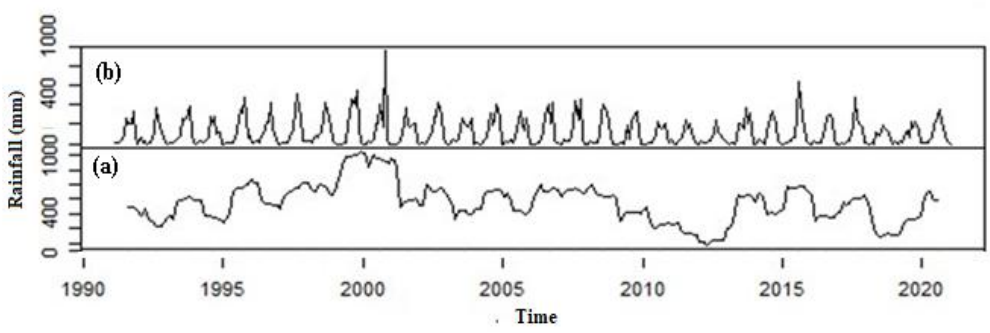

Fig. 3: Rainfall trend with seasonal and random variation

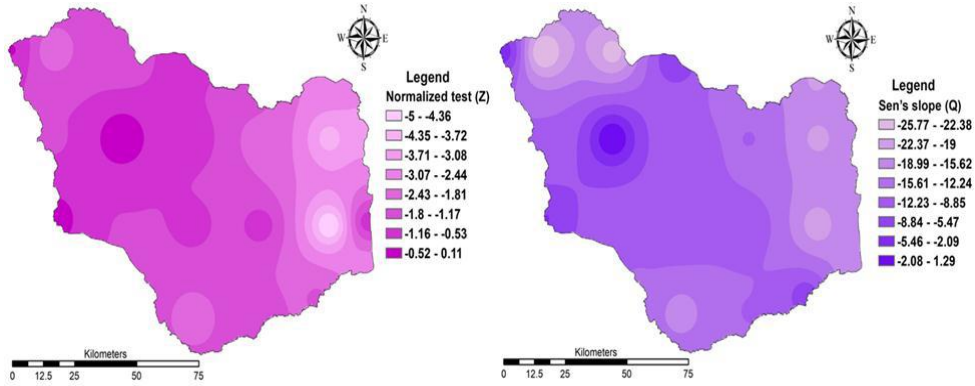

Fig 4: Normalized Z (a) Sen's slope Q (b)

Table 2: Modified Mann Kendall Statistic and Sen's slope estimation

Station	Normalized Test (Z)	Kendall's tau	p-value (Two-tailed)	Sen's slope (Q value)
Basin	-1.67	-0.218	0.035	-10.40
S1	-0.50	-0.070	0.617	-3.980
S2	-2.18	-0.280	0.030	-25.77
S3	-1.70	-0.200	0.089	-23.71
S4	-0.61	-0.089	0.538	-6.020
S5	-1.25	-0.195	0.211	-14.20
S6	-2.68	-0.347	0.007	-19.39
S7	-1.23	-0.200	0.219	-12.14
S8	0.11	0.020	0.91	1.300
S9	-0.69	-0.100	0.492	-10.68
S10	-2.09	-0.241	0.036	-12.11
S11	-4.02	-0.356	<0.05	-19.84
S12	-3.39	-0.301	<0.05	-18.20
S13	-0.21	-0.030	0.830	-5.400
S14	-1.18	-0.150	0.239	-10.07
S15	-0.89	-0.140	0.374	-9.230
S16	-0.86	-0.110	0.392	-9.700
S17	-5.00	-0.370	<0.05	-21.30
S18	-0.86	-0.154	0.388	-15.95
S19	-1.64	-0.210	0.101	-12.37
S20	-2.00	-0.260	0.046	-17.20
S21	-1.61	-0.210	0.108	-12.18
S22	-1.74	-0.150	0.083	-6.880
S23	-2.85	-0.370	0.004	-18.15

Change point of annual rainfall

Various statistical methods, including Pettitt's, SNHT, and Buishand's U tests, were utilized to identify the homogeneity and change points in rainfall patterns. These tests confirmed that a braking point or change point occurred in 2008. Bera et al (2021) stated drought condition extended in the part of Chhota Nagpur Plateau due to low precipitation caused by drastic land use land cover change and modification of cropping pattern. Sankar et al (2023) studied the mining activity of Jharkhand mining area, where the coal mining is the reason of black carbon concentration. Their statistical teste resulted a negative correlation of black carbon mass concentration with rainfall, all of these factors are the

cause of negative trend of rainfall with its step change encountered in 2008. The mathematical models employed in the analysis revealed that the computed p-value, with a confidence interval of 95%, was below the significance level ($\propto$ = 0.05), indicating a notable change in rainfall over the 30-year study period. Concerning individual rainfall stations, the models demonstrated significant breakpoints in annual rainfall at stations S3, S14, S15, S20, and S23 in 2008, at S2 in 2007, and at stations S10, S11, and S12 in 2009. These breakpoints occurred approximately in the middle of the observation period (Table 3). On the other hand, when applying the change-point models (Pettitt's test, SNHT test, Buishand's U test), the calculated p-value exceeded the significance level ($\propto$ = 0.05) at the 95% of confidence interval for 52.17% of the stations (S1, S4, S5, S7, S8, S9, S13, S16, S18, S19, S21, S22). This result indicates that there were no significant changes in rainfall throughout the study period at those particular stations.

Table 3: Change point statistics of the basin

Station	Pettitt's test			SNHT test			Buishand's U test		
	U	t	p 95%	T0	t	P 95%	Q	t	P 95%
Basin	124	2008	0.043	7.395	2008	0.046	0.508	2008	0.032
S1	95	2007	0.287	4.502	2007	0.325	0.226	2007	0.225
S2	153	2007	0.013	10.269	2007	0.012	0.809	2007	0.004
S3	154	2008	0.012	10.045	2008	0.013	0.594	2008	0.020
S4	790	2017	0.522	5.792	2017	0.174	0.107	2017	0.559
S5	124	2008	0.073	7.523	2009	0.067	0.502	2008	0.033
S6	151	2009	0.014	10.291	2009	0.011	0.800	2009	0.004
S7	114	2008	0.122	4.295	2008	0.362	0.286	2008	0.151
S8	940	1996	0.299	4.809	1996	0.285	0.240	2008	0.201
S9	120	2008	0.090	6.378	2008	0.130	0.321	2008	0.114
S10	155	2009	0.011	10.591	2009	0.009	0.591	2009	0.019
S11	153	2009	0.013	10.597	2009	0.008	0.851	2009	0.003
S12	141	2009	0.027	9.338	2009	0.023	0.721	2009	0.008
S13	78	2008	0.541	3.443	2008	0.525	0.248	2008	0.188
S14	116	2008	0.011	5.855	2008	0.167	0.472	2008	0.010
S15	136	2008	0.037	7.599	2008	0.041	0.406	2008	0.046
S16	107	2019	0.171	4.781	2009	0.293	0.284	2009	0.156
S17	148	2002	0.018	9.995	2009	0.014	0.846	2009	0.002
S18	98	2008	0.253	6.791	1994	0.104	0.349	2008	0.097
S19	118	2008	0.100	5.347	2000	0.218	0.366	2000	0.082
S20	140	2008	0.030	7.872	2008	0.054	0.540	2008	0.027
S21	140	2008	0.195	4.801	2008	0.285	0.393	2008	0.070
S22	90	2002	0.350	3.497	2002	0.510	0.263	2002	0.169
S23	152	2008	0.013	8.720	2008	0.031	0.651	2008	0.011

Rainfall seasonality index

The study examined the long-term rainfall patterns in the basin, focusing on individual stations over a 30-year period. The objective was to understand the seasonality of rainfall in the basin. The analysis revealed two predominant classes of Rainfall Seasonality Index (RSI) across the basin: "Very equable" (RSI < 0.19) and "Equable indefinite weather" (RSI between 0.20 and 0.39). When considering the entire 30-year period, 60% of the sampled years exhibited very equal rainfall, while the remaining 40% had equable indefinite weather, which is characteristic of monsoonal rainfall.

Further examination of individual stations (S4, S5, S6, S12, S17, S18, S21, and S23) showed that 60% of the sampled years had consistently equitable rainfall throughout the year. At 52.17% of the stations (S1, S2, S3, S8, S9, S10, S11, S14, S16, S19, S20, and S22), the RSI indicated very equitable and equitable definite weather in 50.00% or more of the sampled years. The decadal analysis of the basin's rainfall seasonality confirmed an equitable pattern.

Spatially, the upper basin experienced higher rainfall intensities with RSI values between 0.20 and 0.39 during the first and second decades. In the third decade, the southern part of the middle and lower basins had RSI values above 0.20. The study area predominantly receives monsoonal rain, and the upper and middle basins exhibit similar rainfall characteristics due to their plateau location and orographic conditions. However, in the lower basin area, which consists of the plain region of the basin, there is a notable difference between very equable and equable definite weather rainfall. On average, 56.67% of the sampled years had very equable rainfall, while 43.33% had equable definite weather rainfall. This disparity may be attributed to the absence of a topographic barrier, leading to increased rainfall uncertainty in the region.

The focal region, primarily encompassing portions of Jharkhand and West Bengal, is chiefly characterized by the presence of the Mayurakshi and Dwarka rivers. Agriculture in this area relies heavily on rainfall and is predominantly mono-crop oriented, resulting in noticeable disparities across different agricultural regions (Chakraborty et al, 2016). Given the significant reliance on rainfall for agricultural activities, analysing the Rainfall Sensitivity Index (RSI) over decades and observing its spatiotemporal variations proves to be a valuable approach for crop selection and mitigating inter-regional agricultural imbalances.

Rainfall anomaly index

The evaluation of the dry and rainy conditions in the basin was conducted based on the Rainfall Anomaly Index (RAI). Over a span of 30 years, the temporal patterns of rainfall were analyzed, revealing that 6.67% of the years were extremely wet, while 16.67%, 13.33%, 6.67%, 13.33%, and 3.33% of the sampled years fell into the categories of very wet, moderately wet, slightly wet, near normal, and slightly dry, respectively. Additionally, 16.67% of the years were identified as extremely dry across the basin.

The spatiotemporal analysis of RAI indicated that 13.33% of the years exhibited extremely wet conditions (>3.00) at 47.83% of the stations (S1, S3, S5, S7, S9, S12, S17, S18, S20, S21). Moreover, extremely dry conditions (<-3.00) were observed in 13.33% of the years at stations S1, S7, S8, S10, S11, S12, S15, S16, S17, S19, and S20 throughout the basin. Very wet conditions were recorded in 13.33% of the years at stations S2, S5, S20, and S25, whereas 10.00% of the years were classified as very wet at stations S6, S8, S10, S12, S15, and S17. The moderately wet condition of RAI was observed in 16.67% of the years across 30.43% of the stations.

Table 4: Rainfall seasonality and decadal status

	RSI Class (Year in percent)		RSI decadal average		
Station	**Very equable (<0.19)**	**Equable in definite weather (0.20-0.39)**	**1991-2000**	**2001-2010**	**2011-2020**
Basin	60.00	40.00	0.19	0.19	0.22
S1	50.00	50.00	0.23	0.20	0.24
S2	50.00	50.00	0.22	0.20	0.23
S3	50.00	50.00	0.20	0.20	0.22
S4	60.00	40.00	0.20	0.17	0.22
S5	60.00	40.00	0.20	0.16	0.22
S6	60.00	40.00	0.19	0.19	0.21
S7	46.67	53.33	0.22	0.21	0.24
S8	56.67	43.33	0.20	0.23	0.20
S9	53.33	46.67	0.21	0.21	0.21
S10	56.66	43.33	0.20	0.20	0.21
S11	56.66	43.33	0.20	0.19	0.22
S12	60.00	40.00	0.19	0.18	0.22
S13	46.67	53.33	0.21	0.22	0.24
S14	50.00	50.00	0.19	0.22	0.23
S15	46.67	53.33	0.20	0.21	0.24
S16	50.00	50.00	0.20	0.19	0.24
S17	60.00	40.00	0.20	0.19	0.22
S18	60.00	40.00	0.21	0.17	0.21
S19	50.00	50.00	0.20	0.20	0.24
S20	53.33	46.67	0.20	0.20	0.24
S21	60.00	40.00	0.20	0.18	0.23
S22	56.67	43.33	0.21	0.19	0.22
S23	63.33	36.66	0.20	0.18	0.21

Among the 23 rainfall stations, the highest occurrence of near normal conditions was found in 26.67% of the years at stations S16 and S19, and in 20.00% of the years at stations S6 and S9. On the other hand, the least frequent near normal condition, accounting for 3.33% of the counted years, was observed at stations S4, S5, S8, and S12. The very dry condition of RAI was prevalent in 23.33% of the years at station S9 and in 20.00% of the years at stations S8 and S19. Similarly, a moderately dry classification was assigned to 13.33% of the years at stations S1, S5, S13, S16, S19, and S21. Overall, the basin experienced a total drought condition in 46.67% of the years, with S2 and S15 being the most affected stations, accounting for 60.00% and 53.33% of the drought years, respectively, among 20.00% of the stations (S1, S3, S7, S16, S19, and S20) (Table 5).

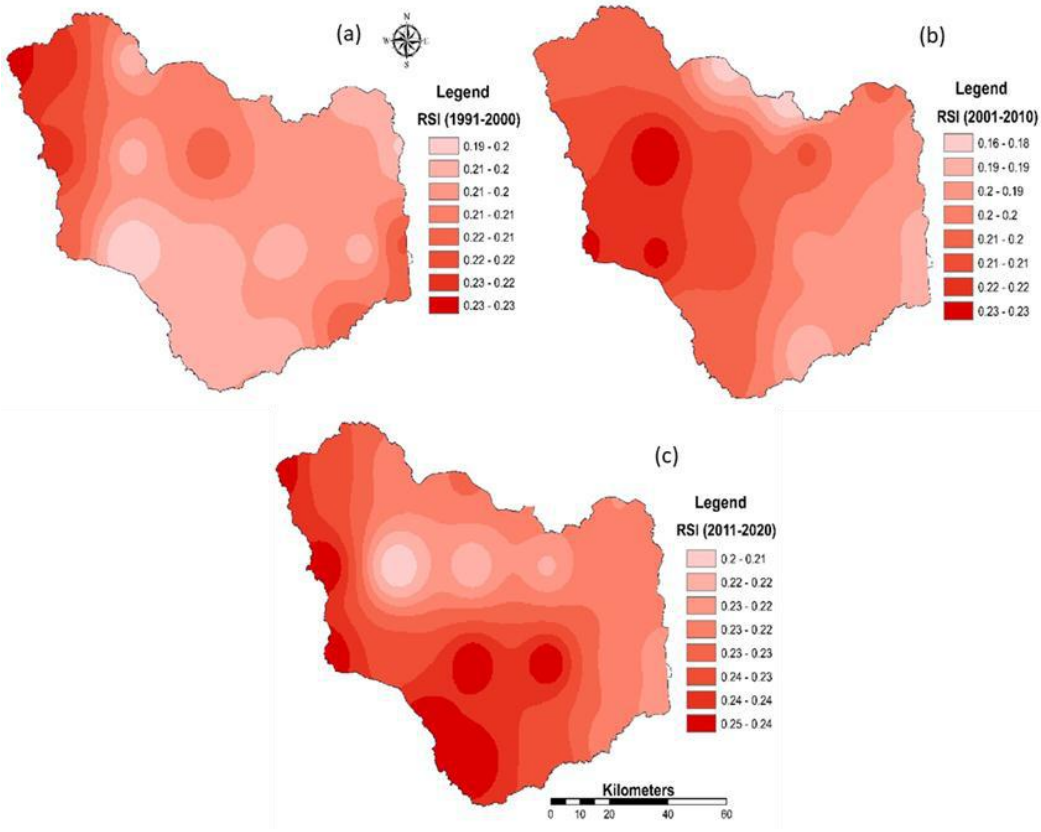

Fig .5: RSI decadal average (a) 1st decade, (b) 2nd decade, (c) 3rd decade

In terms of spatiotemporal variation, the RAI analysis indicated that the years from 2008 to 2014 were characterized by extreme drought conditions, while the period from 1996 to 2001 experienced extreme wet conditions for the basin (Fig 6: Basin). Specifically, S1, S3, S5, and S8 recorded a continuous period of extreme wet conditions from 1997 to 2003. The initial years were predominantly classified as drought years at stations S1, S2, S3, S4, S5, S7, S13, S14, S15, S16, S18, S19, and S20 (Fig 6).

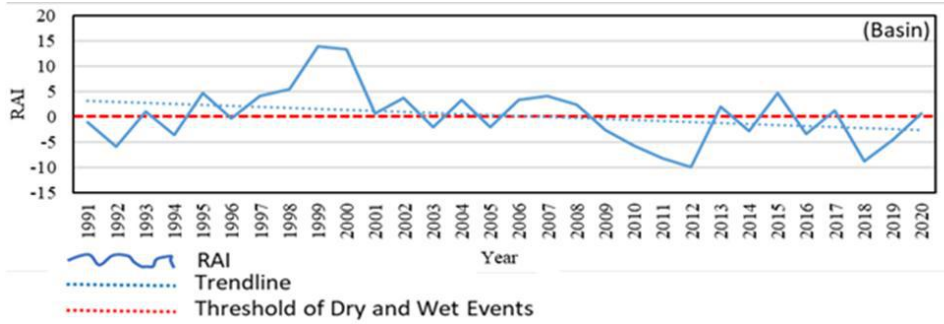

Fig. 6: RAI of individual stations

Table 5: Rainfall anomaly and drought status

Station	Class description (RAI) & years in percentage									Drought year (%)
	Extremely Wet	Very Wet	Moderately Wet	Slightly Wet	Near Normal	Slightly Dry	Moderately Dry	Very Dry	Extremely Dry	
	>3.00	2.00 to 2.99	1.00 to 1.99	0.50 to 0.99	0.49 to -0.49	-0.50 to -0.99	-1.00 to -1.99	-2.00 to -2.99	<-3.00	
Basin	6.67	16.67	13.33	6.67	13.33	3.33	20.00	3.33	16.67	46.67
S1	13.33	6.67	13.33	13.33	0.00	13.33	13.33	13.33	13.33	53.33
S2	10.00	13.33	6.67	6.67	10.00	10.00	20.00	6.67	16.67	60.00
S3	13.33	6.67	20.00	6.67	6.67	0.00	16.67	10.00	20.00	53.33
S4	16.67	0.00	16.67	20.00	3.33	0.00	13.33	13.33	16.67	46.67
S5	13.33	13.33	16.67	10.00	3.33	10.00	10.00	6.67	16.67	46.67
S6	16.67	10.00	6.67	6.67	20.00	6.67	6.67	6.67	20.00	46.67
S7	13.33	0.00	10.00	23.33	0.00	3.33	20.00	16.67	13.33	53.33
S8	10.00	10.00	13.33	10.00	3.33	3.33	16.67	20.00	13.33	56.67
S9	13.33	6.67	3.33	10.00	20.00	10.00	3.33	23.33	10.00	56.67
S10	16.67	10.00	10.00	6.67	16.67	10.00	10.00	6.67	13.33	46.67
S11	16.67	6.67	16.67	10.00	10.00	3.33	20.00	3.33	13.33	50.00
S12	13.33	10.00	16.67	16.67	3.33	0.00	23.33	3.33	13.33	40.00
S13	10.00	6.67	10.00	10.00	13.33	3.33	13.33	16.67	16.67	56.67
S14	10.00	6.67	10.00	10.00	13.33	10.00	10.00	13.33	16.67	50.00
S15	13.33	10.00	16.67	0.00	0.00	20.00	16.67	10.00	13.33	60.00
S16	10.00	6.67	16.67	3.33	26.67	0.00	13.33	10.00	13.33	53.33
S17	13.33	10.00	20.00	6.67	6.67	6.67	20.00	3.33	13.33	50.00
S18	13.33	6.67	16.67	6.67	20.00	3.33	3.33	13.33	16.67	50.00
S19	10.00	3.33	13.33	0.00	23.33	3.33	13.33	20.00	13.33	53.33
S20	13.33	13.33	10.00	6.67	10.00	6.67	16.67	10.00	13.33	53.33
S21	13.33	6.67	13.33	13.33	16.67	6.67	13.33	6.67	10.00	46.67
S22	10.00	6.67	23.33	3.33	13.33	13.33	20.00	0.00	10.00	46.67
S23	10.00	13.33	20.00	10.00	6.66	10.00	6.66	6.66	16.67	40.00

Conclusion

The study was aimed at analyzing the spatiotemporal characteristics of rainfall in the Mayurakshi basin. The findings of long-term rainfall revealed that the upper and middle regions of the basin received the highest rainfall concentrations, ranging from 1500 to 1700 mm, where the maximum and minimum rainfall were recorded as 1717.37 mm and 1172.51 mm, respectively, with a mean annual rainfall of 1398.21 ± 139.95 mm. The upper and

middle areas consistently experienced a significant concentration of rainfall over the long term, while the lower parts of the basin exhibited lower rainfall levels. Statistical analysis, including Kendall's Z test (-1.67), normalized Kendall's tau (-0.218), and Sen's slope value (-10.40), indicated a decreasing trend in rainfall within the basin. Decadal rainfall patterns also indicated a declining nature of rainfall across the basin. To assess the homogeneity and identify the change point of rainfall, statistical tests such as Pettitt's test, the SNHT test, and Buishand's test were employed. The results revealed that the change point occurred in 2008. The Rainfall Anomaly Index (RAI) computed the temporal characteristics of rainfall that were classified as extremely wet (6.67% of the years), very wet (16.67%), moderately wet (13.33%), slightly wet (6.67%), slightly dry (3.33%), and extremely dry (16.67%) across the basin. As previous studies stated, the region is facing an inter-regional imbalance in agricultural development, and the region depends on rainfall for a mono-crop cultivation system. Thus, this rainfall trends its nature (RSI, RAI), and micro-level information obtained from this study will provide valuable insights for crop selection and water resource planning. These findings will aid planners and scientists in crop intensity development, the measures of diverse agricultural indices with emphasis on eradicating regional imbalance in crop management and regional planning to ensure efficient water resource utilization in the basin.

Acknowledgement: The authors would like to thank the Head of the department, Department of Geography and RM, Mizoram University for providing facilities to carry out the present research.

Funding: The authors declare that no funds, grants, or other support were received during the preparation of this manuscript.

Data availability statement: Data will be made available from the corresponding author on reasonable request.

References

1. Ahmad, A., Tang, D., Wang, T. F., Wang, M., & Wagan, B. (2014). Precipitation Trends over Time Using Mann-Kendall and Spearman's rho Tests in Swat River Basin, Pakistan. *Hindawi Publishing Corporation Advances in Meteorology*, 1-16. doi:http://dx.doi.org/10.1155/2015/431860
2. Alexandersson, H. (1986). A Homogeneity Test Applied to Precipitation Data. *Journal of Climatology, 6*(6), 661-675. doi:https://doi.org/10.1002/joc.3370060607.
3. Bera,B., Shit, P.K., Sengupta, N., Saha, S., Bhattacharjee, S. (2021). Trends and variability of drought in the extended part of Chhota Nagpur plateau (Singbhum Protocontinent), India applying SPI and SPEI indices. *Environmental Challenges*.1-10. https://doi.org/10.1016/j.envc.2021.100310
4. Bryson, C., Richard, E., & Adrian, W. (2012). Trend estimation and change point detection in individual climatic series using flexible regression methods. (Vol. 117:D16106.). *J Geophys Res.* doi:doi:10.1029/2011JD017077

5. Buishand, T. (1984). Test for Detecting a Shift in the Mean of Hydrological Time Series (Vol. 73). *Journal of Hydrology.* doi:https://doi.org/10.1016/0022-1694(84)90032-5
6. Chargui, S., Jaberi, A., Cudennec, C., Lachaal, F., Calvez, R., & Slimani, M. (2018). Statistical detection and no-detection of rainfall change trends and breaks in semiarid Tunisia— 50+ years over the Merguellil agro-hydro-climatic reference basin. *Arabian Journal of Geosciences*, 1-14. doi:https://doi.org/10.1007/s12517-018-4001-9
7. Chakraborty, s., Ghosh, S. (2016). Regional Disparity in The Perspective Of Agricultural Development – A Spatio-Temporal Analysis, Ajay-Mayurakshi Interfluve, Birbhum District, West Bengal, India*. IOSR Journal of Economics and Finance.* 43-50
8. Das, J., Mandal, T., Rahman, A. S., & Saha, P. (2021). Spatio-temporal characterization of rainfall in Bangladesh: an innovative trend and discrete wavelet transformation approaches. *Theoretical and Applied Climatology*. doi:https://doi.org/10.1007/s00704-020-03508-6
9. Fischer, T., Gemmer, M., Liu, L., & Su, B. (2012). Change-points in climate extremes in the Zhujiang River basin, South China, 1961–2007. *Climatic Change, 110*, 783–799. doi:https://doi.org/10.1007/s10584-011-0123-8
10. Gajbhiye, S., Meshram, C., Singh, S. K., Srivastava, P. K., & Islam, T. (2015). Precipitation trend analysis of Sindh River basin, India, from 102-year record (1901–2002). *Atmospheric Science Letters, 17*(1), 71-77.
11. Ghosh, S., Sarkar, B., Islam, A., & Shit, P. K. (2022). Assessing the Suitability of Surface Water and Groundwater for Irrigation Based on Hydro-chemical Analysis: A Study of the Mayurakshi River Basin, India. *Air, Soil & Water Research*, *15*.
12. Hamed, K. H., & Rao, A. R. (1998). A modified Mann-Kendall trend test for autocorrelated data. *Journal of Hydrology, 204*(1-14), 182-196. doi: https://doi.org/10.1016/S0022-1694(97)00125-X
13. Hirsch, R. M., Slack, J. R., & Smith , R. A. (1982). Techniques of trend analysis for monthly water quality data. *Water Resources Research, 18*(1), 107-121. doi: https://doi.org/10.1029/WR018i001p00107
14. Islam, A., Barman, S. D., Islam, M., & Ghosh, S. (2020). Role of human interventions in the evolution of forms and processes in the Mayurakshi River Basin. *Anthropogeomorphology of Bhagirathi-Hooghly river system in India*, pp. 135-187. https://doi.org/10.1201/9781003032373
15. Karmeshu, N. (2012). Trend Detection in Annual Temperature and Precipitation using the Mann Kendall Test—A Case Study to Assess Climate Change on Select States in the Northeastern United States. *Master of Environment Studies Capstone project, University of Pennsylvania USA*. Retrieved from http://repository.upenn.edu/mes_capstones/47
16. Kamal, N., & Pachauri, S. (2019). *Mann-Kendall, and Sen's Slope estimators for precipitation trend analysis in north-eastern states of India* (Vol. 177). International Journal of Computer Applications.
17. Ndione, D. M., Sambou, S., Sane, M. L., Kane, S., Leye, I., Tamba, S., & Cisse, M. T. (2017). *Statistical Analysis for Assessing Randomness, Shift and Trend in Rainfall Time*

Series under Climate Variability and Change: Case of Senegal (Vol. 5). Journal of Geoscience and Environment Protection. doi:DOI: 10.4236/gep.2017.513003

18. Pal, S. (2016). Impact of Massanjore Dam on hydro-geomorphological modification of Mayurakshi River, Eastern India. *Environ Dev Sustain, 18*, 921-944. doi:DOI 10.1007/s10668-015-9679-1
19. Pal, S. (2017). Impact of Tilpara barrage on backwater reachof Kushkarni River: a tributary of Mayurakshi River, *Environ Dev Sustain,* 19:2115–2142 *DOI 10.1007/s10668-016-9833-4*
20. Pettitt, A. N. (1997). A Non-Parametric Approach to the Change-Point Problem. *Journal of the Royal Statistical Society. Series C (Applied Statistics), 28*(2), 126-135. . doi:https://doi.org/10.2307/2346729
21. Sarkar, T.K., Ambade, B., Mahato, D.K., Kumar, A., Jangde, R. (2023). Anthropogenic fine aerosol and black carbon distribution over urban environment. Umm Alqura University.472-480.
22. Sen, P. (1968). *Estimates of the regression coefficient based on Kendall's tau* (Vol. 63). Journal of the American Statistical Association.
23. Srivastava, P. K., Han, D., Rico-Ramirez, M. A., & Islam, T. (2014). Sensitivity and uncertainty analysis of mesoscale model downscaled hydro-meteorological variables for discharge prediction. *Hydrological Processes, 28*, pp. 4419–4432.
24. Van-rooy, M. (1965). A Rainfall Anomaly Index (RAI), Independent of the Time and Space. *Notos, 14*, 43-48.
25. Walsh, R., & Lawle, D. (1998). RAINFALL SEASONALITY: DESCRIPTION, SPATIAL PATTERNS AND CHANGE THROUGH TIME. *Department of Geography, University College of Swansea, Department of Geography, University of Birmingham*, 201-208.

The Indian Geographical Journal
Volume 98 (2) December - 2023, pp 176-190
ISSN 0019-4824

HYDROCHEMICAL CHARACTERISTICS OF GROUNDWATER AND MULTIVARIATE STATISTICAL ANALYSIS ALONG THE COASTAL REGIONS OF PONNERI AND TIRUVOTRIYUR TALUKS OF THIRUVALLUR DISTRICT, TAMIL NADU

Ravikumar P[1]., Chandrasekar V[2]., Imrana Banu R[2]., Shaik Mahamad[1]., and Bhaskaran G[3].

[1] Department of Geography, Presidency College (A), Chennai
[2] Department of Geography, Government Arts College for Women, Nilakottai, Dindigul
[3] Department of Geography, University of Madras, Guindy, Chennai

Corresponding author mail id: ravikumarpalaniswamy@gmail.com

Abstract

Groundwater depletion in the Ponneri and Tiruvotriyur coastal regions is worsening due to population growth, urbanization, and industrialization, notably by Ennore Port and Thermal Power Plant. This study is carried out by collecting 37 groundwater samples from open and bore wells during pre-monsoon and post-monsoon seasons indicating high levels of EC, pH, TDS, Na+, and Cl-, rendering 51% of wells are unfit for drinking, and has adversely impacted agricultural production. The multivariate statistical analysis in R has confirmed the saltwater intrusion. The spatial distribution of major ions of groundwater samples are clearly shows the flow of ground water from Southeast to West and Northwest.

Keywords: Groundwater, Coastal Area, GIS, R Language, and Statistical Analysis

Introduction

In India, there has been a significant upsurge in the demand for groundwater, propelled by rapid population growth, intensified industrialization, and urbanization (Prasad B., et.al 2021). Groundwater is the primary water source for drinking, agriculture, and industry, particularly in arid and semi-arid regions. (N Adimalla et al., 2020). Only 0.3% of the world's freshwater is readily available on the surface, such as in rivers, lakes, and reservoirs, while groundwater constitutes 30% of the freshwater reserve (Nitasha Khatri et al., 2014). It is crucial to recognize that nearly 44% of the global population resides within 150 kilometers of coastlines (Atlas, 2010), placing significant pressure on coastal aquifer systems, which are vital resources for human needs (Bachaer Ayed, 2018). Recent research indicates that approximately 69% of total groundwater withdrawals are linked to agricultural activities, 22% to industrial usage, 8% to domestic consumption, and 1% to recreational purposes (Rosegrant et al., 2009). Groundwater contamination primarily stems from wastewater discharge, notably from industries, as well as effluents from human settlements, improper hazardous waste disposal, and pollution from agricultural areas and roads (Ivana Ilić, 2021., Chandrasekar V et al., 2017., Shanmugasundharam et al., 2015).

Groundwater stands as a valuable natural asset, with environmental challenges varying based on geological, hydrological, climatic conditions, and geochemical factors unique to each region.

Water quality degradation can be broadly categorized into two types: those resulting from natural conditions and those stemming from human activities. (Nitasha Khatri, 2014). The extraction or alteration of recharge patterns can modify groundwater flow directions or expose aquifer materials to air, potentially leading to the encounter of clean water with natural contaminants such as radium, salt, arsenic, and fluoride, thereby affecting water quality and causing associated health concerns. Furthermore, chemical and biological contaminants originating from industrial and agricultural sources further deteriorate water quality (Abhay Kumar Soni, 2019).

All groundwater contains minerals dissolved in solution, with the type and concentration of these minerals depend on various factors, such as surface and subsurface environment, groundwater flow rates, and the groundwater source (Jasechko, S, 2024). When precipitation interacts with different soil constituents, it is relatively mineral-free. However, due to water's solvent properties, minerals dissolve and become part of the groundwater as it percolates through the aquifer (Venkateswaran, 2015). The concentrations of cations and anions in groundwater rely on the solubility of minerals in geological formations, the duration of contact with rocks, and the level of dissolved CO2 in the water (Ali, M., et.al, 2022). Chemical alterations in groundwater are influenced by various factors, including interactions with solid phases, groundwater residence time, mixing with saline water pockets, and anthropogenic influences (Stallard, 1983). The quality of groundwater quality is also affected by seawater intrusion in coastal areas which is a natural process. However human exploitation of coastal aquifers exacerbates the issue (Prusty, P et.al., 2020). Besides natural salinity, anthropogenic activities significantly contribute to the deterioration of water quality (Egun, 2010). Therefore, the study aims to assess the quality of coastal groundwater and the spatial distribution of various hydrogeochemical parameters to determine the suitability of groundwater resources in Ponneri and Thiruvottriyur taluk in Northern Coast of Tamil Nadu, which is densely populated and heavily rely on groundwater for domestic and agricultural purposes.

Study Area

Ponneri taluk is situated in the Tiruvallur district of the Indian state of Tamil Nadu, which covers an area of 674 sq.km (Figure 1a). With an average elevation of 16 meters (52 feet), Ponneri serves as the administrative centre of the taluk. As per the 2011 census, Ponneri taluk had a population of 3,85,620, comprising 1,93,043 males and 1,92,577 females (Census of India, 2011). Tiruvottiyur is a small coastal taluk esplanade nestled along the Bay of Bengal coast. Historically, sea encroachment posed significant challenges for local fishermen until the construction of groynes commenced in 2004. Spanning over 4 kilometres, these groynes vary in length from 165 to 300 meters each and stand at a height of four meters above mean sea level. Over time, several acres have been reclaimed with the formation of a beach, aligning with earlier predictions.

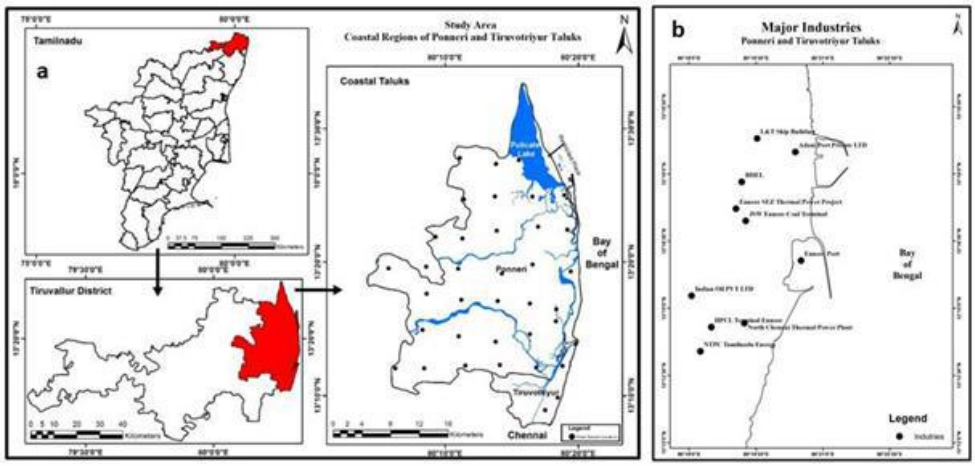

Figure 1. Study area and industries of Ponneri and Tiruvottiyur taluks

Methodology

Groundwater samples were collected from a total of 37 locations, including 23 open wells and 14 bore wells, across the coastal regions as detailed in Table 1, for both the Pre-Monsoon (July) and Post-Monsoon (January) periods in 2023. Approximately 43% of the sample points are located near the shoreline, within a distance of 5 – 7 kilometers. The sampling process followed a systematic grid pattern with defined intervals, as outlined by, A. Shanmugasundharam (2015), and Chandrasekar V (2017). To maintain sample integrity, water samples were collected in plastic bottles that were pre-cleaned with 1 N hydrochloric acid and rinsed 3–4 times with distilled water. Standard methods recommended by the American Public Health Association (APHA, 1999) were employed for water analysis, ensuring consistency and reliability in examining both water and wastewater samples.

The spatial distribution of chemical parameters is depicted in the accompanying images. The primary data was collected at intervals of every five kilometers. The legend accompanying the images comprises five classes: Very Low, Low, Medium, High, and Very High. The Low-level class corresponds to the "Acceptance Limit," while the medium class corresponds to the "Permissible Limit," as defined by the Bureau of Indian Standards (2012). The spatial distribution of groundwater quality has been analyzed for selected parameters such as Ca^{2+}, Na^{+}, Mg^{2+}, Cl^{-}, TDS, EC, pH, and K^{-}. and for multivariate analysis EC (µs/cm), pH, TDS, Ca^{2+}, Mg^{2+}, Na^{+}, K^{+}, Cl^{-}, $SO4^{2-}$, $NO3^{-}$, F parameters were used.

Field measurements of EC and pH were recrded using a calibrated thermometer with a resolution of 0.1 and an Elico portable water quality analyser, respectively. Total dissolved solids (TDS) were determined by multiplying the electrical conductivity (EC) by a factor of 0.64. Total hardness (TH) as CaCO3 and calcium (Ca^{2+}) were analyzed titrimetrically using standard Ethylene Diamine Tetraacetic Acid (EDTA) method. Magnesium (Mg^{2+}) content was calculated by subtracting the calcium (Ca^{2+}) concentration from the total hardness (TH). Chloride (Cl^{-}) levels were determined by silver nitrate ($AgNO_3$) titration.

Table 1. List of Villages (Sample collection site)

S.No	Village	S.No	Village
1	Annaimalaicherry	20	Kodipalam
2	Arasur	21	Kodur
3	Attipattu Pudu Nagar	22	Kuruviagaram
4	Attur	23	New Manali Town
5	Chellappa Nagar	24	Orukaddu
6	Edapalayam	25	Pazhaverkadu
7	Ennore Burma Nagar	26	Penchetty
8	Gounderpalayam	27	Pudupet
9	Illupakkam	28	Puduvoyal
10	Indira Gandhi Colony	29	Telugu Colony
11	Jyothi Nagar	30	Thathaimanji
12	Kadapakkam	31	Thirupallivanam
13	Kalanji	32	Thiruvellavoyal
14	Kaniyambakkam	33	Ooplibedu
15	Kumanoor	34	Vanichatram
16	Karumariamman Nagar	35	Vepathoor
17	Kattavur	36	Vettukuppam
18	Kesvapuram	37	Vichoor
19	Kilmuldalaibedu		

The sodium (Na^+) and potassium (K^+) content in groundwater were estimated using an EEL flame photometer equipped with a proper Air-LPG flame, with sodium and potassium sulphate standards of appropriate concentrations being utilized. All parameters are expressed in milligrams per liter (mg/l), except for pH (no units) and electrical conductivity (EC) is reported in microsiemens per centimeter (µS/cm) at 25°C.

GIS Modelling

GIS has emerged as a potent tool for generating spatial distribution maps, offering insights into the variation in concentrations of various chemical parameters. These maps were prepared using the inverse distance weighted (IDW) raster interpolation technique within the spatial analyst module of ArcGIS (Shanmugasundharam, 2015; Chandrasekar V, 2017). The accuracy of results obtained through IDW interpolation is contingent upon the density and distribution of the sampling points relative to the local variations being modelled. Sparse or uneven sampling may compromise the fidelity of the results, failing to adequately capture the desired surface characteristics.

In the inverse distance weighted (IDW) interpolation method, the predicted value Zp at location $S0$ is calculated using the formula

$$Zp = \sum_{i=1}^{n} \left(\frac{Zi}{dip}\right) / \sum_{i=1}^{n} \left(\frac{1}{dip}\right)$$

Where, n represents the number of measured sample points surrounding the prediction location that is used in the prediction, zi denotes the observed value at location

, and dip signifies the distance between the prediction location $S0$ and the measured sample location Si. The weights assigned to each measured point are inversely proportional to the distance, meaning closer points have more influence on the predicted value. Among several interpolation techniques compared in this study, IDW with a squared distance term yielded more consistent results. Consequently, spatial distribution maps were generated for selected water quality parameters, including pH, TDS, TH, total alkalinity, chloride, nitrates, fluoride, Ca^{2+}, $Mg^{2+,}$ and Water Quality Index (WQI) (D. Janardhana Rao, 2016).

Multivariate Statistical Analysis and Graphical Representation

Various statistical methods and graphs were employed to substantiate the deterioration of groundwater quality. Piper trilinear plots was utilized for hydro-chemical classification. Hierarchical Cluster Analysis (HCA) assessed water chemical profiles, ensuring data accuracy and identifying correlations. A correlation matrix computed R-values, indicating the degree of linear association between parameters. R ranges from -1 to +1, with +1 or close indicating a strong positive correlation, and -1 or close revealing a strong negative correlation, highlighting interrelated parameters influencing water quality in the area. The Gibb's ratio methodology is a hydrogeochemical technique used to assess water composition and understand the processes impacting aquifer systems. It involves calculating ratios of major ions like Na^+/K^+, Na^+/Cl^-, and Ca^{2+}. These ratios help identify dominant processes such as evaporation, rock-water interaction, or precipitation affecting water chemistry. By comparing these ratios with theoretical values associated with specific hydro geochemical processes.

Result and Discussion

The physicochemical parameters of groundwater samples were analyzed, and the descriptive statistics of the analyzed parameters are presented in Table 2. These results are compared with the standard values set by the World Health Organization and the Bureau of Indian Standards (BIS).

Table 2. Comparison of analytical results with international and national standards

Parameters	Post-Monsoon		Pre-Monsoon		Mean		WHO Guidelines (2004)	BIS Guidelines (2012)
	Max	Min	Max	Min	Post-Monsoon	Pre-Monsoon		
EC (µs/cm)	8370	400	7790	490	2584.32	2546.41	1500	-
pH	7.3	5.8	7.8	5.8	6.81	6.97	6.5 -8.5	6.5 – 8.5
TDS	4191	212	4340	250	1417.54	1440.88	1500	500 – 2000
Ca	384	34	460	32	129.02	128.14	200	75 – 200
Mg	316	19	233	10	63.27	68.46	150	-
Na	1051	12	807	12	314.45	296.93	200	200 – 400
K	227	0	74	0	20.05	20.87	12	-
Cl	2233	46	2233	67	509.86	539.31	600	250
SO_4	668	14	1094	7	153.73	163.97	250	200 – 400
NO_3	256	0	549	0	43.51	57.69	-	45
F	1.7	0	1.1	0.01	0.36	0.41	1.5	1.0 – 1.5

pH

The data presented in Table No. 2 illustrates that the pH of groundwater ranged from 5.8 to 7.3 during the post-monsoon period, with an average value of 6.81, indicating nearly neutral conditions. In the pre-monsoon period, pH values ranged from 5.8 to 7.8, with a mean value of 6.97, also indicating neutral conditions in the coastal regions. The lowest post-monsoon pH values were recorded in Vanichatram and Attur villages with 5.8 and 6.2, respectively, indicating acidity. Vepathoor recorded the highest post-monsoon, pH level at 7.3. Approximately, 94.5% of water samples fall within the permissible pH range for drinking, according to BIS 2012, which is 6.5–8.5 (IS: 10500-1991). Most of the samples fall within this range. Similarly, during the pre-monsoon period, Vanichatram village recorded the lowest pH level at 5.8, while Pazhaverkadu recorded the highest pH level at 7.8. Only one sample (Pazhaverkadu) in the northern part exhibited moderately alkaline water, while three samples with an acidic nature were found in the southwestern part of the study area (Figure 2a).

Electrical Conductivity

In the post-monsoon period, the electrical conductivity ranged from 400 to 8370 µS/cm, with an average value of 2584.32 µS/cm (Table 2). The lowest recorded value was observed in Attur village, situated in the western part of the study area. It's worth noting that this village is located above the Cholavaram Tanks. Due to this, water contamination is very low and the aquifer is quickly recharged. In the study area, during the post-monsoon period, the highest electrical conductivity (EC) levels were observed in the eastern and southeastern parts. Karumariamman Nagar recorded the highest EC level at 8370 µS/cm, situated adjacent to the industrial area. This region experiences significant water extraction activities, especially due to the presence of Ennore port and North Chennai Thermal Power station, impacting both the region and the livelihoods of many farmers and anglers (Figure 2b). Approximately, 30% of the water samples exceeded the permissible limit (above 3000 µS/cm) and are deemed unfit for drinking. Only 16% of the study area exhibited EC levels below the acceptance limit, including Puduvoyal, Vanichatram, and Kilmuldalaibedu. These villages are situated away from coastal and industrial regions and are surrounded by numerous tanks. In the pre-monsoon period, Attur village recorded a low EC level of 490 µS/cm, while Karumariamman Nagar recorded 7790 µS/cm. Around 30% of the samples exhibited high EC levels near Ennore Port and Thermal Station, affecting the southern and eastern parts of the study area. Groundwater near these regions is highly contaminated, resembling saltwater, with many wells showing yellowish water. Agricultural production has been significantly impacted due to water contamination. The spatial distribution of EC values depicted in Figure 3 indicates an increase from east to west, implying the direction of flow. The significant variations in EC are primarily attributed to anthropogenic activities and prevailing geochemical processes in the region. EC typically increases along groundwater flow paths due to the combined effects of evaporation, ion exchange, and topographic conditions

Total Dissolved Solids

In the post-monsoon period, the TDS levels ranged from 212 to 4191 mg/l (Table 2). The lowest recorded value was observed in Attur Village, situated in the western part of the study area. This village is positioned above the Cholavaram Tanks, resulting in significant water contamination but rapid aquifer recharge. The highest TDS levels were recorded in the eastern and southeastern parts of the study area, with Karumariamman Nagar registering the highest TDS level at 4191 mg/l (Figure 2c),and this village is located adjacent to the industrial area (Figure.1b). In the pre-monsoon period, data collected in July indicated higher water contamination levels compared to the post-monsoon period. The TDS levels during pre-monsoon ranged from 250 to 4340 mg/l. Attur village exhibited the lowest TDS levels at 250 mg/l, while Karumariamman Nagar recorded the highest TDS level at 4340 mg/l. Approximately, 21.6% of the samples exhibited high TDS levels near Ennore Port and Thermal Station, highlight the significant impact of industrial activities and geomorphological settings on groundwater quality

Calcium

In the post-monsoon season, calcium concentration levels ranged between 34 and 384 mg/l. The lowest calcium concentration was recorded in Puduvoyal and Attur villages, located in the western part of the study area (Figure 2d). Cholavaram tanks situated below Attur village contribute to the natural recharge of aquifers, thereby reducing contamination levels. The highest Ca^{2+} level was observed in the central and eastern parts of the study area. During the pre-monsoon season, calcium levels ranged from 32 to 460 mg/l. Puduvoyal village exhibited the lowest Ca^{2+} level at 32 mg/l, while Karumariamman Nagar recorded the highest Ca^{2+} level at 460 mg/l. Approximately, 16% of the samples collected near Ennore Port and Thermal Station showed high Ca^{2+} levels, indicating saline groundwater. The significant calcium levels near Ennore Port and Thermal Station indicate localized saline groundwater contamination, emphasizing the need for targeted monitoring and remediation efforts.

Magnesium

In the post-monsoon season, Mg^{2+} levels ranged from 19 to 316 mg/l. The lowest magnesium level was recorded in Attur village, situated in the southwestern part of the study area. The highest Mg^{2+} level was observed in the eastern part of the study area, specifically in Karumariamman Nagar at 316 mg/l, attributed to high water extraction activities (Figure 3a). Only 3 samples exceeded the permissible limit, rendering them unfit for drinking. During the pre-monsoon season, magnesium levels ranged from 10 to 233 mg/l. Attur village displayed the lowest Mg^{2+} level at 10 mg/l, while the highest magnesium level was found in New Manali Town at 233 mg/l. indicate the impact of high-water extraction activities and industrial influences on groundwater quality. The presence of elevated magnesium levels in specific areas underscores the need for targeted water management and monitoring strategies to ensure safe drinking water.

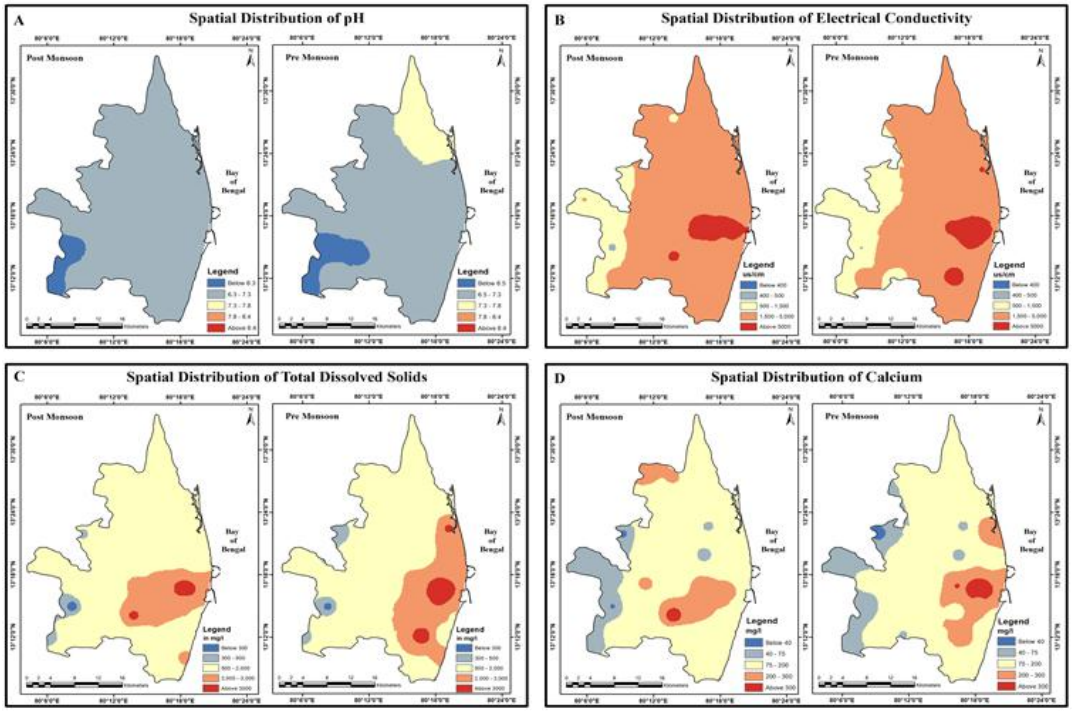

Figure 2. Spatial Distribution of Water Quality Parameters (pH, EC, TDS, Ca2+)

Sodium

In the post-monsoon season Figure 3b, the Na+ levels ranged from 12 to 1051 mg/l (Table 2). The lowest recorded Na+ value was observed in Attur Village, situated above the Cholavaram Tanks in the southwestern part of the study area. Conversely, the highest Na+ level was observed across various parts of the study area, with Karumariamman Nagar recording the highest Na+ level at 1051 mg/l. This village is adjacent to the industrial area, rendering it susceptible to high contamination levels. Approximately, 70% of water samples exceeded permissible limits, rendering them unfit for drinking according to World Health Organization standards (WHO, 2004). During the pre-monsoon season, data collected in July revealed sodium (Na+) levels ranging from 32 to 807 mg/l. Attur village exhibited the lowest sodium level at 32 mg/l, while Karumariamman Nagar recorded the highest level at 807 mg/l. Approximately, 46% of the samples exhibited high Na+ levels, primarily concentrated near the Ennore Port and Thermal Station.

Potassium

In the post-monsoon season, the K+ levels ranged from 0 to 227 mg/l (Table 2). The lowest values were recorded in 21 villages, primarily located in the southern part of the study area. The villages with low potassium levels are situated in the western region, characterized by lesser water contamination and abundant lakes and tanks, leading to rapid aquifer recharge. The highest K+ levels were observed in the eastern part of the study area

(Figure 3c). Pudupet recorded the highest potassium level at 227 mg/l, while Vichoor recorded 203 mg/l. These villages are located adjacent to industrial areas, where water extraction rates are notably high. Approximately 32% of water samples exceeded permissible limits, rendering them unsuitable for drinking. Comparatively, water contamination levels were higher during the pre-monsoon period. During the pre-monsoon season, potassium levels ranged from 0 to 74 mg/l. Seven villages and Kadapakkam exhibited low potassium levels, with Kadapakkam recording 74 mg/l. The presence of high potassium levels exceeding permissible limits in 32% of samples indicates an urgent need for enhanced groundwater management and pollution control measures to protect water resources.

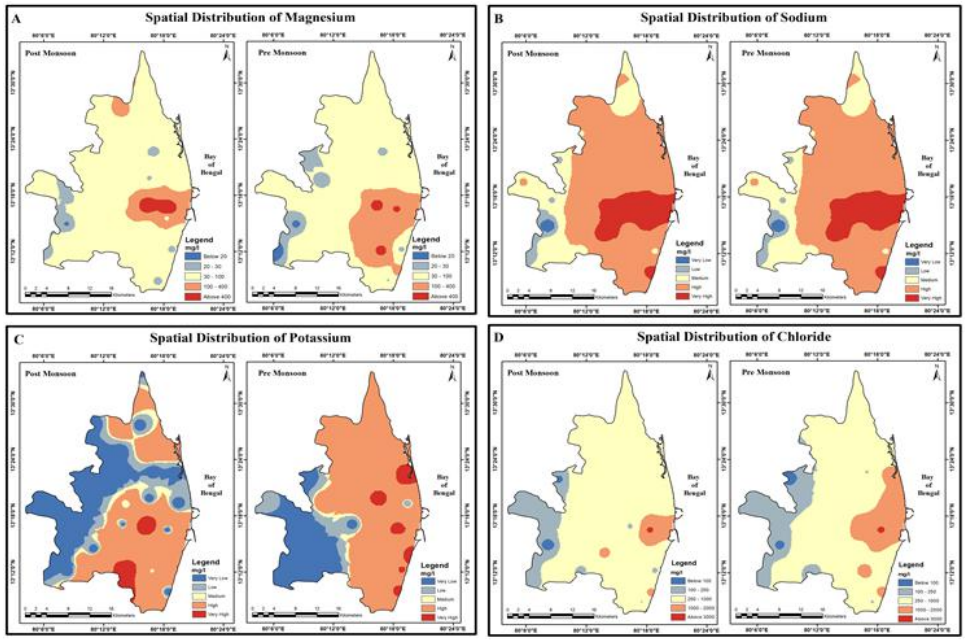

Figure 3. Spatial Distribution of Water Quality Parameters (Mg2+, Na+, K^+, Cl-)

Chloride

In the post monsoon season, the concentration of chloride ranged from 46 to 2233 mg/l. The lowest values of Cl^- concentration were recorded in Attur and Puduvoyal Villages, with 46 and 60 mg/l, respectively. Conversely, the highest Cl^- level was observed in the eastern part of the study area (Figure 3d), with Karumariamman Nagar recording the highest Cl^- level at 2233 mg/l. Data collected during the pre-monsoon period in July, when water contamination levels are comparatively high, revealed Cl^- concentration levels ranging from 67 to 2233 mg/l. Attur village exhibited the lowest Cl^- levels at 67 mg/l, while Karumariamman Nagar recorded the highest Cl^- level at 2233 mg/l. The consistently high chloride levels in Karumariamman Nagar emphasize the critical impact of industrial activities and the necessity for rigorous groundwater monitoring and effective pollution mitigation strategies.

Piper Diagram:

The graphical representation of Piper's diagram (Figure 4) illustrates that the majority of water samples cluster within the Na-Cl field, resembling seawater characteristics, indicating a prevalence of sodium and chloride ions. However, there are a few stations that fall into the mixed Ca-Mg field. This distribution on the Piper diagram underscores those alkalis (Na^+ and K^+) exceed alkaline earth elements (Ca^{2+} and Mg^{2+}), and chloride predominates over other anions in the water samples. This analysis provides valuable insights into the chemical composition and characteristics of the groundwater samples, emphasizing the dominance of specific ions and the prevailing chemical patterns.

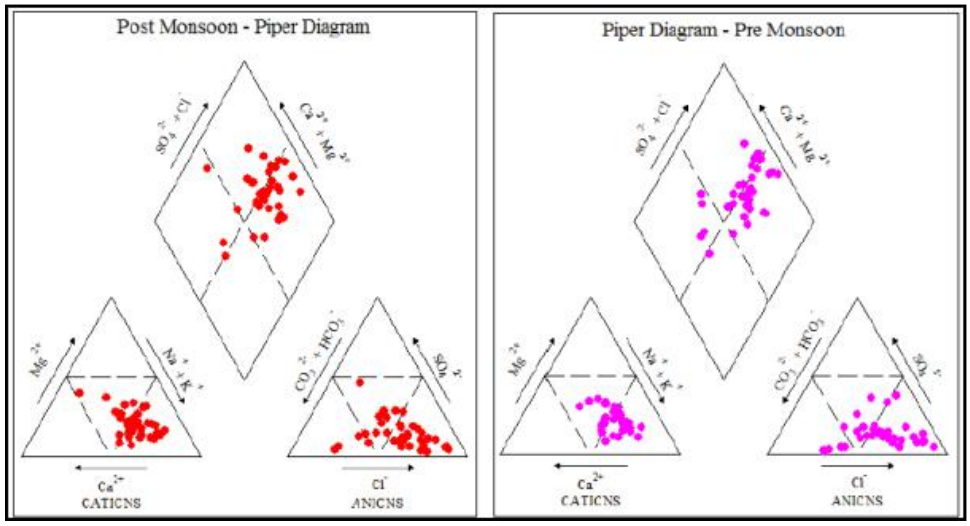

Figure 4. Piper diagram displaying the hydrological facies of the samples

Multivariate Statistical Analysis for the Groundwater

Post-Monsoon Correlation

During the post-monsoon period (Figure 5), a strong positive correlation is observed between EC and TDS, indicating that as EC increases, and TDS levels also tend to rise. This correlation extends to sodium (Na^+), magnesium (Mg^{2+}), and calcium carbonate (CaCO3), suggesting a common origin or shared influence among these elements. Furthermore, strong correlations are noted between Mg-Na, Na-Cl, and Mg-Cl, implying a common source or similar geochemical processes affecting these elements. Moderate correlations are also observed among calcium (Ca^{2+}), bicarbonate ($HCO3^-$), sulphate ($SO4^{2+}$), chloride (Cl^-), and total alkalinity, indicating potential associations or shared origins among these parameters. Conversely, weaker correlations are found with fluoride (F^-), nitrate ($NO3^-$), and potassium (K^+), suggesting less pronounced relationships or diverse sources for these elements. In terms of interdependencies, moderate correlations are observed between Ca-Na, Ca-SO4, Mg-Cl, Cl-Ca, and Cl-Mg, indicating potential interactions or influences among these pairs of elements. However, weaker correlations are

noted between EC-K, EC-F, EC-NO3, Ca-Mg, Ca-K, Ca-NO3, Mg-K, Mg-NO3, Mg-F, Na-K, and K-SO4, suggesting less significant relationships or varying sources for these particular combinations of elements. These weaker correlations may reflect the influence of diverse sources or geochemical processes on these elements during the post-monsoon period.

Pre- Monsoon Correlation

During the pre-monsoon (Figure 5) period, strong positive correlations are observed between EC and TDS with calcium (Ca^{2+}), magnesium (Mg^{2+}), sodium (Na^{+}), chloride (Cl^{-}), and calcium carbonate (CaCO3), indicating that these ions significantly contribute to TDS levels and play crucial roles in water quality. The strong correlations between TDS and major ions such as Na^{+}, Mg^{2+}, Ca^{2+}, Cl^{-}, and $SO4^{2-}$ further suggest their predominant contribution to increased TDS levels. The robust correlations between major ions and both EC and TDS underscore that these ions are primary factors influencing water electrical conductivity and total dissolved solids. Factors contributing to these correlations may include evaporation, rock-water interactions, and silicate weathering processes. Moderate correlations are identified among various ion pairs, including Ca-K, Mg-SO4, Na-K, Na-SO4, K-Na, K-Cl, NO3, and Cl-K. Additionally, moderate correlations are observed between Ca-HCO3, Ca-SO4, Ca-NO3, Mg-K, Mg-HCO3, Mg-NO3, Cl-HCO3, Cl-SO4, Cl-NO3, Na-HCO3, Na-NO3, K-Ca, K-Mg, and K-SO4. Weak correlations are noted between fluoride and various ions, with some values indicating negative correlations, suggesting potential complex interactions. The prevalence of low correlations with $NO3^{-}$ implies diverse influences on this ion, while fluoride exhibits numerous negative correlations with other ions. Overall, the observed correlations highlight the complex interplay among various ions and factors influencing groundwater chemistry during the pre-monsoon period.

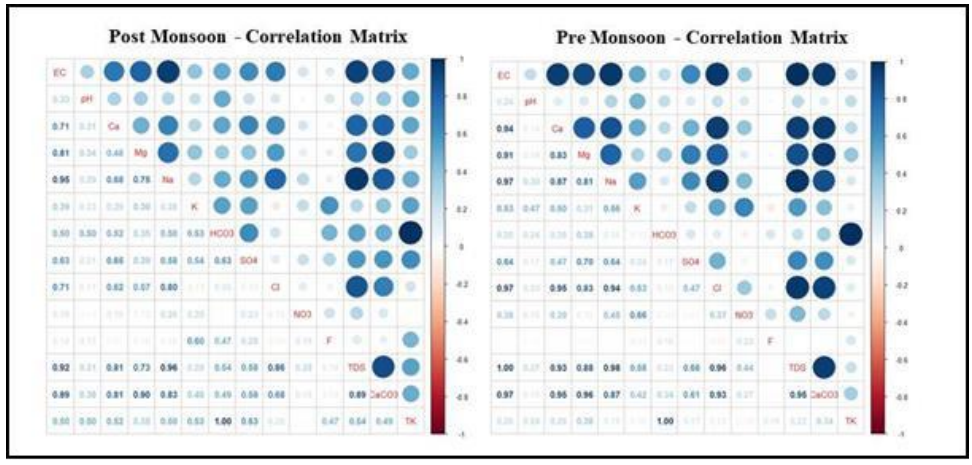

Figure 5. Post and Pre- Monsoon Correlation Matrix

Gibbs Ratio

The Gibbs diagram is commonly employed to validate the connection between water composition and aquifer lithological traits, delineating three distinct fields: evaporation

dominance, rock-water interaction dominance, and precipitation dominance. In post-monsoon (2017), the predominant samples fall in the evaporation dominance and rock water Interaction field of the Gibbs diagram (Figure 6a). The area under rock–water interaction dominance field indicates the interaction between rock chemistry and the chemistry of the percolated waters under the subsurface. In pre-monsoon (2017), figure 6b, the predominant samples fall in the evaporation dominance and Rock water Interaction field of the Gibbs diagram. This plot explains the relationship between water chemistry and aquifer lithology. Such a relationship helps to identify the factors controlling the groundwater chemistry

Gibbs Ratio (I) (For Cations): $(Na^+ + K^+)/(Na^+ + K^+ + Ca^{2+})$ Eq - 1

Gibbs Ratio (II) (For Anions): Cl-/(Cl-+HCO3-) Eq – 2

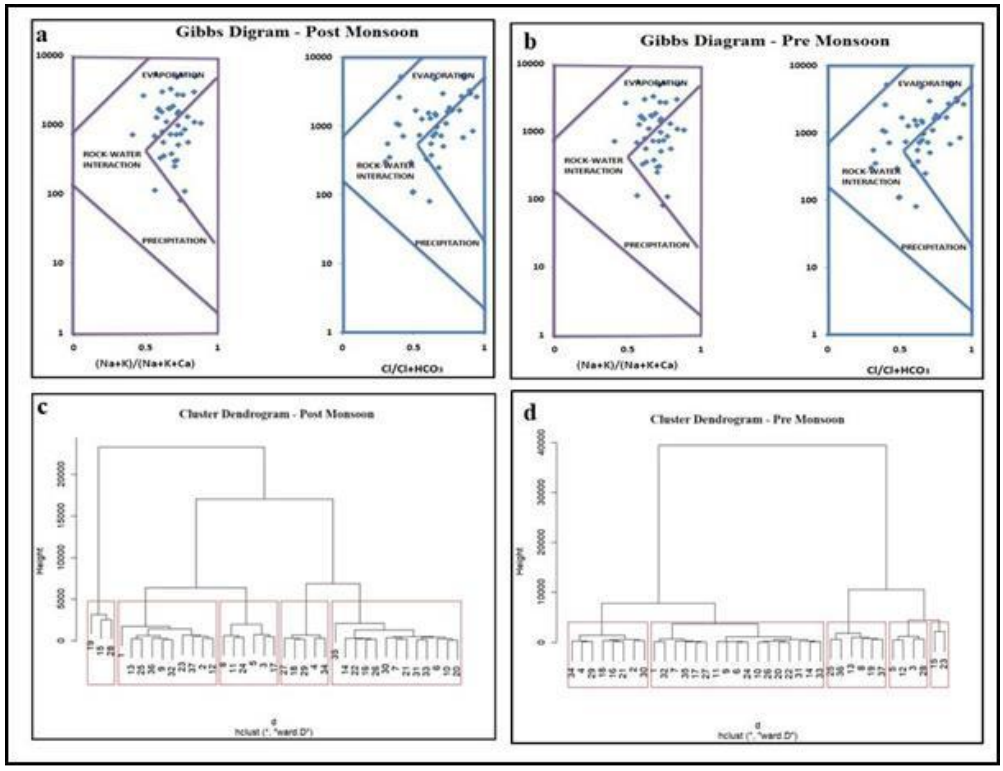

Figure 6. Gibbs Ratio and Cluster Dendrogram of Water Quality

Hierarchical cluster analysis (HCA)

In the current study, cluster analysis has been instrumental in revealing groups of sampled stations sharing similarities, generating a dendrogram using the ward method for both post-monsoon and pre-monsoon periods. In the post-monsoon analysis (Fig. No. 6c), the dendrogram effectively delineates five statistically significant clusters from the 37

sampling stations. The initial cluster encompasses three locations (19, 15, 28), the second cluster comprises samples from 10 locations (13, 25, 36, 9, 32, 23, 37, 2, and 12), the third cluster includes six samples (8, 11, 24, 5, 3, and 17), and the fourth cluster includes five samples (27, 18, 29, 4, and 34), while the remaining samples collectively form the fifth and final cluster with 13 samples. This hierarchical clustering approach enables meaningful categorization of water samples based on their hydrogeochemical characteristics, with differences reflecting variations in morphology and anthropogenic pollution. Notably, sampling sites under clusters 4 and 5, located in commercial and coastal areas, exhibit extensive human activity and water source pollution.

Similarly, in the pre-monsoon analysis (Fig. No. 6d), the hierarchical clustering approach categorizes water samples into distinct groups. The initial cluster encompasses eight locations (34, 4, 29, 18, 16, 21, 2, and 30), the second cluster comprises samples from 17 locations (1, 32, 7, 35, 17, 27, 11, 9, 6, 24, 10, 26, 20, 22, 31, 14, 33), the third cluster includes six samples (25, 36, 13, 8, 19, 37), the fourth cluster includes four samples (5, 12, 3, 28), while the remaining samples collectively form the fifth and final cluster with two samples. Again, sampling sites under clusters 4 and 5, situated in commercial and coastal areas, exhibit significant human activity and water source pollution.

Conclusion

The study highlights significant physicochemical variations in groundwater quality in Ponneri and Tiruvottriyur taluks of Tiruvallur district. Anthropogenic activities, particularly industrialization and urbanization, contribute to elevated pH, electrical conductivity, and total dissolved solids, impacting water suitability. The spatial distribution reveals localized contamination near industrial zones, affecting aquifers and livelihoods. Sodium and potassium levels exceed permissible limits in certain areas, nearly 51% locations are unsuitable for drinking.

The hydrogeochemical analysis of groundwater samples, illustrated through Piper-trilinear plots, multivariate statistical analysis, and hierarchical cluster analysis, provides a comprehensive understanding of the complex interactions and variations in water quality. The Piper diagram emphasizes the prevalence of Na-Cl characteristics in most samples. The multivariate analysis reveals strong correlations among various ions, indicating shared origins or geochemical processes. The area under rock–water interaction dominance field indicates the interaction between rock chemistry and the chemistry of the percolated waters under the subsurface. Hierarchical cluster analysis effectively categorizes sampling stations based on hydrogeochemical characteristics, emphasizing the impact of anthropogenic activities and environmental factors on groundwater quality during both post-monsoon and pre-monsoon periods.

Declaration

It is declared that the manuscript submitting to IGS journal is original work of the author(s) and it is not published already or submitted elsewhere for publication.

References

1. Soni, A. K. (2019). Mining of Minerals and Groundwater in India. *Groundwater - Resource Characterisation and Management Aspects*. DOI: 10.5772/intechopen.85309
2. Ali, M., Jha, N. K., Pal, N., Keshavarz, A., Hoteit, H., & Sarmadivaleh, M. (2022). Recent advances in carbon dioxide geological storage, experimental procedures, influencing parameters, and future outlook. *Earth-Science Reviews*, 225, 103895.
3. APHA (1989). Standard methods for the examination of water and wastewater, 17th ed. Washington, DC, *American Public Health Association*.
4. Atlas U (2010). Atlas U.N.: 44 Percent of us live in Coastal Areas. http://coastalchallenges.com/2010/01/31/un-atlas-60-of-us-live-in-thecoastalareas/⟩
5. Ayed, B., Jmal, I., Sahal, S., & Bouri, S. (2018). The seawater intrusion assessment in coastal aquifers using GALDIT method and groundwater quality index: the Djeffara of Medenine coastal aquifer (Southeastern Tunisia). *Arabian Journal of Geosciences,* 11, 609. https://doi.org/10.1007/s12517-018-3966-8
6. Boukari, M., Gaye, C. B., Faye, A., & Faye, S. (1996). The impact of urban development on coastal aquifers near Cotonou, Benin. *J Afr Earth Sci*, 22(4), 403–408.
7. Census of India (2011). Provisional Population Totals - Tamil Nadu-Census 2011 Sub District (Taluk) Level.
8. Chandrasekar, V., Shaik, M., & Ravikumar, P. (2017). An Assessment of Groundwater Quality in Coastal Taluks of Tiruvallur Districts in Tamil Nadu, India. *International Journal for Research in Applied Science & Engineering Technology*, 5(8).
9. Chilton, J. (1996). Water Quality Assessments - A Guide to Use of Biota, Sediments and Water in Environmental Monitoring - Second Edition. Chapter 9 *Groundwater.* Edited by Deborah Chapman.
10. Igibah, C. E., & Tanko, J. A. (2019). Assessment of urban groundwater quality using Piper trilinear and multivariate techniques: a case study in the Abuja, North-central, Nigeria. *Environmental Systems Research*.
11. Egun, N. K. (2010). Effect of channelling wastewater into water bodies: a case study of the Orogodo River in Agbor, Delta State*. J Hum Ecol,* 31(1), 47–52.
12. Foppen, J. W. A. (2002). Impact of high-strength wastewater infiltration on groundwater quality and drinking water supply: the case of Sana'a, Yemen. *J Hydrol*, 263, 198–216.
13. Ilić, I., Puharić, M., & Ilić, D. (2021). Groundwater Quality Assessment and Prediction of Spatial Variations in the Area of the Danube River Basin (Serbia). *Water Air Soil Pollution*, 232, 117. https://doi.org/10.1007/s11270-021-05069-4
14. Jasechko, S., Seybold, H., Perrone, D., et al. (2024). Rapid groundwater decline and some cases of recovery in aquifers globally. *Nature*, 625, 715–721. https://doi.org/10.1038/s41586-023-06879-8
15. Adimalla, N., Dhakate, R., Kasarla, A., & Taloor, A. K. (2020). Appraisal of groundwater quality for drinking and irrigation purposes in Central Telangana, India. *Groundwater for Sustainable Development,* 10. https://doi.org/10.1016/j.gsd.2020.100334
16. Adimalla, N., & Venkatayogi, S. (2018). Geochemical characterization and evaluation of groundwater suitability for domestic and agricultural utility in semi-arid region of Basara,

Telangana State, South India. *Applied Water Science*, 8, 44. https://doi.org/10.1007/s13201-018-0682-1

17. Khatri, N., & Tyagi, S. (2014). Influences of natural and anthropogenic factors on surface and groundwater quality in rural and urban areas. *Frontiers in Life Science*, 8(1). https://doi.org/10.1080/21553769.2014.933716
18. Prasad, B., Rao, P. R., & Tigga, A. (2021). Groundwater quality assessment using the weighted arithmetic index method in the selected villages of Butchayyapeta Mandal, Visakhapatnam, Andhra Pradesh, India. *Environmental Monitoring and Assessment*, 193, 1-17.
19. Prusty, P., & Farooq, S. H. (2020). Seawater intrusion in the coastal aquifers of India-A review. *HydroResearch,* 3, 61-74.
20. Silva-Madera, R. J., Salazar-Flores, J., Peregrina-Lucano, A. A., Mendoza-Michel, J., Ceja-Gálvez, H. R., Rojas-Bravo, D., Reyna-Villela, M. Z., & Torres-Sánchez, E. D. (2021). *Water Air Soil Pollution*, 232, 43.
21. Rosegrant, M. W., Ringler, C., & Zhu, T. (2009). Water for agriculture: maintaining food security under growing scarcity. *Annu Rev Environ Resour*, 34(1), 205–222. https://doi.org/10.1146/annurev.envir
22. Shanmugasundharam, G., Kalpana, S. R. M., Sudharson, E. R., & Jayaprakash, M. (2015). Assessment of Groundwater quality in Krishnagiri and Vellore Districts in Tamil Nadu*, India. Applied Water Science*, 7, 1869–1879.
23. Stallard, R. F., & Edmond, J. M. (1983). Geochemistry of the Amazon River. The influence of the geology and weathering environment on the dissolved load. *J Geophys Res*, 88, 9671-9688.
24. Steinhorst, R. K., & Williams, R. E. (1985). Discrimination of groundwater sources using cluster analysis, MANOVA, canonical analysis and discriminant analysis. *Water Resour Res*, 21, 1149–1156.
25. Subba Rao, N. (2006). Seasonal variation of groundwater quality in a part of Guntur District, Andhra Pradesh, *India. Environ Geol*, 49, 413–429.
26. Venkateswarana, S., & Deepa, S. (2015). Assessment of Groundwater Quality using GIS Techniques in Vaniyar Watershed, Ponnaiyar River, Tamil Nadu. *Aquatic Procedia*, 4, 1283–1290. doi: 10.1016/j.aqpro.2015.02.167
27. World Health Organization (WHO) (2011). Guidelines for drinking water quality, 4th edn. *World Health Organization*, Geneva.

The Indian Geographical Journal
Volume 98 (2) December - 2023, pp 191-194
ISSN 0019-4824

News and Notes

National Conference on
Frontier Areas of Teaching and Research in Geography (FATRG)
Centenary Year of Establishment of Geography Department in IASE
3 & 4, February 2024

Organisers

The Indian Geographical Society (IGS), Department of Geography, University of Madras, Chennai
Department of Geography, Tamil Nadu Open University, Chennai
Institute of Advanced Study in Education (IASE), Chennai
Indian Society of Remote Sensing – Tiruchirappalli Regional Chapter (ISRS-TRC),
Department of Geography, Bharathidasan University, Tiruchirappalli
Science City, Department of Higher Education, Government of Tamil Nadu, Chennai

****

Background of the Conference

Indian geography is developing in the areas of curriculum, teaching and research over the last one hundred years of its existence in the country. The momentum began only when the founder economics professor Dr. Gilbert Slater found the ignorance of geographic knowledge among the students of Madras University. He raised the issue in Madras University Senate Meeting. As a consequence, a Committee was appointed to look into the matter and submit a report. Based on the Committee's recommendation, among other things, a separate Geography Department in Teachers' Training College in Chennai was established in 1923. Before this, the history teachers were giving a superficial training in geography. Mr. Lakshmana Iyer, was appointed as the full time geography teacher in1923, followed by Mr. N. Subrahmanyam in 1925. Earlier, the traditional geography contained only what and where type of traditional geography, which was taught by and among the teachers of history. During 1920s, why, how and wherefore type of Modern Geography with practical applications in weather study, surveying and field works were introduced and adopted in L.T Geography curriculum of Madras University. A national level geographic revolution was witnessed during the regime of Mr. N.Subrahmanyam. After the retirement Mr. N.Subrahmanyam on 14.1.1940; Mr.S.Muthukrishna Ayyar continued his legacy. To commemorate the centenary event of establishment of Geography Department in AICE, formerly known as Teachers' Training College, the Indian Geographical Society, which was established by the vibrant Geography faculty member of the college. We intend to celebrate the occasion through a National Conference of this kind.

Besides the Conference, the Tiruchirappalli Regional Chapter of the Indian Society of Remote Sensing ISRS TRC, housed at the Department of Geography, Bharathidasan University, Tiruchirappalli, which organizes regularly a variety of academic programs to disseminate the ISRO activities in this part of India, is organizing a Quiz competition to Winners of Talent Test 2024 and Toppers of Talent Test participants from the geography Institutions across Tamil Nadu and distribute prizes and Awards. Thus, the Two-Day National Conference is aimed to sharpen the teaching and research methodology of

Geography by adopting the latest remote sensing, geospatial and geoinformatics knowledge and methods to teachers and students.

The Indian Geographical Society (IGS)

The Indian Geographical Society (IGS), the oldest Geographical Society in India, was established in Chennai (Madras) on 16.3.1926 at Presidency College Campus by a team of Indian and British Geographers, lead by Mr. N. Subrahmanyam M.A., L.T., F.R.G.S., the Chair of Geography at Teachers' College, Saidapet, Chennai. At present, the Society is housed at the Department of Geography, University of Madras, Chennai. The IGS is bi-annually publishing The Indian Geographical Journal since 1926. From its inception, the Journal is maintaining its quality and contributing to the development of geography in various spheres of the discipline. In 1941, the Madras Geographical Journal was renamed as the Indian Geographical Journal, with the ambition to broaden its scope to a national level.

You may visit www.igschennai.org for further details about the activities of the Society.

Institute of Advanced Study in Education – Department of Geography

Chennai, popularly known as Teachers ' College is the premier Teacher Training institution in our country and the first of its kind in Asia. IASE is also the largest Teacher Training Center in Tamil Nadu. Its origin is to be traced back to the Government Normal School started in Vepery in 1856. The affiliation of the Normal School with the University of Madras in 1887 marks the most important milestone in its history. The Institution then came to be called the Teachers' College and the college was shifted to Saidapet, the present premises the same year. The college building was constructed in 1889. In 1952, this Collegiate Teachers' Certificate course was affiliated to the University of Madras and came to be known as the Shortened B. T. Course. M. Ed. Class on Inter-collegiate basis was introduced in the college in 1953. In 1972 the University re-organized the B. T. course and gave its present name, the B. Ed, course. The M. Ed. Course (Evening Class) was introduced in the college in 1974. The college celebrated its Post Centenary Silver Jubilee (125th year) on 30.03.1981. M. Phil. Course was introduced in 1986. The college has been recognized for conducting research leading to Ph. D. in Education both on part-time and full-time basis from the academic year 1986. The college was upgraded as IASE with liberal assistance from the Central Government from the year 1990. Institute of Advanced Study in Education was accredited with FOUR stars by NAAC in 1999. Institute of Advanced Study in Education was reaccredited with B+ from March 2007. The college was granted AUTONOMOUS status by the UGC from the academic year 2005-2006. The college celebrated its POST CENTENARY GOLDEN JUBILEE on 30.03.2006.

Tamil Nadu Open University (TNOU)

Started in 2002, the Academic Programmes of TNOU were duly recognized by UGC-DEB, NCTE, RCI and AICTE. The University has been accorded with 12B Status of the UGC. The academic operations were commenced in 2003-04. The growth of the University during the past 20 years has been phenomenal. With a cumulative student strength of over one million in 234 Programmes of study across various disciplines and skills at different levels from Certificate to Post Graduate Programmes that are imparted through 11 Academic Schools, 5 Support Divisions, 1 Media Centre and a robust network of Learner Support Centres and the Community Colleges across the State. As per UGC-DEB approval, the TNOU started its M.Phil. and Ph.D. programme (in Regular Mode) in 2017.

These Skill Education and Training Programmes are now offered at Short Term, Certificate, Vocational Diploma and Advanced Vocational Diploma levels in TNOU. Since its inception, the University has been catering to the learning needs of the disadvantaged and deprived in the society. With a view to increasing the access to higher education and improve the quality of higher education offered through the open and distance learning modes by coordinating with such provisions in the State, the Government of Tamil Nadu established the Tamil Nadu Open University. The School of Science, established in the year 2004, has been offering the B.Sc. and M.Sc. programs in Mathematics, B.Sc. Mathematics with Computer Application. Physics, Chemistry, Botany, Zoology Geography and Apparel Fashion Design have come under the School. The School is also offering the Ph.D. Research Programs in all the above said subjects, Diplomas, Vocational Diploma Programme and Certificate Programmes.

Indian Society of Remote Sensing – Tiruchirappalli Regional Chapter (ISRS - TRC)

Indian Society of Remote Sensing (ISRS) was established in 1969 with the main objective of advancement and dissemination of remote sensing technology in the fields of mapping, planning and management of natural resources and environment by organising seminars/symposia and by publishing a monthly journal (JISRS), bulletins, proceedings, etc. Starting with 56 members, the Society has now grown into a premier professional body with membership of over 6250 members. Currently, ISRS is a member of the International Society of Photogrammetry and Remote Sensing (ISPRS) and Asian Association on Remote Sensing (AARS). The ISRS TRC is established in 2013 at the Department of Geography, Bharathidasan University, Tiruchirappalli and is regularly organising a variety of academic programs to disseminate the ISRO activities in this part of India.

Sub Themes of the Conference

- Development of geography in India
- New methods of teaching physical geography
- Latest methods of teaching human geography
- Development of cartography & remote sensing
- Teaching & research using geospatial technology
- Applied geoinformatics
- Curriculum development issues in geography
- Prospects and issues of employment & entrepreneurship

Abstract Submission

Research papers are invited for oral presentation in various technical sessions of the Conference. The participants are requested to submit their abstract (s) not exceeding 250 words, typed in MS-Word font size 12 in Times New Roman in single line space. The title should be bold, followed by author(s) name, designation and address.

Registration for Participation

There is no registration fee for the participation. Interested participants can send their abstract to the organisers through mail (coordinatorigs1926@gmail.com) on or before 31.01.2024.

Talent Test 2024 & Remote Sensing Quiz Competition

• The Indian Geographical Society is organising the State-wide 14th Talent Test for Young Geographer – 2024 for the final year UG and PG students of Geography Departments in Tamil Nadu on 5th January, 2024 (Friday) through online mode with the support of Head of the Colleges/Institutes/Geography Departments.

• The Results of the winners of UG & PG Talent Test 2024 will be published on the same day and the participation certificates will be sent separately to the individual participants.

• The winners are requested to participate the National Conference on Frontier Areas of Teaching and Research in Geography being organised at the Institute of Advanced Study in Education (IASE), Saidapet, Chennai-600 015, Tamil Nadu on 3&4, February 2024 and receive the award and certificates.

• The winners are requested to come along with their parents or faculty members of the Department to receive the award and certificates.

• There will be a Quiz Competition among the winners of Talent Test 2024 on 4th February 2024 at the Institute of Advanced Study in Education (IASE), Saidapet, Chennai-600 015. All the institutes which participated in the Talent Test 2024 may depute a maximum of two candidates from UG and PG programmes for the quiz competition. The winners of the quiz competition will be awarded with separate awards and certificates.

Note:

• Those who require accommodation are requested to contact the conference organisers on or before 01.02.2024.

• All the winners of Talent Test 2024 and the Quiz competition participants are informed to bring their ID card issued by the institutes.

Advisory Committee

Prof. S. Arumugam Honourable Vice Chancellor, TNOU, Chennai
Prof. P.S. Tiwari Former Professor Department of Geography, University of Madras, Chennai
Prof. N. Sivagnanam President, The Indian Geographical Society, Chennai
Prof. Sulochana Shekhar Professor & Head, Department of Geography, CUTN, Thiruvarur
Prof. A. Subramani Principal - Institute of Advanced Study in Education, Chennai

Organising Committee

Prof. K. Kumaraswamy Editor, Indian Geographical Society Bharathidasan University, Tiruchirappalli
Prof. D. Venkataraman Former Head, Department of Geography AAISC, Chennai
Prof. R. Jaganathan Secretary, The Indian Geographical Society, Chennai
Prof. V. Emayavaramban Professor & Head, Department of Geography, M.K. University, Madurai
Prof M. Sakthivel Professor, Department of Geography, University of Madras, Chennai
Prof G. Bhaskaran Professor, Department of Geography, University of Madras, Chennai
Prof. R. Jegankumar Professor & Head, Department of Geography, Bharathidasan University, Tiruchirappalli
Dr. T. Ravimanickam Associate Professor & Chairperson, School of Sciences, TNOU, Chennai
Dr. S Sanjeevi Prasad Assistant Professor, Department of Geography, University of Madras, Chennai
Dr. P. Masilamani Assistant Professor, Department of Geography, Bharathidasan University, Tiruchirappalli